Fault Diagnosis and Identification of Electro Mechanical Systems - Methods for Closed Loop Systems.

Sekunda, André Krabdrup

Publication date:
2018

Document Version
Publisher's PDF, also known as Version of record

Fault Diagnosis and Identification of Electro - Mechanical Systems

Methods for Closed Loop Systems

André Krabdrup Sekunda

Technical University of Denmark
Kgs. Lyngby, Denmark, 2017

English title of the thesis:
Fault Diagnosis and Identification of Electro - Mechanical Systems
– Methods for Closed Loop Systems

Afhandlingens danske titel:
Fejl Diagnose og Identifikation af Elektro Mekaniske Systemer
– Methoder for Lukket Sløjfe Systemer

PhD Student:
André Krabdrup Sekunda
aksek@elektro.dtu.dk
ORCID: 0000-0002-0094-0743

Supervisors:
Hans Henrik Niemann
hhn@elektro.dtu.dk
ORCID: 0000-0002-1518-4979

Niels Kjølstad Poulsen
nkpo@dtu.dk
ORCID: 0000-0002-8476-0052

Ilmar Santos
ifs@mek.dtu.dk
ORCID: 0000-0002-8441-5523

Technical University of Denmark
Department of Electro Engineering
Section of Automation and Control
Elektro vej, Building 326
DK-2800 Kgs. Lyngby
Denmark
Phone: (+45) 45 25 34 76
Email: info@elektro.dtu.dk
www.elektro.dtu.dk

Summary (English)

We are on the verge of the fourth industrial revolution also known as industry 4.0[1]. The goal of industry 4.0 is to increase the incorporation of sensor information into decision making for machinery. This in turn increases the popularity of feedback control, and by extension, closed loop schemes. With the increasing popularity of closed loop control it is important that the impact of the feedback loop is handled appropriately. Because of the feedback loop, signals that might normally be uncorrelated are suddenly not and assumptions often used for identification and fault diagnosis schemes are no longer realistic to achieve.

The thesis aims at introducing the reader to design methods with proper handling of noise for closed loop systems. In order to achieve this goal, it is investigated how to transform a closed loop identification problem into an open loop identification problem. Such a transformation is already well known, however the excitation signal design is not intuitive when applying such a transformation. The shape of the excitation signal is of paramount importance for the quality of the identified model. By making the design of the excitation signal more intuitive, it should be possible to increase the quality of identified models.

Another interesting closed loop application is fault diagnosis. More and more systems will be part of a closed loop scheme in the future in accordance with industry 4.0. Often, systems are designed without sensor redundancy, and with disturbance rejecting controllers. Methods which are not limited in isolability due to sensor redundancy, and which decouple the effect of the disturbance rejecting controller, are therefore of huge interest. Active fault diagnosis obtains the required information through a known excitation signal instead of the sensor redundancy. Design of detectors based on active fault diagnosis can therefore make fault diagnosis possible for systems where installation of extra sensors are too cost demanding.

The methods were developed with a piezoelectric rotor-bearing application in mind. The bearing is using air as the lubricant between the bearing and the shaft and is therefore referred to as a gas bearing. Gas bearings have relative low damping compared to high friction bearings such as ball bearings. Feedback control is therefore employed to increase the damping of the Gas Bearing. This makes Gas Bearings a prime example of technology following with the industry 4.0 standard.

The PhD has been carried out in collaboration with DTU Department of Mechanical

Engineering, and DTU Department of Applied Mathematics and Computer Science, both of which contributed with their respective expertise. Furthermore, DTU Department of Mechanical Engineering provided an experimental gas bearing test rig with which to conduct experimental validation of the methods developed. The scientific results of the research have been summarised in 3 conference papers which have been published and presented, 1 published journal paper, 1 journal paper accepted for publication and 1 journal paper which have been submitted.

Resumé (Dansk)

Vi er på tærsklen til den fjerde industrielle revolution, også kendt som industri 4.0 [1]. Målet med industri 4.0 er at øge brugen af sensorinformation i styring af maskiner. Dette som konsekvens øger populariteten af regulering og tilbagekobling. Med den stigende popularitet af regulering ved brug af tilbagekobling er det vigtigt at tilbagekoblingssløjfens effekt håndteres korrekt. På grund af regulatoren bliver signaler der normalt ikke er korrelerede pludselig korrelerede. Antagelser, der ofte anvendes til identifikation og fejldiagnose, bliver derved urealistiske.

Afhandlingen sigter mod at introducere læseren til designmetoder der tager højde for støjs indflydelse i lukketsløjfe systemer. For at nå dette mål undersøges det, hvordan man omdanner et lukketsløjfe identifikationsproblem til et åbensløjfe identifikationsproblem. En sådan transformation er allerede velkendt, men design af excitation signalet er ikke intuitivt, når der bruges en sådan transformation. Excitationssignalet er af afgørende betydning for kvaliteten af den identificerede model. Ved at gøre designet af excitationssignalet mere intuitivt bør det være muligt at øge kvaliteten af de identificerede modeller.

En anden interessant lukketsløjfe anvendelse er fejldiagnose. Flere og flere systemer vil blive styret af en regulator i fremtiden i overensstemmelse med industri 4.0. Ofte er systemer designet uden sensorredundans og med regulatorer designet til at undertrykke forstyrrelser. Metoder, som ikke bliver begrænset af sensor redundans, og som afkobler effekten af regulatoren, er derfor af stor interesse. Aktiv fejldiagnose opnår den nødvendige information gennem et kendt excitationssignal i stedet for sensor redundans. Design af detektorer baseret på aktiv fejldiagnose kan derfor gøre fejldiagnose mulig for systemer, hvor ekstra sensorer er for omkostningskrævende.

De præsenterede metoder blev udviklet med et piezoelektrisk luftleje i tankerne. Lejet anvender luft som smøremiddel mellem lejet og akslen og betegnes derfor som et luftleje. Luftlejer har relativt lav dæmpning i forhold til højfriktionslejer såsom kuglelejer. Tilbagekobling er derfor anvendt til at øge luftlejets dæmpning. Dette gør luft lejer til et perfekt eksempel på teknologi, der følger med standarden fra industri 4.0.

Ph.d.-uddannelsen er udført i samarbejde med DTU Institut for Mekanisk Teknologi og DTU Institut for Matematik og Computer Science, der har bidraget med deres respektive ekspertise. Desuden leverede DTU Institut for Mekanisk Teknologi en eksperimentel testopstilling til at udføre eksperimentel validering af de udviklede metoder på. De

videnskabelige resultater er opsummeret i 3 konferenceartikler, der er blevet udgivet og præsenteret, 1 tidsskrift der er publiceret, 1 tidskrift der er blevet accepteret for publicering og 1 tidsskrift der er indsendt.

Preface

This thesis is submitted as a prerequisite to obtain a Danish PhD degree. The PhD-thesis is based on the contributions described in 3 conference and 3 journal papers which are included as part of the thesis. Besides the 6 papers, the thesis consists of a summary which links the contributions from all the articles together. The work has primarily been carried out at the Section of Automation and Control (AUT), Department of Electrical Engineering, Technical University of Denmark (DTU). The PhD project was fully funded by the section of Automation and Control without contributions from external stakeholders.

The project was supervised by associate professor Hans Henrik Niemann, and co-supervised by associate professor Niels Kjølstad Poulsen and professor Ilmar Ferreira Santos. The supervisor composition gave me unique possibilities to enhance existing ideas and develop new methods within the field of mechatronics. I would like to thank my supervisors for their invaluable through and competent guidance, especially my main supervisor Hans Henrik Niemann who has always made time in his busy schedule when I needed help. Furthermore, his interest in the project has always made it enjoyable for me to come by his office to discuss new ideas and results. I would also like to thank Professor Steven Ding which I got to know during my short but fruitful stay at the University of Duisburg-Essen. It was extremely helpful with much insightful discussion regarding fault diagnosis and closed loop systems.

I would like to thank Lukas Roy Svane Theisen who patiently introduced me to the test rig and how to use his model of the gas bearing. His work and guidance saved me many frustrating hours in the lab. I would also like to thank Andreas Søndergaard Pedersen, Dan Hermann, Jonas Skjødt Lauridsen and Dimitrios Papageorgiou for their help and technical discussions, as well as sharing with me the burdens encountered during a PhD. I need to also thank Adriana Gabriela Zsurzsan for listening to all my complaints, and Elbert Hendricks for his endless tries at making me a better writer, which hopefully has made this thesis more enjoyable to read. Furthermore, a general thanks goes out to my colleagues at AUT.

I want to thank my family, and last but definitely not least, I would like to recognise the amazing support of my girlfriend Tara Amirkhizi. You have always let my work go before your wishes, and I deeply appreciate your understanding and support.

Contents

Summary (English) i

Resumé (Dansk) iii

Preface v

Contents vii

Abbreviations and nomenclature xi

1 Introduction 1
- 1.1 Motivation . . . 1
- 1.2 State of the art - literature survey . . . 2
  - Close loop identification of active gas bearings . . . 2
  - Active Fault Diagnosis of Closed Loop Systems . . . 3
  - Fault diagnosis of rotation machinery . . . 4
  - Summary of the literature survey . . . 5
- 1.3 Original Contribution . . . 6
  - Paper P1: Identifying parameters in active magnetic bearing system using LFT formulation and Youla factorisation. By Jonas S. Lauridsen, André K. Sekunda, Ilmar F. Santos and Henrik Niemann. . . . 6
  - Paper P2: Closed loop identification using a modified Hansen scheme. By André K. Sekunda, Henrik Niemann, Niels Kjølstad Poulsen and Ilmar F. Santos. . . . 6
  - Paper P3: Active Fault Detection Based on a Statistical Test. By André K. Sekunda, Henrik Niemann and Niels Kjølstad. . . . 7
  - Paper P4: Detector Design for Active Fault Diagnosis in Closed Loop Systems. By André K. Sekunda, Henrik Niemann and Niels Kjølstad. 7
  - Paper P5: Parametric Fault Diagnosis of an Active Gas Bearing. By André K. Sekunda, Henrik Niemann, Niels Kjølstad Poulsen and Ilmar F. Santos. . . . 8
  - Paper P6: Closed-loop Identification of an Active Gas Bearing. By André K. Sekunda, Henrik Niemann, Niels Kjølstad Poulsen and Ilmar F. Santos. . . . 8
- 1.4 Structure of the Thesis . . . 8

2 YJBK Theory 9

2.1 Coprime factorisation . . . 9
2.2 Bezout Identity . . . 10
2.3 All Stabilising Controllers . . . 10
2.4 All Stabilised Plants . . . 12
2.5 Relationship between S and Q . . . 13
2.6 Parametrisation in S . . . 14
2.7 Coprime Factorisation of Controllers . . . 15
Coprime Factorisation given a Stable Controller . . . 16
2.8 Perspective . . . 17

3 Experimental Test Rig **19**
3.1 Experimental Test Rig . . . 19
Objective . . . 20
Model . . . 22
Implementation . . . 24

4 System Identification **27**
4.1 Closed Loop Identification . . . 28
4.2 Identification of Parametric Uncertain Parameters . . . 29
4.3 Hansen Scheme . . . 32
4.4 Modified Hansen Scheme . . . 34
4.5 Initial Results Closed loop Identification of Gas Bearing . . . 35
4.6 Method Comparison for Closed Loop Identification . . . 37
4.7 Experimental Results . . . 37
Order Reduction . . . 39
4.8 Contributions . . . 39

5 Fault Diagnosis **41**
5.1 Active Fault Diagnosis . . . 43
5.2 Whitening filter . . . 45
5.3 Matching filters . . . 46
Model Uncertainty . . . 49
5.4 Design of excitation signal . . . 49
5.5 Experimental Diagnosis . . . 51
Noise analysis . . . 53
Controller Design . . . 53
Fault Diagnosis . . . 54
5.6 Contributions . . . 57

6 Conclusion **59**
6.1 Future Perspectives . . . 60

Bibliography **63**

P1 Identifying parameters in active magnetic bearing system using LFT formulation and Youla factorisation **69**

P2 Closed loop identification using a modified Hansen scheme **87**

P3 Active Fault Detection Based on a Statistical Test 105

P4 Detector Design for Active Fault Diagnosis in Closed Loop Systems 131

P5 Parametric Fault Diagnosis of an Active Gas Bearing 163

P6 Closed Loop Identification of a Piezo Electrically-Controlled Radial Gas Bearing - Theory & Experiment 201

Abbreviations and nomenclature

This nomenclature covers the thesis summary. The nomenclatures of the appended publications may differ.

Abbreviations

N4SID	Numerical Subspace State Space System Identification
MOESP	Multi-variable Output Error State Space
PEM	Prediction Error Method
YJBK	Youla-Jabr-Bongiorno-Kucera
LQR	Linear Quadratic Regulator
SISO	Single Input Single Output
MIMO	Multiple Input Multiple Output
gcd	Greatest Common Divisor
LFT	Linear Fractional Transformation
FAR	False Alarm Rate
LCF	Left coprime factorisation
RCF	Right coprime factorisation
WGN	White Gaussian Noise
PDF	Probability Density Function
AMB	Active Magnetic Bearing
FEM	Finite Element Model
CUSUM	Cumulative Sum
FD	Fault Detection
LTI	Linear Time Invariant

Latin symbols

K	Stiffness matrix $[\frac{N}{kg \cdot \mu m}]$
D	Damping matrix $[\frac{N}{kg \cdot \mu m}]$
B	Input gain matrix $[\frac{N}{kg \cdot \mu m}]$
H	Hypothesis $[-]$
s	Laplace variable $[j\omega]$
$\|\| \cdot \|\|_x$	The x-norm $[-]$
θ	Parametric fault or Parametric uncertainty diagonal matrix [-]

θ_i Specific parametric fault or parametric uncertainty [-]

Notation

$\left(\begin{array}{c|c} A & B \\ \hline D & D \end{array}\right)$ Shorthand notation for the state space realisation $C(sI-A)^{-1}B+D$

$\begin{bmatrix} G_{11} & G_{12} \\ G_{21} & G_{22} \end{bmatrix}$ Partition of the system G into four subsystems

$\star$ Star product $G \star K := \begin{bmatrix} \mathscr{F}_l(G,K_{11}) & G_{12}(I-K_{11}G_{22})^{-1}K_{12} \\ K_{21}(I-G_{22}K_{11})^{-1}G_{21} & F_u(K,G_{22}) \end{bmatrix}$

$\mathscr{F}_l(G,\theta)$ Shorthand notation for lower LFT:$= G_{11}+G_{12}\theta(I-G_{22}\theta)^{-1}G_{21}$

$\mathscr{F}_u(G,\theta)$ Shorthand notation for upper LFT:$= G_{22}+G_{21}\theta(I-G_{11}\theta)^{-1}G_{12}$

Chapter 1

Introduction

1.1 Motivation

Research into low friction bearings has been a hot topic for the last decade. Active gas bearings is one such bearing technology. These bearings have several advantages that make them suitable for specialised industries. Another low friction bearing type is the Active Magnetic Bearing (AMB), unlike gas bearings, AMB's are open loop unstable. This makes gas bearings preferable for systems where controller failures is a possibility. Other popular applications of gas bearings are in air-conditioning systems of closed environments such as aeroplanes and in the food industry. The reason for gas bearings being popular in these applications is that gas bearings use air as a lubricant and therefore do not pose the danger of leaking toxic lubricants.

Until recently there were no models that could predict the behaviour of active gas bearings for control design purposes[2]. An experimental test setup containing an active gas bearing was therefore constructed at DTU [3, 4, 5]. It is shown that it is possible in [6, 7, 8, 9] to create a Finite Element Model (FEM) that appropriately predicts the dynamics of the active gas bearing. Such models consist of an inconvenient high number of states for the design of feedback controllers. This is mainly because the purpose of such models is to help in the design phase of the plant, which requires a lot of information that is unimportant for control purposes. It was thus the task in [10] to identify low order models appropriate for design of feedback control. Initial success was achieved with a fourth order model in [11] which disregarded the actuator dynamics. The model was found to have discrepancies because of the actual actuator dynamic, and was improved in [12] identifying the actuator dynamics as well. This approach resulted in a 10'th order model. Lastly, it is shown possible in [13] to reduce the order of the model so that a 6'th order model could capture the main dynamics of the plant.

All previous identified models were identified and verified using open loop experiments. It is often not possible to identify a plant using open loop experiments. This can be due to safety related issues, or the plant simply not being open loop stable. For active gas bearings this is especially true. Active gas bearings is a technology meant for precision operation in systems with a low downtime. It is therefore seen as advisable to conduct identification with feedback control active.

Because of the importance of low downtime for active gas bearings, it is furthermore

essential to only conduct maintenance when required. Fault diagnosis is a promising tool to determine when machinery requires maintenance. As for the identification, it is important that the fault diagnosis is usable while the plant is subject to a feedback loop. Besides the closed loop requirement, the active gas bearing experimental test rig used for experiments is supplied with a fixed sensor setup. In order to be able to conduct exact diagnosis of faults, it is natural to investigate the possibilities of active fault diagnosis. With such a fault diagnosis scheme, the downtime can be reduced to a minimum where the active gas bearing can show its full potential compared to other types of bearings.

The goal of the thesis can be summarised into 3 points.

- Identify the active gas bearing when part of a closed loop scheme.
- Design methods for closed loop active fault diagnosis.
- Conduct active fault diagnosis on the active gas bearing.

The thesis is a product of simulation and experimental results. Such an approach has been chosen because it is able to cover the entire range from idea to application.

1.2 State of the art - literature survey

In this section state of the art literature is presented. This section is separated into 3 subsections, each dealing with one of the goals of the thesis.

Close loop identification of active gas bearings

Identification is an intensively studied subject with base line defining contributions such as [14, 15]. In [15] it was argued that closed loop identification methods can be divided into three main categories

- Direct identification
- Indirect identification
- Joint input-output identification

Direct identification is similar to ignoring the feedback loop. The risk of identifying the controller instead of the plant with direct identification is shown in [15, 14]. Indirect identification methods deal with identification of the closed loop system using an external excitation signal. Afterwards, the knowledge of the feedback loop is used to determine the plant. One method in this category is known as the Hansen scheme [16, 17]. This method is based on the Youla-Jabr-Bongiorno-Kucera (YJBK) parametrisation of the plant first introduced in [18] for the Single Input Single Output (SISO) case, and in [19] for the Multiple Input Multiple Output (MIMO) case. The Hansen scheme transforms the identification problem from a closed loop problem to an open loop problem as illustrated in Figure 1.1. This is achieved by formulating the identification problem as identifying the Youla deviation system, instead of the plant the plant to identify, and therefore indirectly identifying the plant.

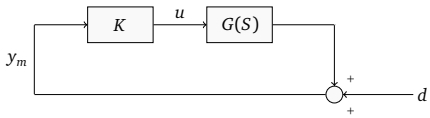

(a) Block representation of a closed loop system. The goal is to identify the plant G using the measurable input u and the measurable output u. It is clear from the block diagram that both u and y depend on the noise d.

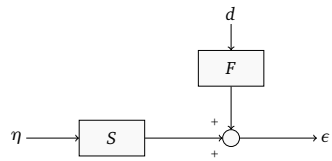

(b) Reformulation of the identification problem using the Youla deviation system S. The goal is to identify the Youla deviation system S using the known input η and the known output ϵ. The noise d is subject to a linear filter F. It is clear that the reformulation makes the input η independent of the noise d.

Figure 1.1: Block diagram illustration of the transformation from a closed loop to open loop identification problem using the Hansen Scheme.

Identification of the Youla deviation system is an open loop identification problem as shown in [16, 17]. It can be problematic to identify the Youla deviation system simply because required a priori knowledge might not be obtainable. Subspace identification methods have shown promising results when it comes to identification of the Youla deviation system. They, for example, make it possible to identify the Youla deviation system easily for both the SISO and MIMO case. Several different subspace identification methods have been developed with some of the more well-known methods being the Multi-variable Output Error State Space (MOESP) [20, 21] and the Numerical Subspace State Space System Identification (N4SID) [22] algorithms. An overview of the different subspace identification methods and their strengths and weaknesses is given in [23].

Active Fault Diagnosis of Closed Loop Systems

Model based fault diagnosis has been shown to be applicable for different applications [24, 25, 26, 27]. All of these schemes are based on a passive fault diagnosis approach. By passive it is understood that the fault diagnosis is conducted based only on monitoring the input and output signals. It was first proposed in [28] to design a diagnosis scheme which used an external signal to diagnose faults. In this thesis a diagnosis scheme that uses external signals for diagnosis is referred to as an active fault diagnosis scheme. Active fault diagnosis has been applied to several different diagnosis problems. One such example is [29] where pitch actuator faults on a wind turbine were simulated. The main objective of active fault diagnosis schemes is to determine the optimal external signal for diagnosis. This issue was discussed from a deterministic viewpoint in [30] and was based on set theory. It was argued that often the plant to be diagnosed is subject to a feedback loop. Controllers are often designed for disturbance rejection which essentially tries to hide faults on the monitored signals. Active fault diagnosis has the advantage, compared to passive schemes, that the excitation signal can be designed to reveal such hidden faults. Methods for the design of optimal excitation signals for closed loop systems have also been considered in [31, 32].

Often active fault diagnosis schemes are stated as an output fitting problem. The problem of determining which fault that has occurred is solved by creating a bank of

plants, where each plant represents a specific fault. The objective is then to determine which plant that produces the output that best resembles the measured output. The method is illustrated on Figure 1.2 where G_0 is the fault free system, and G_1 to G_n are the models given each of the possible faults.

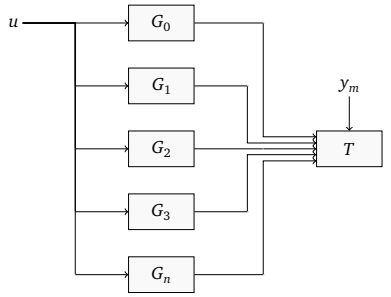

Figure 1.2: Illustration of the active fault diagnosis problem using a bank of possible plants representing the fault free case G_0, and the different possible faulty cases G_1 to G_n together with the measured output y_m.

The problem illustrated in Figure 1.2 is to determine which plant in the bank produces the output which mimic y_m the best. Some examples of this problem description can be found in [33, 34].

The research conducted throughout this thesis investigates how to apply the YJBK-parametrisation for fault diagnosis purposes of closed loop systems instead. The framework was first described in [35, 36]. It was argued by the authors that it is possible to construct a fault signature system which is zero in the fault free case, and non-zero in the case of a fault for closed loop systems. A scheme was therefore constructed where a signal was applied to the fault signature system, and diagnosis was based on the attributes of the signal measured from the fault signature system. The scheme was extended with a statistical test based on a Cumulative Sum (CUSUM) detector in [37]. It is here shown possible to diagnose small faults using a linearised version of the fault signature system.

Fault diagnosis of rotation machinery

Most of the experimental work conducted in this thesis has been completed using a rotating machinery test rig, or more specifically an active gas bearing test rig. The test rig consist of a shaft held in a selected position by an active gas bearing and is shown in Figure 1.3.

Fault diagnosis of rotating machinery is within the framework of industry 4.0, the goal of which is to implement intelligence into the existing systems. In [38] the authors show that it is possible to diagnose faults on a bearing rotating between 10 and 60 RPM. The diagnosis is conducted using the vibrations created due to mass unbalance during rotation inside the bearing. The bearing in itself is passive and cannot be excited directly. Fault diagnosis based on neural networks was applied in [39] to diagnose faults in induction motors. The authors pointed out that often machinery can be subject to one or more faults without failing. The production cost might however increase, thus fault diagnosis is important to keep the production cost low. As stated in [6], until

Figure 1.3: Picture of an experimental test rig consisting of a shaft with a disc attached to the end and a position controlled by an active gas bearing.

recently, models have not been available for fault diagnosis of active gas bearings. It is shown possible here for the first time to adequately predict the dynamics of an active gas bearing. The model was designed using the FEM method and was of too high an order to be used for control purposes. A 6'th order model was presented in [40]. The model has proven able to identify the main dynamics of the system, and is therefore useful for model based fault diagnosis.

Summary of the literature survey

Research into active gas bearings has been intensified during the last decade. This is partly due to the trends identified in industry 4.0 that predict sensor information to have an increasing impact on the industry in the future. All identification of active gas bearings has so far been conducted using open loop schemes. Because modelling of active gas bearings is still in its infancy, proof of concept has been the goal of the modelling so far.

Equivalently, active fault detection based on the fault signature system has still not been applied to any real systems. The method has shown great promise with

simulations, but the issues with regards to implementation have not been studied yet.

Examples of various kinds of fault diagnosis on rotating machinery have become popular. Not until recently have the models for active gas bearing matured enough to apply model based fault diagnosis. The most recent models however, have the order and accuracy believed to be required for successfully applying active fault diagnosis.

1.3 Original Contribution

The contributions in each of the attached papers are highlighted in this section. The papers are presented in chronological order.

The thesis has 3 main contributions. A novel approach to the experimental setup regarding identification using the Hansen scheme is presented in paper P1, P2 and P6, whereas paper P1 focuses on identifying specific parameters in AMB's, and paper P2 and P6 focus on identification of active gas bearings. The second contribution is a method for active fault diagnosis based on a matched filter design described in paper P3 and P4. The diagnosis method presented is the first method where test statistics have been developed for active fault diagnosis based on the YJBK-parametrisation. The last contribution is the implementation of active fault diagnosis of active gas bearings. It is shown possible in paper P5 to diagnose both sensor and actuator faults without modifying the setup used in the laboratory.

Paper P1: Identifying parameters in active magnetic bearing system using LFT formulation and Youla factorisation. By Jonas S. Lauridsen, André K. Sekunda, Ilmar F. Santos and Henrik Niemann.

Presented at IEEE Multi-Conference on Systems and Control, September 2015. Published in Control Applications (CCA), 2015 IEEE Conference on page 430-435.

It is shown in the conference paper P1 how to identify uncertain parameters for AMB's. A FEM is constructed, and it is shown with simulation examples that it is possible to identify uncertain stiffness parameters for the AMB. Since AMB's are open loop unstable all identification and verification was conducted in closed loop. The uncertain parameters were isolated using a Linear Fractional Transformation (LFT) approach. Because of the high order usually associated with the FEM approach, a comparison between model identification with the full order model, and a model obtained through model reduction, was conducted. It was proposed in the paper to apply the excitation signal inside the controller for a simpler optimisation.

Paper P2: Closed loop identification using a modified Hansen scheme. By André K. Sekunda, Henrik Niemann, Niels Kjølstad Poulsen and Ilmar F. Santos.

Presented at Advanced Control & Diagnosis conference, November 2015. Published in "Journal of Physics": Conference Series Vol. 659, No. 1, page 012009

In conference paper P2, a modification to the Hansen scheme is proposed for simplification of the identification process. The idea introduced in paper P1, with direct

excitation inside the controller, is formalised to the Hansen scheme framework. The original version of the Hansen scheme required the excitation signal to indirectly excite the Youla deviation system in order to be identified. By introducing the excitation in the controller, it was shown possible to directly excite the Youla deviation thus skipping a step in the identification procedure. This new identification scheme was named the modified Hansen scheme. A reformulation of the controller was introduced in order to generalise the method to work for any linear controller setup. The method was presented using an active gas bearing for experimental validation of the identification scheme. An observer based controller was implemented such that the gas bearing was working as part of a closed loop environment. It was shown possible to identify the active gas bearing using the modified Hansen scheme.

Paper P3: Active Fault Detection Based on a Statistical Test. By André K. Sekunda, Henrik Niemann and Niels Kjølstad.

Presented at 3´rd International Conference on Control and Fault-Tolerant Systems, September 2016. Published in "Control and Fault-Tolerant Systems" (SysTol), 2016 3rd Conference on page 511-518

A method for active fault diagnosis using a statistical detector based on the YJBK parametrisation was first introduced in paper P3. A linearised version of the fault signature system was used in order to be able to cope with small faults. A novel detector design was presented based on a desired false alarm rate (FAR). The detector design used a moving window to be able to give a probability of detection and the probability of a false alarm occurring. This was made possible by using a sinusoidal excitation signal with a known frequency and amplitude. The approach was furthermore able to diagnose several different faults using a single sensor. This was shown possible with a simulation example where two different actuators were having a fault imposed at different times.

Paper P4: Detector Design for Active Fault Diagnosis in Closed Loop Systems. By André K. Sekunda, Henrik Niemann and Niels Kjølstad.

Published in International "Journal on Adaptive Control and Signal Processing"

The journal paper P4 introduces the framework for active fault diagnosis based on the fault signature system without linearisation. The main contribution of the paper is a detector design which is able to cope with faults no matter the magnitude. It was shown that the residual generator used in P3 resulted in the noise being coloured in the fault free case. A whitening filter was therefore introduced, to be used both for open loop stable and unstable systems. Finally, the choice of excitation signal was discussed and a solution was proposed to choose the frequency of the signal. The fault diagnosis scheme was presented using a simulation example where it was shown possible to diagnose faults on different parameters. The impact of parametric uncertainties was investigated for dealing with implementation on a real experimental test rig.

Paper P5: Parametric Fault Diagnosis of an Active Gas Bearing. By André K. Sekunda, Henrik Niemann, Niels Kjølstad Poulsen and Ilmar F. Santos.

Submitted to "Journal of Control, Automation and Systems"

Journal paper P5 dealt with implementing active fault diagnosis based on the fault signature system on an active gas bearing. The method introduced in paper P4 was implemented, and it was shown possible to diagnose faults introduced on both actuators and sensors. The method was shown to be able to diagnose several different faults using only one sensor. Several different experiments were conducted to show the method with feedback control using P-control and more complex observer based controllers. The main contribution of the paper was to show that it was possible to implement active fault diagnosis on active gas bearings with the potential to reduce downtime.

Paper P6: Closed-loop Identification of an Active Gas Bearing. By André K. Sekunda, Henrik Niemann, Niels Kjølstad Poulsen and Ilmar F. Santos.

Accepted for publication in "Journal of Systems and Control Engineering"

It was in paper P2 shown possible to identify the active gas bearing as part of a closed loop system using the modified Hansen scheme framework. In journal paper P6, identification using the modified Hansen scheme is compared with Prediction Error Method (PEM) identification and direct subspace identification. All methods are given the same inferior nominal model and a comparison of the different methods ability to identify a model is conducted. Simulations of the system have been employed to find characteristics of the different identification methods. The characteristics found were experimentally verified. Experimental work was conducted using the active gas bearing test rig both with and without the disc rotating.

1.4 Structure of the Thesis

The thesis is structured as follows: In Chapter 2 the theory forming the basis for the methods developed and applied throughout the thesis is presented. The experimental test rig consisting of the active gas bearing is described in Chapter 3. The results and experience obtained with regards to closed loop system identification are given in Chapter 4. In Chapter 5, active fault diagnosis is discussed, and methods for active fault diagnosis are presented. Furthermore, the results obtained in regards to fault diagnosis theoretically and experimentally are given. Lastly, a conclusion is given in Chapter 6 summarising the presented contributions and future research subjects. The 6 papers containing the foundation for the thesis are included in the appendix.

Chapter 2

YJBK Theory

The control tools used throughout the thesis are based on results obtained through the use of ring theory. The subject of ring theory is described in [41]. A survey of the YJBK parametrisation, together with proofs, can be found in [42]. The work is based on the possibility of parameterising all systems stabilised by a known controller using a stable system S. The stable system S is in this thesis denoted as either the fault signature system or the Youla deviation system. Different schemes dealing with the use of the Youla deviation system are summarised in [43]. The schemes relevant for identification and fault diagnosis as conducted throughout the thesis are introduced in this chapter.

2.1 Coprime factorisation

In order to introduce the reader to the YJBK parametrisation we first need to discuss the meaning of coprimeness. Two numbers are coprime if their greatest common divisor (gcd) is 1. Tightly written in Eq. (2.1) where a and b are two arbitrary real numbers.

$$gcd(a, b) = 1 \tag{2.1}$$

For polynomials the gcd is equivalent to the two polynomials sharing no common factor. It is possible to write any linear SISO system as two polynomials, one for the nominator and one for the denominator. This is shown in Eq. (2.2) where $n(s)$ and $m(s)$ are two polynomials describing the transfer function $H(s)$.

$$H(s) = \frac{n(s)}{m(s)} \tag{2.2}$$

It is evident that if $n(s)$ and $m(s)$ are coprime, a minimal representation of the transfer function $H(s)$ is given by Eq. (2.2). This in turn means that the transfer function does not contain any pole-zero cancellations. Based on the notion of a minimal representation, extending the definition of coprimeness to MIMO systems, is rather straight forward, from the SISO case. Two MIMO systems are said to be coprime if they contain no pole-zero cancellations. Because the order is important for matrices, two

different kinds of coprimeness are needed when working with MIMO systems. A system is said to be left coprime if:

$$G = \tilde{M}^{-1}\tilde{N} \quad \tilde{M},\tilde{N} \in RH_\infty \tag{2.3}$$

Throughout the thesis ˜ denotes the left coprime systems. Equivalently a system is said to be right coprime if:

$$G = NM^{-1} \quad M,N \in RH_\infty \tag{2.4}$$

It is important to note that even though the system G might be unstable, the coprime pairs $\{N,M\}$ and $\{\tilde{N},\tilde{M}\}$ are all stable systems.

2.2 Bezout Identity

The Bezout identity is presented in this section. The Bezout identity is a powerful tool used to prove properties when using the coprime factorisation of plant and controller. The Bezout identity is based on a coprime factorisation of both the controller and the plant. The coprime factorisation of the plant is given in Eq. (2.5).

$$G = NM^{-1} = \tilde{M}^{-1}\tilde{N} \quad \tilde{M},\tilde{N},M,N \in RH_\infty \tag{2.5}$$

Likewise, to the plant it is possible to describe the controller using a coprime pair of systems. Such a description is given in Eq. (2.6).

$$K = UV^{-1} = \tilde{V}^{-1}\tilde{U} \quad \tilde{V},\tilde{U},V,U \in RH_\infty \tag{2.6}$$

It is assumed that the controller K stabilises the plant G which makes the following statements possible. For a coprime factorisation of plant and controller Eq. (2.7) and Eq. (2.8) is furthermore true.

$$I = \tilde{V}M - \tilde{U}N \tag{2.7}$$
$$I = \tilde{M}V - \tilde{N}U \tag{2.8}$$

It is possible to write Eq. (2.7) and Eq. (2.8) more tightly using a matrix representation. This is known as the Bezout identity and is shown in Eq. (2.9).

$$\begin{bmatrix} I & 0 \\ 0 & I \end{bmatrix} = \begin{bmatrix} M & U \\ N & V \end{bmatrix}\begin{bmatrix} \tilde{V} & -\tilde{U} \\ -\tilde{N} & \tilde{M} \end{bmatrix} = \begin{bmatrix} \tilde{V} & -\tilde{U} \\ -\tilde{N} & \tilde{M} \end{bmatrix}\begin{bmatrix} M & U \\ N & V \end{bmatrix} \tag{2.9}$$

2.3 All Stabilising Controllers

One of the main ideas behind reformulating the plant and controller using the coprime factorisation is to be able to describe all stabilising controllers. Given a stabilising controller K for the plant G it is possible to describe all stabilising controllers $K(Q)$ as in Eq. (2.10).

$$K(Q) = (U + MQ)(V + NQ)^{-1} = (\tilde{U} + Q\tilde{M})^{-1}(\tilde{V} + Q\tilde{N}) \quad Q \in RH_\infty \tag{2.10}$$

Using Eq. (2.10) it is possible to design any controller that stabilises the plant G by choosing an arbitrary system Q that is stable. A block diagram of the controller setup is shown in Figure 2.1 using the Left coprime factorisation (LCF).

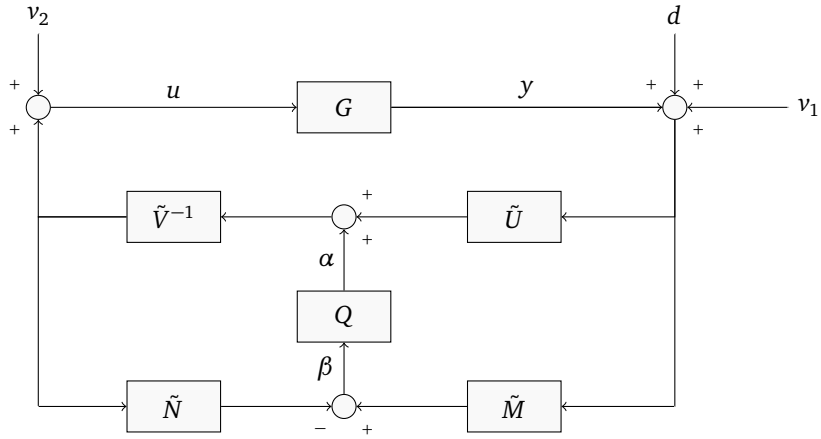

Figure 2.1: Representation of a YJKB parametrised controller for generation of signals for identification.

Any linear controller can be reformulated into the control scheme showed in Figure 2.1. The signals v_1 and v_2 represent possible external signals, whereas the signal d denotes the noise. It is possible to write any linear controller using the Right coprime factorisation (RCF) as well. This controller scheme based on the RCF is, however, rarely used as it does not have a direct translation to the observer residual signal. The closed loop system can be represented in a more familiar way as shown in Figure 2.2.

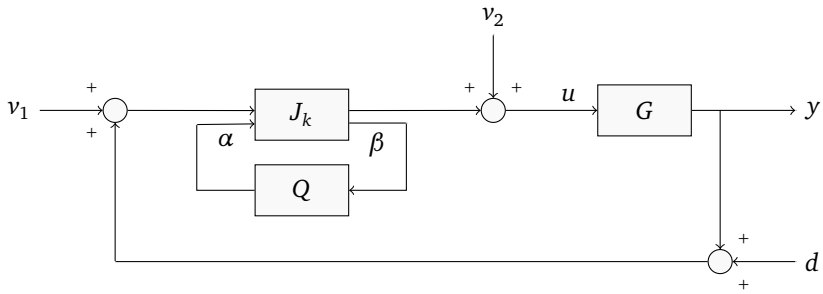

Figure 2.2: Block diagram of the closed loop system using the augmented controller.

Here J_k, together with the system Q, is a compact representation of Eq. (2.10). The augmented controller J_k is given in Eq. (2.11) using the coprime representation of the controller and plant.

$$J_k = \begin{bmatrix} UV^{-1} & \tilde{V}^{-1} \\ V^{-1} & -V^{-1}N \end{bmatrix} \tag{2.11}$$

From Figure 2.2 and Eq. (2.11) it is clear that the controller simplify to the nominal controller if Q is 0. With Q disconnected, the augmented controller description can be utilized for active fault diagnosis.

2.4 All Stabilised Plants

It has been shown how to describe all controllers that stabilise a nominal plant. However, often full knowledge of the controller is possible whereas it is not for the plant. It is here shown how, given a stabilising controller, all plants that will be stabilised can be found. Given a nominal controller K stabilising the nominal plant G, it is possible to describe all stabilised plants $G(S)$ using Eq. (2.12).

$$G(S) = (N + VS)(M + US)^{-1} = (\tilde{M} + S\tilde{U})^{-1}(\tilde{N} + S\tilde{V}) \quad S \in RH_\infty \tag{2.12}$$

Here S is a stable system describing the deficiencies between the nominal plant and the real plant. Using Eq. (2.12) has great potential due to the possible a priori knowledge when designing controllers. For a controller stabilising the plant to be identified, the search space is considerably reduced when identifying S instead of $G(S)$. This is because S has to be a stable system, and all unstable systems are therefore not needed to be considered. A block diagram of the closed loop system scheme is shown in Figure 2.3 when the plant is described using Eq. (2.12).

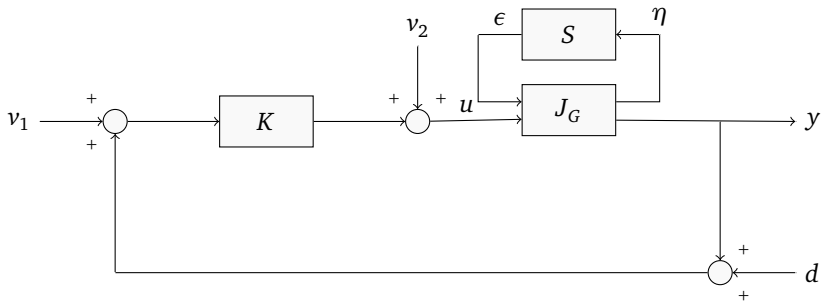

Figure 2.3: Block diagram of the closed loop system with the nominal stabilising controller and the augmented plant.

Here J_G together with S is a compact matrix representation of the real system based on Eq. (2.12). The augmented system J_G is given in Eq. (2.13).

$$J_G = \begin{bmatrix} -M^{-1}U & M^{-1} \\ \tilde{M}^{-1} & NM^{-1} \end{bmatrix} \tag{2.13}$$

The closed loop scheme simplify to a closed loop representation of the nominal controller and plant if S is 0, in which case the nominal plant is equal to the true plant.

By using this knowledge it is possible to indirectly identify the plant by identifying the Youla deviation system S.

2.5 Relationship between S and Q

So far the chapter has dealt with what the YJBK parametrisation is and how to derive it using coprime factorisation. This section is instead focussed on giving the reader some motivation for using the framework. It is not possible to directly obtain the signals η and ϵ due to the location inside the plant. However, in many applications determining S is of interest. On the other hand it is possible to measure β, and impose α directly due to their location inside the controller. The control signals α and β are therefore more convenient to use than the signals η and ϵ. A relationship between S and Q was shown in [43].

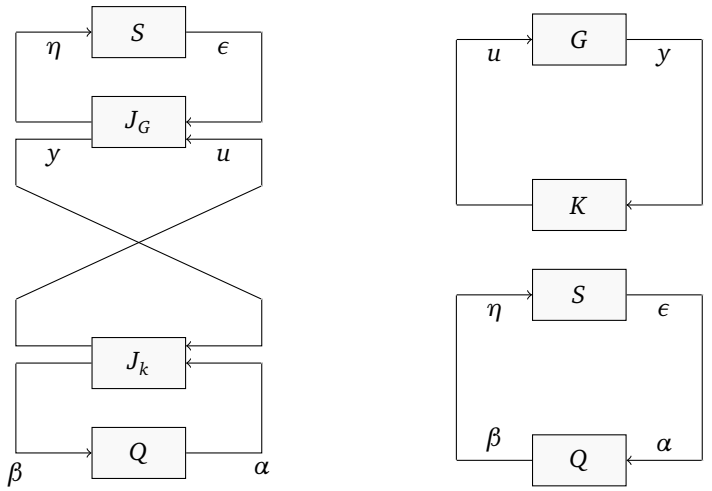

Figure 2.4: Block diagram of the relationship between S and Q

It is shown in Figure 2.4 how to divide the closed loop system into what is a priori known, illustrated by the top right block diagram and what is a priori undetermined, illustrated by the bottom right block diagram. The controller scheme makes it possible to either design Q to adapt the controller to system changes or identify unknown dynamics through S. Using Figure 2.4 it is possible to show that Eq. (2.14) holds.

$$I = J_G \star J_K \tag{2.14}$$

This in turn implies a relationship between the signals in the controller and plant as shown in Eq. (2.15).

$$\begin{bmatrix} \alpha \\ \beta \end{bmatrix} = \begin{bmatrix} I & 0 \\ 0 & I \end{bmatrix} \begin{bmatrix} \eta \\ \epsilon \end{bmatrix} \tag{2.15}$$

The relationship found in Eq. (2.15) is used to gain easier access to problems related to the system S and thus the plant.

2.6 Parametrisation in S

The previous sections have dealt with the relationship between the parametrised plant and controller. In this section, focus is instead on how to obtain a physical understanding of S in relation to possible parametric deviations. In (2.16) a nominal plant has been augmented with two additional signals z and w to accommodate for these parametric deviations.

$$\begin{bmatrix} z \\ y \end{bmatrix} = G_{aug} \begin{bmatrix} w \\ u \end{bmatrix} = \begin{bmatrix} G_{zw} & G_{zu} \\ G_{yw} & G_{yu} \end{bmatrix} \begin{bmatrix} w \\ u \end{bmatrix} \tag{2.16}$$

The signals w and z are the error signals describing the deviation between the nominal plant G_{yu} and the true plant $G(S)$. The error signals are related to the parametric deviations θ as given in Eq. (2.17).

$$w = \theta z = diag(\theta_i) z \tag{2.17}$$

Here $diag(\theta_i)$ denotes a diagonal matrix where each parametric deviation is a diagonal element. A block diagram of the relationship is shown in Figure 2.5.

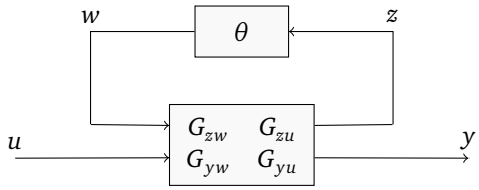

Figure 2.5: Block diagram of the plant augmented G_{aug} with the parametric deviations θ.

The plant is thus possible to describe, using the known augmented plant G_{aug} and the parametric deviation diagonal matrix θ, as a LFT as shown in Figure 2.5. It is shown in [44] that such a LFT description can be expressed as Eq. (2.18).

$$G(\theta) = G_{yu} + G_{yw}\theta(I - G_{zw}\theta)^{-1}G_{zu} = \mathscr{F}_u(G_{aug}, \theta) \tag{2.18}$$

Equivalent to Eq. (2.18) which expresses the plant based on the nominal plant and parametric deviations, it is possible to express S as a function of the parametric deviations and augmented plant as shown in Eq. (2.19).

$$S(\theta) = \tilde{M}G_{yw}\theta(I - (G_{zw} + G_{zu}U\tilde{M}G_{yw})\theta)^{-1}G_{zu}M \tag{2.19}$$

This relationship between the parametric deviation and the system S makes it possible to obtain knowledge about the structure of S given different possible parametric deviations. There are several important points to gain from comparing $G(\theta)$ from Eq. (2.18) with $S(\theta)$ from Eq. (2.19). Firstly it is noted that while $G(\theta)$ simplify to G_{yu} when the parametric deviation goes to 0, $S(\theta)$ simplify to 0, stated in Eq. (2.20).

$$S = 0|_{\theta=0} \tag{2.20}$$

Secondly, the impact of the controller is integrated in $S(\theta)$ which is not the case for $G(\theta)$. This makes an analysis of the impact of the parametric deviation easier when using $S(\theta)$ than when using $G(\theta)$. By combining Figure 2.4 and Figure 2.5, a fault detector is designed as shown on Figure 2.6 based on the fault signature system S.

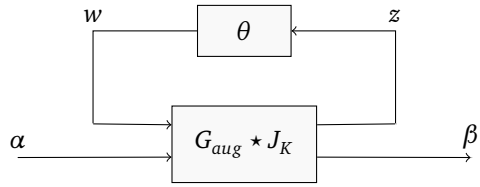

Figure 2.6: Block diagram of the residual generation based on the impact of the parametric faults θ on S. Here $G_{aug} \star J_K$ denotes the star product between the two systems G_{aug} and J_K.

Based on the relationship between the controller and the plant, it is possible to extract the control signals shown on Figure 2.6 for active fault diagnosis.

2.7 Coprime Factorisation of Controllers

It has been shown possible to represent all plants stabilised by a nominal controller and all controllers stabilising a nominal plant, using an YJBK parametrisation. In order to be able to design such a scheme we must be able to derive the coprime factorisation given different controller design schemes. The coprime factorisations have been derived in [43] and [45]. A state space description of the nominal plant is given in Eq. (2.21).

$$G = \left(\begin{array}{c|c} A & B \\ \hline C & 0 \end{array}\right) \tag{2.21}$$

The most simple controller used is a standard proportional controller. Such a controller is presented in state space form in Eq. (2.22).

$$K = \left(\begin{array}{c|c} 0 & 0 \\ \hline 0 & P \end{array}\right) \tag{2.22}$$

Here P is the proportional gain and can be either a scalar or matrix. With the proportional gain defined as in Eq. (2.22), the RCF of controller and plant is given by Eq. (2.23) and the LCF is given in Eq. (2.24).

$$\begin{bmatrix} M & U \\ N & V \end{bmatrix} = \left(\begin{array}{c|cc} A+BF & B & 0 \\ \hline F & I & P \\ C & 0 & I \end{array}\right) \tag{2.23}$$

$$\begin{bmatrix} \tilde{V} & -\tilde{U} \\ -\tilde{N} & \tilde{M} \end{bmatrix} = \left(\begin{array}{c|cc} A+BPC & -B & BP \\ \hline F-PC & I & -P \\ C & 0 & I \end{array} \right) \tag{2.24}$$

Here F is a fictitious gain which satisfy that all poles of $A+BF$ are contained in the stable left half plane. With the coprime factorisation it is possible to implement the controller using the controller scheme presented in Figure 2.1 with the system Q disconnected. Another common control design is the full order observer. A state space description of the full order observer is given in Eq. (2.25) where the direct gain is 0.

$$K = \left(\begin{array}{c|c} A+BF+LC & -L \\ \hline F & 0 \end{array} \right) \tag{2.25}$$

For a controller scheme based on the full order observer, the RCF is given in Eq. (2.26) and the LCF is given in Eq. (2.27).

$$\begin{bmatrix} M & U \\ N & V \end{bmatrix} = \left(\begin{array}{c|cc} A+BF & B & -L \\ \hline F & I & 0 \\ C & 0 & I \end{array} \right) \tag{2.26}$$

$$\begin{bmatrix} \tilde{V} & -\tilde{U} \\ -\tilde{N} & \tilde{M} \end{bmatrix} = \left(\begin{array}{c|cc} A+LC & -B & L \\ \hline F & I & 0 \\ C & 0 & I \end{array} \right) \tag{2.27}$$

Here the observer gain is denoted L and state feedback gain is denoted F. It is possible to use the same implementation based on the scheme presented in Figure 2.1. If the interest lies in the signals denoted α and β it was shown in [46] how to obtain these signals from the classic full order observer scheme. A block diagram of the full order observer is shown in Figure 2.7 where the signals α and β are added.

It is seen in Figure 2.7 that the signal β is equivalent with the innovation signal. This link between the signal β and the innovation signal is useful for design of controllers.

Coprime Factorisation given a Stable Controller

Previously, methods using the state space form of the controller and plant to generate a coprime factorisation have been presented. The solutions presented so far have all relied on a stabilising observer gain, fictitious or not. Here, instead is given a method easily implemented when working with transfer functions and standard linear controllers. The factorisation method was first presented in [47]. Given a stable linear controller K, it is possible to write the 8 systems as in Eq. (2.28) to Eq. (2.35).

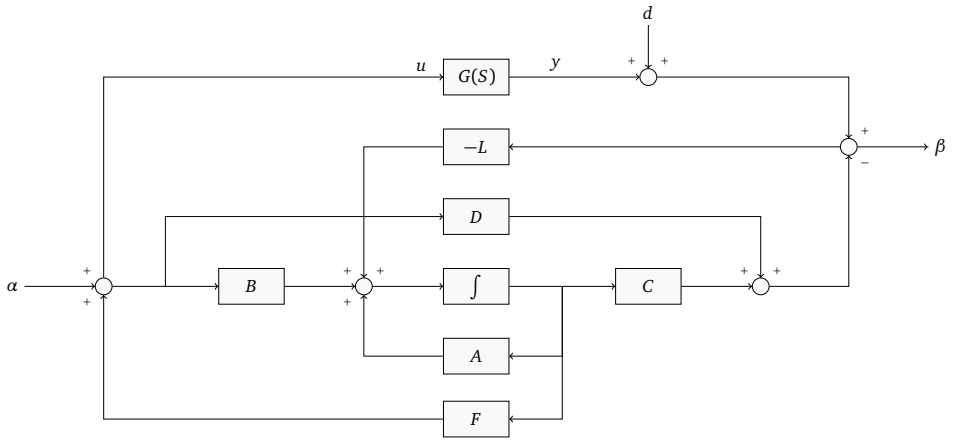

Figure 2.7: Block diagram of the full order observer scheme. The signals α and β have been added for comparison with Figure 2.1

$$M = (I + KG)^{-1} \tag{2.28}$$
$$N = G(I + KG)^{-1} \tag{2.29}$$
$$V = I \tag{2.30}$$
$$U = K \tag{2.31}$$
$$\tilde{M} = (I + GK)^{-1} \tag{2.32}$$
$$\tilde{N} = (I + GK)^{-1}G \tag{2.33}$$
$$\tilde{V} = I \tag{2.34}$$
$$\tilde{U} = K \tag{2.35}$$

Here, G is the nominal plant, and I is an identity matrix of appropriate size. The factorisation method is useful for when a state space description of the nominal plant and controller is not given.

2.8 Perspective

In this chapter, the YJBK-parametrisation using a coprime factorisation of plant and controller was presented. The relationship between signals in the plant and controller were established. Furthermore, an interpretation of S given parametric deviations from the nominal plant was discussed. These relationships have been taken advantage of for the identification and fault diagnosis methods to be presented further on in this thesis. Furthermore coprime factorisations of plant and controller were given for different controller schemes and for state space models, as well as systems described using transfer functions. The basis for the identification and fault diagnosis methods presented in this thesis is thus outlined in this chapter. In addition, the tools for how to implement the methods are given using Eq. (2.23), (2.24), (2.26) and (2.27) and the framework was shown in Figure 2.1.

Chapter 3

Experimental Test Rig

Throughout this thesis, several theoretical contributions are presented on identification and fault diagnosis. This theoretical work is backed up by a benchmark study to validate the given assumptions and further prove the validity of the methods presented. The experimental work is conducted using an active gas bearing experimental test rig. The design of the test rig was presented in [48] and modelling of the active gas bearing was presented in [49], from a mechanical point of view. Lastly, a model of appropriate order for control purposes was introduced in [10].

3.1 Experimental Test Rig

The experimental test rig consists of a rigid shaft held in position by a ball bearing and an active gas bearing. A disc is attached at the end of the rigid shaft and has its vertical and horizontal positions measured using position sensors. A picture of the whole system is shown on Figure 3.1.

While the ball bearing is passive, the gas bearing is actively controlled using 4 piezo electric actuators. The gas bearing is known as an active gas bearing due to the possibility to control the inflow of air. On Figure 3.1 the active gas bearing can be seen with its 4 piezo electric actuators denoted b and c which controls the vertical and horizontal flow of air into the bearing. The actuators have been lumped together such that the two vertically oriented actuators denoted **b** are controlled as one input, and the two horizontally oriented actuators denoted **c** are controlled as a single input as well. By grouping the actuators together it is possible to have one input controlling the vertical position, and one input controlling the horizontal position. By controlling the inflow of air into the gas bearing, it is also possible to increase the damping inside the bearing. A schematic of the active gas bearing is shown on Figure 3.2a.

Figure 3.2 is a simple schematic of the active gas bearing. In Figure 3.2 a cross sectional view of the gas bearing is shown with the actuators and valve inlets. The air is pumped into the gas bearing through the tubes denoted a and the flow is actively controlled using the piezo electric actuators denoted b and c. A schematic of how the actuator functions is shown in Figure 3.2b. The flow of air into the gas bearing is controlled by moving the actuator towards and away from the shaft, located at the middle of the bearing. For simplicity, the two actuators positioned in the vertical

Figure 3.1: Picture of the experimental test rig, used for experimental validation of the methods introduced. The different parts of the test rig is as follows: **b** are the piezo actuators pumping air into the controllable gas bearing in the vertical direction, **c** are the piezo actuators pumping air into the controllable gas bearing in the horizontal direction, **d** is the flexible shaft, **e** is the sensor measuring the vertical displacement of the disc, **f** is the disc and **g** is the sensor measuring the horizontal displacement of the disc.

direction have been lumped together as one. Likewise, the two actuators positioned in the horizontal direction have been lumped together as one actuator. It is thus possible to control the vertical and horizontal position of the shaft using the piezo electric actuators.

Objective

Besides the gas bearing, the test rig consists of a shaft with a disc attached in one end. The disc is denoted f on Figure 3.1. The system has two distance sensors attached, denoted e and g on Figure 3.1. The sensors are placed orthogonal of each other so one measures the position of the disc in the vertical direction while the other measures the position in the horizontal direction. A schematic of the full test rig is shown in Figure

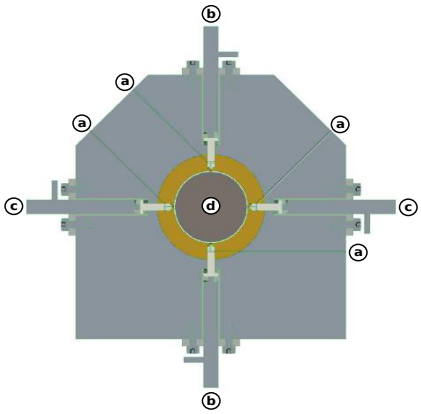

(a) A cross section schematic of the active gas bearing. The air is pumped in through the 4 tubes denoted by **a**. The piezo actuators denoted **c** open and close the flow of air from the horizontal direction. Likewise, the piezo actuators denoted **c** open and close the flow of air towards the shaft **d** in the vertical direction.

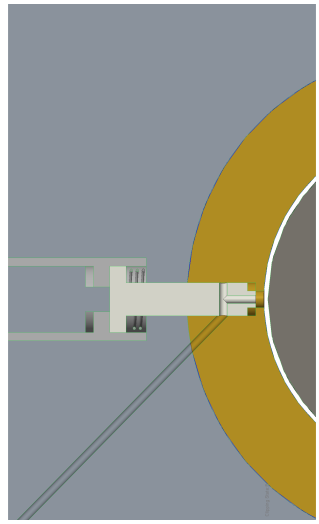

(b) Schematic of the piezo electric actuator used to inject air into the bearing. The actuator is able to change position horizontally such that the gap increases or decreases between the air tube and the small tube inside the actuator.

Figure 3.2: Schematic of the active gas bearing seen on Figure 3.1

3.3.

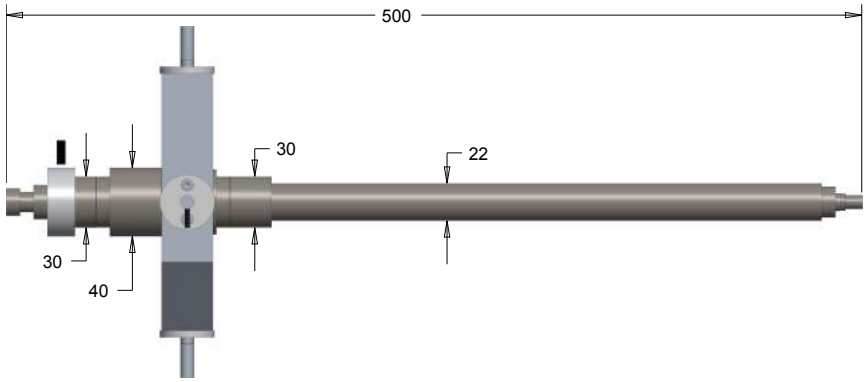

Figure 3.3: Side view schematic of the test rig with measurements given in mm.

It is the goal of the control effort to keep the disc in a fixed position by injecting air into the gas bearing in the horizontal and vertical directions. The movement of the disc is limited to 10 μm in each direction in order to prevent the test rig from getting damaged. Control schemes are designed with the primary goal of increasing the overall

damping of the system. Furthermore, the disc attached to the shaft contributes to a mass imbalance when the shaft is rotating due to imperfections. Such a mass unbalance is equivalent to a sinusoidal disturbance with the same frequency as the rotational speed of the shaft. The control design thus needs to compensate for the mass imbalance in the frequency range that the system has when it is rotating.

Model

It is imperative to have an adequate model of the plant for feedback control design. Models to describe the active gas bearing have been based on two different modelling methods. A FEM was developed in [7] which was able to describe the dynamics of the plant. The model gave a good physical understanding of the plant. This was however obtained at the cost of a model containing 144 states. Such a high order model is inconvenient for controller design, which gets especially clear for observer design. The first attempt at a low order model was presented in [12]. The FEM was based on a mass springer damper model of the movement of the disc when a voltage was applied to the piezo electric actuator. The mass spring damper equation is shown in Eq. (3.1).

$$\ddot{l} - D\dot{l} - Kl = Bu \tag{3.1}$$

Here l is a vector with the position displacement in the horizontal and vertical direction, K is the specific stiffness matrix and is in $[\frac{N}{kg\ \mu m}]$, D is the specific damping matrix expressed in $[\frac{Ns}{kg\ \mu m}]$ and B is the actuator gain matrix in $[\frac{N}{kg\ V}]$. Based on Eq. (3.1) a state vector is defined in Eq. (3.2)

$$x = \begin{bmatrix} l \\ \dot{l} \\ u \end{bmatrix} \tag{3.2}$$

The model developed in [12] consist of the dynamics of the gas bearing given by Eq. (3.3).

$$G_{rb} = \left[\begin{array}{ccc|c} 0 & I & 0 & 0 \\ K & D & 2B\tau & -B \\ 0 & 0 & -\tau & I \\ \hline I & 0 & 0 & 0 \end{array}\right] \tag{3.3}$$

The model given in Eq. (3.3) consist of 6 states. Furthermore, the actuators are modelled as 4'th order system given in Eq. (3.4)

$$G_{act} = \begin{bmatrix} G_{a,x} & 0 \\ 0 & G_{a,y} \end{bmatrix} \tag{3.4}$$

Here $G_{a,x}$ describes the dynamics of the horizontal actuator, and $G_{a,y}$ describes the dynamics of the vertical actuator. Each of the actuators are modelled as a second order system as shown in Eq. (3.5)

$$G_{a,j} = \frac{\kappa_{a,j}}{(\frac{1}{p_{1,j}\ s+1})(\frac{1}{p_{2,j}\ s+1})} \tag{3.5}$$

Here κ is the actuator gains, and $p_{1,j}$ and $p_{2,j}$ are the two poles of the actuator transfer function. The two systems G_{act} and G_{rb} are lumped together in series to represent the full dynamics of the test rig as shown in Eq. (3.6).

$$G_{bearing} = G_{act} G_{rb} \tag{3.6}$$

Because G_{rb} contains 6 states, and G_{act} contains 4 states, the plant $G_{bearing}$ consists of 10 states. The full system using the model from Eq. (3.6) is shown in Figure 3.4. Here a controller is added to illustrate the signals used for the model and for control of the active gas bearing.

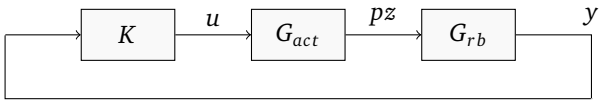

Figure 3.4: Block diagram of the full system using the gas bearing model given in Eq. (3.6). The input to the system u is a voltage (in volts). The signal pz between G_{act} and G_{rb} is the opening position of the piezoelectric actuators. Lastly, the output y is the displacement of the disc given in micrometers.

A new first principle model was developed in [13] which only used 6 states instead of 10 to describe the plant dynamics. The physical understanding of the plant was somewhat sacrificed to obtain such a low order model. The model has proven advantageous for control design purposes due to it being a linear relatively low order model. However, the model parameters depend on the gas pressure of the air flowing into the piezo electric actuators and the rotational speed of the disc. The papers presented in this thesis uses the model presented in [13] as state of the art using a fixed rotational speed and air pressure. With air pressure and rotational speed fixed, it is possible to treat the model as a simple Linear Time Invariant (LTI) model.

With the state vector defined in Eq. (3.2) a state space description of the plant is given in Eq. (3.7)

$$\mathbf{G_{bearing}} = \left[\begin{array}{ccc|c} 0 & I & 0 & 0 \\ K & D & B & 0 \\ 0 & 0 & -P & P \\ \hline I & 0 & 0 & 0 \end{array}\right] \tag{3.7}$$

Here K is the stiffness matrix, D is the damping matrix and B is the input gain matrix. The matrix is designed as a diagonal matrix with each element h_j defined by Eq. (3.8) as a first order low pass filter.

$$h_j(s) = \frac{p_j}{s + p_j} \qquad j \in \{1, 2\} \tag{3.8}$$

The system h_j describes the actuator dynamics and was the last extension to the model described in [50]. The parameters of the matrices are identified using greybox PEM identification. An example of identified parameters of the system, when it is not rotating, using the 6'th order model are shown in Eq. (3.9) to Eq. (3.12).

$$D = \begin{bmatrix} -224.9 & 3.97 \\ 9.12 & -267.7 \end{bmatrix} \tag{3.9}$$

$$K = \begin{bmatrix} -1.869 \cdot 10^6 & -8577 \\ -9510 & -1.737 \cdot 10^6 \end{bmatrix} \tag{3.10}$$

$$B = \begin{bmatrix} -6.126 \cdot 10^6 & 3.154 \cdot 10^5 \\ -1.571 \cdot 10^5 & -4.516 \cdot 10^6 \end{bmatrix} \tag{3.11}$$

$$P = \begin{bmatrix} 989 & 0 \\ 0 & 942.5 \end{bmatrix} \tag{3.12}$$

Implementation

Besides the active gas bearing, a desktop computer is associated with the test rig. All controller schemes are implemented on the computer using real time software through the simulink interface. A picture of the computer with the real time software is shown in Figure 3.5.

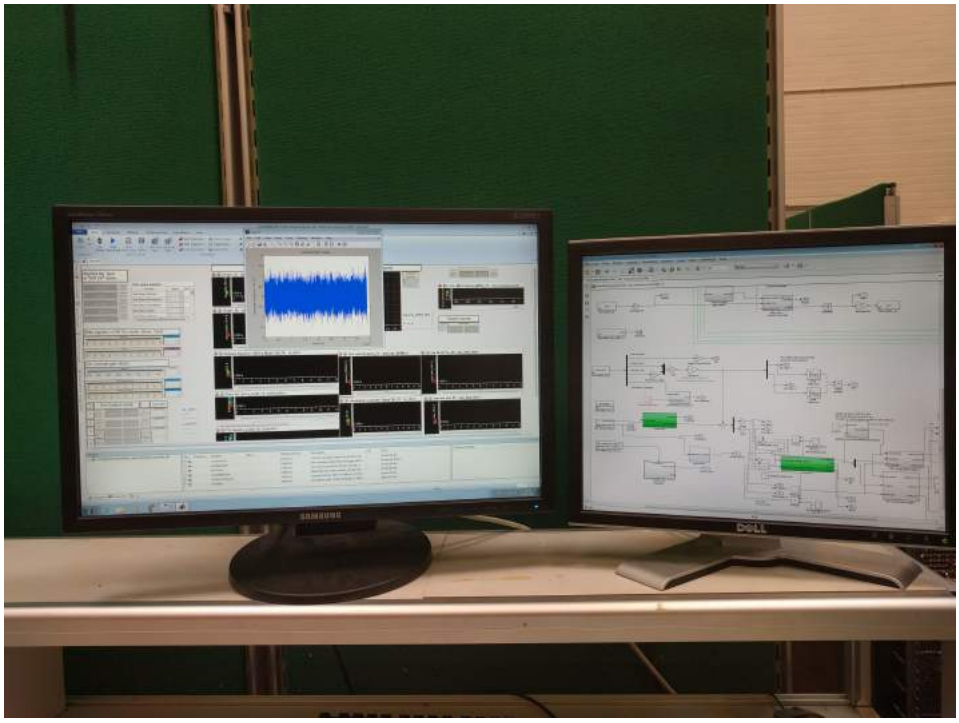

Figure 3.5: Picture of the computer with the real time software open. On the right screen is the simulink system shown while on the left screen dSpace software is seen.

The control architecture is implemented using matlab simulink as shown on the right computer screen in Figure 3.5. The program dSpace, shown on the left screen in Figure 3.5, is used for online interaction with the actuators and sensors of the experimental test rig. The experimental test rig uses a sampling speed of 0.2 ms and it is possible to acquire data sequences of up to 14 seconds. Real time is ensured by the software, and a warning will be given if it is not possible to comply with the sampling speed.

Chapter 4

System Identification

In this chapter, closed loop identification is discussed and methods used for identification of stable and unstable plants are presented. The chapter is organised with a short introduction into the issue of identifying systems as part of a closed loop. An initial solution is presented for identifying parameters where the structure of the model is perfectly known beforehand. Using this approach, identifications results for a simulated AMB are given. The Hansen scheme method is presented and a modification is proposed to the process. Lastly, the results using the modified Hansen scheme on an active gas bearing are presented, and a summary of the contributions presented in this chapter is given.

The main points used from Chapter 2 are summarised in Figure 4.1 which illustrate the scenarios investigated in this chapter for identification purposes.

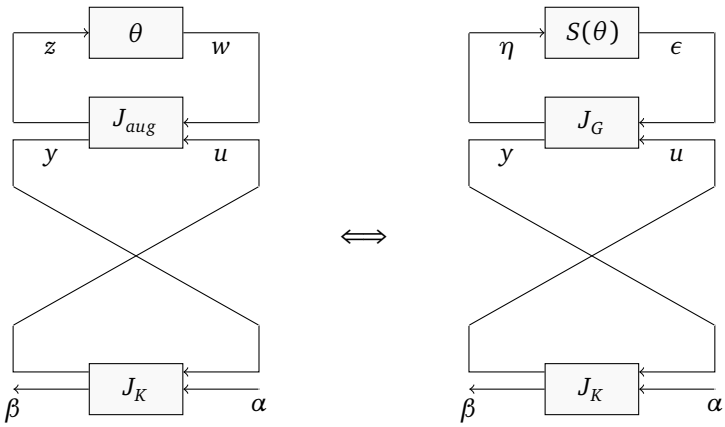

Figure 4.1: On the left, a block diagram is shown representing the relationship between the augmented controller signals (α,β) and the parametric uncertainties θ. On the right we see a block representation of the relationship between the augmented controller signals (α,β) and the Youla deviation system $S(\theta)$.

On the left it is illustrated how to find the parametric uncertainties directly using the signals from the augmented controller J_K. On the right it is illustrated how to identify

the parametric uncertainties through S by the use of the signals from the augmented controller J_K.

4.1 Closed Loop Identification

It is often the case that it is not possible to obtain identification data from open loop experiments. There can be several different reasons for this such as safety issues, cost of taking the system offline, or it might simply be an open loop unstable system. Whichever the reason, data is only possible to obtain while a feedback loop is active.

The subject of closed loop identification has been of great interest for many of the most influential researchers within identification. Indeed, two of the most recognised books within the field [14, 15] have both devoted a considerable space to cover the issue. In order to discuss closed loop systems it is important to define what is meant by the term. In this thesis, closed loop systems are defined as shown in Figure 4.2.

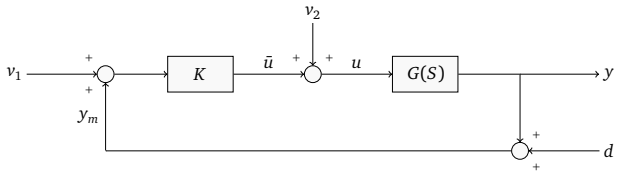

Figure 4.2: Block diagram of a plant $G(S)$ as part of a closed loop system with the controller K. The signal d is unknown noise while v_1 and v_2 are possible external input signals.

Here, $G(S)$ is the plant to be identified, K is the controller, d is the unknown noise signal, and v_1 and v_2 are possible known external signals. For such a system the goal is to identify the plant $G(S)$ and the most simple way is using Eq. (4.1) which can be rewritten as in Eq. (4.2) based on the spectral density of the signals.

$$y_m = G(S)u + d \tag{4.1}$$

$$\Phi_{y_m u} = G(S)\Phi_u + \Phi_d \tag{4.2}$$

Here, y_m, u and d are data vectors of the same length, $G(S)$ is time domain system, $\hat{G}$ is the estimated system and Φ denotes the spectral density. The system is usually identified using the input and measurement signal as shown in Eq. (4.3). For the case where the noise and input are uncorrelated using a sufficient amount of data, Eq. (4.3) will simplify to Eq. (4.4).

$$\hat{G} = \frac{\Phi_{y_m u}}{\Phi_u} = G(S) + \frac{\Phi_d}{\Phi_u} \tag{4.3}$$

$$\lim_{t\to\infty} \frac{\Phi_{y_m u}}{\Phi_u} = G(S) \tag{4.4}$$

Eq. (4.4) is however, based on the assumption that the noise d and input u are not correlated which is clearly not the case when the feedback loop is active. For this

example, inspired by [15], we use v_2 as the external excitation signal. First the two signals y_m and u have to be found based on the external signals v_2 and d.

$$\Phi_{y_m} = \frac{1}{1-G(S)K}(G(S)\Phi_{v_2} + \Phi_d) \tag{4.5}$$

$$\Phi_u = \frac{1}{1-G(S)K}(\Phi_{v_2} + K\Phi_d) \tag{4.6}$$

Again, the identification is based on the correlation of the input and output signals as shown in Eq. (4.7).

$$\frac{\Phi_{y_m}}{\Phi_u} = \frac{G(S)\Phi_{v_2} + \Phi_d}{\Phi_{v_2} + K\Phi_d} \tag{4.7}$$

It is easy to see that if the excitation signal v_1 is dominant relative to the noise signal d Eq. (4.7) simplify to Eq. (4.8).

$$\lim_{\frac{\|v_2\|_2}{\|d\|_2}\to\infty} \frac{\Phi_{y_m}}{\Phi_u} = G(S) \tag{4.8}$$

Here, the identification succeeds and it is possible to identify the plant $G(S)$ using the input and output signal. However, the issue arises when the noise becomes significant. Indeed, if the noise is dominant relative to the excitation signal, Eq. (4.9) becomes true.

$$\lim_{\frac{\|v_2\|_2}{\|d\|_2}\to 0} \frac{\Phi_{y_m}}{\Phi_u} = \frac{1}{K} \tag{4.9}$$

Suddenly $\frac{1}{K}$ is identified using the signals u and y_m for identification. This fact comes from the correlation between the input signal and the unknown noise. The above example is shown for SISO systems, the inclusion of MIMO systems is rather straightforward. It was however chosen with this example, to strive for transparency to introduce the reader to the issues associated with identification of closed loop systems. Furthermore, the problem showed above is related to identification using spectral methods. A whole set of possible fallacies when conducting closed loop identification using different methods was discussed in [14]. Here, both PEM and subspace identification methods are mentioned, as well as the spectral methods. In this work the possible fallacies have tried to be avoided by decorrelation of the input signal, used for the identification process, and the noise.

4.2 Identification of Parametric Uncertain Parameters

In this section a method is presented as to how to identify specific parameters for an a priori known model structure. Given a diagonal matrix θ, containing all the parameter uncertainties, it is possible to state the real plant as an LFT of the nominal plant and the uncertainty. The LFT can be shown as a system description as on Figure 4.3.

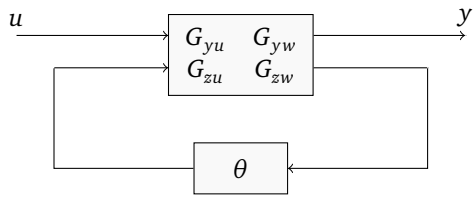

Figure 4.3: Lower lft description of $G(\theta)$.

Equivalently the gain from input (u) to output (y) is given in Eq. (4.10) for uncertainties θ.

$$\mathscr{F}_l = G_{yu} + G_{yw}\theta(1 - G_{zw}\theta)^{-1}G_{zu} \tag{4.10}$$

This can be written in a slightly more compact form as given in Eq. (4.11).

$$G(\theta) = \mathscr{F}_l\left(\begin{bmatrix} G_{yu} & G_{yw} \\ G_{zu} & G_{zw} \end{bmatrix}, \theta\right) \tag{4.11}$$

Methods for how to select G_{yw} G_{zw} and G_{zu} can be found in [44], and depends on the type of the specific parametric uncertainty. In order to identify parameters for a plant, the parameter uncertainties θ have been defined as in Eq. (4.12) throughout this analysis.

$$p(\theta_i) = p(0)(1 + \theta_i) \tag{4.12}$$

Here, $p(0)$ is the initial estimate of the parameter, and θ_i is the uncertainty and is the diagonal element i of the diagonal matrix θ containing all the uncertainties. Uncertainties are thus treated as relative parameter changes.

Instead of defining the uncertainties as part of the full system, it is possible to use the dual Youla parametrisation to define the uncertainties based on the deviation between the real plant and initial model. Hence, the uncertainties need to be formulated as a function of S. With the uncertainties given as defined in Eq. (4.12), S can be formulated as a function depending on the parameter uncertainties θ as shown in Eq. (4.13).

$$S(\theta) = \mathscr{F}_l\left(\begin{bmatrix} 0 & \tilde{M}G_{yw} \\ G_{zu}M & G_{zw} + G_{zu}U\tilde{M}G_{yw} \end{bmatrix}, \theta\right) \tag{4.13}$$

It is possible to write the lower LFT as a transfer function shown in Eq. (4.14).

$$S(\theta) = \tilde{M}G_{yw}\theta(I - (G_{zw} + G_{zu}U\tilde{M}G_{yw})\theta)^{-1}G_{zu}M \tag{4.14}$$

Determining $S(\theta)$ in Eq. (4.14) is a non-linear problem. In order to solve the problem, an YJKB parametrised controller as shown in Figure 4.4 is used with Q set to

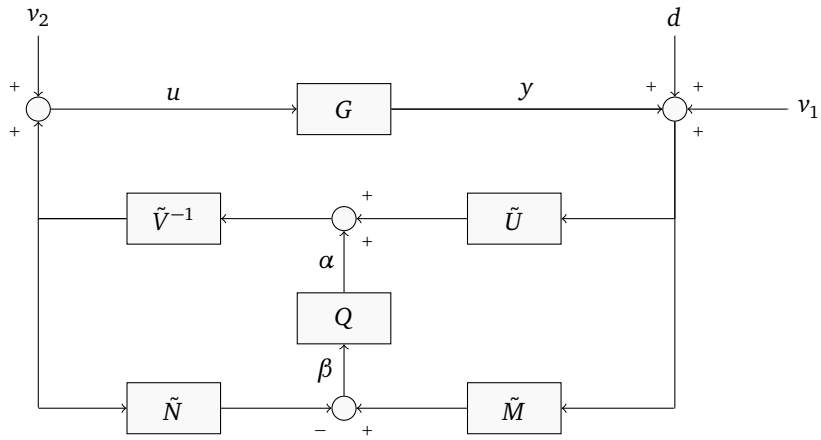

Figure 4.4: Representation of a YJKB parametrised controller for the generation of signals for identification.

0. It is then possible to inject a signal α into the system whereby the signal β can be measured.

The goal is thus to be able to isolate the signal going from α to β, from the disturbance signal as shown in Eq. (4.15). The signal α, is for this purpose chosen to be a sinusoidal wave defined in Eq. (4.16).

$$\beta = S(\theta)\alpha + \bar{d} \tag{4.15}$$

$$\alpha = Asin(\omega_0 t) \tag{4.16}$$

For simplicity Eq. (4.13) can be written as Eq. (4.17).

$$S(\theta) = S_{12}\theta(I - S_{22}\theta)^{-1}S_{21} \tag{4.17}$$

Here, S_{12}, S_{21} and S_{22} are all a priori known systems. In order to identify the uncertainty parameters a cost function is used. The cost function is given in Eq. (4.18), and shaped to make it an approximately quadratic problem.

$$J(\theta) = \frac{1}{2}\|\beta(t) - S(\theta)\alpha(t)\|_1^2 \tag{4.18}$$

The 1-norm is used here, but other norms might be convenient due to a priori knowledge. A visualisation of a possible cost plane is shown in Figure 4.5 given two possible uncertainties.

The goal is to minimise the cost function $J(\theta)$. The minimum of a cost function as shown in Eq. (4.18) can be found using non-linear programming methods such as the one presented in [51].

The method was used to show it possible to identify specific parameters on an AMB which had a high uncertainty from the construction phase. A FEM, of a shaft kept held in a constant position using two AMB's, was developed. It was shown possible to reduce the order of the model while isolating specific parameters at the same time.

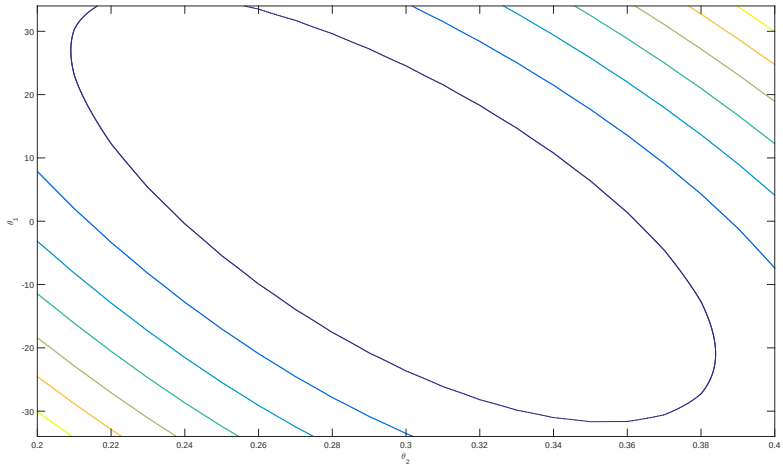

Figure 4.5: Contour plot of $J(\theta)$ given two parametric uncertainties.

4.3 Hansen Scheme

In the previous section a simple method was given for how to determine specific parameters in a predetermined model framework for closed loop systems. The complexity of the method explodes when the amount of uncertain parameters increases. In this section an introduction is given to a method developed in [16] in order to reformulate the closed loop identification problem into an open loop problem. The formulation was further simplified in [17] where a block diagram as shown in Figure 4.6 was presented.

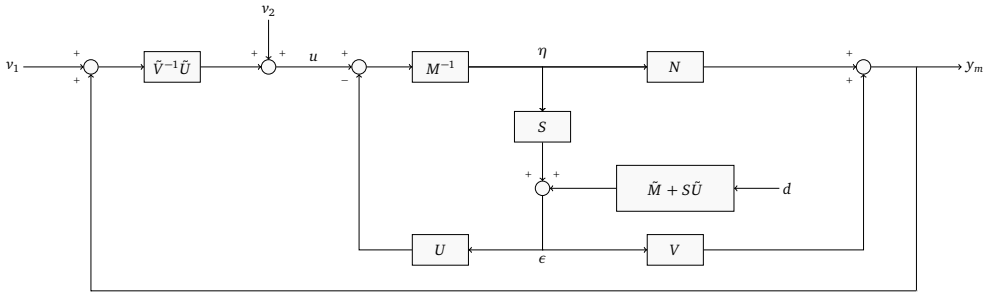

Figure 4.6: Block diagram of the Hansen Scheme as presented in [17].

The idea with the Hansen scheme, as presented in Figure 4.6, is to identify the unknown system S using the signals η and ϵ instead of identifying the plant G using the signals u and y. As explained in Section 4.1, the issue with identification of a plant subject to a feedback loop arises from the correlation between the input and noise signals. However, where u is correlated with d the signal η is not. It was shown in [16] that η can be solely expressed using v_1 and v_2 as in Eq. (4.19).

$$\eta = \tilde{U}v_1 + \tilde{V}v_2 \tag{4.19}$$

It is not obvious from Figure 4.6 that Eq. (4.19) is true. A proof is given in Eq. (4.20) to Eq. (4.25). The proof is based on the bezout identity presented in Chapter 2.

$$u = (M + US)\eta + U(\tilde{M} + S\tilde{U})d \tag{4.20}$$
$$y_m = (N + VS)\eta + V(\tilde{M} + S\tilde{U})d \tag{4.21}$$
$$\tilde{V}u - \tilde{V}(M + US)\eta = \tilde{U}y_m - \tilde{U}(N + VS)\eta \tag{4.22}$$
$$\tilde{V}(\tilde{V}^{-1}U(v_1 + y) + v_2) - \tilde{V}(M + US)\eta = \tilde{U}y_m - \tilde{U}(N + VS)\eta \tag{4.23}$$
$$\tilde{U}v_1 + \tilde{V}v_2 = \tilde{V}(M + US)\eta - \tilde{U}(N + VS)\eta \tag{4.24}$$
$$\eta = \tilde{U}v_1 + \tilde{V}v_2 \tag{4.25}$$

The signal η is thus not correlated with the noise d which is the main motivation behind the reformulation of the identification problem. The signal ϵ can be estimated using Eq. (4.26).

$$\epsilon = \tilde{M}y_m - \tilde{N}u \tag{4.26}$$

Again a proof is given in Eq. (4.27) to Eq. (4.31) and is based on the bezout identity.

$$M\eta = u - U\epsilon \tag{4.27}$$
$$N\eta = y_m - V\epsilon \tag{4.28}$$
$$\tilde{N}u - \tilde{N}U\epsilon = \tilde{M}y_m - \tilde{M}V\epsilon \tag{4.29}$$
$$\tilde{M}y_m - \tilde{N}u = (\tilde{M}V - \tilde{N}U)\epsilon \tag{4.30}$$
$$\epsilon = \tilde{M}y_m - \tilde{N}u \tag{4.31}$$

It is thus possible, using only known signals, to create the signals η and ϵ. The identification problem is thus possible to formulate as Eq. (4.32).

$$\epsilon = S\eta + (\tilde{M} + S\tilde{U})d \tag{4.32}$$

The identification problem of identifying S is thus an open loop identification problem. It is worth noticing that S represents all the dynamics not represented in the initial model. For this reason it can be extremely difficult to predict the structure of S beforehand.

Subspace identification methods require no a priori knowledge about the structure of the system to identify. The methods excel in identifying systems where the order and structure is not known beforehand. Subspace identification methods are therefore very convenient to use for identifying S. With the system S identified, the plant G can be calculated, as shown in Chapter 2, using either the right factorised form as in Eq. (4.33) or the left factorised form as in Eq. (4.34).

$$G(S) = (N + VS)(M + US)^{-1} \tag{4.33}$$
$$G(S) = (\tilde{M} + S\tilde{U})^{-1}(\tilde{N} + S\tilde{V}) \tag{4.34}$$

The Hansen scheme has thus indirectly identified the plant by reformulating the closed loop problem, of identifying G, into the open loop problem of identifying S. The downside of the method comes with the loss of physical understanding. When using Eq. (4.33) or Eq. (4.34) to construct the plant $G(S)$, any a priori physical knowledge used to create the nominal model $G(0)$ is lost in the parameters of the identified model.

4.4 Modified Hansen Scheme

The Hansen scheme has proven to be an effective method for transforming a closed loop identification problem into an open loop identification problem. The method however, is based on using the signals η and ϵ for identification. These signals are internal plant signals and therefore impossible to directly measure or impose. The goal is to modify the Hansen scheme such that it is possible to both directly impose the identification signal and measure the output signal. A method able to produce such results is for the future denoted a modified Hansen scheme.

For design of the modified Hansen scheme, the nominal controller is augmented with two new signals α and β, such that an augmented controller as presented on Figure 4.7 is constructed. This augmented controller was first introduced in Chapter 2 when discussing the relationship between the system Q in the controller, and the system S in the plant. It is important to notice that the controller simplify to the nominal controller when the two newly introduced signals are left unused.

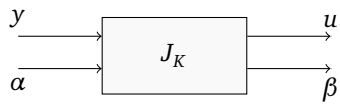

Figure 4.7: Representeation of the augmented controller with the two newly introduced signals α and β.

With an augmented controller as shown in Figure 4.7, the relationship between the signals α and β in the controller and the signals η and ϵ in the plant was shown in Section 2. This relationship is repeated in Eq. (4.35).

$$\begin{bmatrix} \alpha \\ \beta \end{bmatrix} = \begin{bmatrix} I & 0 \\ 0 & I \end{bmatrix} \begin{bmatrix} \eta \\ \epsilon \end{bmatrix} \tag{4.35}$$

The relationship as shown in Eq. (4.35) makes it possible to use the signals from the augmented controller, which can be obtained and imposed directly, instead of indirect approach corresponding with using η and ϵ. A graphical comparison of the two identification methods is shown in Figure 4.8a where the Hansen scheme is depicted and in Figure 4.8b where the modified Hansen scheme is given instead.

Using the modified Hansen scheme the identification problem changes from Eq. (4.32) to Eq. (4.36).

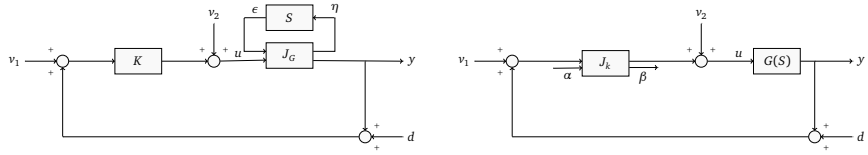

(a) Block diagram of the original Hansen scheme, using the signals η and ϵ for identification.

(b) Block diagram of the modified Hansen scheme, using the signals α and β for identification.

Figure 4.8: Comparison of the Hansen scheme and the modified Hansen scheme.

$$\beta = S\alpha + (\tilde{M} + S\tilde{U})d \tag{4.36}$$

As for the Hansen scheme, the identification problem is again an open loop problem. It is clear that the signals α and d are not correlated. As with the original Hansen scheme, standard identification methods can be used to identify S when using the modified Hansen scheme.

4.5 Initial Results Closed loop Identification of Gas Bearing

The modified Hansen scheme has been used to identify the active gas bearing which was presented in Chapter 3 with an active feedback loop. A simulation of the active gas bearing was conducted in order to examine whether the method would be feasible. A nominal insufficient model of the active gas bearing was used, and the signals α and β were obtained using the scheme presented in Figure 2.1 with Q omitted. Given that the real plant is known, which is the case for a simulation example, it is possible to compare the identified S with the real S. The real S can for such examples be calculated as in Eq. (4.37)[43].

$$S = \tilde{V}^{-1}(I - G(S)K)^{-1}(G(S) - G(0))M \tag{4.37}$$

Here, $G(S)$ is the plant to be identified, as shown in Figure 4.2. For simulations this is treated as a known LTI system. This, in turn, is of course unrealistic for real systems which is why the comparison is only possible during simulations. Using the signals α and β and the subspace identification method N4SID it is possible to identify the unknown dynamics as the system S. An example of an identified S for a simulation example is shown in Figure 4.9 where it is compared with the real S calculated using Eq. (4.37).

The identified S is seen to have a similar gain to the real S. However, the identified system was chosen of an order such that it was not possible to identify the peak gain. It is interesting to examine the impact of using a low order approximation for reconstructing the plant. This is possible by comparing the identified plant with the real and nominal plant such as shown in Figure 4.10.

The result shown in Figure 4.10 shows that it is possible to reach the true system from the nominal system through the identification process. Simulation experiments, such as

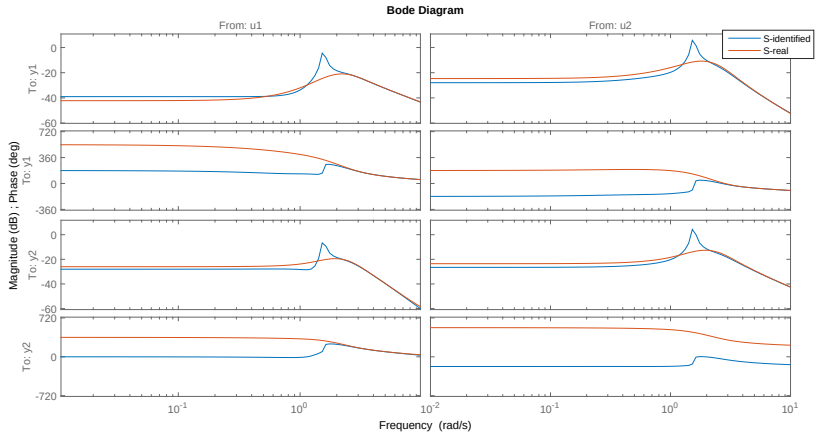

Figure 4.9: Bode plot comparison of an identified S and the true S calculated using Eq. (4.37).

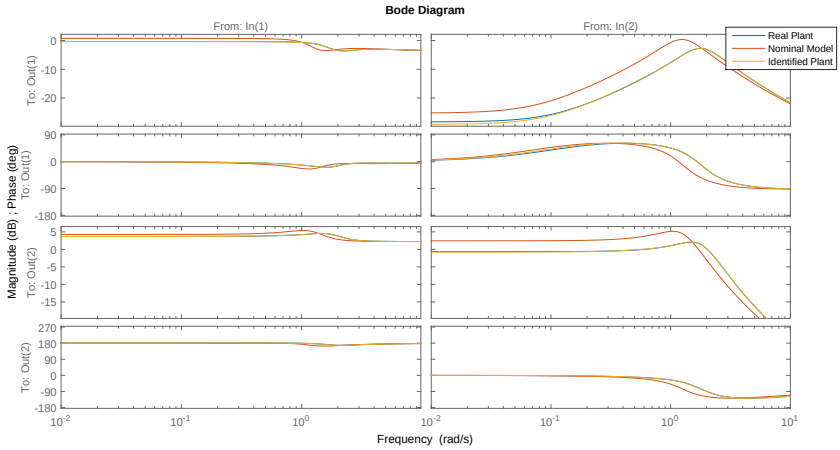

Figure 4.10: Bode plot comparison of an identified $G(S)$ the true $G(S)$ calculated using Eq. (4.37) and the nominal $G(0)$.

the example shown in Figure 4.9 and Figure 4.10, suggest that it is possible to identify the active gas bearing as part of a closed loop system. It should however be noted, that the identified system using the modified Hansen scheme is of an inconvenient high order relative to the nominal model. This is because of the step where the identified plant is calculated using Eq. (4.33). This is a well-known issue with identification based on the Hansen scheme, and makes a model reduction step required. The impact of conducting model reduction will be discussed later.

4.6 Method Comparison for Closed Loop Identification

It has been shown possible in Section 4.5 to identify the gas bearing using the modified Hansen scheme. A comparison with more commonly used identification schemes is seen as required in order to be able to justify using this fairly complex identification scheme. A qualitative measure for the identified models is needed to be able to determine the quality of the identification results for the different methods. In this work, a R^2 measure as shown in Eq. (4.38) is used for this purpose.

$$R^2 = 1 - \frac{||y - \hat{y}||_2}{||y - \bar{y}||_2} \tag{4.38}$$

Here R^2 is the goodness of the fit and should be as close to 1 as possible. The measured output is denoted y whereas the estimated output is $\hat{y}$ and $\bar{y}$ is the mean of all the measured output values y. The purpose of the R^2 is thus to estimate the goodness of the fit where outliers are given less importance.

For comparison, the identification scheme is compared with direct identification using a grey box PEM. Two possible scenarios have been explored to study the effect of using the modified Hansen scheme for identification.

A study into the impact of a priori insufficient knowledge about the system dynamics was conducted. A numerical study was conducted where the ability of each identification scheme to reconstruct the real plant, given a degraded nominal model, were investigated. The study used 300 imperfect nominal models obtained using Eq. (4.39).

$$A_{model} = (1 - \theta) \cdot A_{real} \tag{4.39}$$

Here, A_{real} is the true systems system matrix, A_{model} is the system matrix of the nominal model, and θ is a uniformly distributed scalar between 0 and 1. Using the 300 nominal models, both identification schemes were applied, and the quality of the identification schemes were found relative to θ. Identification results are shown in Figure 4.11 using Eq. (4.39) for construction of the nominal models.

The results as shown on Figure 4.11 suggest that it is advantageous to use the modified Hansen scheme when a priori knowledge of the system dynamics is insufficient. Simulations suggest that it can be advantageous to use the modified Hansen scheme for closed loop identification when a priori knowledge is lacking.

4.7 Experimental Results

It was suggested through simulation results, that identification using the modified Hansen scheme would produce superior results to direct identification using PEM when the initial nominal model does not represent the system well.

The results obtained from the simulation experiments have been investigated on the active gas bearing. Several different experiments were conducted to compare direct PEM identification with the modified Hansen scheme.

For the first set of experiments conducted, the nominal model was designed to mimic the dynamics of the active gas bearing well. The gas bearing was rotating with 2500 RPM, and both identification and verification sequences were obtained. The

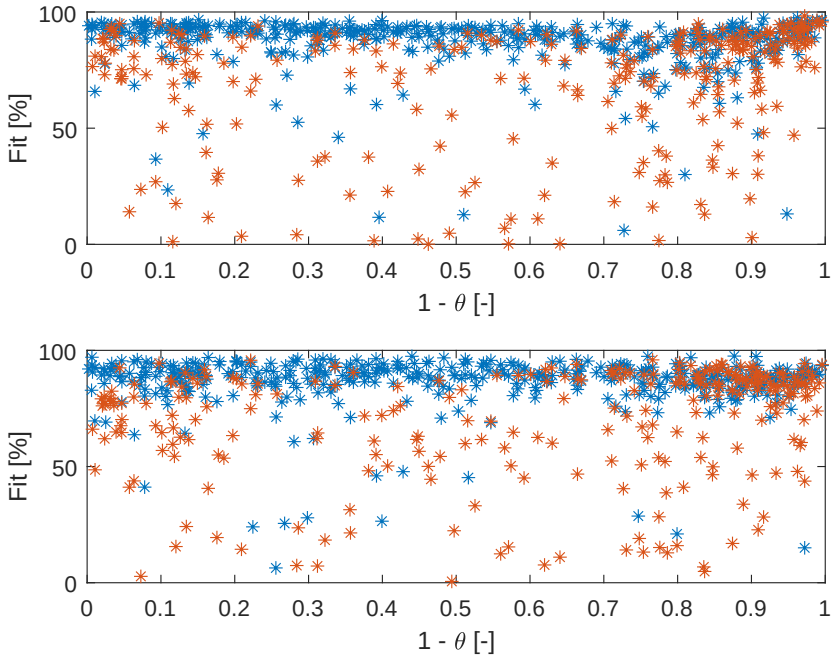

Figure 4.11: Comparison of the R^2 fit relative to θ using the modified Hansen scheme (blue), and direct PEM identification (red). The top plot shows the fit for the horizontal direction, and the bottom plot shows the fit in the vertical direction.

identification schemes are under such circumstances both able to identify the active gas bearing with the PEM getting slightly better results. The identification results from the experiments are shown in the first column of Table 4.1.

For the second set of experiments, the nominal model was chosen to mimic the dynamics well, while the rotation of the gas bearing was set to 0 RPM. The nominal model has a very high R^2 fit, and both identification schemes are only able to improve the result in the vertical direction. The result of the identification schemes are shown in the third column in Table 4.1. Again, the PEM identification scheme achieves slightly better results, however, both identification schemes produce models of similar quality to the nominal case.

The last set of experiments was executed using a nominal model lacking knowledge of the plant dynamics. The results of the experiments are shown in the second column of Table 4.1. For such a nominal model, the modified Hansen scheme clearly outperforms the PEM identification. The model identified using the modified Hansen scheme produces similar results to the models identified based on a good nominal model as shown in the third column of Table 4.1. Such results correspond with the simulations result shown in Figure 4.11 and confirms that the method can be advantageous when a priori knowledge is insufficient.

Order Reduction

The models identified using the modified Hansen scheme and direct PEM identification has so far been directly compared. This is seen as being unfair due to the order difference between the models generated using the two different schemes. The models generated using the PEM have the same order as the nominal model, whereas the order of the models generated using the modified Hansen scheme are of a much higher order. In order to get similar models which are comparable model reduction of the models generated using the modified Hansen scheme is needed. The low order model approximation is denoted $G_{red}(S)$, and $G(S)$ is the original model identified using the modified Hansen scheme. The model reduction technique used is described in [52]. The technique is used to obtain approximated models of the same order as the nominal model. The identification results using the full order models, and the models obtained using model reduction techniques are shown in Table 4.1.

	2500 RPM		high deviation 0 RPM		small deviation 0 RPM	
	Horizontal	Vertical	Horizontal	Vertical	Horizontal	Vertical
Nominal model	51.36%	54.13%	3.19%	3%	83.21%	76.12%
Open loop PEM model	62.87%	75.78%	48.91%	39.47%	83.9%	84.63%
Modified Hansen scheme $G(S)$	61.94%	69.19%	76.76%	83.58%	83.53%	81.18%
Modified Hansen scheme $G_{red}(S)$	60.71%	69.33%	76.73%	83.53%	83.07%	79.59%

Table 4.1: Model R^2 fit using each of the two identification methods.

4.8 Contributions

The work presented in the chapter is based on the results presented in publication P1, P2 and P6. The chapter introduced methods for the identification of systems that are subject to feedback control. The first contribution presented in the chapter was parameter identification for open loop unstable high order systems. The method was based on initial knowledge about the structure of the model and specific parametric uncertainties in the design phase. The method was first presented in P1 where an AMB model was used as the example.

The second contribution of the chapter is the modification to the Hansen scheme. Here it is shown how to design an identification scheme with the same properties as the Hansen scheme, while still possible to directly impose an excitation signal. The method was first presented in P2, and was used to identify an active gas bearing while a feedback loop was active.

Lastly, a comparison between PEM identification and identification using the modified Hansen scheme was presented. It was shown advantageous to use the modified Hansen scheme when a priori knowledge about the dynamics of the active gas bearing was lacking. The results of the comparison between the two identification schemes and closed loop identification of the active gas bearing was presented in P6.

Chapter 5

Fault Diagnosis

It has always been a huge driving force for control engineers to acquire precise models making it possible to design advanced control architectures. The controllers are designed to satisfy beforehand chosen requirements. However, due to faults and uncertainties, the system might change over time, and the a priori decided requirements might become infeasible. For known uncertainties and possible faults, robust controllers are often employed to keep up with performance requirements. However, the possible faults might be so severe that designing a robust controller is unachievable. Another approach is to conduct fault diagnosis, examining when the system has changed in such a way that the current control scheme is not able to satisfy the a priori defined requirements, and then repair the system accordingly. Fault diagnosis thus consists of determining whether a system is in its nominal or faulty state. Design of residual signals and kernel design have been studied widely and some approaches for kernel design are given in [24, 53, 54, 26]. Recently, research into using the Youla deviation system, introduced in Chapter 2 for kernel design, was conducted [37, 36]. It is in this chapter presented how to apply the YJBK-parametrisation and the augmented controller design presented in Chapter 2 for fault diagnosis design.

Fault diagnosis usually focuses on 4 different possible states. The first state is no fault (NF) which is when the plant is fault free and no fault is detected. The second state is false alarm (FA) which is when a fault is detected but the plant is fault free. The third state is missed alarm (MA) which is when no fault is detected, but the plant is experiencing a fault. Lastly, the fourth possible state is fault detected (FD) which is a fault being detected when the plant is experiencing a fault. This is illustrated in Table 5.1 where each of the possible states for a fault diagnosis scheme are shown.

	$\mathscr{H}_0$	$\mathscr{H}_1$
$\hat{\mathscr{H}}_0$	NF	FA
$\hat{\mathscr{H}}_1$	MA	FD

Table 5.1: Possible states when using a fault diagnosis scheme. The fault free case is denoted $\mathscr{H}_0$, while $\mathscr{H}_1$ correspond to system state being faulty. The $\hat{\cdot}$ is to be understood as the detectors estimate of the system state.

Usually, the goal of a fault diagnosis scheme is to maximise the diagonal elements in Table 5.1 relative to the off-diagonal elements. This is often accomplished by deciding on an allowed FAR, and optimising based on the detection probability. The FAR is defined in Eq. (5.1) based on N_F and F_A.

$$FAR = \frac{F_A}{N_F + F_A} \tag{5.1}$$

The quality of most FD schemes are therefore measured on their ability to detect faults given a beforehand chosen FAR.

Some different methods for residual design are given in [24], such as the null space method and structural analysis. A common kernel used for residual generation is shown in Eq. (5.2).

$$r = y - G(0)u \tag{5.2}$$

Here, noise has been omitted for simplicity, and it is clear that the residual is 0 in the fault free case, and different from 0 in the faulty case. It is advantageous to design such residuals where the fault free case is easy to distinguish from the different possible faulty cases. This advantage comes in the form of easier threshold design and calculation of FAR. It is not possible to conduct open loop FD on all systems. There can be plenty of reasons for it not to be possible to conduct FD using an open loop scheme. The plant might be unstable without feedback control, performance might not be possible to maintain without feedback control, or it might simply not be feasible to disconnect the controller. For example, residual generation using Eq. (5.2) is clearly impossible to realise when the plant is open loop unstable. The fault diagnosis conducted in this thesis are based on a closed loop scheme instead. Such a scheme is presented in Figure 5.1.

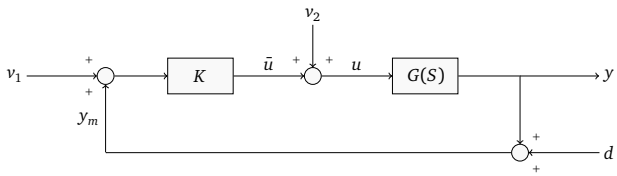

Figure 5.1: Block diagram of a plant $G(S)$ as part of a closed loop system with the controller K. The signal d is unknown noise while v_1 and v_2 are possible reference signals.

For such a system description, the closed loop kernel representation was presented in [55] where the kernel is based on the LCF of the plant. Unlike Eq. (5.2), the kernel presented ensures a stable residual generator for both open loop stable and unstable plants. The kernel presented in [55] is given in Eq. (5.3).

$$r = R\tilde{M}(y - G(0)u) \tag{5.3}$$

Here r is the residual vector, and R is a stable filter which can be used to shape the residual signal appropriately. The system $\tilde{M}$ ensures that the residual generator is stable for both open loop stable and unstable plants. The problem of optimizing FD is usually counterproductive to the goal of the designed controllers. Often, controllers are designed for disturbance rejection which has similar characteristics to faults. In order to determine the detectability of a fault, the impact of the controller thus needs to be taken into account. One such method is the k-gap metric [56, 57] based on the gap metric [58] which measures the gap between the fault free plant, and a given faulty plant given feedback control.

5.1 Active Fault Diagnosis

Passive fault diagnosis is a well-established research area. For passive fault diagnosis schemes, isolation of different faults is conducted using sensor redundancy information. Such redundancy is for many systems not possible, and it is indeed a goal for most companies to use only the minimal required amount of sensors. Active fault diagnosis uses a known excitation signal instead to obtain sufficient information for isolation of different faults. Active fault diagnosis using the input and output signal of the plant to conduct diagnosis has been studied intensively [59, 60]. Such fault diagnosis schemes has many similarities to direct identification. The active fault diagnosis schemes often work with a discrete bank of possible systems such as shown in [61, 62, 31, 33]. An alternative approach was introduced in [36] which bases the fault diagnosis on the fault signature system instead of the plant directly. Recall the YJBK-parametrisation from Chapter 2, the fault signature system can be shown to fulfil Eq. (5.4) in the fault free case, and Eq. (5.5) in the faulty case.

$$S(\theta) = 0|_{\theta=0} \tag{5.4}$$
$$S(\theta) \neq 0|_{\theta\neq 0} \tag{5.5}$$

The main advantage of using the fault signature system for fault diagnosis comes from Eq. (5.4) and Eq. (5.5) which states that the fault signature system is 0 in the fault free case, and different from 0 when a fault occurs. Hypothesis testing becomes easier and a CUSUM detector was introduced for fault diagnosis using the fault signature system in [37]. It is possible to express the fault signature system as a function of the faults as shown in Eq. (5.6).

$$S(\theta) = \tilde{M}G_{yw}\theta(I-(G_{zw}+G_{zu}U\tilde{M}G_{yw})\theta)^{-1}G_{zu}M \tag{5.6}$$

Here G_{yw}, G_{zu} and G_{yw} are all defined in Eq. (4.13) as part of the augmented plant consisting of the nominal plant and the considered faults. Active fault diagnosis using the fault signature system is similar to the standard closed loop kernel presented in Eq. (5.3) when the filter R is identity. This can easily be shown by recalling the Hansen scheme from Chapter 4. It was possible to express the output of S as given in Eq. (5.7) based on a right YJBK-parametrisation of the plant.

$$\epsilon = \tilde{M}y - \tilde{N}u \tag{5.7}$$
$$\epsilon = \tilde{M}(y - \tilde{M}^{-1}\tilde{N}u) \tag{5.8}$$
$$\epsilon = \tilde{M}(y - G(0)u) = r \tag{5.9}$$

It is clear that the output of S denoted ϵ in Eq. (5.9) is equal to the residual generated for the closed loop kernel in Eq. (5.3). For active fault diagnosis the system S is excited with a known signal η, and the output of S is the residual. Since it is not possible to directly use the signals η and ϵ as explained in Chapter 2, the equivalent controller signals α and β are used instead by augmenting the controller. The standard active fault detection scheme for this thesis is shown in Figure 5.2.

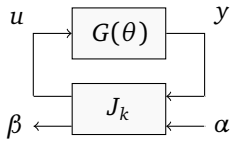

Figure 5.2: Block diagram of the standard active fault diagnosis scheme using an augmented controller J_k.

Here, J_k is given in Eq. (5.10), and is the controller augmented to accommodate for the signals α and β as shown in Chapter 2. It is easy to see from Eq. (5.10) that the augmented controller simplifies to the nominal when the excitation signal α is unused. The nominal performance is therefore kept for the time periods where fault diagnosis is not conducted.

$$J_k = \begin{bmatrix} UV^{-1} & \tilde{V}^{-1} \\ V^{-1} & -V^{-1}N \end{bmatrix} \tag{5.10}$$

So far noise has not been considered in the fault diagnosis scheme. For simplicity, all noise is in this analysis treated as White Gaussian Noise (WGN) output noise. This is a simplification used for transparency. It can be shown that all noise on linear systems can be modelled as WGN on the output subject to some filter. This filter is here treated as identity, but it is straightforward to extend the analysis to cover examples where that is not the case. A block diagram with the noise incorporated is shown in Figure 5.3.

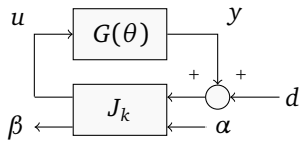

Figure 5.3: Block diagram of the standard active fault diagnosis scheme using an augmented controller J_k. Noise is treated as output noise and represented by the signal d.

With an active fault diagnosis scheme as presented in Figure 5.3 the closed loop system is given in Eq. (5.11).

$$\begin{bmatrix} y \\ u \\ \beta \end{bmatrix} = \begin{bmatrix} (N+VS)\tilde{U} & N+VS \\ (M+US)\tilde{U} & M+US \\ \tilde{M}+S\tilde{U} & S \end{bmatrix} \begin{bmatrix} d \\ \alpha \end{bmatrix} = P_{cl}(S) \begin{bmatrix} d \\ \alpha \end{bmatrix} \tag{5.11}$$

The residual signal with the noise considered is given by Eq. (5.12) for the active diagnosis scheme presented in Figure 5.3.

$$\beta = S(\theta)\alpha + (\tilde{M} + S(\theta)\tilde{U})d \tag{5.12}$$

It is worth noticing that Eq. (5.12) is equviavalent to the identification problem stated in Chapter 4 when using the modified hansen scheme. For active fault diagnosis schemes based on the fault signature system, the goal is to detect the signal α through $S(\theta)$ in the measurable signal β given Eq. (5.12). There are plenty of methods to conduct such detection with the CUSUM method presented in [37] and the Matched Filter detector, which is presented in P4.

5.2 Whitening filter

The detection method to be presented in Section 5.3 is based on the assumption that the residual signal consists of only WGN in the fault free case. This assumption does not hold for a residual as given in Eq. (5.12) even though the noise signal d is WGN. In the fault free case the residual signal β is given in Eq. (5.13).

$$\beta = \tilde{M}d \tag{5.13}$$

The method introduced in Section 5.3 uses a threshold based on an allowed FAR. A correlator design is introduced which in the fault free case uses the whiteness of the noise to determine the variance of the detector signal. For coloured noise the method fails and produces a higher amount of F_A than expected due to correlation in the noise signal. It is therefore important to introduce a filter which makes the noise white in the fault free case.

This section introduces 2 different cases and their respective solutions. The first case is output noise as shown on Figure 5.3 with an open loop stable plant. This is the simplest case, and a residual generator as shown in Eq. (5.14) will translate to the noise being white in the fault free case.

$$r = \tilde{M}^{-1}\beta = \tilde{M}^{-1}(\tilde{M}y - \tilde{N}u) = y - G(0)u \tag{5.14}$$

Here, the transfer function from the excitation signal to the residual is $\tilde{M}^{-1}S(\theta)$ instead of $S(\theta)$. It is worth noticing that the kernel is equivalent to the open loop kernel presented in Eq. 5.2. For this reason the residual generator will be unstable if the plant is unstable.

The second case is again based on the scheme presented in Figure 5.3. For this case the plant is open loop unstable which means that the filter $\tilde{M}^{-1}$ will be unstable. The

goal is to obtain a stable filter denoted W^{-1} with the same spectrum as $\tilde{M}^{-1}$. This can be achieved using spectral factorisation as described in [63]. A stable residual generator for an open loop unstable plant is shown in Eq. (5.15).

$$r = W^{-1}\beta = W^{-1}(\tilde{M}y - \tilde{N}u) = W^{-1}\tilde{M}(y - G(0)u) \tag{5.15}$$

This residual generator is of the same type as the closed loop stable residual generator shown in Eq. (5.3), where W^{-1} is used as the filter R. The transfer function from the excitation signal to the residual is here $W^{-1}S(\theta)$, and from the noise signal d to the residual is given in Eq. (5.16) for when the plant is fault free.

$$r = W^{-1}\tilde{M}d = Hd|_{\theta=0} \tag{5.16}$$

Here, H is a diagonal matrix which describes the difference between the variance of d and the variance of the residual signal. The next section is based on the residual given in Eq. (5.15) which is the general case. However, for plants where $\tilde{M}^{-1}$ is possible to use as the filter, H simplify to an identity matrix.

5.3 Matching filters

Matching filter detection is based on the idea of estimating the Probability Density Function (PDF) most likely to be observed. The method is based on the Neyman-Pearson lemma and is described in [64]. By using the fault signature system for the fault diagnosis, the residual signal only consist of noise in the fault free case. It is therefore possible to design a $\mathscr{H}_0$ as in Eq. (5.17) for the fault free case. For active fault diagnosis, the excitation signal is a known entity. Therefore, a $\mathscr{H}_1$ as introduced in Eq. (5.18) with a known signal but a delay and amplitude that depends on the specific fault occurring, is possible.

$$\begin{aligned} \mathscr{H}_0 : r[n] &= Hd[n], & n = 0,1,....,N-1 \quad (5.17)\\ \mathscr{H}_1 : r[n] &= A_{S_\theta}\alpha[n-n_0] + (H + WS(\theta)\tilde{U})d[n], & n = 0,1,....,N-1 \quad (5.18) \end{aligned}$$

Here, d is the output noise signal, H is a diagonal matrix designed using the whitening filter, W is the whitening filter, A_{S_θ} is a fault dependent amplitude and n_0 is a fault dependent delay. For the derived method the noise is assumed white in the fault free case, which is true when the whitening filter is applied. It is thus possible to determine whether the $\mathscr{H}_1$ is true by detecting a known signal with an unknown delay and amplitude. For simplicity of the method, the excitation signal is expected to be a sinusoidal wave. Both the unknown delay and amplitude can be shown to belong to a set that depends on the possible faults. For the delay this set is denoted τ and is determined by the parametric faults considered, compactly written in Eq. (5.19).

$$n_0 \in \tau(\theta) \tag{5.19}$$

The matched filter method consist of 2 steps. First step is to determine which fault that might have occurred. For this step, the method employs a correlation filter with a

fixed moving window to determine which fault from the set of faults that is most likely to have occurred. The correlation filter is given in Eq. (5.20) which chooses the delay with the highest correlation.

$$\phi = \arg\max_{n_0 \in \tau}\left(\sum_{n=n_0}^{n_0+N-1} r[n]\alpha[n-n_0]\right) \tag{5.20}$$

Here, N is the window length chosen for the detector, $r[n]$ is the residual signal and α is the excitation signal. The correlator gives the best estimate of the delay corresponding with S. In the fault free case the residual signal r is white noise and the correlator is equally likely to choose any of the possible delays. The second step for the matched filter method is to determine whether a fault has occurred or not. For this, it is necessary to be able to decide whether the $\mathscr{H}_0$ or $\mathscr{H}_1$ is found to be true. A detector is implemented as shown in Eq. (5.21) to determine the probability that the actual signal is observed.

$$T(r) = \sum_{n=\phi}^{\phi+N-1} r[n]A_0\alpha[n-\phi] \tag{5.21}$$

Here, A_0 is a predetermined gain and T is the decision variable. The decision variable is used to determine which hypothesis to be true deciding on the $\mathscr{H}_0$ if Eq. (5.22) and on $\mathscr{H}_1$ if Eq. (5.23) is true.

$$\mathscr{H}_0 : T \leq \gamma \tag{5.22}$$

$$\mathscr{H}_1 : T > \gamma \tag{5.23}$$

Here, γ is the threshold which has to be determined beforehand based on the allowed FAR as illustrated in Table 5.1. A graphical illustration of the detector introduced in Eq. (5.21) is shown in Figure 5.4. A fault is introduced after 5 seconds to the system which makes the detector signal rise above the threshold line. The change introduced by the fault makes Eq. (5.22) become true instead of Eq. (5.22).

It is possible to determine the threshold as shown in Figure 5.4 based on a desired FAR using Eq. (5.24) as shown in [64]. The possibility of designing the threshold based on a desired FAR makes the method easy to integrate with functionality requirements.

$$\gamma = \sqrt{\sigma^2 \nu} Q^{-1}(FAR) \tag{5.24}$$

Here, σ^2 is the variance of the noise in the fault free case shown in Eq. (5.17), ν is the energy contained in the signal for one window length and $Q(\cdot)$ is the complementary cumulative distribution. It is assumed for Eq. (5.24) that the system consist of no uncertainties. In reality this is not the case, and the model uncertainties will result in a higher FAR than expected using Eq. (5.24). The energy contained in a sinusoidal signal is given in Eq. (5.25) as used for determining the threshold limit.

$$\nu = N\frac{A_0^2}{2} \tag{5.25}$$

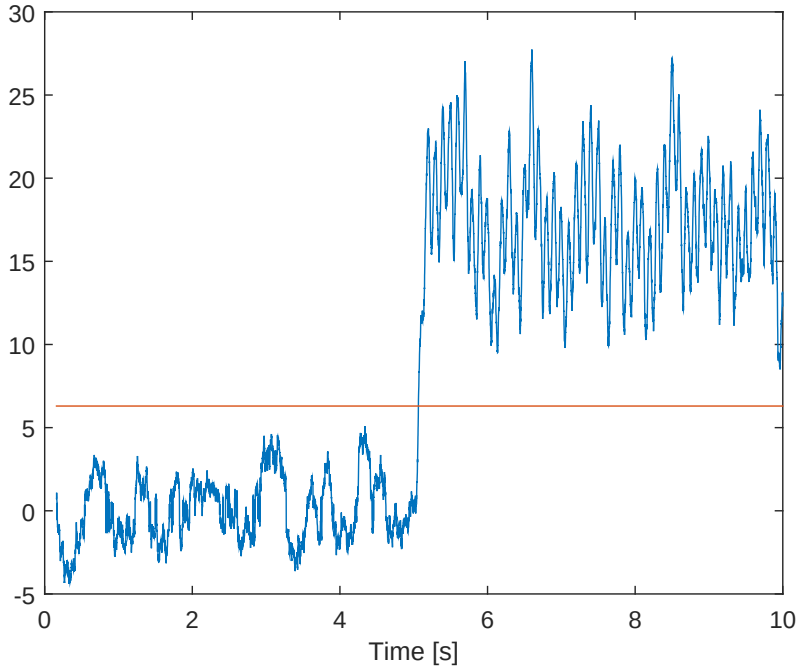

Figure 5.4: Graphical example of the detector signal $T(r)$ given a fault free plant subject to a fault after 5 seconds. The fault introduced to the plant is detected when $T(r)$ rises above the threshold line and $\mathcal{H}_1$ becomes true.

The calculation of the energy contained in the residual signal is based on a sinusoidal excitation wave. Another type of excitation signal can be used, however Eq. (5.25) would have to be modified accordingly. The final active fault detection scheme is shown in Figure 5.5 with the detector implemented as the T block.

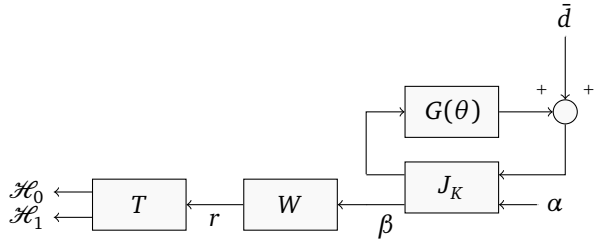

Figure 5.5: Block diagram of the active fault diagnosis scheme with a hypothesis testing implemented.

The fault diagnosis method is thus based on a threshold design given by an a priori chosen FAR. The design procedure does not as such give insight into the detectors ability to detect the possible parametric faults. The probability of detection can be defined

based on the last row in Table 5.1 as shown in Eq. (5.26).

$$P_D = \frac{F_D}{M_A + F_D} \tag{5.26}$$

The quality of detection is thus measured by how often a fault is detected relative to how often that it is missed. A P_D close to 1 is therefore seen as a good detector design, while a P_D close to 0 means that the detector is unable to detect the given fault. It is possible to calculate the probability of detection for each specific fault based on the energy of the correlator signal in the faulty case and the variance of the noise. The probability of detection is given in Eq. (5.27).

$$P_D = Q(Q^{-1}(FAR) - \sqrt{D}) \tag{5.27}$$

$$D^2 = \frac{(E(T;\mathscr{H}_1|\theta_k) - \chi)E(T;\mathscr{H}_1|\theta_{A_0}) - \chi)}{var(T;\mathscr{H}_0)} \tag{5.28}$$

Here, D is the deflection coefficient which was introduced in [64] as defined in Eq. (5.28), θ_k denotes the specific considered fault, θ_{A_0} denotes the fault used to determine the gain A_0 and Xi is the expected value of the detector signal given the plant is fault free also written in Eq. (5.29).

$$\chi = E(T;\mathscr{H}_0) \tag{5.29}$$

Model Uncertainty

The detector scheme previously presented is based on the assumption of perfect model knowledge for the fault free case. However, identified parameters are often associated with an uncertainty. It is possible to modify the detector scheme to accommodate for such uncertainties. The $\mathscr{H}_0$ can be reformulated as shown in Eq. (5.30), and the $\mathscr{H}_1$ can be reformulated as shown in Eq. (5.31).

$$\mathscr{H}_0 : r[n] = A_{S_\mu}\alpha[n] + (H + W^{-1}S(\mu)\tilde{U})d[n] \tag{5.30}$$

$$\mathscr{H}_1 : r[n] = A_{S_{(\theta,\mu)}}\alpha[n - n_0] + (H + W^{-1}S(\theta,\mu)\tilde{U})d[n] \tag{5.31}$$

Here, μ denotes the parametric uncertainties. The uncertainties make the residual signal consist of both a sinusoidal signal and non-white noise in the fault free case. It is assumed that the noise is approaching white noise in the fault free case. The parametric uncertainties can be shown to translate into an uncertainty band on the phase shift used for isolation. Furthermore, parametric uncertainties will add a constant gain to $T(r)$ in the fault free case. Such a gain is possible to compensate for with an equivalent increase to the threshold.

5.4 Design of excitation signal

Passive FD is based on observing the plant in steady state, and detecting discrepancies between the measured and expected output. The faults are there isolated based on

information from extra sensors. Such diagnosis schemes are not disturbing the ongoing process, and are therefore supposed to always be active. Active fault diagnosis uses information from an excitation signal to gain insight into the isolation of faults. The process is therefore disturbed while active fault diagnosis is being conducted. It is therefore preferred to conduct active fault diagnosis for short intervals and reduce the disturbance introduced during these periods. To do this, it is desired to find the excitation signal that gives the best probability of detection relative to the disturbance on the output of the plant. The following procedure is based on the use of a single frequency sinusoidal excitation signal. Other types of excitation signals might yield better results for specific systems, but are disregarded to keep in line with the matched filter method. Based on Eq. (5.6), and the whitening filter presented in Section 5.2, the transfer function from the excitation signal to the residual is given in Eq. (5.32).

$$\xi_r(\omega) = |W^{-1}\tilde{M}G_{yw}\theta(I-(G_{zw}+G_{zu}U\tilde{M}G_{yw})\theta)^{-1}G_{zu}M| \tag{5.32}$$

Here, θ is the specific fault considered. The optimal frequency therefore depends both on the type and magnitude of the specific fault. It is therefore clear that the analysis needs to be conducted for each fault to be considered. The transfer function from the excitation signal to the output is less complicated, as shown in Eq. (5.33). Whereas for Eq. (5.32), each of the faults has to be considered, here the goal is just to minimize the disturbance on the output in the fault free case.

$$\xi_y(\omega) = \bar{\sigma}(N(\omega)) \tag{5.33}$$

Here, $\bar{\sigma}(\cdot)$ is the highest singular value. By using the highest singular value it is possible to find the highest gain between the excitation and output signal [65]. Eq. (5.33) is therefore based on the fault free case why it does not depend on the specific fault. The efficiency is defined in Eq. (5.34) using the transfer function from the excitation signal to the residual, in the faulty case, defined in Eq. (5.32) and the transfer function from the excitation to the output, in the fault free case, defined in Eq. (5.33).

$$f_\alpha(\omega) = \min_{\theta=\Delta} \frac{\xi_r(\theta,\omega)}{\xi_y(\omega)} \tag{5.34}$$

The goal of Eq. (5.34) is to find the lowest efficiency between all the possible faults at each frequency. The lowest efficiency is believed to be the only important parameter to optimise, since all other faults will be possible to detect if that specific fault is detectable. The method is illustrated in Figure 5.6 with a simple plant with two possible parametric faults.

By using the new function $f_\alpha(\omega)$ it is possible to find the optimal frequency of the excitation signal for detecting the fault with the lowest efficiency. This search for the optimal frequency of the excitation signal is shown in Eq. (5.35)

$$\omega_\alpha = \arg \max_{\omega_1 \leq \omega \leq \omega_2} f_\alpha(\omega) \tag{5.35}$$

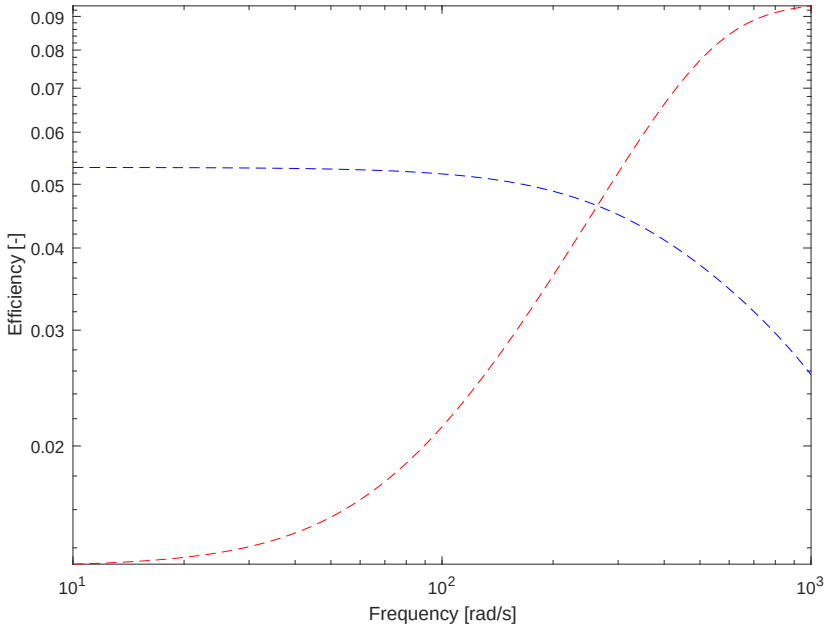

Figure 5.6: Plot of $\frac{\xi_r(\theta,\omega)}{\xi_y(\omega)}$ for two possible faults. For this example $f_\alpha(\omega)$ is equal to the red stippled line until ω is around 300 rad/s where the two lines cross. From ω is 300 rad/s and upwards $f_\alpha(\omega)$ is the blue line instead.

Here, ω_α is the optimal frequency for the excitation signal, ω_1 is the lower bound for the frequency and ω_1 is the upper bound for the frequency. These bounds usually come naturally from the specific plant and operation. Indeed, for the active gas bearing the lower bound is determined based on how many full wave lengths is desired during a test which is limited to 14 seconds. The upper bound is chosen based on the sampling rate used during diagnosis on the gas bearing. An upper limit of the frequency is chosen such that the sinusoidal signal is still smooth.

5.5 Experimental Diagnosis

In this section an implementation example, of the active fault diagnosis scheme, on an active gas bearing is presented. The description of the active gas bearing and its state space model was given in Chapter 3. In order to design a detector and conduct fault diagnosis the following points have to be addressed first.

- Determine possible faults
- Identify noise model
- Design or obtain a stabilising controller

Fault description	Notation	Bound	Description
Horizontal actuator	θ_1	[0 -1]	The fault on the opening degree of the horizontal actuator is $100 \cdot (-\theta_1)$% of its expected value. This results in a reduction of the horizontal input gain.
Vertical actuator	θ_2	[0 -1]	The fault on the opening degree of the vertical actuator is $100 \cdot (-\theta_2)$% of its expected value. This results in a reduction of the vertical input gain.
Horizontal sensor	θ_3	[0 -1]	The fault on the measured distance of the horizontal displacement sensor is $100 \cdot (-\theta_3)$%. This is equivalent to a reduction in the horizontal output gain, and the controller is then demanding wrong actuation.
Vertical sensor	θ_4	[0 -1]	The fault on the measured distance of the vertical displacement sensor is $100 \cdot (-\theta_4)$%. This is equivalent to a reduction in the vertical output gain, and the controller is then demanding wrong actuation.

Table 5.2: Lookup table for the different possible faults

With the points above addressed the detector design is found using the following steps.

- Calculate coprime factorisation of controller and plant
- Construct the augmented plant based on the possible faults
- Define the fault signature system (S)
- Determine optimal excitation signal
- Choose the window length based on a decided FAR
- Calculate the phase shift of possible faults

For the design of active fault diagnosis, the analysis is conducted using 4 different possible faults. The four possible faults considered are faults on the sensor in either the vertical or horizontal direction, and faults on the actuator in either the vertical or horizontal direction. The faults are described in further detail in Table 5.2.

The diagonal fault matrix Δ is designed as shown in Eq. (5.36). Each of 4 faults is deemed possible to occur, and the isolation process is therefore trying to determine which fault is most likely.

$$\theta = \begin{bmatrix} \theta_1 & 0 & 0 & 0 \\ 0 & \theta_2 & 0 & 0 \\ 0 & 0 & \theta_3 & 0 \\ 0 & 0 & 0 & \theta_4 \end{bmatrix} \tag{5.36}$$

With a fault description as given in Eq. (5.36), the plant can be described as an upper LFT as shown in Eq. (5.37).

$$G(\theta) = \mathscr{F}_u(G_{aug}, \Delta) \tag{5.37}$$

Where the augmented system is defined as in Eq. (5.38).

$$G_{aug} = \begin{bmatrix} G_{zw} & G_{zu} \\ G_{yw} & G_{yu} \end{bmatrix} \tag{5.38}$$

The four subsystems are defined by Figure 2.5 which describes the relationship between the faults and the nominal plant. Based on Eq. (5.38) the augmented plant G_{aug} is shown in Eq. (5.39).

$$G_{aug} = \left[\begin{array}{ccc|ccc} 0 & \mathbf{I} & 0 & 0 & 0 & 0 \\ K & D & B & 0 & 0 & 0 \\ 0 & 0 & -P & P & 0 & P \\ \hline \mathbf{I} & 0 & 0 & 0 & 0 & 0 \\ 0 & 0 & 0 & 0 & 0 & \mathbf{I} \\ \mathbf{I} & 0 & 0 & 0 & \mathbf{I} & 0 \end{array}\right] \tag{5.39}$$

Each element in Eq. (5.39) is a $2x2$ matrix with the elements defined in Chapter 3. The system G_{zw} has 4 input and 4 output, the system G_{zu} has 2 input and 4 output, the system G_{yw} has 4 input and 2 output and the system G_{yu} consists of 2 input and 2 output. The augmented plant is used for the design of the fault signature system for analysis of the impact of the different possible faults.

Noise analysis

For design of a statistical based detection scheme, the noise influencing the plant needs to be properly identified. Such identification is conducted in open loop, and it was found possible to model all noise as output noise to follow the detector scheme given in Figure 5.5. Because it is possible to model the noise as WGN on the output, a filter as presented in Section 5.2 can be implemented on the residual. The whitening filter is given in Eq. (5.40) for active fault diagnosis on the active gas bearing.

$$W^{-1} = \tilde{M}^{-1} \tag{5.40}$$

It is possible to use the filter introduced in Eq. 5.40 due to the plant being open loop stable. With this whitening filter, the variance is unchanged between the measured output and the residual. A histogram of the residual with the whitening filter implemented is shown in Figure 5.7. The data is obtained without any excitation signal, such that discrepancies between the model and real plant does not influence the experiment.

The histogram shows the distribution of the noise to be gaussian. Furthermore, no direct or cross correlation is found for the noise in the fault free case. Using the model of the noise, a threshold can be decided based on a window length of the detector and the amplitude of the excitation signal using Eq. (5.24).

Controller Design

In order to conduct active closed loop fault diagnosis a controller is required. Two different control designs have been implemented in order to investigate the modularity of the detector design. The first controller is a simple proportional controller as presented in Eq. (5.41).

$$K = k\begin{bmatrix} 1 & 0 \\ 0 & 1 \end{bmatrix} \tag{5.41}$$

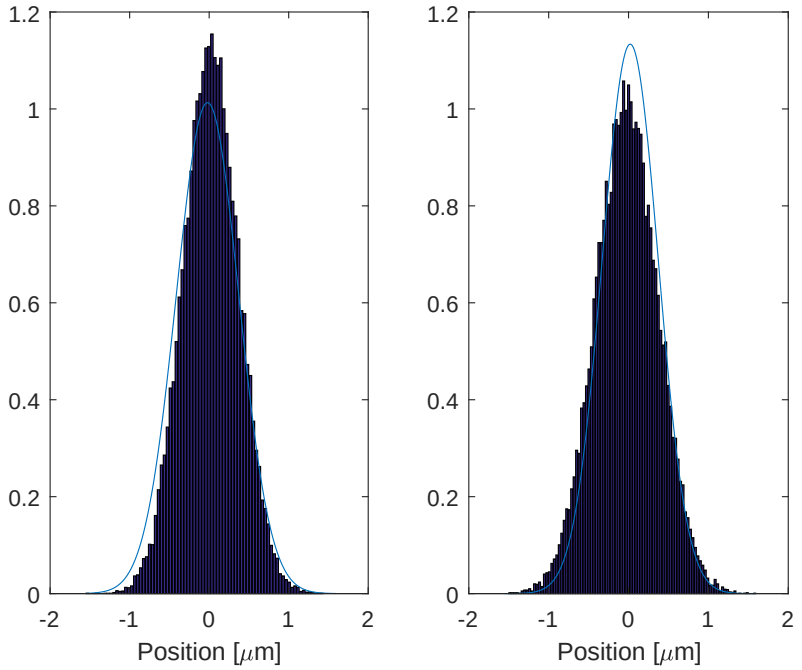

Figure 5.7: Histogram of the residual measurements obtained from an experiment without any input signal and with a fault free plant. The left histogram is for the horizontal residual measurement and the right histogram is for the vertical residual measurement.

Here, k is a scalar which results in a symmetric controller for the horizontal and vertical direction. The implemented proportional controller is thus without any gain in the off diagonal. The design is chosen in order to show that it is possible to detect faults using only the cross coupling in the plant.

The second control design is a Linear Quadratic Regulator (LQR) controller designed using a full order observer. The observer gain and the state feedback gain are both fully populated matrices with non-zero elements. The two controllers therefore, differ both in structure and solution to the control problem. Where the proportional controller is trying to treat each direction as independent, the LQR controller is trying to take advantage of the cross coupling to increase the damping. A gain plot of the closed loop plant given each controller, and the nominal open loop plant is shown in Figure 5.8.

Fault Diagnosis

Based on a known controller, it is possible to conduct an analysis to determine the expected phase shift given each of the considered faults. For each of the possible faulty sensors and actuators, the magnitude of the fault is chosen as shown in Eq. (5.42).

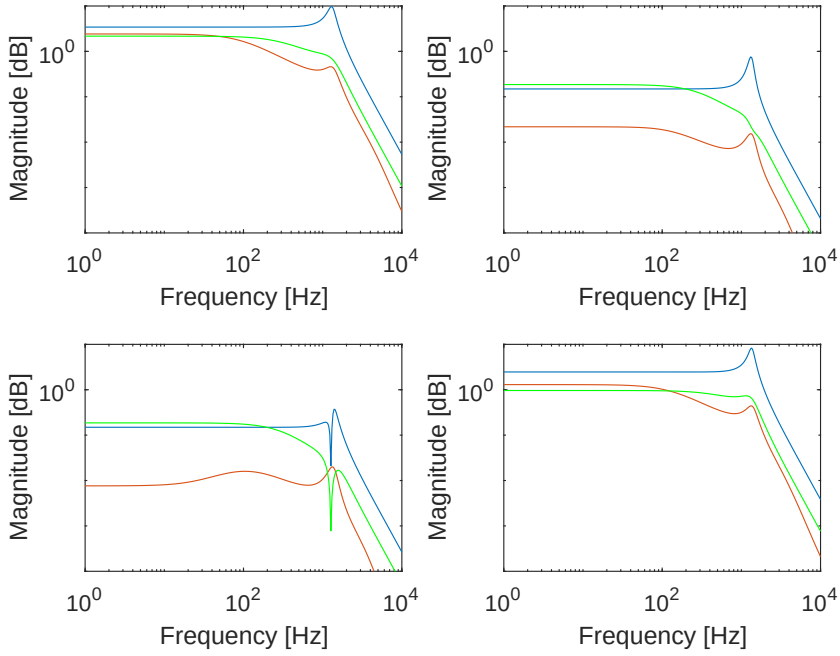

Figure 5.8: Bode plot of the gain from a disturbance, in form of a displacement, to the displacement of the rotor. The left column is for a disturbance in the horizontal direction, while the right column is for a disturbance in the vertical direction. Equivalently the top row is for the position of the rotor in the horizontal direction, while the bottom row is for the position in the vertical direction. The blue line represents the gas bearing without any control, the red line represents the gas bearing with the LQR controller implemented and the green line represents the gas bearing with the proportional controller implemented.

$$\theta_i = 0.5 \tag{5.42}$$

This gives the possibility of 4 different faults on the active gas bearing. Based on the severity of the faults considered, the optimal frequency for the excitation signal can be determined using the method described in Section 5.4. Recall that the efficiency parameter was based on the transfer function from the excitation signal to the output, and from the transfer function from the excitation signal to the detector. Such a ratio can be described as in Eq. (5.43).

$$f_{\alpha_i}(\omega) = \frac{\xi_r(\theta_i, \omega)}{\xi_y(\omega)} \tag{5.43}$$

Using Eq. (5.43) a plot of the efficiency parameter f_α given each of the 4 possible

faults is then shown in Figure 5.9 using the horizontal excitation signal and vertical residual signal.

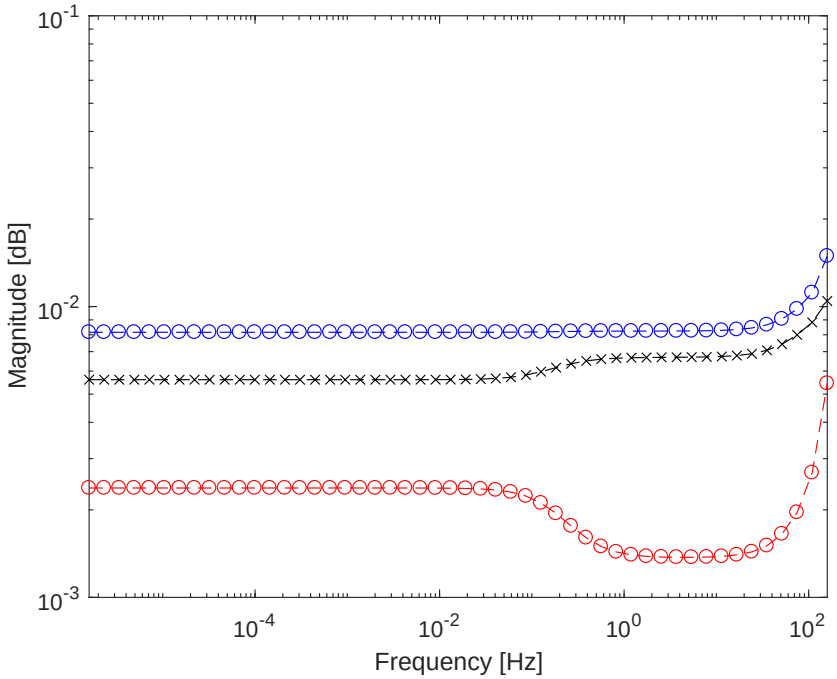

Figure 5.9: Plot of f_α versus the frequency of the excitation signal where α_h and β_v are used. The blue line represents f_α given a fault on the horizontal actuator, the red line is for a fault on the vertical actuator and the black line represents the vertical sensor. The horizontal sensor cannot be detected in the signal which is why it is not shown.

Using Figure 5.9, the frequency of the excitation signal is found using Eq. (5.35). Based on the decided frequency, the delay given each of the faults can be calculated using faulty system and whitening filter. With this information it is possible to apply the detector as given in Eq. (5.21).

The efficiency plot on Figure 5.9 suggests that it is only possible to detect 3 of the faults in each of the residual directions. The reason is that it is impossible to detect and isolate faults on the sensor which is not used to design the residual. Hence, faults on the horizontal sensor can only be detected when using β_h, and faults on the vertical sensor can only be detected when using β_v. A plot of this phenomena is shown in Figure 5.10. There, a horizontal excitation signal is applied, and the vertical residual signal is used for fault diagnosis. Each of the four subplots corresponds to one of the four different faults being introduced to the active gas bearing and using the detector design described in Eq (5.20) and Eq. (5.21).

Figure 5.10 shows how the detector is unable to detect faults introduced on the horizontal sensor when using the vertical residual signal. It is, however, possible to detect all four faults by the use of both the vertical and horizontal residual signal. Furthermore, the isolation based on the phase shift introduced by the excitation signal

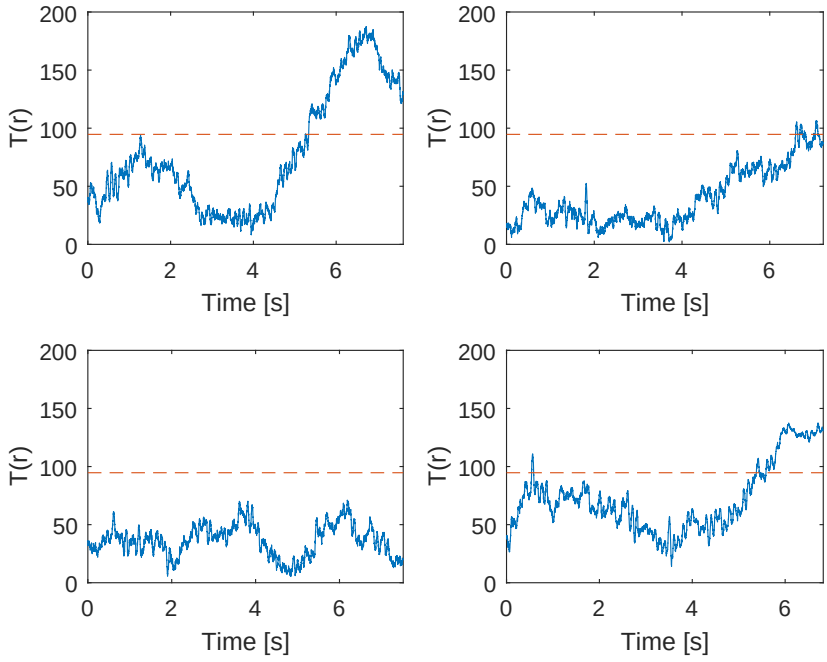

Figure 5.10: Plot of $T[n]$ for the gas bearing when each of the 4 possible parametric faults is introduced respectively. A horizontal excitation signal is applied and the vertical output of the fault signature system is used for detection purposes. The top left plot is for a fault on the horizontal actuator whereas the top right is for a fault on the vertical actuator. On the bottom left plot a fault is introduced on the horizontal sensor, and on the bottom right a fault has been introduced on the vertical sensor instead.

going through S was shown to be able to isolate the actual occurring fault.

5.6 Contributions

The chapter summarises the contributions of publication P3, P4 and P5. A method for active fault diagnosis based on a matching filter design with a moving window was first introduced in P3. The detector derived in P3 was based on a linearized version of the fault signature system. Initial detection and isolation of parametric faults was introduced and shown possible using a simulation example. The method was extended to use the nonlinear fault signature system in P4. The whitening filter was presented as well to get the residual signal as presented in Section 5.2. The choice of frequency for the excitation signal was furthermore discussed, and a solution was proposed. Lastly, the results from using the method to diagnose faults on an active gas bearing was presented in P5. The publication presented the detector process and identified the most interesting faults to detect. It was shown possible in P5 to diagnose several different faults on an active gas bearing using the proposed active fault diagnosis method.

Chapter 6

Conclusion

Closed loop identification and fault diagnosis schemes offer methods which handle the influence of the feedback loop introduced by most control systems. This project has investigated methods for identification and active fault diagnosis of systems subject to such a feedback loop. Extra focus has been on applying such methods to an active gas bearing. Closed loop identification is seen as crucial for many applications because of the use of sensor feedback. There can be several different reasons for feedback control to be required; it might not be safe to excite the system without feedback, the plant might simply not be stable without it, or it might not be feasible to disconnect the controller. Identification of systems with low damping such as gas bearings is one example of this. To show that it is possible to apply closed loop methods to an active gas bearing is therefore of great relevance. For this, the Hansen scheme was investigated. It was proposed to augment the controller such that signals in the controller could be used for closed loop identification.

For fault diagnosis, most methods require a large number of sensors to isolate different faults. Such a sensor requirement might not be desirable, and indeed many systems are designed without such possibilities. In the case of the experimental active gas bearing test rig, the sensor setup is indeed without redundancy. Injecting a known disturbance into the system is an alternative approach for exposing the information required to conduct faults isolation. This project has contributed with methods applicable for closed loop control problems. A method for design of a statistical detector for active fault diagnosis therefore is proposed. It was found possible to use the active fault diagnosis scheme for detection and isolation of parametric faults on an active gas bearing. The methods were based on a coprime factorisation of controller and plant. Information was given on how to exploit internal controller signals in order to gain insight into the relevant plant dynamics.

Several contributions have been given on closed loop fault diagnosis.

- A comparison between the Hansen scheme and the modified Hansen scheme showed it is possible to identify the plant using direct injection in the controller. This modification made it straightforward to determine the excitation of the fault signature system to be identified.
- The experimental results from the active gas bearing proved that it is also possible to identify the system dynamics using the modified Hansen scheme. It was found

possible to reach a higher R^2 fit using the modified Hansen scheme than direct PEM identification when good a priori knowledge of the system dynamics is not available. The identification approach based on subspace identification of the fault signature system made it easy to determine the order of the fault signature system based on the Hankel singular values.

- It was shown possible to identify uncertain parameters in an AMB. The bearing is open loop unstable, and identification of the uncertain parameters through the stable system S was found to be possible.

Likewise, several new contributions were presented regarding active fault diagnosis with a focus on active gas bearings. The contributions consists of:

- A method for active fault diagnosis using a matched filter detector was introduced. The method used a moving window to correlate the residual signal with the expected signal. The correlation was used to determine which fault that has happened, while the amplitude of the residual was estimated to determine whether the plant is fault free or not. The amplitude of the residual was therefore used for detection, while the delay was used for isolation.

- The residual signal used for active fault diagnosis in [37] was subject to coloured noise in the fault free case. A whitening filter was presented which made the residual signal subject to white noise in the fault free case. Both a filter for open loop stable and open loop unstable systems were presented which ensured a stable fault signature system. A threshold based on an acceptable FAR was constructed using the whitening filter.

- An approach to determine the optimal frequency of the excitation signal for the active fault diagnosis scheme, when considering periodic input signals, was found. The active fault diagnosis approach presented, disturbs the system during diagnosis. A measure of the excitation disturbance on the output, relative to the residual signal, was therefore formulated. A novel formulation was given which determines a single optimal frequency for a sinusoidal wave with regards to the possible faults on the system.

- Experimental results showed that it is possible to diagnose both sensor and actuator faults on the active gas bearing in the vertical and horizontal direction. The approach was shown possible to use with both a simple proportional and an observer based controller. The proportional controller was designed without any cross coupling gain, to show that diagnosis of faults occurring in the orthogonal direction of the residual is possible due to the internal cross coupling in the plant. The experimental results confirmed that the FAR based threshold method successful. The method was furthermore found easy to implement.

6.1 Future Perspectives

As shown above, the project has resulted in several new contributions for closed loop identification and fault diagnosis. There are however plenty of possible future opportunities based on the results from the project:

- The identification scheme used to identify the active gas bearing in closed loop is strongly linked to performance recovery using a Q parameter. It would be interesting to use the identified fault signature system for controller adaptation. Proper order reduction is required such that the controller order does not increase. Furthermore, adaptation needs to be converging which can make noise a possible issue.

- The active fault diagnosis scheme only uses the delay invoked by the fault signature system for fault isolation at this time. Isolation using both amplitude and phase can improve the gap between faults, making isolation less sensitive to noise. The amplitude estimation is only used for the lower bound on the probability of detection in the faulty case with the current design method.

- Applying the identification and fault diagnosis schemes at higher rotational speed is of interest for closer resemblance with a normal operating point for an active gas bearing. Better understanding of the disturbances associated with a higher rotational speed, and how to decouple them, is required to make the schemes work at such an operating point.

- An approach for finding the optimal sinusoidal signal for excitation used in the active fault diagnosis scheme is presented in the thesis. The approach searches for a single frequency which will allow best detection relative to the disturbance on the outputs of the plant. It might be convenient to design an excitation signal which consists of several frequencies instead in order to obtain a higher signal to disturbance ratio. Further adaptation of the approach is required to accommodate excitation signals consisting of several frequencies instead of a single one.

- The active fault diagnosis method was shown able to diagnose faults on an active gas bearing. The quality of a fault diagnosis scheme is often measured as its FAR relative to its FD. So far, the method has not been compared on such parameters with other fault diagnosis schemes, and it could be of great interest to obtain a clear overview under which circumstances the fault diagnosis scheme is superior to other methods. Such a comparison should be performed experimentally.

- It was proven possible to diagnose parametric sensor and actuator faults in both the vertical and horizontal directions on the active gas bearing. Introducing other parametric faults on the gas bearing which are related to the plant dynamics, would improve the experimental results. The experimental test rig would need to be modified so that changes associated with a single parameter are possible.

- It has been shown possible to identify an open loop stable active gas bearing. Since the method is based on a stabilising feedback gain, it would be interesting to use it on an unstable plant. Increasing the rotational speed of the gas bearing will result in it becoming such an open loop unstable plant. Investigation into the treatment of the mass unbalance in closed loop has to be conducted to apply the modified Hansen scheme at higher rotational speed.

Bibliography

[1] A. Gilchrist, *Industry 4.0: the industrial internet of things*. Apress, 2016.

[2] I. F. Santos, "On the future of controllable fluid film bearings," *Mechanics & Industry*, vol. 12, no. 4, pp. 275–281, 2011.

[3] S. Morosi and I. F. Santos, "On the modelling of hybrid aerostatic-gas journal bearings," *Proceedings of the Institution of Mechanical Engineers, Part J: Journal of Engineering Tribology*, vol. 225, no. 7, pp. 641–653, 2011.

[4] S. Morosi and I. F. Santos, "Active lubrication applied to radial gas journal bearings. part 1: Modeling," *Tribology International*, vol. 44, no. 12, pp. 1949–1958, 2011.

[5] S. Morosi and I. F. Santos, "Experimental investigations of active air bearings," in *Proceedings of ASME turbo expo*, vol. 7, 2012, pp. 901–910.

[6] F. G. Pierart and I. F. Santos, "Steady state characteristics of an adjustable hybrid gas bearing–computational fluid dynamics, modified reynolds equation and experimental validation," *Proceedings of the Institution of Mechanical Engineers, Part J: Journal of Engineering Tribology*, vol. 229, no. 7, pp. 807–822, 2015.

[7] F. G. Pierart and I. F. Santos, "Active lubrication applied to radial gas journal bearings. part 2: Modelling improvement and experimental validation," *Tribology International*, vol. 96, pp. 237–246, 2016.

[8] F. G. Pierart and I. F. Santos, "Adjustable hybrid gas bearing–influence of piezoelectrically adjusted injection on damping factors and natural frequencies of a flexible rotor operating under critical speeds," *Proceedings of the Institution of Mechanical Engineers, Part J: Journal of Engineering Tribology*, vol. 230, no. 10, pp. 1209–1220, 2016.

[9] F. G. Pierart and I. F. Santos, "Lateral vibration control of a flexible overcritical rotor via an active gas bearing–theoretical and experimental comparisons," *Journal of Sound and Vibration*, vol. 383, pp. 20–34, 2016.

[10] L. R. S. Theisen, *Advanced Control of Active Bearings-Modelling, Design and Experiments*. Technical University of Denmark, Department of Electrical Engineering, 2016.

[11] L. R. S. Theisen, F. G. Pierart, H. Niemann, I. F. Santos, and M. Blanke, "Experimental grey box model identification and control of an active gas bearing," in *Vibration Engineering and Technology of Machinery*. Springer, 2015, pp. 963–976.

[12] L. R. Theisen, H. H. Niemann, I. F. Santos, R. Galeazzi, and M. Blanke, "Modelling and identification for control of gas bearings," *Mechanical Systems and Signal Processing*, vol. 70, pp. 1150–1170, 2016.

[13] L. R. Theisen, J. F. Camino, and H. H. Niemann, "An application of gain-scheduled control using state-space interpolation to hydroactive gas bearings," in *Control Applications (CCA), 2016 IEEE Conference on*. IEEE, 2016, pp. 1117–1122.

[14] L. Ljung, "System identification," in *Signal Analysis and Prediction*. Springer, 1998, pp. 163–173.

[15] T. Söderström and P. Stoica, *System identification*. Prentice-Hall, Inc., 1988.

[16] F. Hansen, G. Franklin, and R. Kosut, "Closed-loop identification via the fractional representation: Experiment design," in *1989 American Control Conference*, 1989, pp. 1422–1427.

[17] B. D. Anderson, "From Youla-Kucera to identification, adaptive and nonlinear control," *Automatica*, vol. 34, pp. 1485–1506, 1998.

[18] D. Youla, J. d. Bongiorno, and H. Jabr, "Modern wiener–hopf design of optimal controllers part i: The single-input-output case," *IEEE Transactions on Automatic Control*, vol. 21, no. 1, pp. 3–13, 1976.

[19] D. Youla, H. Jabr, and J. Bongiorno, "Modern wiener-hopf design of optimal controllers–part ii: The multivariable case," *IEEE Transactions on Automatic Control*, vol. 21, no. 3, pp. 319–338, 1976.

[20] M. Verhaegen and P. Dewilde, "Subspace model identification part 1. the output-error state-space model identification class of algorithms," *International journal of control*, vol. 56, no. 5, pp. 1187–1210, 1992.

[21] M. Verhaegen and P. Dewilde, "Subspace model identification part 2. analysis of the elementary output-error state-space model identification algorithm," *International journal of control*, vol. 56, no. 5, pp. 1211–1241, 1992.

[22] P. Van Overschee and B. De Moor, "N4SID: Subspace algorithms for the identification of combined deterministic-stochastic systems," *Automatica*, vol. 30, no. 1, pp. 75–93, 1994.

[23] T. Katayama, *Subspace methods for system identification*. Springer Science & Business Media, 2006.

[24] M. Blanke, M. Kinnaert, J. Lunze, M. Staroswiecki, and J. Schröder, *Diagnosis and fault-tolerant control*. Springer, 2006, vol. 2.

[25] C. Lin and V. Makis, "Optimal bayesian maintenance policy and early fault detection for a gearbox operating under varying load," *Journal of Vibration and Control*, vol. 22, no. 15, pp. 3312–3325, 2016.

[26] R. Isermann, "Model-based fault-detection and diagnosis–status and applications," *Annual Reviews in control*, vol. 29, no. 1, pp. 71–85, 2005.

[27] P. Frank, S. Ding, and T. Marcu, "Model-based fault diagnosis in technical processes," *Transactions of the Institute of Measurement and Control*, vol. 22, no. 1, pp. 57–101, 2000.

[28] X. J. Zhang, "Auxiliary signal design in fault detection and diagnosis," 1989.

[29] L. Rakoto, J. Schorsch, and M. Kinnaert, "Modelling hydraulic pitch actuator for wind turbine simulation under healthy and faulty conditions," *IFAC-PapersOnLine*, vol. 48, no. 21, pp. 577–582, 2015.

[30] S. L. Campbell and R. Nikoukhah, *Auxiliary signal design for failure detection*. Princeton University Press, 2004.

[31] G. R. Marseglia and D. M. Raimondo, "Active fault diagnosis: A multi-parametric approach," *Automatica*, vol. 79, pp. 223–230, 2017.

[32] I. Punčochář, J. Širokỳ, and M. Šimandl, "Constrained active fault detection and control," *IEEE Transactions on Automatic Control*, vol. 60, no. 1, pp. 253–258, 2015.

[33] R. Nikoukhah, F. Delebecque, S. Campbell, and K. Horton, "Multi-model identification and the separability index," in *Proceedings of the 14th International Symposium of the Mathematical Theory of Networks and Systems*, 2000.

[34] D. M. Raimondo, R. D. Braatz, and J. K. Scott, "Active fault diagnosis using moving horizon input design," in *Control Conference (ECC), 2013 European*. IEEE, 2013, pp. 3131–3136.

[35] H. Niemann, "Fault tolerant control based on active fault diagnosis," in *American Control Conference, 2005. Proceedings of the 2005*. IEEE, 2005, pp. 2224–2229.

[36] H. Niemann, "A setup for active fault diagnosis," *IEEE Transactions on Automatic Control*, vol. 51, no. 9, pp. 1572–1578, 2006.

[37] N. Poulsen and H. Niemann, "Active fault diagnosis based on stochastic tests," *International Journal of Applied Mathematics and Computer Science*, vol. 18, no. 4, pp. 487–496, 2008.

[38] W. Moustafa, O. Cousinard, F. Bolaers, K. Sghir, and J. Dron, "Low speed bearings fault detection and size estimation using instantaneous angular speed," *Journal of Vibration and Control*, vol. 22, no. 15, pp. 3413–3425, 2016.

[39] J. P. Amezquita-Sanchez, M. Valtierra-Rodriguez, D. Camarena-Martinez, D. Granados-Lieberman, R. J. Romero-Troncoso, and A. Dominguez-Gonzalez, "Fractal dimension-based approach for detection of multiple combined faults on induction motors," *Journal of Vibration and Control*, vol. 22, no. 17, pp. 3638–3648, 2016.

[40] L. R. Theisen, H. H. Niemann, R. Galeazzi, and I. F. Santos, "Enhancing damping of gas bearings using linear parameter-varying control," *Journal of Sound and Vibration*, vol. 395, pp. 48–64, 2017.

[41] M. Atiyah, *Introduction to commutative algebra*. Westview Press, 1994.

[42] M. Vidyasagar, "Control system synthesis: A factorization approachmit press," *Cambridge, MA*, 1985.

[43] T. T. Tay, I. M. Y. Mareels, and J. B. Moore, Eds., *High Performance Control*. Chicago: Birkhauser, 1998.

[44] K. Zhou and J. C. Doyle, *Essentials of robust control*. Prentice hall Upper Saddle River, NJ, 1998, vol. 104.

[45] H. Niemann, "Controller parameterization based on reduced order models," *American Control Conference, ACC18, Milwaukee, WI, USA*, vol. -, no. -, pp. –, 2018.

[46] H. Niemann and N. K. Poulsen, "Estimation of parametric fault in closed-loop systems," in *2015 American Control Conference (ACC)*. IEEE, 2015, pp. 201–206.

[47] T. Sugie and T. Ono, "On doubly coprime factorizations," *Linear Algebra and its Applications*, vol. 122, pp. 681–696, 1989.

[48] S. Morosi, *From Hybrid to Actively-Controlled Gas Lubricated Bearings–Theory and Experiment*. DTU Mechanical Engineering, 2011.

[49] F. G. P. Vásquez, *Model-Based Control Design for Flexible Rotors Supported by Active Gas Bearings-Theory & Experiment*. Technical University of Denmark, 2016.

[50] L. R. Theisen, H. H. Niemann, R. Galeazzi, and I. F. Santos, "Enhancing damping of gas bearings using linear parameter-varying control," *Journal of Sound and Vibration*, 2017.

[51] J. J. Moré, "The levenberg-marquardt algorithm: implementation and theory," in *Numerical analysis*. Springer, 1978, pp. 105–116.

[52] A. Varga, "Balancing free square-root algorithm for computing singular perturbation approximations," in *Decision and Control, 1991., Proceedings of the 30th IEEE Conference on*. IEEE, 1991, pp. 1062–1065.

[53] M. Nyberg and E. Frisk, "Residual generation for fault diagnosis of systems described by linear differential-algebraic equations," *IEEE Transactions on Automatic Control*, vol. 51, no. 12, pp. 1995–2000, 2006.

[54] S. Ding, *Model-based fault diagnosis techniques: design schemes, algorithms, and tools*. Springer Science & Business Media, 2008.

[55] P. Zhang and S. X. Ding, "An integrated trade-off design of observer based fault detection systems," *Automatica*, vol. 44, no. 7, pp. 1886–1894, 2008.

[56] S. Ding, "Application of factorization and gap metric techniques to fault detection and isolation part i: A factorization technique based fdi framework," *IFAC-PapersOnLine*, vol. 48, no. 21, pp. 113–118, 2015.

[57] S. Ding, "Application of factorization and gap metric techniques to fault detection and isolation part ii: Gap metric technique aided fdi performance analysis," *IFAC-PapersOnLine*, vol. 48, no. 21, pp. 119–124, 2015.

[58] T. T. Georgiou, "On the computation of the gap metric," *Systems & Control Letters*, vol. 11, no. 4, pp. 253–257, 1988.

[59] M. Šimandl and I. Punčochář, "Active fault detection and control: Unified formulation and optimal design," *Automatica*, vol. 45, no. 9, pp. 2052–2059, 2009.

[60] S. L. Campbell, K. G. Horton, and R. Nikoukhah, "Auxiliary signal design for rapid multi-model identification using optimization," *Automatica*, vol. 38, no. 8, pp. 1313–1325, 2002.

[61] L. H. Chiang, E. L. Russell, and R. D. Braatz, *Fault detection and diagnosis in industrial systems*. Springer Science & Business Media, 2000.

[62] F. Kerestecioğlu* and I. Cetin, "Optimal input design for the detection of changes towards unknown hypotheses," *International Journal of Systems Science*, vol. 35, no. 7, pp. 435–444, 2004.

[63] F. Gustafsson and F. Gustafsson, *Adaptive filtering and change detection*. Wiley New York, 2000, vol. 1.

[64] S. M. Kay, "Fundamentals of statistical signal processing: Detection theory, vol. 2," 1998.

[65] A. Packard and J. Doyle, "The complex structured singular value," *Automatica*, vol. 29, no. 1, pp. 71–109, 1993.

Publication P1

Identifying parameters in active magnetic bearing system using LFT formulation and Youla factorisation

Identifying parameters in active magnetic bearing system using LFT formulation and Youla factorization

Jonas S. Lauridsen[1], André K. Sekunda[2], Ilmar F. Santos[3] and Henrik Niemann[4]

[1]) Department of Mechanical Engineering, Technical Unversity of Denmark, Kongen Lyngby, Denmark

[2]) Department of Electrical Engineering, Technical University of Denmark, Kongen Lyngby, Denmark

[3]) Department of Mechanical Engineering, Technical Unversity of Denmark, Kongen Lyngby, Denmark

[4]) Department of Electrical Engineering, Technical University of Denmark, Kongen Lyngby, Denmark

E-mail: jonlau@mek.dtu.dk, aksek@elektro.dtu.dk, ifs@mek.dtu.dk, hhn@elektro.dtu.dk

Abstract

In this paper, a method for identifying uncertain parameters in a rotordynamic system composed of a flexible rotating shaft, rigid discs and two radial active magnetic bearings is presented. Shaft and disc dynamics are mathematically described using a Finite Element (FE) model while magnetic bearing forces are represented by linear springs with negative stiffness. Bearing negative stiffness produces an unstable rotordynamic system, demanding implementation of feedback control to stabilize the rotordynamic system. Thus, to identify the system parameters, closed-loop system identification techniques are required.

The main focus of the paper relies on how to effectively identify uncertain parameters, such as stiffness and damping force coefficients of bearings and seals in rotordynamic systems. Dynamic condensation method, i.e. pseudo-modal reduction, is used to obtain a reduced order model for model-based control design and fast identification.

The paper elucidates how nodal parametric uncertainties, which are easily represented in the full FE coordinate system, can be represented in the new coordinate system of the reduced model. The uncertainty is described as a single column vector of the system matrix A of the full FE model while it is represented

as several elements spread over multiple rows and columns of the system matrix of the reduced model. The parametric uncertainty, for both the full and reduced FE model, is represented using Linear Fractional Transformation (LFT). In this way the LFT matrices represent the mapping of the uncertainties in and out of the full and reduced FE system matrices. Scaling the LFT matrices easily leads to the amplitudes of the uncertainty parameters.

Youla Parametrization method is applied to transform the identification problem into an open-loop stable problem, which can be solved using standard optimization methods.

An example shows how to decouple and identify an uncertainty in the linear bearing stiffness of a reduced FE rotordynamic system.

1 Introduction

The Active Magnetic Bearing (AMB) has many advantages compared to conventional fluid film bearings and ball bearings, such as no mechanical contact, no lubrication, low maintenance, practically no friction, low vibration level and high rotational speed, which makes it extremely useful in special environments such as cleantech, subsea among others. Today the AMB is widely used on several types of industrial applications such as centrifugal compressors, turbo expanders, blood pumps, centrifuges, machine drilling tools, energy storage flywheel etc. The AMBs have been applied in turbomachinery equipment with capacities that range from a few kilowatts up to 29,000 kW and with operation speed up to 60,000 RPM.

Rotors levitated by AMB's are essentially unstable systems whose properties cause several challenges to the design of active control system due to: gyroscopic effects, mass unbalance, rotor flexibility, aerodynamic excitations among others. It is essential to have a global mathematical model which precisely predicts the real plant dynamics, in order to design a high performance control system and to predict its stability and performance.

Due to assembly tolerances and simplified model assumptions, discrepancies between the model and real plant typically exist and adjustment of some of the model parameters are often needed. System identification techniques should therefore be applied to find the deviation between model and the real plant, toward more accurate global mathematical models, which in turn makes improved controller design possible.

Due to the fact that AMB systems are open-loop unstable, input-output data is only possible to gather in a closed-loop scheme with a stabilizing controller. Standard open-loop identification methods are therefore ill suited [3] since they typically assume that the measurement noise is uncorrelated with the system

inputs and outputs, which does not holds, once the controller action links input and output signals.

There are several methods which take into account that the plant is part of a closed loop scheme [3, 7, 14]. Each method has advantages and the method used in this paper is chosen for the easy translation to fault diagnosis of parameters. In this paper a method for closed-loop identification of the rotordynamic system (turboexpander) using a coprime factorization is proposed. The method is based on the well known Hansen scheme [17]. However classical identification using the Hansen scheme makes it difficult to take advantage of physical knowledge of the plant. The method proposed in this paper is therefore an extension which makes it possible to identify specific plant parameters through the identification of the open loop error dynamics. The method proposed in this paper has also been applied to estimate parametric faults in systems[1, 2].

The main originality of the work relies on parametrization and identification of uncertainties in FE rotordynamic systems. Focus is put on how LFT representation of a reduced system can be obtained based on a full FE representation of a rotordynamic system.

This paper deals with a 700 kW turboexpander supported by AMB designed for air separation units. The turboexpander can essentially be considered as a flexible rotor spinning at angular velocities up to 31500 RPM, levitated by AMB forces. In this paper the modelling of the shaft is carried out using FE method including gyroscopic effects [11, 12], and the forces of the AMB have been characterized using the basic laws of electromagnetism [10].

The paper is structured as follows: Section II introduces the identification method of unstable systems based on Youla parmetrization; Section III contains a description of the system to be identified, modelling and reduction of the system, followed by representation of the uncertainty; Section IV discuss results obtained from a simulation example of applying the identification method to a plant with parameter uncertainties; Section V contains a conclusion on the results presented in the paper.

2 Method

Identification of system using Coprime factorization

In this section a method for identification of closed-loop systems using coprime factorization is given. The method uses the coprime factorisation of plant and controller and is based on the theory outlined in [4]. The closed-loop scheme is given as shown in Fig. 0.1. Let $G = G(0)$ be the nominal plant i.e. initial

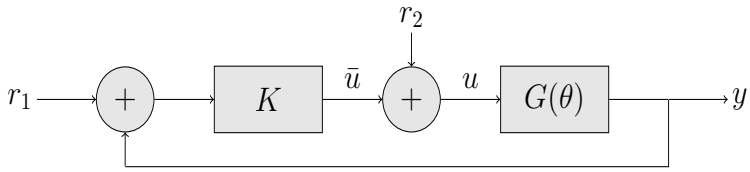

Figure 0.1: Closed-loop system representation.

model guess and K be a stabilising controller to both the real plant $G(\theta)$ and the nominal plant G, where θ is the parameter uncertainty. Then G and K are given as:

$$G = NM^{-1} = \tilde{M}^{-1}\tilde{N} \tag{1}$$

$$K = UV^{-1} = \tilde{V}^{-1}\tilde{U} \tag{2}$$

For the 8 matrices given in Eq. (1) and Eq. (2) to be coprime factors, the double Bezout identity shown in Eq. (3) have to be satisfied.

$$\begin{bmatrix} I & 0 \\ 0 & I \end{bmatrix} = \begin{bmatrix} \tilde{V} & -\tilde{U} \\ -\tilde{N} & \tilde{M} \end{bmatrix} \begin{bmatrix} M & U \\ N & V \end{bmatrix} = \begin{bmatrix} M & U \\ N & V \end{bmatrix} \begin{bmatrix} \tilde{V} & -\tilde{U} \\ -\tilde{N} & \tilde{M} \end{bmatrix} \tag{3}$$

With a coprime factorization of the nominal plant G and of the controller K stabilizing both the real plant $G(\theta)$ and the nominal plant $G(0)$, Eq. (4) gives a parametrization of all stabilizing controllers, for the nominal plant, using the stable transfer matrix Q, from ϵ to η shown in Fig. 0.2 [4].

$$K(Q) = (\tilde{V} + Q\tilde{N})^{-1}(\tilde{U} + Q\tilde{M}) \tag{4}$$

This controller can be represented as a LFT [6].

$$K(Q) = \mathcal{F}_l\left(\begin{bmatrix} UV^{-1} & \tilde{V}^{-1} \\ V^{-1} & -V^{-1}N \end{bmatrix}, Q\right) \tag{5}$$

$$= \mathcal{F}_l(J_k, Q) \tag{6}$$

Equivalent, all plants stabilized by K can be parameterized as Eq. (9). Taking advantage of the relationship given in Eq. (7) between the parametrized controller $K(Q)$ and the parametrized plant $G(S)$ [4], it is possible to show that Eq. (9) is a parametrization of all plants stabilized by the controller K using the stable system $S(\theta)$ being the transfer matrix from η to ϵ shown in Fig. 0.2.

$$S = \mathcal{F}_l(J_k, G(S)) \tag{7}$$

$$\epsilon = S(\theta)\eta \tag{8}$$

$$G(S) = (\tilde{M} + S\tilde{U})^{-1}(\tilde{N} + S\tilde{V})^{-1} \tag{9}$$

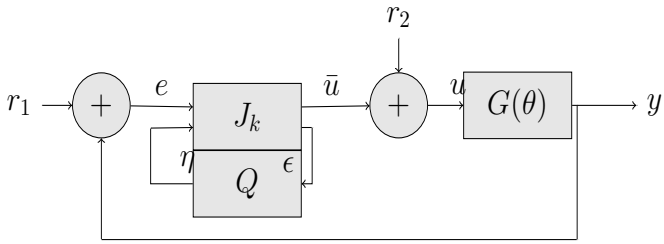

Figure 0.2: Closed-loop system representation with all stabilizing controllers parametrised using a stable transfer matrix Q.

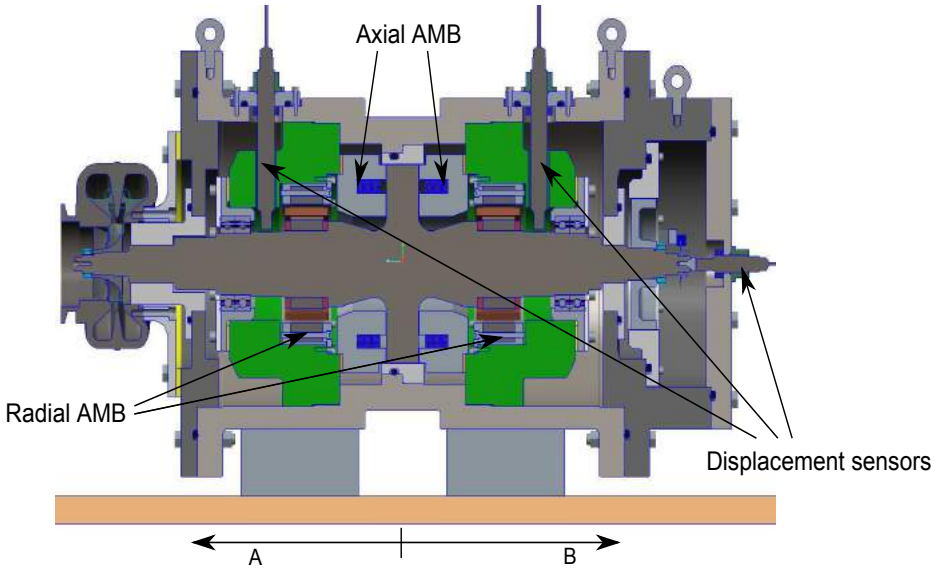

Figure 0.3: Cross-section of the turboexpander testrig.

If the nominal plant is equal to the real plant, $S(\theta)$ is zero. As the nominal plant differs from the real plant, $S(\theta)$ increases and can thus be considered as a expression of the deviation between the nominal and the real plant.

A standard Luenberger observer is used for implementation of $S(\theta)$ for simulation examples. However any controller with its associated coprime factorization can be used. For a system such as shown in Fig. 0.2, the closed-loop transfer function can be written as [1].

$$\begin{bmatrix} y \\ u \\ \epsilon \end{bmatrix} = T_{cl}(S) \begin{bmatrix} r_1 \\ r_2 \\ \eta \end{bmatrix} \tag{10}$$

$$T_{cl}(S) = \begin{bmatrix} (N+VS)\tilde{U} & (N+VS)\tilde{V} & N+VS \\ (M+US)\tilde{U} & (M+US)\tilde{V} & M+US \\ \tilde{M}+S\tilde{V} & \tilde{N}+S\tilde{U} & S \end{bmatrix} \tag{11}$$

With input and output of the system defined, the uncertainties need to be given in regards to $S(\theta)$. Parameter uncertainties are given using a LFT description. Plant uncertainties are therefore given as in Eq. (12).

$$G(\theta) = \mathcal{F}_l \left(\begin{bmatrix} G_{yu} & G_{yw} \\ G_{zu} & G_{zw} \end{bmatrix}, \theta \right) \tag{12}$$

Here θ is a diagonal matrix with a parameter uncertainty in each diagonal element. It is worth noticing that $G(0)$ is equivalent to the nominal plant. A description of how to represent the parameter uncertainties as an LFT is shown in Section 3. With the uncertainties defined as in Eq. (12), $S(\theta)$ is found in [1] to be

$$S(\theta) = \mathcal{F}_l \left(\begin{bmatrix} 0 & \tilde{M}G_{yw} \\ G_{zu}M & G_{zw} + G_{zu}U\tilde{M}G_{yw} \end{bmatrix}, \theta \right) \tag{13}$$

Due to η not being correlated with the disturbances r_1 and r_2, Eq. (10) can be used for identification of the open loop error S. Estimation of the open loop error S from η to ϵ simplifies to Eq. (14), which can be considered as an open-loop identification problem of the stable system $S(\theta)$ with uncorrolated noise in the prediction [4].

$$\epsilon = S(\theta)\eta + D_1 r_1 + D_2 r_2 \tag{14}$$

Identification of parameter uncertainties using a LFT scheme is a well studied subject in open-loop identification of Linear Parameter Varying (LPV) systems [7, 8, 9]. The approach is to define a cost function and minimize the error between the measured and calculated output of the system. The cost function is given in Eq. (15) in its approximate quadratic form.

$$J(\theta) = \int_0^t \frac{1}{2}(\epsilon - S(\theta)\eta)^2 dt \tag{15}$$

The goal is to find the global minima of (15) which can be done using several different methods. In this paper the MATLAB function `fminsearch` is used,

which is an general unconstrained nonlinear optimization method. Other methods, like gradient methods, has shown to yield faster convergence for specific types of plants, however this has not been the main focus.

3 System and Uncertainty Representation

In this section, the rotordynamic system is described and it is shown how dynamic uncertainties from such a system can be extracted and represented in Linear Fractional Transformation (LFT) form.

The real system

A cross-section schematic of the turboexpander investigated is shown in Fig. 0.3. The turboexpander essentially consists of a shaft levitated using axial and radial AMBs. It is assumed that the only forces acting on the rotor are the left and right radial AMB. The displacement sensors are placed close to the AMBs. The placement of the sensors and actuators will be denoted by A_x, A_y and B_x, B_y.

The analysis will be focused on rotor lateral movements and for simplicity the rotor axial movements will not be investigated. The term AMB will therefore refer to the radial AMBs in the following.

Model of AMBs

The model of the magnetic bearing is simplified to describe the forces acting on the rotor as function of the rotor lateral displacements s and the control current i_x. The linearized expression of the forces are given as [10]

$$f_b(i_x, s) = K_i i_x + K_s s \tag{16}$$

where K_i are K_s are constants. K_s can be considered as the stiffness of the bearing forces which is negative and thus makes the system open-loop unstable. The dynamics of the electromechanical system including the inductance of the coil and the amplifiers have been neglected.

Model of shaft

The rotating shaft has been modelled using the FE method and Bernoulli-Euler beam theory taking into account the gyroscopic effects of the shaft and discs [11, 12]. The shaft have been dicretized in 40 node points with 4 degrees of freedom each, which is x and y direction, and the rotation around the x and y axes, which

yields 320 states in total. The discretization of node points of the shaft and the placement of sensors and AMBs is shown in Fig. 0.4. The goal is to control the rigid body motion of the rotating shaft and it is possible to obtain a reduced model of the rotor-bearing system with 8 states by using pseudo-modal reduction [15, 16] and removing all flexible modes, described in the following section. The reduction method are later used for LFT representation of uncertainties in the reduced FE plant model G.

Hence a MIMO system with 4 inputs (control current) and 4 outputs (rotor displacement) and 8 states have been obtained.

Model Reduction

The full order rotordynamic system G_f consisting of the finite element model of the shaft and negativ stiffness forces from the AMB can be written in state space form

$$\dot{x}_f = A_f x_f + B_f u, \quad y = C_f x_f \tag{17}$$

The system left and right eigenvectors (U_l and U_r) are found by solving the eigenvalue problem

$$A_f U_r = \lambda U_r \tag{18}$$

$$A_f^T U_l = \lambda U_l \tag{19}$$

The system can be sorted by the undamped natural frequencies, $|\mathcal{I}(\lambda)|$, since only the low frequency dynamics are of interest. The eigenvectors for the cor-

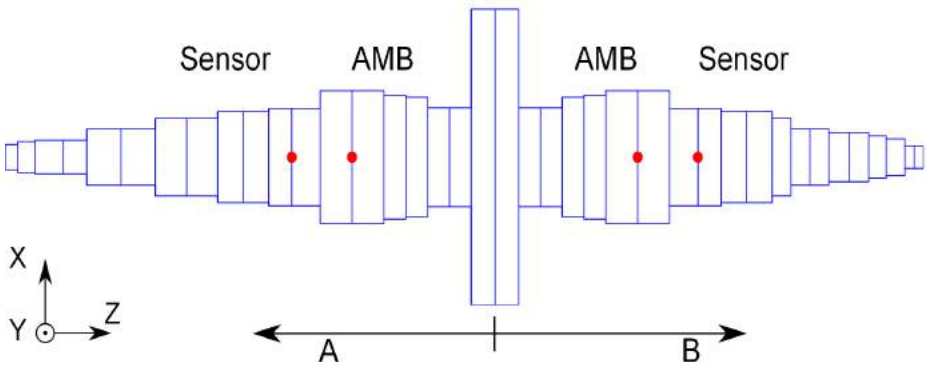

Figure 0.4: Discretization of the shaft. Placement of sensors and AMBs are shown.

responding eigenvalues are used to create right and left transformation matrices

$$T_r = \begin{bmatrix} U_{r_1} & U_{r_2} & \dots & U_{r_n} \end{bmatrix} \tag{20}$$

$$T_l = \begin{bmatrix} U_{l_1} & U_{l_2} & \dots & U_{l_n} \end{bmatrix} \tag{21}$$

The reduced system is then given as

$$\dot{x}_c = A_c x_c + B_c u_c, \quad y_c = C_c x_c \tag{22}$$

where

$$x_c = {T_l}^T x_f \tag{23}$$

$$A_c = {T_l}^T A_f T_r \tag{24}$$

$$B_c = {T_l}^T B_f \tag{25}$$

$$C_c = C_f T_r \tag{26}$$

In this way the system is decomposed into a reduced system A_c which contains the dominant dynamics and the residual system A_{res} containing the residual dynamics, as shown below

$$\begin{bmatrix} \dot{x}_c \\ \dot{x}_{res} \end{bmatrix} = \begin{bmatrix} A_c & 0 \\ 0 & A_{res} \end{bmatrix} \begin{bmatrix} x_c \\ x_{res} \end{bmatrix} + \begin{bmatrix} B_c \\ B_{res} \end{bmatrix} u \tag{27}$$

Fig. 0.5 shows the singular values of the full and the reduced system. It is seen that the reduced 8 states system fits the dynamics very well up to approx. 20×10^3 rad/s which is above the frequency range of interest. The singular values are shown for the rotordynamic system when angular velocity is 31500 RPM since the system identification is assumed to take place at nominal operational conditions.

Complex separation

The reduced state space model obtained by modal reduction consist of complex coefficients. This model can be rewritten to real form with $2n$ states, one state to represent the real part and one for the imaginary part [13]. This can be done by transforming the T_l^T and T_r to

$$T_{r_{sep}} = \begin{bmatrix} \mathcal{R}(T_{r_1}) & -\mathcal{I}(T_{r_1}) & \dots & \mathcal{R}(T_{r_n}) & -\mathcal{I}(T_{r_n}) \end{bmatrix} \tag{28}$$

$$T_{l_{sep}} = \begin{bmatrix} \mathcal{R}(T_{l_1}) & \mathcal{I}(T_{l_1}) & \dots & \mathcal{R}(T_{l_n}) & \mathcal{I}(T_{l_n}) \end{bmatrix} \tag{29}$$

Such that the new system G_s with new state vector x_s and the matrices A_s, B_s and C_s are given as

$$\dot{x}_s = A_s x_s + B_s u, \quad y = C_s x_s \tag{30}$$

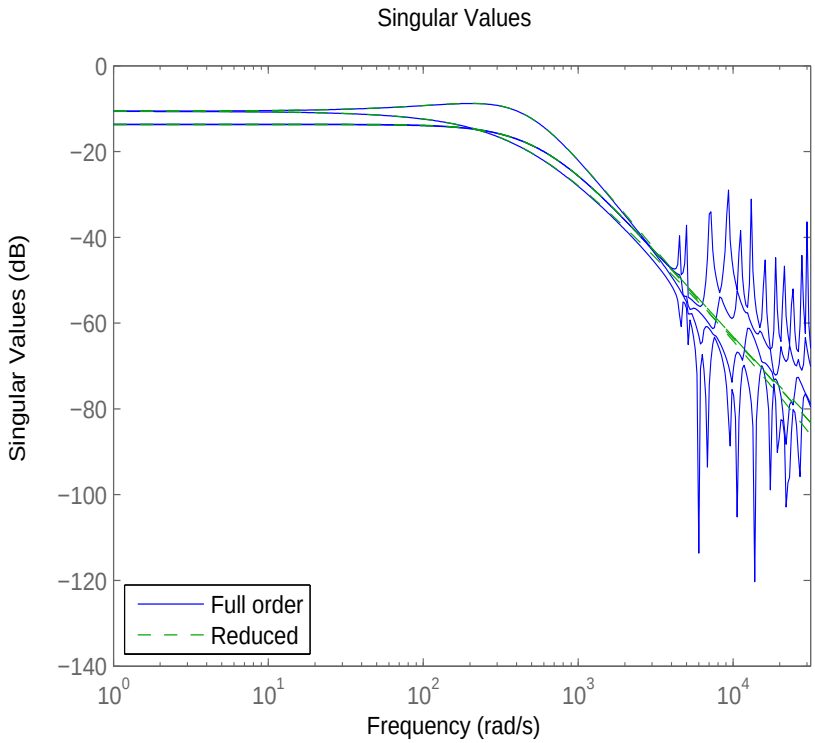

Figure 0.5: Singular values of the full and the reduced rotor dynamic system shown at nominal angular velocity of 31500 RPM

$$x_s = \begin{bmatrix} \mathcal{R}(x_{c_1}) & \mathcal{I}(x_{c_1}) & \dots & \mathcal{R}(x_{c_n}) & \mathcal{I}(x_{c_n}) \end{bmatrix}^T, \tag{31}$$

$$A_s = \begin{bmatrix} \ddots & & 0 \\ & A_{c_{ii}} & \\ 0 & & \ddots \end{bmatrix}, \qquad A_{c_{ii}} = \begin{bmatrix} \mathcal{R}(\lambda_i) & -\mathcal{I}(\lambda_i) \\ \mathcal{I}(\lambda_i) & \mathcal{R}(\lambda_i) \end{bmatrix}, \tag{32}$$

$$B_s = [\mathcal{R}(B_{c_1}), \mathcal{I}(B_{c_1}) \dots \mathcal{R}(B_{c_n}), \mathcal{I}(B_{c_n})]^T, \tag{33}$$

$$C_s = [\mathcal{R}(C_{c_1}), -\mathcal{I}(C_{c_1}) \dots \mathcal{R}(C_{c_n}), -\mathcal{I}(C_{c_n})], \tag{34}$$

Reduction of uncontrollable and unobservable modes

After complex separation the system consist of $2n$ states. By considering which states that is controllable and which are observable it becomes clear that some states are uncontrollable and can be removed. A similarity transform T_{sim} exists

which transforms the complex separated system G_s into a controllable part and an uncontrollable part which can be removed

$$\bar{A} = T_{sim} A_s T_{sim}^T \tag{35}$$
$$\bar{B} = T_{sim} B_s \tag{36}$$
$$\bar{C} = C_s T_{sim}^T \tag{37}$$

and the transformed system has the form

$$\bar{A} = \begin{bmatrix} A_{ncon} & 0 \\ A_{21} & A_{con} \end{bmatrix}, \; \bar{B} = \begin{bmatrix} 0 \\ B_{con} \end{bmatrix}, \; \bar{C} = \begin{bmatrix} 0 \\ B_{con} \end{bmatrix} \tag{38}$$

where A_{con}, B_{con}, C_{con} represents the controllable system.

The final transformation matrices denoted T_R and T_L can thus be found as the lower part of the products $T_{r_{sep}} T_{sim}^T$ and $T_{l_{sep}}^T T_{sim}$

$$T_{r_*} = T_{r_{sep}} T_{sim}^T \tag{39}$$
$$T_{l_*} = T_{sim} T_{l_{sep}}^T \tag{40}$$
$$T_R = T_{r_*}(:\,,\; n{+}1{:}2n) \tag{41}$$
$$T_L = T_{l_*}(n{+}1{:}2n\;,\; :) \tag{42}$$

Thus the final reduced system matrices can be written as

$$A = T_L A_f T_R \tag{43}$$
$$B = T_L B_f \tag{44}$$
$$C = C_f T_R \tag{45}$$

The transformation matrices T_R and T_L will later be used to map the uncertainty from the full system to the reduced system.

Identification of parameter uncertainty using LFT of full system

LFT can be used for representing a nominal system with a parameter uncertainty. A lower LFT can be written as [6]

$$\mathcal{F}_l(G, \theta) = G_{yu} + G_{yw}\theta(I - G_{zw}\theta)^{-1} G_{zu} \tag{46}$$

If G_{zw} is zero, the LFT representation can be simplified to

$$\mathcal{F}_l(G, \theta) = G_{yu} + G_{yw}\theta G_{zu} \tag{47}$$

G_{yw} and G_{zu} can be considered as the mapping of the uncertainty in and out of the the states of the system, where G_{yu} can be considered as the nominal system as if the uncertainty is zero ($G(0)$).

It is chosen to investigate the possibility of identifying the uncertainty of a parameter in the system. A change in the negative bearing stiffness in a single direction, in a single position, is considered, which happens at e.g. B_y, see Fig. 0.4.

It is therefore investigated if the change in negative stiffness can be described by an LFT using G_{yw_f} and G_{zu_f} scaled by θ, on the form shown in Eq. (47). The subscript f denotes the full system i.e. the full finite element system with 40 nodes and 320 states (before model reduction). It can be proved that a change in stiffness (or damping) at a single direction at e.g. B_y corresponds to a change in a single column of system matrix A, which corresponds to the node j where the stiffness has changed.

$$A_{\Delta_f} = \begin{bmatrix} 0 & \dots & 0 & a_{1,j} & 0 & \dots & 0 \\ 0 & \dots & 0 & a_{2,j} & 0 & \dots & 0 \\ \vdots & \ddots & \vdots & \vdots & \vdots & \ddots & \vdots \\ 0 & \dots & 0 & a_{i,j} & 0 & \dots & 0 \end{bmatrix} \tag{48}$$

G_{yw_f} and G_{zu_f} can then easily be obtained by selecting G_{yw_f} to be the column of system matrix A which has changed

$$G_{yw_f} = \begin{bmatrix} a_{1,j} \\ a_{2,j} \\ \vdots \\ a_{i,j} \end{bmatrix} \tag{49}$$

and select G_{zu} to be

$$G_{zu_f} = \begin{bmatrix} 0 & 0 & \dots & 1 & \dots & 0 & 0 \end{bmatrix} \tag{50}$$

where 1 should be placed at the position of column which has changed in A (node position). θ is simply selected to 1 which would correspond to a 100% change in the system parameter.

LFT of reduced system

The LFT of the reduced system can now simply be described using the transformation matrices given in Eq. (41) and Eq. (42) to transform the uncertainty mapping G_{yw_f} and G_{zu_f} from the full finite element system to the reduced system

on modal form given by Eq. (43).

$$G_{yw} = T_L G_{yw_f} \tag{51}$$
$$G_{zu} = G_{zu_f} T_R \tag{52}$$

4 Results

This section demonstrates that it is possible to identify an uncertainty using the method introduced in Section 2 on a rotordynamic system and uncertainty representation as presented in Section 3.

Before identification of the plant is conducted, it is shown why open-loop identification of the plant is not possible. On Fig. 0.6 the poles and zeros of real plant $G(\theta)$ is shown, hence the real plant to be identified. It is easy to see that any input given to the plant would make the output increase to infinity, due to poles in the right half plane. Such right half plane poles are not present in $S(\theta)$, as can be seen in Fig. 0.7, why open-loop identification of $S(\theta)$ is possible. A simulation is conducted with a controller stabilizing both nominal model plant and the real plant. A stiffness reduction of 50 % ($\theta = 0.5$) is introduced to the real plant compared to the nominal plant model.

The frequency response of the nominal and real plants are shown in Fig. 0.8. The plot shows that the uncertainty injected through the LFT change the dynamics of the system.

For the identification, a random binary signal is chosen for η and both r_1 and r_2 are set to 0. The variables η, r_1 and r_2 are shown in Fig. 0.2. A time period of 0.5 s and a time step of 0.001 s are chosen. The uncertainty, θ, is identified to be 0.502 which is practically the same as the theoretical result ($\theta = 0.5$).

5 Conclusion

The problem of estimating uncertain dynamics in a rotordynamic system supported by AMB is considered. Finite element and modal reduction methods are applied to establish a reduced model of the system and to parametrize uncertain dynamics in the system into uncertain parameters, which then can be identified. Youla parametrization theory is applied to show how the unstable system in connection with a standard observer based feedback structure can be used to transform the identification problem into an open loop stable formulation describing the change of dynamics between the modelled system and the real system. This method is proposed for rotordynamic systems, in which the

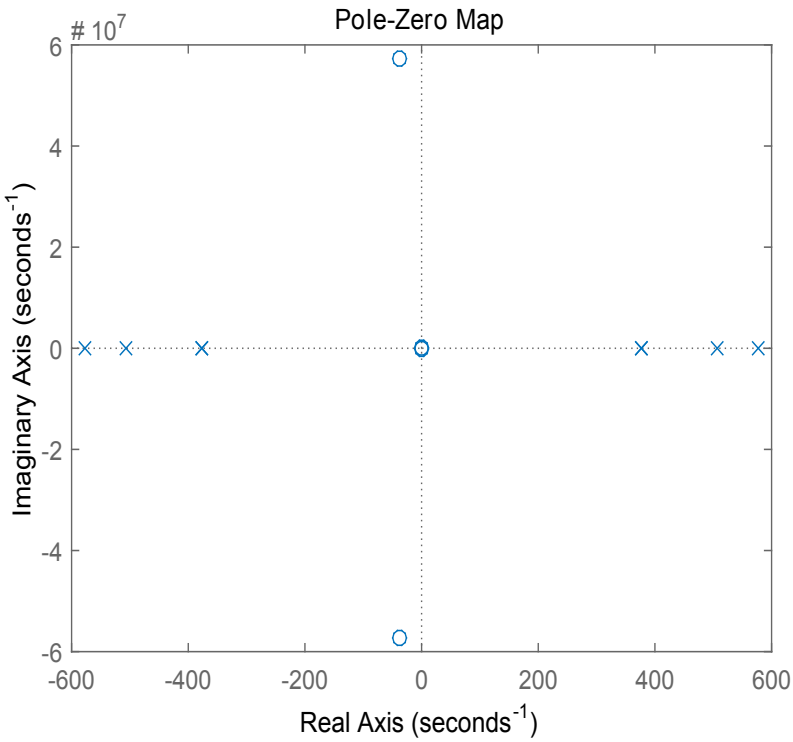

Figure 0.6: Pole-Zero plot of $G(\theta)$. Poles are marked using $\times$'s and zeros are marked using $\circ$'s.

finite element model of shaft is known in advance, but where e.g. bearing or seal dynamics is uncertain.

From the example it can be concluded that the method works when considering an ideal case where the bearing stiffness in one direction is uncertain. The ideal case is used to give a clear overview of the methodology proposed. The example shows that the bearing stiffness is efficiently identified, while the shaft is spinning at nominal angular speed.

There are various possibilities to be investigated with this method such as to extend the shaft model to include flexible modes, identify multiples parameters simultaneously, investigate the effect of disturbances, investigate the effect of uncertain shaft dynamics and carry out experimental tests.

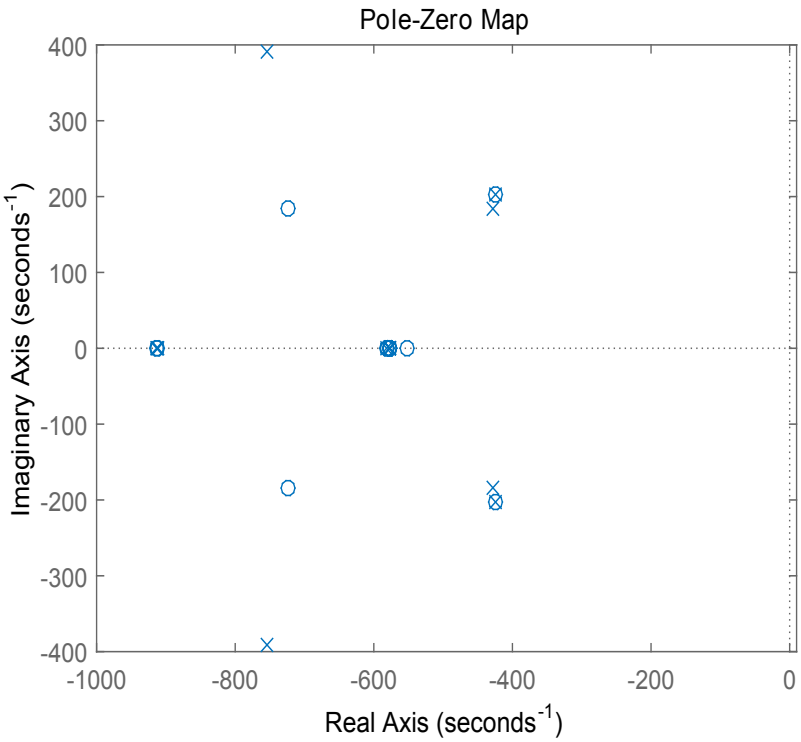

Figure 0.7: Pole-Zero plot of $S(\theta)$. Poles are marked using $\times$'s and zeros are marked using $\circ$'s.

Bibliography

[1] Niemann H. and Poulsen N. K, Estimation of parametric fault in closed-loop systems, 2015 American Control Conference(ACC) June 1-3, Chicago, Illinois, USA.

[2] Niemann H., Stoustrup J., and Poulsen N. K, "Controller modification applied for active fault detection." American Control Conference (ACC), 2014.

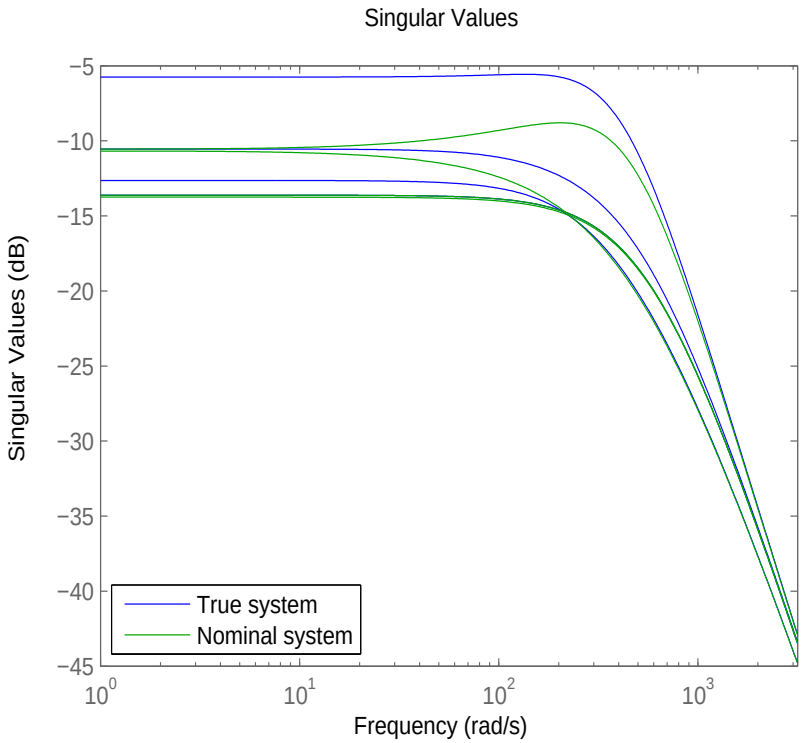

Figure 0.8: Comparison of the singular values of the real system to be identified and the nominal system

[3] Anderson B. D. O., "From Youla Kucera to identification, adaptive and nonlinear control." Automatica 34.12 1998: 1485-1506.

[4] Tay, T. T., Mareels I., and Moore J. B., "High performance control" Springer Science & Business Media, 1998.

[5] Niemann H., "Architecture for fault diagnosis and fault-tolerant control", Department of Electrical Engineering DTU, 2015.

[6] Zhou K., and Doyle J. C. "Essentials of robust control", Vol. 180. Upper Saddle River, NJ: Prentice hall, 1998.

[7] Wolodkin G., Rangan S. and Poolla K. "An LFT approach to parameter estimation." American Control Conference, 1997. Proceedings of the 1997. Vol. 3. IEEE, 1997.

[8] Hsu K, et al. "An LFT approach to parameter estimation." Automatica 44.12 (2008): 3087-3092.

[9] Casella F. and Marco L., "LPV/LFT modelling and identification: overview, synergies and a case study." Computer-Aided Control Systems, 2008. CACSD 2008. IEEE International Conference on. IEEE, 2008.

[10] H Bleuler, et al. "Magnetic bearings: theory, design, and application to rotating machinery", Eds. Gerhard Schweitzer, and Maslen E. H., Springer Science & Business Media, 2009.

[11] Nelson, H. D., and McVaugh, J. M., "The dynamics of rotor-bearing systems using finite elements." Journal of Manufacturing Science and Engineering 98.2 (1976): 593-600.

[12] Nelson, H. D., "A finite rotating shaft element using Timoshenko beam theory." Journal of mechanical design 102.4 (1980): 793-803.

[13] Christensen, R. H., and Santos I. F., "Design of active controlled rotor-blade systems based on time-variant modal analysis." Journal of sound and vibration 280.3 (2005): 863-882.

[14] Söderström T., and Stoica P. "System Identification", London, UK: Prentice hall, 1989.

[15] Roehrle, H. (1980) "Reduktion von Freiheitsgraden bei Strukturdynamikaufgaben", VDI Reihe 1, Nr. 72.

[16] Bucher, C. (1985) "Contributions to the Modeling of Flexible Structures for Vibration Control", PhD Thesis, Swiss Federal Institute of Technology Zrich, Switzerland.

[17] Hansen F., Franklin G. and Kosut Robert(1989), Closed-Loop Identification via the Fractional Representation: Experiment Design, In Proc. Amer. Control Conf., pp. 386-391

Publication P2

Closed loop identification using a modified Hansen scheme

Closed loop identification using a modified Hansen scheme

André K. Sekunda[1], H Niemann[1], N Kjølstad Poulsen[2] and Ilmar F. Santos[3]

[1]) Department of Electrical Engineering, Technical Unversity of Denmark, Kongen Lyngby, Denmark

[2]) Department of Applied Mathematics and Computer Science, Technical Unversity of Denmark, Kongen Lyngby, Denmark

[3]) Department of Mechanical Engineering, Technical Unversity of Denmark, Kongen Lyngby, Denmark

E-mail: aksek@elektro.dtu.dk, hhn@elektro.dtu.dk, nkpo@dtu.dk, ifs@mek.dtu.dk

Abstract

It is often not feasible or even impossible to identify a plant in open loop. This might be because the plant contains unstable poles, or it is simply too expensive to remove the plant from its intended operation, among other possibilities. There are several methods for identifying a plant in closed loop [4], and one such method is the Hansen scheme [1]. Standard identification using Hansen scheme demands generating the identification signals indirectly. In this paper it is instead proposed to use the relationship between the Youla factorization of a plant and its stabilizing controller to directly measure the signals used for identification. A simulation example and identification of a gas bearing is given to show the method in action. Rotors supported by controllable gas bearings are open loop stable systems. However as the rotational speed is increased feedback control is necessary in order to keep the system stable. Furthermore because the dynamics of such a system depends on the rotational speed it is needed to conduct an identification while the system is part of a closed loop scheme. The authors believe the paper able to contribute towards a simpler and more direct way of identifying closed loop plants using Hansen scheme.

1 Introduction

Identification of closed loop systems is of great interest for many practical application. It is often not possible to conduct open loop identification on a plant.

This can be due to several reasons, such as the system being open loop unstable, or disconnecting the controller being too costly. The Hansen scheme is a method for identification of closed loop systems, proposed by Fred Hansen [1]. The method takes advantage of the parametrization of all plants stabilized by a specific controller.

The experimental design procedure proposed by Fred Hansen demands the use of signals, which are not directly measurable from the plant G. It is therefore necessary to recreate the signals from known signals sent through predefined filters. The advantage of the method proposed in this paper is to get rid of the step of recreating the signals and instead measure directly the equivalent signals from the controller. Such a change will eliminate any need of a priori knowledge of the system states and reduce the amount of numerical inaccuracies related to the identification procedure.

In this paper the control architecture is based on a Luenberger observer design. The identification method proposed will be shown theoretically as well as experimentally, using data from a rotor-bearing system linked to a controllable gas bearing. However the method can easily be used with other controller architectures.

The paper is structured as follows: Section 2 introduces Hansen scheme and how to conduct identification of closed loop systems; Section 3 introduces the coprime factorization of plant and controller together with a Youla parametrization; Section 4 presents results from a simulation example for the reader; Section 5 presents an identification example of a gas bearing; Section 6 contains a conclusion on the results presented in the paper.

2 Closed loop identification using the Hansen Scheme

The Hansen scheme is a method originally introduced by Fred Hansen [1] for identification of plants connected as part of a closed loop scheme. In this section a brief description of the Hansen scheme is given together with a motivation for modification. The method takes advantage of the coprime factorisation of plant and controller and is based on the theory outlined in [7]. A standard setup for a plant as part of a closed loop scheme can be seen in Fig. 0.1. Here the signals r_1 and r_2 can be both known or unknown disturbance input. Let G be the nominal plant and K be the nominal controller, a coprime factorization of the nominal plant is then given in Eq. (1) and a coprime factorization of the nominal controller is given in Eq. (2), given the 8 matrices satisfies the double Bezout identity shown in Eq. (3).

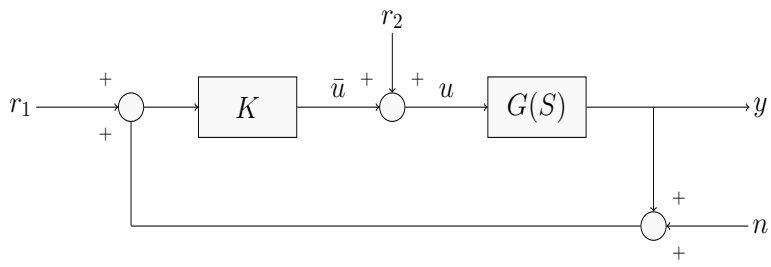

Figure 0.1: Closed-loop system representation.

$$G = NM^{-1} = \tilde{M}^{-1}\tilde{N} \tag{1}$$
$$K = UV^{-1} = \tilde{V}^{-1}\tilde{U} \tag{2}$$

$$\begin{bmatrix} I & 0 \\ 0 & I \end{bmatrix} = \begin{bmatrix} \tilde{V} & -\tilde{U} \\ -\tilde{N} & \tilde{M} \end{bmatrix} \begin{bmatrix} M & U \\ N & V \end{bmatrix} = \begin{bmatrix} M & U \\ N & V \end{bmatrix} \begin{bmatrix} \tilde{V} & -\tilde{U} \\ -\tilde{N} & \tilde{M} \end{bmatrix} \in \mathbf{RH}_\infty \tag{3}$$

With a coprime factorization of the nominal plant G and of the controller K stabilizing the nominal plant $G(0)$, Eq. (4) gives a parametrization of all plants stabilized by the nominal controller K [3].

$$G(S) = (N + VS)(M + US)^{-1} = (\tilde{M} + S\tilde{U})^{-1}(\tilde{N} + S\tilde{V}) \tag{4}$$

The goal of the identification method is to find a signal uncorrelated with the output disturbance, n, to use for identification of the open loop error system, denoted S in Eq. (4).

The real plant can be described using the nominal controller and nominal plant together with the open loop error. Such a description is shown in Fig. 0.2 [1]. Here the output noise have been moved to inside the plant. This representation is believed to make it easier to determine the impact of the noise on the identification process.

For the representation shown in Fig. 0.2 it is possible to recreate the signal η from the 2 input, r_1 and r_2 which are independent of the input and output noise. The calculation of η is given by Eq. (5) to Eq. (10).

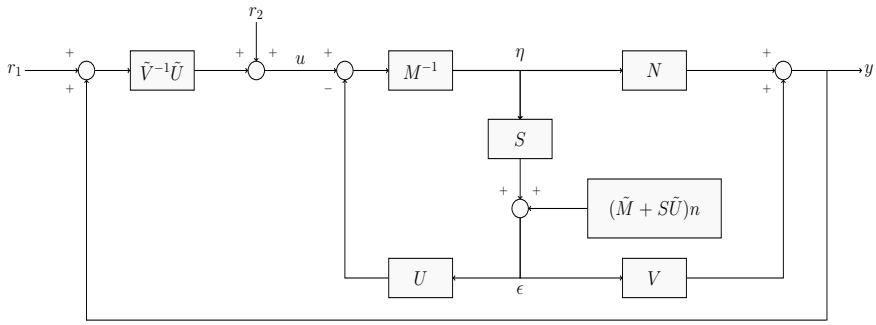

Figure 0.2: Block representation of the Hansen Scheme.

$$u(t) = (M + US)\eta(t) + U(\tilde{M} + S\tilde{U})n(t) \tag{5}$$

$$y(t) = (N + VS)\eta(t) + V(\tilde{M} + S\tilde{U})n(t) \tag{6}$$

$$\tilde{V}u(t) - \tilde{V}(M + US)\eta(t) = \tilde{U}y(t) - \tilde{U}(N + VS)\eta(t) \tag{7}$$

$$\tilde{V}(\tilde{V}^{-1}U(r_1(t) + y(t)) + r_2(t)) - \tilde{V}(M + US)\eta(t) = \tilde{U}y(t) - \tilde{U}(N + VS)\eta(t) \tag{8}$$

$$\tilde{U}r_1(t) + \tilde{V}r_2(t) = \tilde{V}(M + US)\eta(t) - \tilde{U}(N + VS)\eta(t) \tag{9}$$

$$\eta(t) = \tilde{U}r_1(t) + \tilde{V}r_2(t) \tag{10}$$

In a similar fashion it is possible to calculate ϵ using only the input measurements u and the output measurements y. How to calculate ϵ is derived in Eq. (11) to Eq. (15).

$$M\eta(t) = u(t) - U\epsilon(t) \tag{11}$$

$$N\eta(t) = y(t) - V\epsilon(t) \tag{12}$$

$$\tilde{N}u(t) - \tilde{N}U = \tilde{M}y(t) - \tilde{M}V\epsilon(t) \tag{13}$$

$$\tilde{M}y(t) - \tilde{N}u(t) = (\tilde{M}V - \tilde{N}U)\epsilon(t) \tag{14}$$

$$\epsilon(t) = \tilde{M}y(t) - \tilde{N}u(t) \tag{15}$$

With the signals η and ϵ it is possible to identify the open loop error system S as shown in Eq. (18), which is an open loop identification problem.

$$\eta(t) = \tilde{U}r_1(t) + \tilde{V}r_2(t) \tag{16}$$
$$\epsilon(t) = \tilde{M}y(t) + \tilde{N}u(t) \tag{17}$$
$$\epsilon(t) = S\eta(t) + d(t) \tag{18}$$

Because the signals η and ϵ are internal signals in the plant it is impossible to measure them directly. It is therefore necessary to create them from the already known signals, as shown in Eq. (16) and Eq. (17). This approach might give lead to numerical problems because of how the signals are calculated, while the input signals are also led through a filter shaping the excitation signal. Furthermore initial conditions might increase the uncertainty of the signal estimation. It is therefore believed by the authors that it is a huge advantage to measure the signals directly instead.

The rest of the paper will outline a method for how to directly apply a signal equivalent to η and how to measure a signal equivalent to ϵ using a full order observer based controller. A simulation example will be given and results from applying it to a gas bearing is finally presented.

3 Controller plant relationship

In this section the relationship between the parametrization of all controllers stabilised by a specific plant and all plants stabilized by a specific controller investigated. The results stated in the following section can also be found in [3] [8].

As shown in [3] [7] all controllers stabilising a specific plant is given in Eq. (19).

$$K(Q) = (U + MQ)(V + NQ)^{-1} = (\tilde{V} + Q\tilde{N})^{-1}(\tilde{U} + Q\tilde{M}) \mid Q \in \mathbf{RH}_\infty \tag{19}$$
$$K(Q) = \mathcal{F}_l(J_k, Q) \tag{20}$$
$$J_k = \begin{bmatrix} K & \tilde{V}^{-1} \\ V^{-1} & -V^{-1}N \end{bmatrix} \tag{21}$$

It is easy to see that the parametrization can be represented as a lower linear fractional transformation [5]. Such a controller can be implemented as seen in Fig. 0.3. Here Q is chosen to be zero, a set up which will be used throughout the rest of the paper. It is easy to see in Fig. 0.3 that by closing the loop from β to α using Q, the controller is given as in Eq. (19).

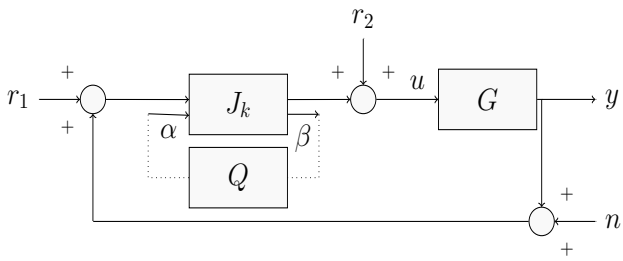

Figure 0.3: Closed loop description with a controller given as in Eq. (19), where the system Q is disconnected.

Equivalently it is possible to state all plants stabilised by a specific controller as shown in Eq. (22).

$$G(S) = (N + VS)(M + US)^{-1} = (\tilde{M} + S\tilde{U})^{-1}(\tilde{N} + S\tilde{V}) \mid S \in \mathbf{RH}_\infty \quad (22)$$

$$G(S) = \mathcal{F}_u(J_G, S) \quad (23)$$

$$J_G = \begin{bmatrix} -M^{-1}U & M^{-1} \\ \tilde{M}^{-1} & G \end{bmatrix} \quad (24)$$

Again it is possible to represent $G(S)$ as an upper LFT as shown in Fig. 0.4. It is important to notice that the signals η and ϵ shown in Fig. 0.4 are the same η and ϵ signals as shown in Fig. 0.2.

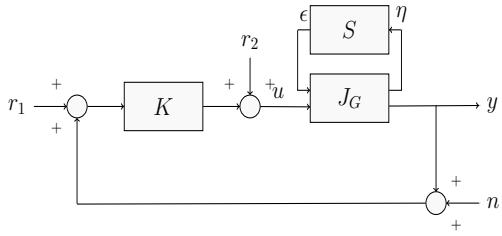

Figure 0.4: General lower LFT description of $G(S)$.

Combining J_k and J_G as shown in Fig. 0.5 it is possible to calculate the transfer function from each input to the two outputs.

It is easy to see that the cross coupling of J_k and J_G in Fig. 0.5 can be calculated as a redheffer star product. The gains of the block is shown in Eq. (25).

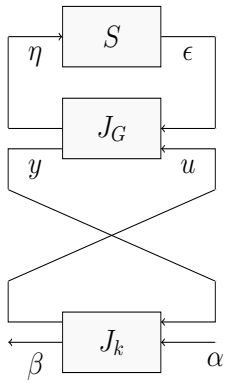

Figure 0.5: Block representation of the relationship between $G(S)$ and $K(Q)$.

$$J_G \star J_k = \begin{bmatrix} \mathcal{F}_l(J_G, K) & M^{-1}(\mathbf{I} - KG)^{-1}\tilde{V}^{-1} \\ V^{-1}(\mathbf{I} - GK)^{-1}\tilde{M}^{-1} & \mathcal{F}_u(J_k, G) \end{bmatrix} \tag{25}$$

In order to determine the relationship between the signals on each side of the system Q and the system S the gains of the redheffer starproduct shown in Eq. (25) are calculated. First the transfer function from the output of S to the input of S is found:

$$\begin{aligned}
\mathcal{F}_l(J_G, K) &= -M^{-1}U + M^{-1}K(I - GK)^{-1}\tilde{M}^{-1} && (26)\\
&= -M^{-1}U + M^{-1}UV^{-1}(I - GK)^{-1}\tilde{M}^{-1} && (27)\\
&= -M^{-1}U + M^{-1}UV^{-1}(I - \tilde{M}^{-1}\tilde{N}UV^{-1})^{-1}\tilde{M}^{-1} && (28)\\
&= -M^{-1}U + M^{-1}UV^{-1}V(\tilde{M}V - \tilde{N}U)^{-1}\tilde{M}\tilde{M}^{-1} && (29)\\
&= -M^{-1}U + M^{-1}U(\tilde{M}V - \tilde{N}U)^{-1} && (30)\\
&= -M^{-1}U + M^{-1}U(\mathbf{I})^{-1} && (31)\\
&= 0 && (32)
\end{aligned}$$

The transfer function from the output of Q to the input of Q can in a similar fashion be proved to be 0. It is therefore only left to show the transfer function respectively from the output of Q to the input of S, which can be seen in Eq. (34) and from the output of S to the input of Q, which can be seen in Eq. (33).

$$
\begin{aligned}
M^{-1}(\mathbf{I}-KG)^{-1}\tilde{V}^{-1} &= M^{-1}(\mathbf{I}-\tilde{V}^{-1}\tilde{U}NM^{-1})^{-1}\tilde{V}^{-1} \\
&= M^{-1}M(\tilde{V}M-\tilde{U}N)^{-1}\tilde{V}\tilde{V}^{-1} \\
&= (\tilde{V}M-\tilde{U}N)^{-1} = \mathbf{I} \qquad (33) \\
V^{-1}(\mathbf{I}-GK)^{-1}\tilde{M}^{-1} &= V^{-1}(\mathbf{I}-\tilde{M}^{-1}\tilde{N}UV^{-1})^{-1}\tilde{M}^{-1} \\
&= V^{-1}V(\tilde{M}V-\tilde{N}U)^{-1}\tilde{M}\tilde{M}^{-1} \\
&= (\tilde{M}V-\tilde{N}U)^{-1} = \mathbf{I} \qquad (34)
\end{aligned}
$$

Combining the results from Eq. (32),(33) and (34) the relationship between α and β can be described as in Eq. (35). The result can be found in [3] where the relationship between Q and S, to the best of the authors knowledge, was examined for the first time.

$$\beta = S\alpha \qquad (35)$$

It is thus proved that the input signal of S is equal to the output signal of Q and the output signal of S is equal to the input signal of Q. It is therefore possible to directly measure the signals equivalent to η and ϵ from the parametrized controller as the signals α and β respectively. To the best knowledge of the authors this approach is not limited to a specific controller architecture, but can be applied to any controller implemented as showed in Fig. 0.6.

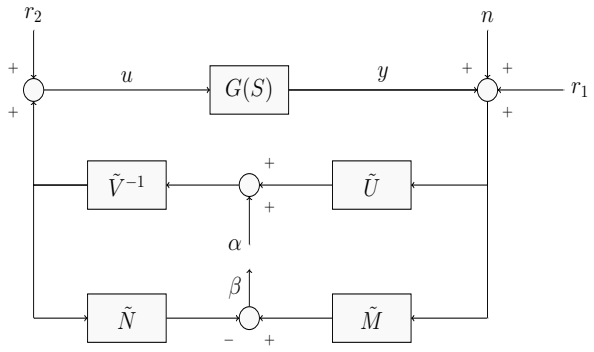

Figure 0.6: General controller scheme using a coprime plant and controller description.

The approach demands that it is possible to find the signals α and β in the controller. This is in this paper done using an observer based controller. It

is important to notice the order of the recast controller is increased by twice the order of the nominal plant model. It can therefore be convenient to use an observer based control scheme, where the order of the controller is 2 times the order of the nominal plant, which is the minimal order possible for such a controller set up.

For a controller given as in Fig. 0.6 as part of a closed loop as shown in Fig. 0.1 the closed loop transfer functions are given in Eq. (36), where α is a free signal to choose for identification purposes.

$$\begin{bmatrix} y \\ u \\ \beta \end{bmatrix} = \begin{bmatrix} (N+VS)\tilde{U} & (N+VS)\tilde{U} & (N+VS)\tilde{V} & N+VS \\ (M+US)\tilde{U} & (M+US)\tilde{U} & (M+US)\tilde{V} & M+US \\ \tilde{M}+S\tilde{U} & \tilde{M}+S\tilde{U} & \tilde{N}+S\tilde{V} & S \end{bmatrix} \begin{bmatrix} n \\ r_1 \\ r_2 \\ \alpha \end{bmatrix} \tag{36}$$

By applying a known disturbance signal on both the observer input and the plant input, hence the α signal, it is possible to measure β as the difference between the predicted output by the observer and the output from the plant $G(S)$. This method is seen as superior in regards to the freedom of the identification signal compared to the method proposed in [1], where the excitation signal is imposed through r_1 and r_2. It is clear from Eq. (36) that the 3 excitation signals and the disturbance signal are uncorrelated why open loop identification can be conducted.

4 Simulation example

A simulation example is presented to give the reader some insight into the identification procedure. A random open loop stable plant with 2 inputs, 2 outputs and 4 states is generated. The nominal plant is chosen such that the system matrix (A_{model}) is 70% of the actual system matrix (A_{real}) as shown in Eq. (37).

$$A_{model} = 0.7 \cdot A_{real} \tag{37}$$

The nominal plant have thus both an dynamic and steady state error that needs to be identified. The test set up is shown in Fig. 0.7 where both the unknown disturbance signal, n, and the excitation signal (α) are implemented as white noise signals. The amplitude of the noise was chosen to be 10% of the β signal. Furthermore only output noise, r_1, was used for this simulation.

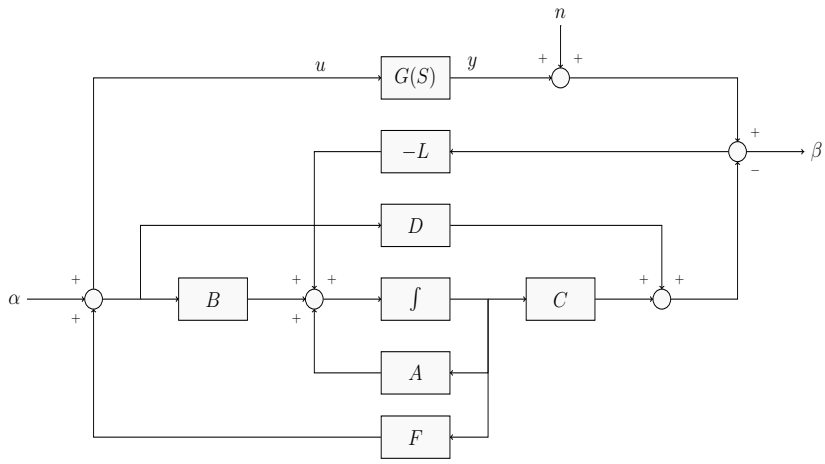

Figure 0.7: Block diagram of simulation example. The observer is designed for a plant where the elements of the system matrix is only 70 % of the actual values of the elements of the system matrix. The state feedback is designed using LQR design and the observer poles are placed to have insignificant dynamics compared to the state feedback poles.

The order of the state space model is chosen by calculating the real open loop error, which was found to be a 12'th order system. It is therefore possible to identify the real open loop error, S, as a 12'th order system, why the open loop error is identified as a 12'th order state space model.

In order to be able to determine the goodness of a model an error signal is calculated using Eq. (38).

$$\phi(t) = G_{real}u(t) - G_{model}u(t) \tag{38}$$

An error signal sequence of respectively the nominal model and the identified plant, using Eq (38), can be seen in Fig. 0.8. It is clearly seen that the identified plant reduce the output error why it can be concluded possible to improve the nominal model, which was on purpose designed to be imperfect. The dynamics are identified although there is still a small deviation between the identified and the real plant, which is due to numerical issues and presence of output noise on the identification signal. It is important to note that there is not applied any noise to the validation data shown in Fig. 0.8 why any deviation from zero corresponds to a deviation between the real plant and respectively the nominal or identified plant.

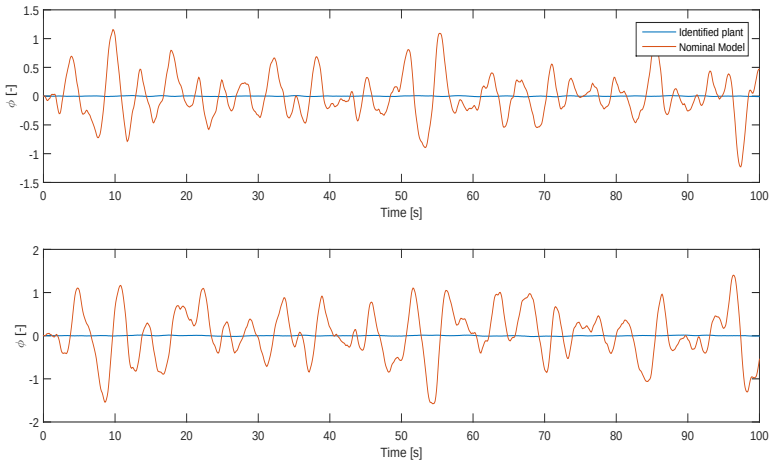

Figure 0.8: Goodness of fit of Nominal and identified plant. Each signal is calculated using Eq. (38). The top plot shows respectively nominal and identified model for the first output, while the lower plot shows the signal for output 2. The identified plant have a better goodness fit which can be seen from the variance in the signal being lower than for the nominal model while the mean is at 0.

A bode plot of respectively the real plant, the identified plant and the plant model is shown in Fig. 0.9. It is easily seen from the bode plot that the model does not agree with the real plant. However the identified plant have successfully minimized the error over the whole frequency span.

For validation of the identification procedure it is also possible to compare the real S with the one identified through the identification procedure. A bode plot of the identified and real S are shown in Fig. 0.10.

5 Lab experiment

Identification of a gas bearing test rig is given to show the identification procedure with data obtained from a real system. A photo of the gas bearing test rig is shown in Fig. 0.11.

A block diagram of the test rig is shown in Fig. 0.12. Here $\mathbf{K_s}$ describes the direct stiffness and cross stiffness of the gas bearing, $\mathbf{D_d}$ the direct damping and cross damping of the gas bearing and $\mathbf{B}$ is the direct input gain and cross input gain of the gas bearing.

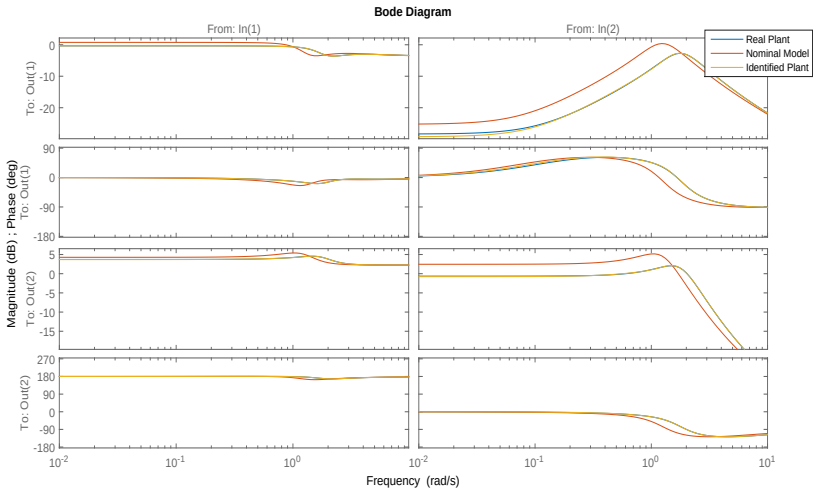

Figure 0.9: Bode plot of the real plant, the identified plant and the plant model. The plant model and real plant are clearly not the same, while the identified plant have almost same frequency response as the real plant.

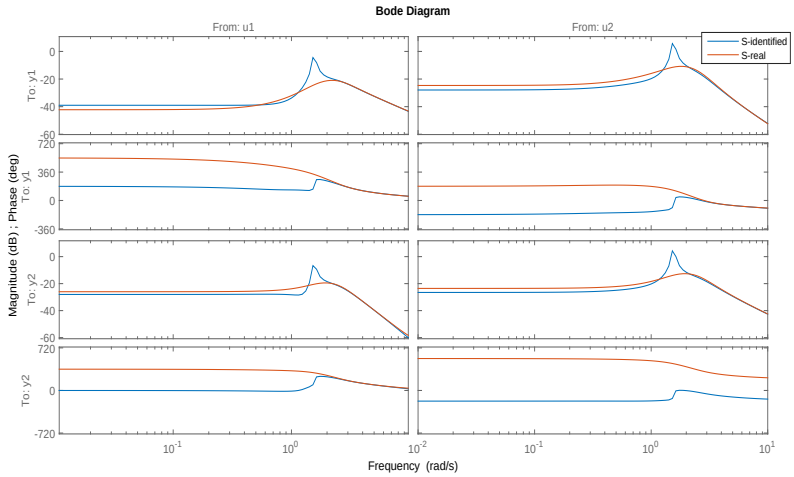

Figure 0.10: Bode plot of the real S calculated as described in [3] and the identified S using the procedure described in section 3.

The rotor-bearing system thus consists of 8 states, 2 inputs and 2 outputs. A model for this set up have been derived and identified in [9] where the gas bearing is not a part of a closed loop Scheme. The identification shown in this

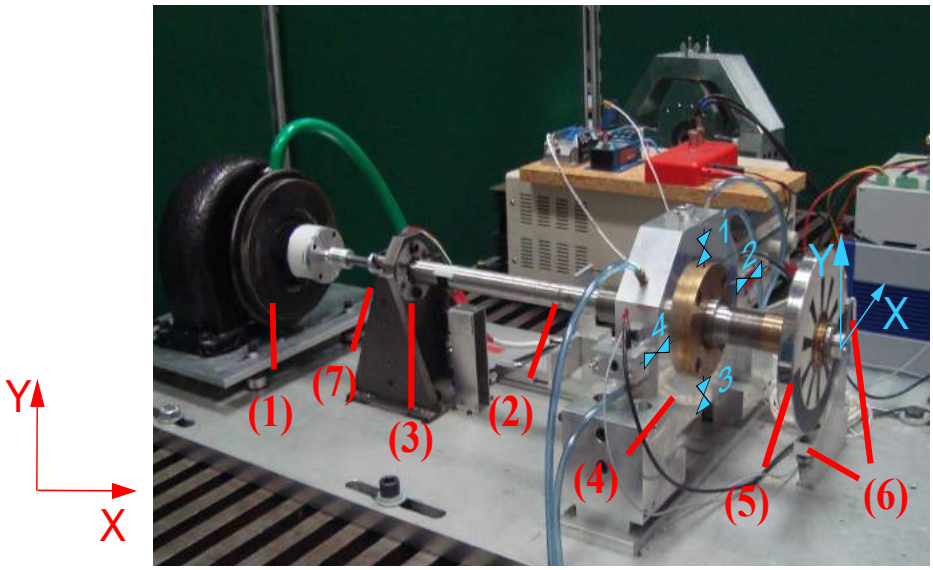

Figure 0.11: Photo of the gas bearing test rig. Here (1) is the turbine, (2) is the flexible shaft, (3) is a ball bearing, (4) is the gas bearing, (5) is a disc used for preload the journal and (6) is the displacement sensors.

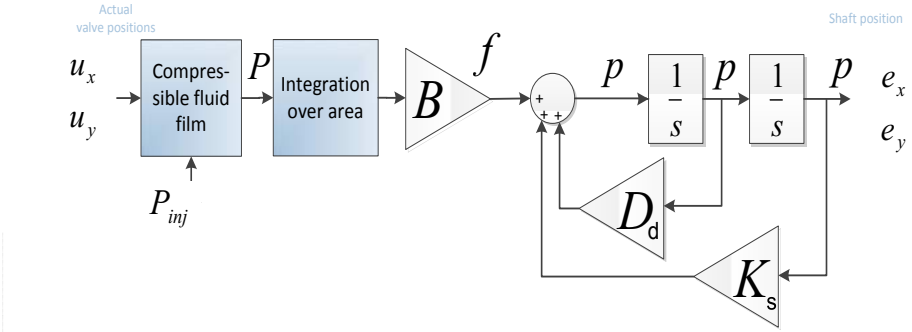

Figure 0.12: Block diagram representation of the gas bearing test rig.

section is based on non-rotating shaft levitated by the externally presented gas bearing shown in Fig. 0.11, as part of a closed loop scheme. The controller implemented is designed as a standard Luenberger observer where the observer gain and state feedback gain is chosen using lqr design. It is important to note that the gas bearing is open loop stable at zero rotational speed. It is therefore possible to identify the plant using open loop techniques. However the

point is to show that the method is applicable why it will be possible to use the same method for higher rotational speeds. At higher rotational speed the rotor-bearing is open loop unstable why only closed loop identification will be possible.

For identification an observer with state feedback is designed and as for the simulation example showed in section 4 a white noise excitation signal is applied as the η signal in the horizontal and vertical direction. The open loop error, S, is estimated as a 8'th order system, same order as the nominal model, which is found to produce a good identification result.

An error plot as described in Eq. (38) is presented in Fig. 0.13 using both the nominal model and the identified model. For validation the excitation signal is only applied in the horizontal direction. It is worth noticing that the nominal model is a good representation of the test rig, why the error is relative small compared to the output noise which is measured to have an amplitude of 1 μm.

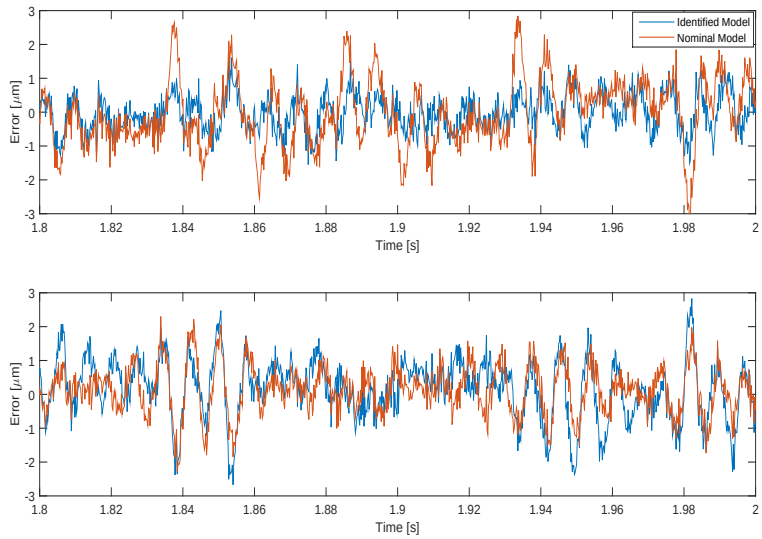

Figure 0.13: Plot of the error between the predicted output and measured output for horizontal and vertical direction. The top plot shows the error in the horizontal direction, while the bottom plot shows the error in the vertical direction.

From Fig. 0.13 it can be seen that the identification have produced a more accurate model for prediction of the horizontal direction (the top plot), while there is no significant improvement in the vertical direction. The error in the

horizontal direction is reduced to close to 1 μm which is the level of the output noise induced by the displacement sensors. The result suggests that it has been possible to identify the direct gains from horizontal input to horizontal output while the cross coupling between the two inputs have not been improved through the identification. It is believed possible to identify the direct gain in the vertical direction with a pure vertical excitation signal in a likewise manner.

6 Conclussion

Identification using Hansen scheme has so far been conducted using indirect excitation signals for identification. Such an approach makes it difficult to determine the frequency response of the excitation signal. In this paper a method is given, on how to use the equivalent signals in the controller, for identification of the open loop error system S, thus letting the excitation be imposed without pre filtering which is the case with the original method proposed in [1]. It is therefore believed that the Hansen scheme is a more limiting special case of the identification approach outlined in this paper. The paper outline an approach for how to excite a plant and measure the needed signals for identification, given an observer based controller. The paper furthermore shows how it is possible to recast any controller such that it is possible to excite and measure the signals used here for identification. Using a simulation example and a Gas Bearing system for identification the method is proven to work.

Bibliography

[1] HANSEN, Fred; FRANKLIN, Gene; KOSUT, Robert. Closed-loop identification via the fractional representation: Experiment design. In: 1989 American Control Conference. 1989. p. 1422-1427.

[2] ANDERSON, Brian DO. From YoulaKucera to identification, adaptive and nonlinear control. Automatica, 1998, 34.12: 1485-1506.

[3] TAY, Teng-Tiow; MAREELS, Iven; MOORE, John B. High performance control. Springer Science & Business Media, 2012.

[4] SÖDERSTRÖM, Torsten; STOICA, Petre. System identification. Prentice-Hall, Inc., 1988.

[5] ZHOU, Kemin, et al. Robust and optimal control. New Jersey: Prentice hall, 1996.

[6] NIEMANN, Henrik; POULSEN, Niels Kjolstad. Estimation of parametric fault in closed-loop systems. In: American Control Conference (ACC), 2015. IEEE, 2015. p. 201-206.

[7] VIDYASAGAR, M. Control system synthesis: a factorization approach, 1985. Cambridge, Massachusetts.

[8] NIEMANN H., "Architecture for fault diagnosis and fault-tolerant control", Department of Electrical Engineering DTU, 2015.

[9] THEISEN, Lukas Roy Svane, et al. Experimental Grey box model identification and control of an active gas bearing. In: Vibration Engineering and Technology of Machinery. Springer International Publishing, 2015. p. 963-976.

Publication P3

Active Fault Detection Based on a Statistical Test

Active Fault Detection Based on a Statistical Test

André K. Sekunda[1], H Niemann[1] and N Kjølstad Poulsen[2]
[1]) Department of Electrical Engineering, Technical Unversity of Denmark, Kongen Lyngby, Denmark
[2]) Department of Applied Mathematics and Computer Science, Technical Unversity of Denmark, Kongen Lyngby, Denmark
E-mail: aksek@elektro.dtu.dk, hhn@elektro.dtu.dk, nkpo@dtu.dk

Abstract

In this paper active fault detection of closed loop systems using dual Youla-Jabr-Bongiorno-Kucera(YJBK) parameters is presented. Until now all detector design for active fault detection using the dual YJBK parameters has been based on CUSUM detectors. Here a method for design of a matched filter detector is proposed instead, based upon the Neyman-Pearson criterion for optimal detector design. Furthermore alternative ways to design the excitation signal which relates to indirect identification methods are presented. Examples are given on detection of actuator faults using a simulated gas bearing for both one and multiple possible parametric faults.

1 Introduction

Fault detection is a well studied subject which has been a popular research area for many years [1, 2]. Usually fault detection is divided into two subgroups, active and passive fault detection. Passive fault detection is based on the use of redundancy equations to generate residuals which detect and isolate the faults in the system [3]. Equivalently active fault detection is based on applying excitation signals to a system in order to detect residual signals which point towards specific parametric changes. In this paper focus is put on detector design for active fault detection, based on the huge amount of research which have been conducted in the area of statistical test design [4, 5].

Since no redundancy equations are needed in active fault detection the amount of sensors required are less than for passive fault detection in order to get the same amount of possible detectable faults. However this advantage comes at the cost of degradation of performance while active fault detection is conducted due to the auxiliary signal. Application of active fault detection is therefore advantageous when detection of a fault is non critical such that constant detection is not required or when adding extra sensors hugely influence the cost compared to the performance degradation.

The study of active fault detection have historically been divided into two main categories. The two philosophies for active fault detection differ in regards to the approach used when determining the auxiliary signal[6]. One branch look into the method of trying to determine which model, from a set of models, describe the system behaviour the best. Such a method is based on knowledge of the magnitude of faults that might occur. The method is presented in [7, 8] and design of the auxiliary signal is discussed in [9, 10, 11].

In this paper active fault detection based instead on the Youla-Jabr-Bongiorno-Kucera(YJBK) parameters is presented. This method was first introduced in [12] and have been extensively described in [13, 14, 6, 12]. Where the first method was based on finding the model that best describe the system behaviour from a set of models, the method presented in [12] is based on the error system associated with a system given a chosen model. It was shown in [14] how to isolate parameters from such an error system and a linearisation of the problem was introduced, while introduction of the CUSUM detector to the detection problem was presented in [6].

In this paper a matched filter detector is designed instead of the CUSUM detector and test statistics are calculated based on the auxiliary signal. Using a matched filter instead of a CUSUM detector is advantageous in several ways. With a matched filter it is possible to quantify how long time it is needed to wait before it is possible to determine whether a fault has occurred, such information is not possible to obtain for a CUSUM detector. Furthermore the properties of a matched filter makes it extremely useful for fault isolation in case of multiple hypothesis testing. Such a statistical based detector has never before been shown in regards to active fault detection based on the Youla-Jabr-Bongiorno-Kucera parameters.

To give an example the matched filter detector is applied to a gas bearing simulation. The model used for the gas bearing was first developed and verified in [15] where it was shown possible to increase performance of the gas bearing by design of feedback control. Furthermore gas bearings are used for high performance equipment with low maintenance requirements. It is seen as critical

for such a system to be able to keep in running until a fault occur. A system using gas bearings is therefore seen as the perfect application of active fault detection.

This paper limits to only show detection of actuator faults in the examples. However it is possible to detect faults on any model parameter with the approach presented. The actuator faults are chosen since they have been identified as the most critical parts of a gas bearing. It is therefore seen as relevant for future work to show it possible to detect faults on the actuators.

The paper is structured as follows: Section 2 introduce the state of the art; Section 3 presents the model of the gas bearing used in the examples; Section 4 discuss the design of the excitation signal; Section 5 presents the detector design given a single fault and Section 6 presents the detector design given multiple faults. Lastly a conclusion is given in section 7.

2 System formulation

The work presented in this paper is based on the use of a coprime description of plant and controller. The nominal plant denoted $G(0)$ and controller denoted K are therefore given respectively in Eq. (1) and Eq. (2)

$$G(0) = NM^{-1} = \tilde{M}^{-1}\tilde{N}, \quad N, M, \tilde{N}, \tilde{M} \in \mathcal{RH}_\infty \tag{1}$$

$$K = UV^{-1} = \tilde{V}^{-1}\tilde{U}, \quad U, V, \tilde{U}, \tilde{V} \in \mathcal{RH}_\infty \tag{2}$$

Here N and M, $\tilde{N}$ and $\tilde{M}$, U and V, $\tilde{U}$ and $\tilde{V}$ are each coprime pairs respectively. In Eq. (1) and Eq. (2) the plant and controller using the systems denoted with a tilde are known as the left factorizations where as the non-tilde pairs are known as the right factorized form. These 8 matrices thus satisfy the bezout identity given in Eq. (3).

$$\begin{bmatrix} I & 0 \\ 0 & I \end{bmatrix} = \begin{bmatrix} M & U \\ N & V \end{bmatrix} \begin{bmatrix} \tilde{V} & -\tilde{U} \\ -\tilde{N} & \tilde{M} \end{bmatrix} \tag{3}$$

Taking advantage of the coprime factorization of the nominal plant and controller, all plants stabilized by a given controller, K, can be expressed as in Eq. (4) using the right factorized form and as in Eq. (5) using the left factorized form.

$$G(S) = (N + VS)(M + US)^{-1}, \ S \in \mathcal{RH}_\infty \tag{4}$$

$$G(S) = (\tilde{M} + S\tilde{U})^{-1}(\tilde{N} + S\tilde{V}), \ S \in \mathcal{RH}_\infty \tag{5}$$

Here S is known as the open loop error [16]. It can be seen from Eq. (4) and Eq. (5) that as S increases the real plant deviate from the nominal plant defined in Eq. (1). Assuming perfect knowledge of the plant a fault will therefore be seen as the open loop error deviating from 0. The goal of the active fault detection is therefore to describe the faults independent of each other using the open loop error. For this it is needed to define an appropriate excitation signal to use for detection through the open loop error. The method described here for design of the excitation signal was first presented in [14, 13]. Throughout the rest of the paper the true plant is defined using Eq. (6) and the control law imposed is given in Eq. (7).

$$y = G(S)u \tag{6}$$

$$u = Ky_m \tag{7}$$

The closed loop system is shown on Fig. 0.1, where the two known external signals r_1 and r_2 are introduced together with the output noise denoted n.

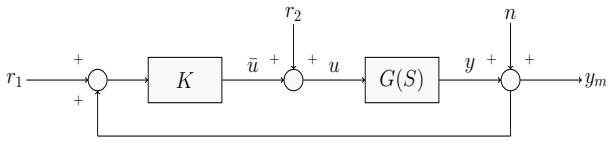

Figure 0.1: Closed loop system setup.

The closed loop system presented on Fig. 0.1 can be expanded using the definition of $G(S)$ given in Eq. (4). The closed loop system is represented using the coprime factorization on Fig. 0.2, which makes it more clear how the open loop error influence the plant.

Here the output noise have been moved using simple block transformation rules in order to make the impact of the noise on the open loop error more transparent. It was shown in [17] that the signal η is independent of the noise. The advantage of detecting changes in the open loop error is therefore twofold. Firstly any change in behaviour from the nominal case is directly translated to a change in S diverging from zero, this makes it into a more simple problem of detection since in the healthy case the signal to detect is only containing noise. Secondly, because the signal η is independent of the noise signal, the detection signal and the noise are independent of each other which is used for implementation of the detector.

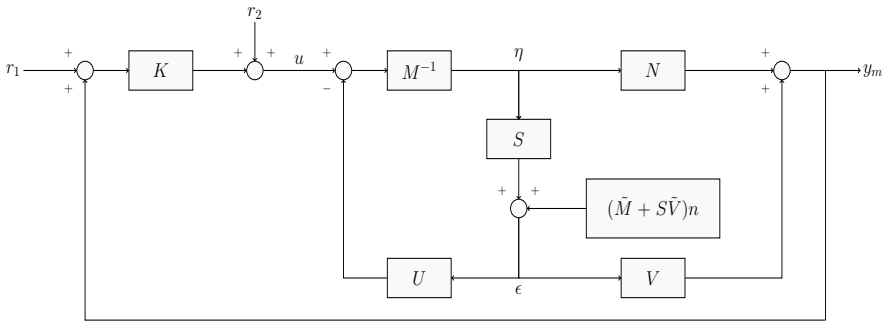

Figure 0.2: Closed loop system setup using the coprime factorisation of the plant.

Parametrisation of faults

As it is possible to represent the true plant, $G(S)$, using Eq. (4) it is also possible to represent all controllers stabilising the nominal plant by the use of Eq. (8) which is known as the right factorised form, while the left factorised form is given in Eq. (9).

$$K(Q) = (U + MQ)(V + NQ)^{-1},\ Q \in \mathcal{RH}_\infty \tag{8}$$

$$K(Q) = (\tilde{V} + Q\tilde{N})^{-1}(\tilde{U} + Q\tilde{M}),\ Q \in \mathcal{RH}_\infty \tag{9}$$

Such a controller can also be represented using a linear fractional transformation as shown in Eq. (10).

$$K(Q) = \mathcal{F}_l(J_K, Q) \tag{10}$$

$$J_K = \begin{bmatrix} UV^{-1} & \tilde{V}^{-1} \\ V^{-1} & -V^{-1}N \end{bmatrix} \tag{11}$$

A block diagram of the controller setup is shown on Fig. 0.3. Here the connections to Q are stippled to represent that Q is disconnected from the system. The signals α and β shown on Fig. 0.3 are the signals being used for the fault detection.

It was proved in [18] that the output signal of the open loop error S is equal to the input signal for Q and the output signal from Q is equal to the input signal for S. The transfer function from α to β was thus shown in [18] to be given as in Eq. (12).

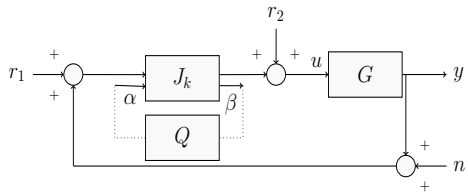

Figure 0.3: Closed loop system setup using the coprime factorisation of the controller.

$$\beta = S\alpha + (\tilde{M} + S\tilde{V})n \tag{12}$$

$$\tag{13}$$

Combining Eq. (12) with Fig. 0.3, following connection between (α, β) and (η, ϵ) is directly given in Eq. (14).

$$\alpha = \eta \wedge \beta = \epsilon \tag{14}$$

For fault detection the two external inputs, r_1 and r_2 are disregarded in this work. If preferred these two inputs could be used for the fault detection. Using the relationship given in Eq. (14) and letting Q be equal to zero, it is possible to state the closed loop system as in Eq. (15) using the two external inputs.

$$\begin{bmatrix} y \\ u \\ \beta \end{bmatrix} = T_{cl}(S) \begin{bmatrix} n \\ \alpha \end{bmatrix} = \begin{bmatrix} (N + VS)\tilde{U} & N + VS \\ (M + US)\tilde{U} & M + US \\ \tilde{M} + S\tilde{V} & S \end{bmatrix} \begin{bmatrix} n \\ \alpha \end{bmatrix} \tag{15}$$

With the impact of the external inputs on the open loop error given in Eq. (15) a connection between the open loop error, S, and the parametric faults, θ, need to be established. In [19] the connection between the open loop error and specific parameters is thoroughly examined. Expressing the open loop error using the parametric faults was shown possible to express as in Eq. (16) [14].

$$S(\theta) = \tilde{M} G_{yw} \theta (I - (G_{zw} + G_{zu} U \tilde{M} G_{yw})\theta)^{-1} G_{zu} M \tag{16}$$

It is easy to see from Eq. (16) that the open loop error is zero when the faults are zero. This is based on an assumption of perfect knowledge of the system.

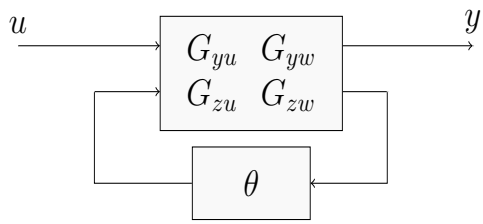

Figure 0.4: LFT description of system faults.

The systems, G_{yw}, G_{zw} and G_{zu} can be found by use of the linear fractional transformation shown on Fig. 0.4. Furthermore θ is a diagonal matrix where the faults are the diagonal elements.

The goal of the fault detection is to detect the faults from Eq. (16) in Eq. (17) where noise(w) is added.

$$\beta = S(\theta)\alpha + (\tilde{M} + S\tilde{V})n \tag{17}$$

$$\beta = S(\theta)\alpha + w \tag{18}$$

Since $S(\theta)$ is a non-linear function it was proposed in [14] to linearise $S(\theta)$ around $\theta = 0$ which corresponds to no fault. This linearised version will be denoted $\bar{S}(\theta)$ and is given in Eq. (19).

$$S(\theta) \approx \bar{M} G_{yw} \theta G_{zu} M \tag{19}$$

Here θ is a diagonal matrix with each diagonal element corresponding to a fault in the system. Such a linearisation is seen as appropriate when detecting small faults where θ is close to zero.

Multiple faults

Using $\bar{S}(\theta)$ from Eq. (19) the impact of multiple faults on the signal is rather straightforward. Due to the linearisation each fault is independent and the amplitude of the signal is simply a summation of the impact of all faults as shown in Eq. (21).

$$\beta = \sum_{i=1}^{k} (\tilde{M} G_{yw_i} G_{z_i u} M \theta_i \alpha) + w \tag{20}$$

$$\beta = (\bar{S}_1\theta_1 + \bar{S}_2\theta_2 + .. + \bar{S}_i\theta_i)\alpha + w = \sum_{i=1}^{k} (\bar{S}_i\theta_i\alpha) + w \tag{21}$$

Here i is used to specify which fault is considered, why i describe which input of Gyw_i and output of $G_{z_i u}$ is used. Detection and isolation of fault is in the rest of this paper based on Eq. (21).

3 Model of active gas bearing

Fault diagnosis conducted throughout this paper is applied to an simulation example of a disc held in place by an active gas bearing. A model for such a test rig is based on experiments conducted on the flexible shaft held in place by a gas bearing which is shown on Fig. 0.5. The system showed on Fig. 0.5 is designed to keep the disc(5) in a fixed position. Through feedback control of the active gas bearing(4) it is possible to increase the damping of the system and thus increase the disturbance rejection.

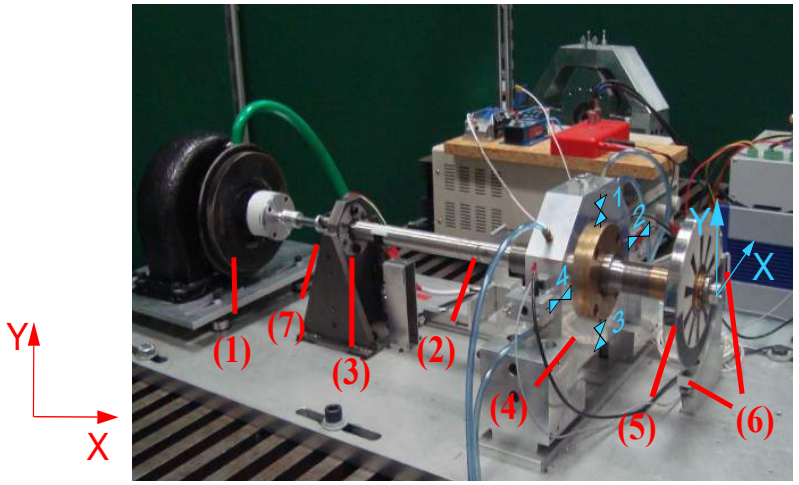

Figure 0.5: Photo of the gas bearing test rig. Here (1) is the turbine, (2) is the flexible shaft, (3) is a ball bearing, (4) is the gas bearing, (5) is a disc used for preload the journal, (6) is the displacement sensors and (7) is the connector between the turbine and the flexible shaft.

A model of the system was presented and verified in [15] and it was shown possible to model the plant as a 6'th order system with 2 inputs and 2 outputs. The model inputs represent the air injected in the horizontal and vertical direction to the gas bearing, while the system outputs is the vertical and horizontal position of the disc. A block diagram of the system modelled is shown on Fig. 0.6.

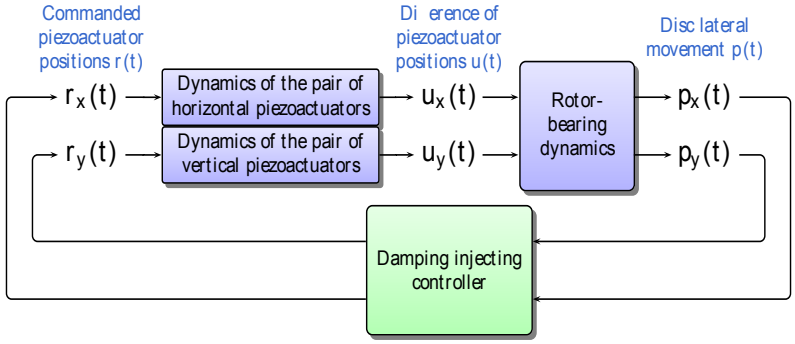

Figure 0.6: Block diagram of the model used for simulation examples.

The states of the plant are sorted with the two first representing the position of the disc, the next two states representing the velocity of the disc, while the two last states are a product of the Tustin approximation of the delay in the system. The structure of the state space model is given in Eq. (22) to Eq. (25). Here each element in the state space system denotes a 2x2 matrix, hence the dynamics governing the horizontal and vertical movement are modelled in an identically.

$$\mathbf{A}=\begin{bmatrix} 0 & \mathbf{I} & 0 \\ K & D & 2B\tau \\ 0 & 0 & -\tau \end{bmatrix} \tag{22}$$

$$\mathbf{B}=\begin{bmatrix} 0 \\ -B \\ \mathbf{I} \end{bmatrix} \tag{23}$$

$$\mathbf{C}=\begin{bmatrix} \mathbf{I} & 0 & 0 \end{bmatrix} \tag{24}$$

$$\mathbf{D}=\begin{bmatrix} 0 \end{bmatrix} \tag{25}$$

Here K denotes the stiffness, D denotes the damping, B denotes the actuator gain and τ denotes the Tustin approximation of the delay. The model thus describes the relation between the opening degree of the valves controlling the

flow of air to the gas bearing and the position of the disc at the end of the rotating shaft.

The actuators of the active gas bearing are identified as the components which are most susceptible to tear and wear. It is therefore seen as necessary to be able to detect faults on the actuators, which is equivalent to a change in the input gains. The faults are modelled as multiplicative faults as shown in Eq. (26) which is the input matrix modified with the possible faults identified for the plant.

$$\mathbf{B}(\theta) = \begin{bmatrix} 0 \\ -B \\ \mathbf{I} \end{bmatrix} \begin{bmatrix} \mathbf{I} + \theta \end{bmatrix} \tag{26}$$

Here θ is a diagonal matrix denoting the magnitude of the faults on each of the actuators in the diagonal elements. Both faults (θ_1, θ_2) are limited to the interval 0 to -1, where 0 corresponds to no fault and -1 corresponds to a complete failure. The faults are therefore only present in the input matrix. In the fault free case both faults are zero and Eq. (27) hold.

$$G(S|_{\theta=0}) = G_{yu} = NM^{-1} = \tilde{M}^{-1}\tilde{N} \tag{27}$$

Going from the fault free to the faulty case therefore corresponds to the open loop error S diverging from zero. The relationship between the faults and the open loop error is thus given in Eq. (28).

$$S(\theta) = 0 \mid_{\theta=0} \tag{28}$$

This is an extremely useful property which means that no signal will be generated in the healthy case, which greatly simplify detection.

4 Detection Signal

For active fault detection an excitation signal is needed. It is decided here to look into the use of a sinusoidal wave. The excitation signal, α, is therefore defined in Eq. (29).

$$\alpha = A_\alpha \sin(\omega t) \tag{29}$$

From a detection point of view the excitation signal has to be chosen such that the fault give the maximum amplification of the excitation signal and hence makes it the easiest to detect a fault. For the gas bearing model the frequency response of $\bar{S}$ for a fault on respectively the horizontal and vertical actuator is given on Fig. 0.7 when considering signals from the horizontal input to the horizontal output.

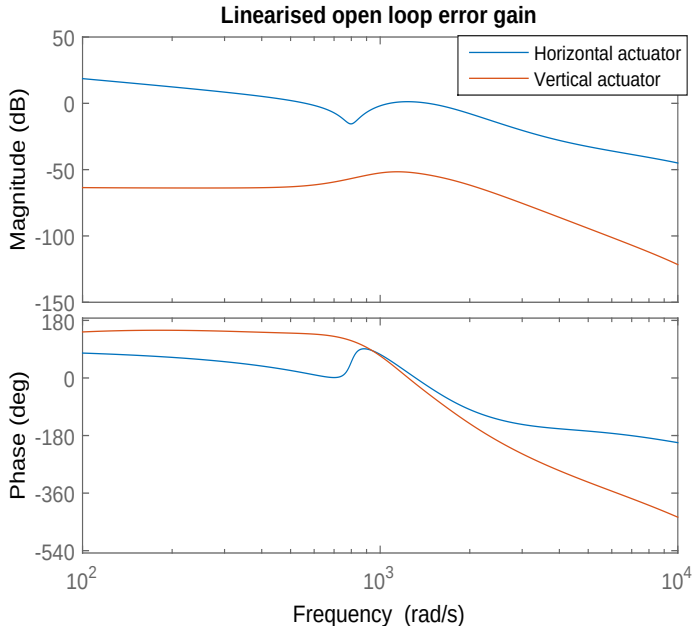

Figure 0.7: Gain of the linearised system $\bar{S}_i$ given a fault on each of the two actuators. The bode plot shows the transfer function from an excitation signal on the horizontal input to the horizontal output. The phase is shifted 180 degrees since the fault can only be negative.

It can be seen from Fig. 0.7 that a fault on the horizontal actuator is easiest to detect by excitation of input 1. This corresponds well with input 1 representing the horizontal actuators and input 2 representing the vertical actuators. Using Fig. 0.7 the excitation signal used to detect faults is chosen to be a $1030 rad/s$ sine wave on the horizontal input. The frequency of the excitation signal is chosen such that faults on the vertical actuator is amplified the most, which maximise the smallest gain.

With a known excitation signal, a known nominal model and a known controller it is possible to define the residual to detect as in Eq. (30).

$$\beta(t) = \sum_{i=1}^{k} (\bar{S}_i \theta_i A_\alpha \sin(\omega t)) + w(t) \tag{30}$$

It might be convenient to keep the original non-factorised controller on the system or not excite the system by the use of the external input α. In such cases instead of using α as the excitation signal, r_1 or r_2 shown on Fig 0.1 can be used. The excitation signal of the open loop error will then be subject to a phase shift and gain change depending on the external input used. The transfer function from the 3 outputs to the residual signal are given in Eq. (31). It is thus possible to use any of the 3 known inputs and compensate from the phase shift introduced due to the excitation used.

$$\beta = S\alpha + (\tilde{N} + S\tilde{U})r_1 + (\tilde{M} + S\tilde{V})r_2 \tag{31}$$

The extra systems introduced when using the two alternative inputs, r_1 and r_2 can easily be compensate for by reformulating the residual signal. In the case r_1 is used the residual signal is reformulated to $\bar{\beta}_{r_1}$ as shown in Eq. (32) and the residual signal is thus a proper residual signal as shown in Eq. (33). The same procedure for reformulation of the residual signal is shown when using r_2 as the excitation signal in Eq. (34) and Eq. (35).

$$\bar{\beta}_{r_1} = \beta - \tilde{N} \tag{32}$$
$$\bar{\beta}_{r_1} = S\tilde{U}r_1 \tag{33}$$
$$\bar{\beta}_{r_2} = \beta - \tilde{M} \tag{34}$$
$$\bar{\beta}_{r_2} = S\tilde{V}r_2 \tag{35}$$

5 Detector design for a single fault

In order to design the detector a model of the noise signal is needed. A normalized histogram of respectively the vertical and horizontal output signals in the fault free case have been obtained from a real gas bearing test rig. The normalized histogram for each residual is shown on Fig. 0.8 and a normal distribution with a zero mean and a variance of 0.11 is found to be the best fit of the noise.

In Eq. (30) the only unknown parameter is the magnitude of the fault why a detector should be able to detect a known signal with an unknown amplitude.

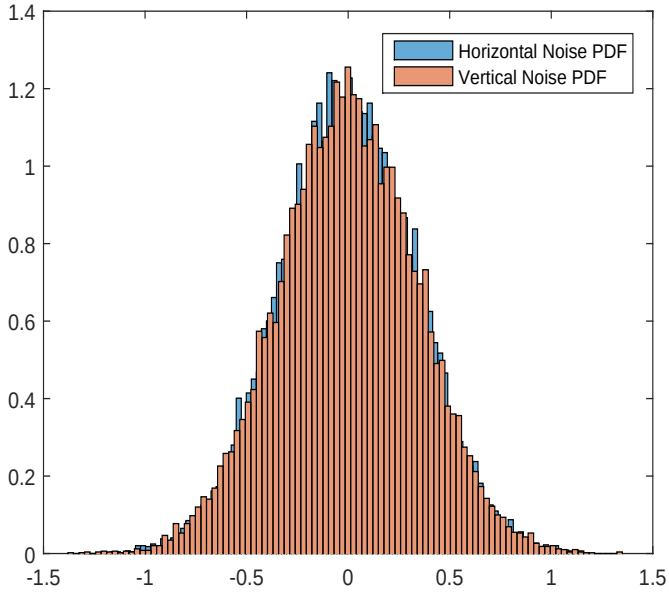

Figure 0.8: Normalized histogram of the vertical and horizontal residual, given a steady state of zero and no excitation signal imposed.

For such a problem it is possible to design a null hypothesis as in Eq. (36) and a one hypothesis as in Eq. (37).

$$\mathcal{H}_0 : \beta[n] = w[n] \qquad n = 0, 1, ..., N-1 \tag{36}$$
$$\mathcal{H}_1 : \beta[n] = Ax[n] + w[n] \qquad n = 0, 1, ..., N-1 \tag{37}$$

Here $w[n]$ is white gaussian noise with variance 0.11 found from the measurements of the residual signal in the fault free case, due to the output noise from Fig. 0.8. The known signal is denoted $x[n]$ and A is the unknown amplitude due to the magnitude of the fault. For such a detection problem it is usually not possible to design an optimal detector [4] due to the detection being two sided, hence A can be both smaller or larger than 0. However due to only degradations in performance are considered θ is limited to $[-1\ 0[$ why the amplitude is only negative and the detection is therefore one sided. A Neyman Pearson detector can therefore be implemented [4]. In order to detect the sinusoidal signal in the residual signal β a matched filter detector is designed. The detection signal, $T(\beta)$ for a matched filter is given in Eq. (38).

$$T(\beta) = \sum_{n=0}^{N-1} \beta[n]x[n] \tag{38}$$

The energy of the detector signal is needed in order to determine the threshold and depends on the window size and the characteristics of the excitation signal. Given a sinusoidal excitation signal, the energy of the signal can be expressed as in Eq. (39).

$$\varepsilon = N\frac{A^2}{2} \tag{39}$$

Here N is the window size as shown in Eq. (38) and A is the amplitude of the residual signal given in Eq. (30). The amplitude can be determined from Eq. (40). It is worth noticing that the amplitude depends on the magnitude of the fault, the test statistic therefore depends on the expected magnitude of the fault [14].

$$A = \bar{S}_i \theta_i A_\alpha \tag{40}$$

With the energy of the detection signal, ε defined in Eq. (39) and the variance of the residual signal, σ^2, the threshold can be found using Eq. (41) based on the allowed frequency of false alarms.

$$\gamma = (\sigma^2 \varepsilon)^{0.5} Q^{-1}(P_{FA}) \tag{41}$$

Similarly with the threshold, the probability of detection can be determine as in Eq. (42), given an allowed probability of false alarm.

$$P_D = Q\left(Q^{-1}(P_{FA}) - (d)^{0.5}\right) \tag{42}$$

In Eq. (42) d is known as the deflection coefficient and is defined in Eq. (43).

$$d^2 = \frac{\varepsilon}{\sigma^2} = \frac{(E(T;H_1) - E(T;H_0))^2}{var(T;H_0)} \tag{43}$$

Example

A simulation example using the gas bearing model introduced in [15] is presented next. For simplicity only a fault on the horizontal actuator is considered. Because only a fault on the horizontal actuator is considered the residual with the greatest gain as shown on Fig. 0.7 is from the horizontal input to the horizontal output. Given the white gaussian output noise with a variance of 0.11 the PDF of the residual in the faulty and healthy case are shown on Fig 0.9.

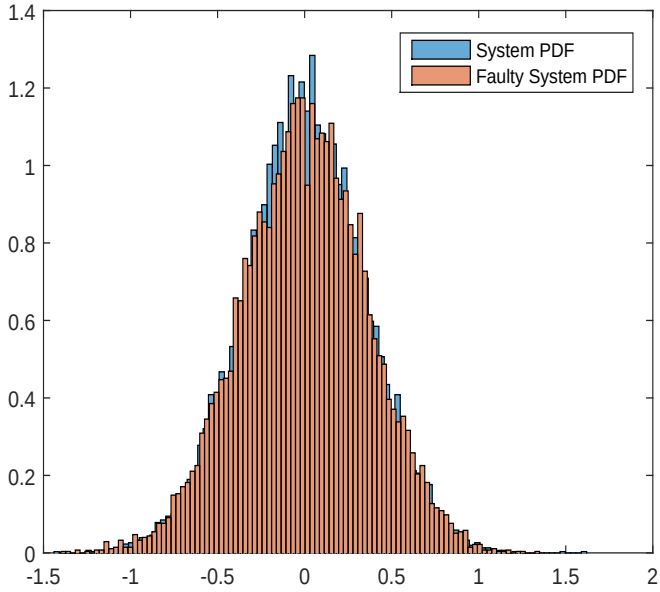

Figure 0.9: PDF of the residual signal β for the case of a fault free system and in the case a fault has happened.

Using the residual signal generated when no fault is happening the variance of the residual, σ, was found to be 0.11. The amplitude of the sinusoidal wave was chosen such that the signal could be detected without an inappropriate window length, but disturbing the system as little as possible, hence keep the amplitude of the excitation signal as small as possible. The residual signal both with and without a fault on the system is shown on Fig. 0.10 where the sinusoidal wave is chosen to have a frequency of $1030 rad/s$. Distinguishing between the residual in the healthy and the faulty case is not trivial why a matched filter detector can be used.

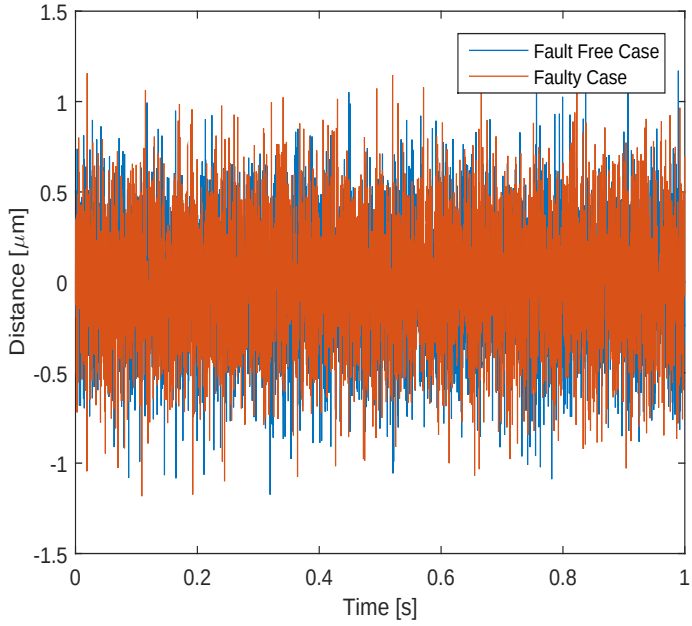

Figure 0.10: Residual signal β with and without a fault on the horizontal actuator respectively. The system have been excited with a sinusoidal signal as described in Eq. (29) and both output signals have been subject to white Gaussian noise with a variance of 0.11.

In order to determine the threshold and probability of detection, it is chosen that one alarm is allowed to happen once every 10'th second on average, hence P_{FA} is equal to the one tenth the sampling time. Furthermore the gain of the residual was determined with an expected magnitude of the fault of 10% and using the gain of $\bar{S}$ at $1030 rad/s$ found on Fig. 0.7. The window size is chosen to be 420 and the energy of the signal can thus be found using Eq. (44).

$$\varepsilon = N\frac{A^2}{2} = 560\frac{0.12^2}{2} = 2.9 \tag{44}$$

With the energy of the signal determined, the threshold is calculated in Eq. (45)

$$\begin{aligned}\gamma &= (\sigma^2\varepsilon)^{0.5}Q^{-1}(P_{FA}) \\ &= (0.11^2 \cdot 2.9)^{0.5}Q^{-1}(0.1 \cdot Ts) = 2.3\end{aligned} \tag{45}$$

With the threshold calculated it is possible to design the detector and simulate a system where a fault of 10% occur after half a second. On Fig. 0.11 the matched filter detector is implemented and it can be seen there is a clear distinction between the detector signal in the healthy and faulty case.

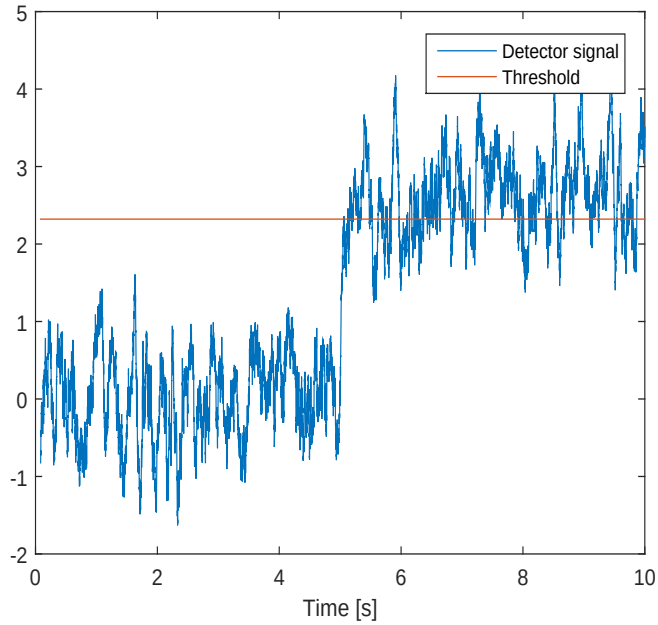

Figure 0.11: Detection signal using a matched filter detector with a window size of $N = 420$ with an expected fault of 10%. The excitation signal is designed as a sinusoidal signal with a frequency of 1030 rad/sec which was found to correspond with the greatest gain of the residual signal in case of a fault. The gas bearing is initially fault free and a fault of 10% is at 5 seconds introduced to the horizontal actuator.

With a detector as described in this section the probability of detection can be calculated using Eq. (42). The probability of detection is found to be 80% which corresponds well with what is seen on Fig. 0.11.

6 Detector Design for Multiple Faults

So far design of an optimal detector have been considered with one possible fault for the system. In this section the method is extended to cover design of an optimal detector given multiple faults. Again the faults are assumed to be

small in which case it is appropriate to linearise Eq (16). The residual signal to detect is therefore given as in Eq. (46).

$$\beta = \sum_{i=1}^{k} (\tilde{M} G_{yw_i} G_{z_i u} M \theta_i)\alpha + w \tag{46}$$

Given only one fault can happen at a specific time and a known sinusoidal excitation signal, the residual signal to detect is a sinusoidal signal with a known frequency but unknown amplitude and phase. The unknown amplitude comes from the magnitude of the fault which is not known, where the phase depends on which fault is occurring and is therefore treated as unknown from a known set related to the faults considered. The detection problems $\mathcal{H}_0$ hypothesis is therefore given in Eq. (47) and corresponds to no fault has happened and the $\mathcal{H}_1$ hypothesis is given in Eq. (48), and correspond to any fault has happened. The unknown phase shift is treated as an unknown delay and the unknown amplitude A is the unknown amplitude.

$$\mathcal{H}_0 : \beta[n] = w[n] \qquad n = 0, 1, ..., N-1 \tag{47}$$

$$\mathcal{H}_1 : \beta[n] = Ax[n - n_0] + w[n] \quad n = 0, 1, ..., N-1 \tag{48}$$

Such a detector is described in [4] and is somewhat similar to the detector designed in the case of a single fault in section 5. The unknown amplitude depends on both the magnitude of the fault(θ) and which parametric fault that has happened. It is easily seen from Fig. 0.7, how the gain depends on the specific parametric fault. In the case of a single fault considered A was guessed to be the gain given a 10% degradation of the parameter, used in order to calculate the test statistics. It is needed to give an estimate of the amplitude A in order to calculate the test statistics. The test is therefore based on the gain open loop error gain given a 10% fault of the faulty parameter given fault $1(f_1)$. The gain is for this case denoted A_0 and is used for determining the delay and probability of detection. It was shown in [4] that the delay can be found by maximising the correlation between the measured signal and the known part of the predicted signal. The unknown delay is therefore possible to determine by maximizing Eq. (49).

$$\phi = \arg\max_{n_0 \in \mathcal{T}} \Big(\sum_{n=n_0}^{n_0+M-1} \beta[n] A_0 x[n - n_0] \Big) \tag{49}$$

Even though the phase(n_0) is unknown some information is still known about it which makes the evaluation of Eq. 49 much simpler. Given each specific

fault the detector is designed to detect, the phase shift is known from Eq (46). Evaluation of Eq. (49) is therefore only needed for each of the delays imposed by each possible fault. The set of possible delays given the faults considered is thus denoted by $\mathcal{T}$. Using Eq. (49) the detection problem simplifies to the case of detecting a known signal with an unknown amplitude in gaussian white noise. Using a matched filter optimal detector is therefore seen as appropriate and is given in Eq. (50).

$$T(\beta) = \sum_{n=0}^{N-1} \beta[n]x[n - n_0] \tag{50}$$

Again as in the case of 1 fault the threshold can be determined from Eq. (51).

$$\gamma = (\sigma^2\varepsilon)^{0.5}Q^{-1}(P_{FA}) \tag{51}$$

It is here worth noticing that the threshold is independent of the faults considered, and the number of faults considered will therefore not influence the threshold. The probability of detection does depend on the faults considered, and it is needed to calculate the probability for each of the faults considered. The probability of detection is given in Eq. (52).

$$P_D = Q(Q^{-1}(P_{FA}) - (d_i)^{0.5}) \tag{52}$$

The deflection coefficient d_i depends on the fault considered and the magnitude of the fault. The probability of detection therefore depends on the energy in the signal, which in turn depends on the amplitude of the matched signal. The deflection coefficient is given in Eq. (53).

$$d_i^2 = \frac{(E(T; H_1|_{f_1}) - E(T; H_0))(E(T; H_1|_{f_i}) - E(T; H_0))}{var(T_0; H_0)} \tag{53}$$

It can be seen from Eq. (53) that when the reference fault is considered the deflection coefficient simplifies to Eq. (43).

Example

Again the example is based on a simulation using the gas bearing model introduced in [15]. However while only a fault on the horizontal actuator was

considered in section 5, it is in this example possible that a fault can occur both on the horizontal and vertical actuator. The detector design therefore need to be able to both detect when a fault occurs and determine which actuator is faulty. Using the residual signal, generated in the fault free case, the variance of the residual, σ, was found to be 0.11. The residual signal both with and without a fault on the system is shown on Fig. 0.12 where the sinusoidal wave is chosen to have a frequency of 1030 rad/sec. The fault in this example is chosen to be a 10% reduction of the vertical actuator gain. Once again it is shown that distinguishing between the residual in the healthy and the faulty case is not trivial.

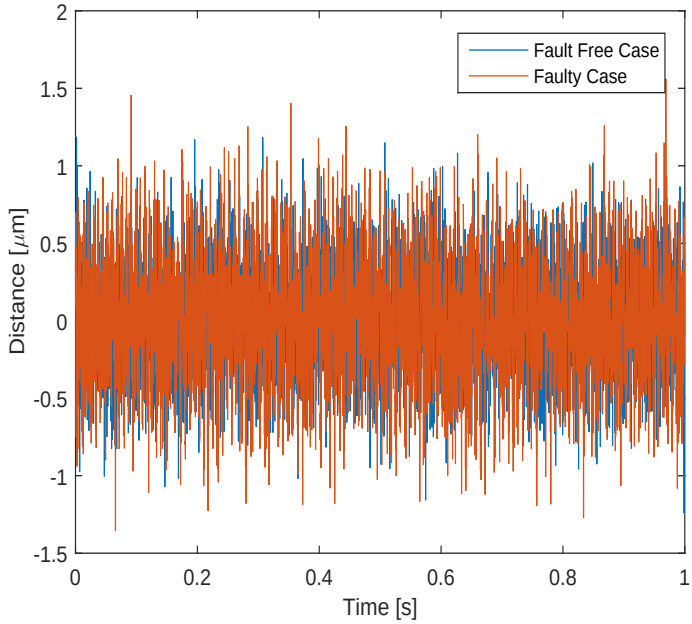

Figure 0.12: Residual signal β with and without a fault on the vertical actuator respectively. The system have been excited with a sinusoidal signal as described in Eq. (29) and both output signals have been subject to white Gaussian noise with a variance of 0.11.

In order to determine the threshold and probability of detection, the probability of a false alarm is chosen to be the same as in the previous example. Furthermore the gain of the residual was determined with an expected magnitude of the fault, on the vertical actuator, of 10% and using the gain of $\bar{S}$ at 1030 rad/sec found on Fig. 0.7. The window size was chosen to be 60 which

made it possible to distinguish between the faulty and fault free case. The energy of the signal can thus be found using Eq. (54).

$$\varepsilon = N\frac{A^2}{2} = 60\frac{0.3^2}{2} = 2.7 \tag{54}$$

With the energy of the signal determined, the threshold is calculated in Eq. (45)

$$\gamma = (\sigma^2\varepsilon)^{0.5}Q^{-1}(P_{FA}) = (0.11^2 \cdot 2.7)^{0.5}Q^{-1}(0.1 \cdot Ts) = 2.2 \tag{55}$$

With the threshold calculated it is possible to design the detector and simulate a system where a fault on the vertical actuator of 10% occur after five seconds. On Fig. 0.11 the matched filter detector is implemented and it can be seen there is a clear distinction between the detector signal in the healthy and faulty case.

With a detector as described in this section the probability of detection can be calculated using Eq. (42). The probability of detection is found to be 80% which corresponds well with what is seen on Fig. 0.11. Since the amplitude of the residual would be greater in the case of a fault on the horizontal actuator the probability of detection would be higher.

In order to determine which fault has happened Eq. (49) is used. The phase shift of the residual signal in case of each of the faults is found using Fig. 0.7 and at each time step it is checked which of the two phase shifts maximise the detector signal. A plot of the decision at each time step is shown on Fig. 0.14. The decision algorithm clearly choose a fault at random in the fault free case, while the vertical actuator is chosen continuously when a fault happens at 5 seconds.

7 Conclusion

So far detectors for active fault detection using dual YJBK parameters have been based on waiting sufficient amount of time for detection to happen. Such CUSUM detectors were designed without regard to a threshold based on the accepted probability of false alarm. In this paper a matched filter detector was designed instead. Methods for determining an appropriate threshold and probability of detection was given based on the allowed false alarm rate. The problem of detecting parametric changes was shown possible to formulate in such a way that standard hypothesis testing was possible. Using the designed

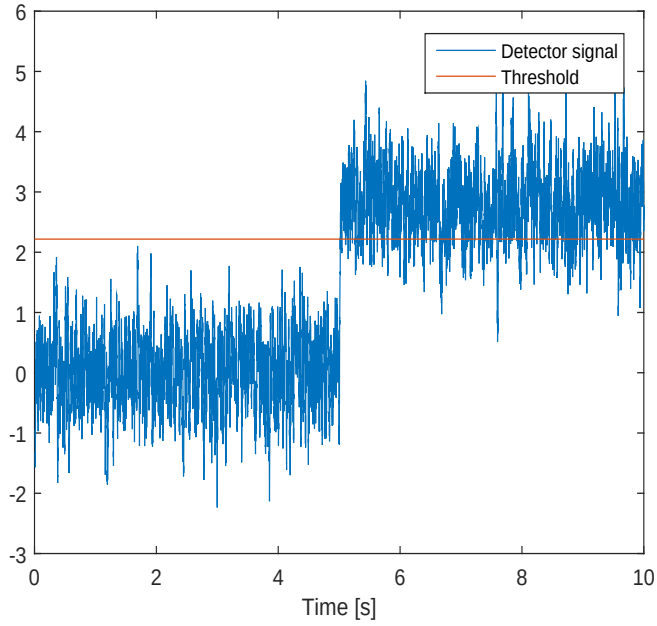

Figure 0.13: Detection signal using a matched filter detector with a window size of $N = 60$ with an expected fault of 10% on the vertical actuator. The excitation signal is designed as a sinusoidal signal with a frequency of 1030 rad/sec which was found to correspond with the greatest gain of the residual signal in case of a fault. The gas bearing is initially fault free and a fault of 10% is at 5 seconds introduced to the vertical actuator.

matched filter detector it was shown possible to detect actuator faults in a detector signal corrupted by Gaussian noise using a gas bearing model for the simulation example. The detection procedure was conducted using a sinusoidal excitation signal, however in theory the excitation signal could be of any shape. The frequency of the sinusoidal wave was determined by maximising the gain from the excitation signal to the parametric fault most difficult to detect. It was thus shown possible to minimize the disturbance introduced by the excitation signal relative to the probability of detecting a specific parametric fault.

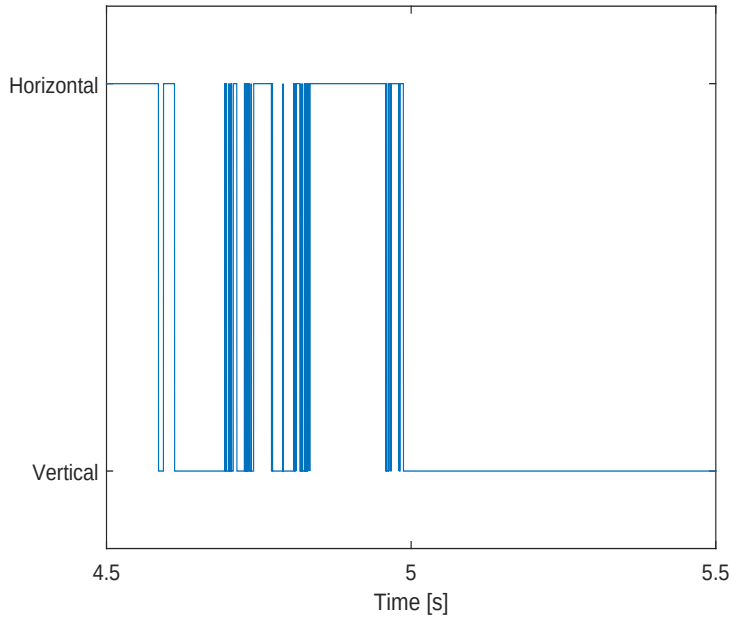

Figure 0.14: Plot of the decision taken by Eq. (49) at each time step. The plot shows how the decision algorithm goes from randomly choosing the fault to only deciding the vertical fault after a fault occur at 5 seconds. The random behaviour of the algorithm in the fault free case corresponds well with the noise being white.

Bibliography

[1] R. Isermann, "Model-based fault-detection and diagnosis–status and applications," *Annual Reviews in control*, vol. 29, no. 1, pp. 71–85, 2005.

[2] R. Isermann and P. Ballé, "Trends in the application of model-based fault detection and diagnosis of technical processes," *Control engineering practice*, vol. 5, no. 5, pp. 709–719, 1997.

[3] M. Blanke, M. Kinnaert, J. Lunze, M. Staroswiecki, and J. Schröder, *Diagnosis and fault-tolerant control*, 2nd ed. Springer, 2006.

[4] S. M. Kay, "Fundamentals of statistical signal processing: Detection theory, vol. 2," 1998.

[5] M. Basseville, I. V. Nikiforov *et al.*, *Detection of abrupt changes: theory and application*. Prentice Hall Englewood Cliffs, 1993.

[6] N. Poulsen and H. Niemann, "Active fault diagnosis based on stochastic tests," *International Journal of Applied Mathematics and Computer Science*, vol. 18, no. 4, pp. 487–496, 2008.

[7] S. L. Campbell, K. G. Horton, and R. Nikoukhah, "Auxiliary signal design for rapid multi-model identification using optimization," *Automatica*, vol. 38, no. 8, pp. 1313–1325, 2002.

[8] R. Nikoukhah, F. Delebecque, S. Campbell, and K. Horton, "Multi-model identification and the separability index," in *Proceedings of Mathematical Theory Networks and Systems (MTNS)*, 2000.

[9] F. Kerestecioğlu* and I. Cetin, "Optimal input design for the detection of changes towards unknown hypotheses," *International Journal of Systems Science*, vol. 35, no. 7, pp. 435–444, 2004.

[10] M. Šimandl and I. Punčochář, "Active fault detection and control: Unified formulation and optimal design," *Automatica*, vol. 45, no. 9, pp. 2052–2059, 2009.

[11] S. L. Campbell and R. Nikoukhah, *Auxiliary signal design for failure detection*. Princeton University Press, 2015.

[12] H. Niemann, "A setup for active fault diagnosis," *IEEE Transactions on Automatic Control*, vol. 51, no. 9, pp. 1572–1578, 2006.

[13] A. Sekunda, H. Niemann, N. K. Poulsen, and I. Santos, "Closed loop identification using a modified hansen scheme," in *Journal of Physics: Conference Series*, vol. 659, no. 1. IOP Publishing, 2015, p. 012009.

[14] H. Niemann and N. K. Poulsen, "Estimation of parametric fault in closed-loop systems," in *2015 American Control Conference (ACC)*. IEEE, 2015, pp. 201–206.

[15] L. R. S. Theisen, F. G. Pierart, H. Niemann, I. F. Santos, and M. Blanke, "Experimental grey box model identification and control of an active gas bearing," in *Vibration Engineering and Technology of Machinery*. Springer, 2015, pp. 963–976.

[16] B. D. Anderson, "From youla–kucera to identification, adaptive and nonlinear control," *Automatica*, vol. 34, no. 12, pp. 1485–1506, 1998.

[17] F. Hansen, G. Franklin, and R. Kosut, "Closed-loop identification via the fractional representation: Experiment design," in *1989 American Control Conference*, 1989, pp. 1422–1427.

[18] T.-T. Tay, I. Mareels, and J. B. Moore, *High performance control*. Springer Science & Business Media, 2012.

[19] H. Niemann, "Dual youla parameterisation," *IEE Proceedings-Control Theory and Applications*, vol. 150, no. 5, pp. 493–7, 2003.

Publication P4

Detector Design for Active Fault Diagnosis in Closed Loop Systems

Detector Design for Active Fault Diagnosis in Closed Loop Systems

André K. Sekunda[1], H Niemann[1] and N Kjølstad Poulsen[2]
[1]) Department of Electrical Engineering, Technical Unversity of Denmark, Kongen Lyngby, Denmark
[2]) Department of Applied Mathematics and Computer Science, Technical Unversity of Denmark, Kongen Lyngby, Denmark
E-mail: aksek@elektro.dtu.dk, hhn@elektro.dtu.dk, nkpo@dtu.dk

Abstract

Fault diagnosis of closed loop systems is extremely relevant for high precision equipment and safety critical systems. Fault diagnosis is usually divided into two schemes, active and passive fault diagnosis. Recent studies have highlighted some advantages of active fault diagnosis based on dual Youla-Jabr-Bongiorno-Kucera (YJBK) parameters. In this paper a method for closed loop active fault diagnosis based on statistical detectors is given using dual YJBK parameters. The goal of the paper is twofold; Firstly the authors introduce a method for measuring a residual signal subject to white noise; Secondly an optimal detector design is presented for single and multiple faults using the amplitude and phase shift of the residual signal to conduct diagnosis. Here both the optimal case of a perfect model and the suboptimal case of a model with uncertainties are discussed. The method is successfully tested on a simulated system with parametric faults.

Keywords— YJBK Parameters, Active Fault Diagnosis, Statistical Test, Closed-loop Systems

1 Introduction

Fault diagnosis has been an intensively studied subject which has branched into two subgroups; passive [1, 2, 3] and active [4, 5, 6] fault diagnosis. Broadly speaking passive fault diagnosis obtain information of faults by the use of residual signals generated by comparing input-output data [7] whereas active fault

diagnosis uses auxiliary signals to obtain extra information about the state of a system to use for fault diagnosis. So far most active fault diagnosis solutions have been based on the assumption of an open loop system description, however, fault diagnosis of closed loop systems is more relevant for critical systems. For open loop processes it is usually possible to assume the characteristics of the noise to be the same for the open loop measurements as for the residual signal. This is however not the case when a feedback law is imposed. It has been shown in [8] how to design a residual generator where the noise characteristics are independent of the feedback loop, using active fault detection of a coprime factorised system.

A method for detecting parametric faults by the use of a nominal fault free model was given in [9]. The method was based on translating different parametric faults to a fault signature system and detecting changes in this fault signature system using a known excitation signal. Furthermore it was shown in [8] how to design a CUSUM detector for such a problem. Research into linearisation of the fault signature system and isolation of faults have been investigated in [10, 11].

Detector design for statistical tests have been presented in [12] and the Neyman-Pearson detector was presented for optimal detection of partially known signals corrupted with noise. Using a statistical detector have the advantage of an easy translation to the false alarm rate and probability of detection, the classical succes criteria for a fault diagnosis scheme. The detectors introduced in [12] assume the noise to be white which was not the case with the solution presented in [8]. A method for isolation of faults based on a sequential detector was proposed in [13] using several excitation signals with different frequencies. An implementation of a statistical detector for detecting faults was proposed first in [14] where the fault signature system was linearised. A simulation of how to detect parametric faults on the actuators of an active gas bearing was presented. The linearised fault signature system was however found ill suited for parametric faults that showed highly non-linear behaviour. Furthermore the residual was subject to coloured noise which resulted in an increase in false alarm occurrences.

In this paper it is proven possible to implement a detector as presented in [12] for active fault detection based on the fault signature system. The system to be detected faults on is part of a closed loop scheme with a known controller. Most systems to be conducted fault detection on are believed to be part of a closed loop scheme. Pre-whitening of the noise has been conducted to improve the results. It is proposed to use the knowledge of the detectors sensitivity towards different faults to enable isolation of several faults using only a single excitation

signal with a known amplitude and frequency. The method presented exploits knowledge about the phase shift and gain impacts of the faults in order to isolate different faults using only a single signal. Basing the fault diagnosis on the magnitude and phase information makes the solution advantageous compared to other methods such as previously shown in [4, 5, 6, 15]. It is shown that it is possible to design the detector based solely on the stochastic model of the noise in addition to the model of the controller and plant. The detector is implemented as a moving window to be able to detect changes over time. The impact of model uncertainties is furthermore discussed. It is believed that a design procedure for residual signals of closed loop systems that ensure the noise on the residual signal to be white is useful for fault diagnosis of closed loop systems.

The paper is structured as follows: Section 2 introduces the reader briefly to the preliminary work conducted; Section 3 presents the residual signal design; Section 4 presents the detector design and isolation procedure; Section 6 shows some examples using the method described; The paper is closed with a conclusion in section 7.

2 Preliminary Results

Most detector designs are based on the assumption that the detector signal is influenced by white noise. Such assumptions are usually valid given open loop problems such as depicted on Figure 0.1. Here the plant $G(\theta)$ is subject to a known input u and the output of the plant y_m is subject to an unknown disturbance d which is in this paper assumed to be white gaussian noise.

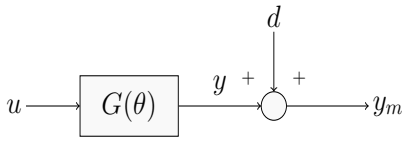

Figure 0.1: Simple open loop plant setup. The plant $G(\theta)$ is only subject to a known input and the output signal(y_m) is generated by the plant and the unknown disturbance d.

Such a system structure as presented on Figure 0.1 is only feasible to use when feedback control is not required and the plant is open loop stable. However most interesting control applications require some form of feedback control. When feedback control is applied, the system representation changes to Figure 0.2, which is the standard implementation used throughout this paper.

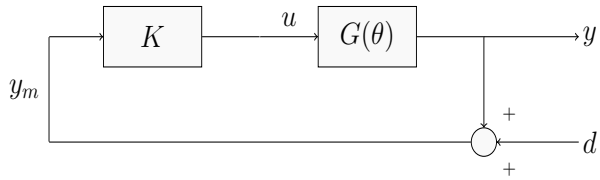

Figure 0.2: Representation of the system description used throughout this paper. The system is here subject to feedback control through the controller K. Again the output is subject to an unknown disturbance signal (d)

From Figure 0.2 it is easy to see that the assumption of white noise on the measurement signal y_m does not hold due to the feedback loop. The noise signal d is treated as white with a Gaussian distribution for simplicity in the paper. However much of the analysis conducted throughout the paper is independent of the noise distribution.

Coprime Representation

In this section a coprime description of the nominal plant and controller are exploited to represent the parametric faults in the plant through the use of the fault signature matrix. Given a nominal plant $G(0)$ and a controller $K(0)$ the coprime factorisation of plant and controller are given in the following two equations respectively.

$$G(0) = NM^{-1} = \tilde{M}^{-1}\tilde{N}, \qquad N, M, \tilde{M}, \tilde{N} \in \mathcal{RH}_\infty \tag{1}$$

$$K(0) = UV^{-1} = \tilde{V}^{-1}\tilde{U}, \qquad U, V, \tilde{V}, \tilde{U} \in \mathcal{RH}_\infty \tag{2}$$

Here the $\tilde{\cdot}$ represent the left coprime factorisation where as systems without, are the right coprime factorisation. Such a left and right coprime factorisation are always possible to find when the plant and controller can be represented as rational functions [16]. Given the eight matrices in Eq. (1) and Eq. (2) the double Bezout identity shown in Eq. (3) is satisfied due to the coprimeness.

$$\begin{bmatrix} I & 0 \\ 0 & I \end{bmatrix} = \begin{bmatrix} M & U \\ N & V \end{bmatrix} \begin{bmatrix} \tilde{V} & -\tilde{U} \\ -\tilde{N} & \tilde{M} \end{bmatrix} = \begin{bmatrix} \tilde{V} & -\tilde{U} \\ -\tilde{N} & \tilde{M} \end{bmatrix} \begin{bmatrix} M & U \\ N & V \end{bmatrix} \tag{3}$$

Given a nominal plant as defined in Eq. (1) it is possible to define all stabilising controllers based on a nominal stabilising controller. Such a controller

is given in Eq. (4) using the right coprime factorisation and in Eq. (5) based on the left coprime factorisation of plant and controller [17].

$$K(Q) = (U + MQ)(V + NQ)^{-1}, \quad Q \in \mathcal{RH}_\infty \tag{4}$$
$$K(Q) = (\tilde{V} + Q\tilde{N})^{-1}(\tilde{U} + Q\tilde{M}), \quad Q \in \mathcal{RH}_\infty \tag{5}$$

$K(Q)$ can be represented as a linear fractional transformation (LFT). A lower LFT of the parametrised controller $K(Q)$ is given by:

$$K(Q) = \mathcal{F}_l(J_K, Q) \tag{6}$$
$$J_K = \begin{bmatrix} UV^{-1} & \tilde{V}^{-1} \\ V^{-1} & -V^{-1}N \end{bmatrix} \tag{7}$$

In principle it is possible to design a realisation as in Eq. (6) of any linear controller. Such a control implementation is shown on Figure 0.3. The system shown in Figure 0.3 is the same as presented in Figure 0.2, however two new signals α and β are introduced to the closed loop system description.

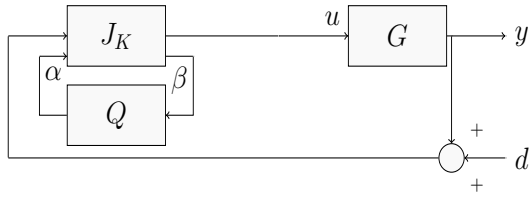

Figure 0.3: Closed loop system setup using the Youla parametrisation of the controller.

It is shown in [17] how to transform some of the most general controller schemes into the form shown on Figure 0.3.

It is possible to parametrise all plants stabilised by the nominal controller. In Eq. (8) and Eq. (9) a parametrisation of all plants stabilised by a nominal controller based on the right and left coprime factorisation are respectively given.

$$G(S) = (N + VS)(M + US)^{-1}, \quad S \in \mathcal{RH}_\infty \tag{8}$$
$$G(S) = (\tilde{N} + S\tilde{V})^{-1}(\tilde{M} + S\tilde{U}), \quad S \in \mathcal{RH}_\infty \tag{9}$$

Equivalently as for the parametrised controller it is possible to represent the parametrised plant as a LFT:

$$G(S) = \mathcal{F}_u(J_G, S) \tag{10}$$

$$J_G = \begin{bmatrix} -M^{-1}U & M^{-1} \\ \tilde{M}^{-1} & NM^{-1} \end{bmatrix} \tag{11}$$

A block diagram of the closed loop system introduced in Figure 0.2 with the parametrised plant using Eq. (10) is shown in Figure 0.4.

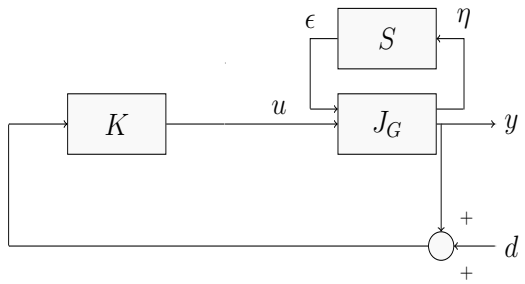

Figure 0.4: Closed loop system setup using the Youla parametrisation of the plant.

Again two new signals are introduced, η and ϵ. The transfer function S parametrising all plants stabilised by the nominal controller have been known as the open loop error between the nominal and real plant [18] and describe the dynamics of the true system omitted from the nominal model. It was shown in [18] that the signal η is independent of the output noise d.

The signals η and ϵ are however not directly measurable. It was shown in [17] that the relationship between the set of signals $\{\alpha, \beta\}$ from Figure 0.3 and the set of signals $\{\eta, \epsilon\}$ from Figure 0.4 can be depicted as in Figure 0.5

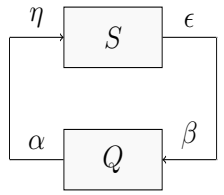

Figure 0.5: Figure showing the relationship between the input-output pair of S and Q.

There are several ways to prove the relationship between the two set of signals $\{\alpha, \beta\}$ and $\{\eta, \epsilon\}$, with one approach to be found in [19]. Whereas it is not possible to directly excite the system using η, it is using the signal α. It is

therefore convenient to use the signals related to the controller for identification and detection purposes.

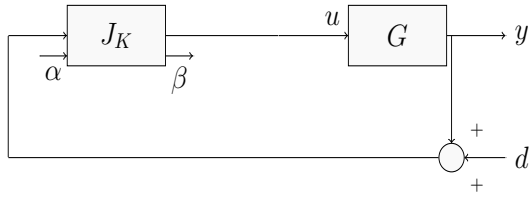

Figure 0.6: Alternative controller representation based on a coprime factorisation of the controller and plant model.

The system setup in Figure 0.6 is equivalent to the setup shown in Figure 0.3 but with Q omitted. Furthermore it is also straightforward to see from Figure 0.6 that the controller is not changed from the nominal one as long as Q is disconnected.

In order to state the detection problem the closed loop system with regards to the external inputs is required. The transfer functions are shown in Eq. (12) and are derived from Figure 0.4 with the input and output vector defined as in Eq. (12) as well as the connection of the signals shown in Figure 0.5.

$$\begin{bmatrix} y \\ u \\ \beta \end{bmatrix} = \begin{bmatrix} (N+VS)\tilde{U} & N+VS \\ (M+US)\tilde{U} & M+US \\ \tilde{M}+S\tilde{U} & S \end{bmatrix} \begin{bmatrix} d \\ \alpha \end{bmatrix} = P_{cl}(S) \begin{bmatrix} d \\ \alpha \end{bmatrix} \tag{12}$$

Here the β output is considered the detection or residual signal. The input signal d is considered an unknown input, while α is the controllable input used for active fault detection.

Fault diagnosis in the YJBK setup

In order to detect faults in the system based on the fault signature system S, it is necessary to translate the behaviour of parametric faults from the input-output pair u, y to the signal pair η, ϵ. Such a parametrisation was first introduced in [20] and methods to represent different parametric faults were first presented in [21]. This method is based on a coprime factorisation of a nominal model of the implemented plant and controller in order to design a residual signal which is zero for the fault free case and non zero when a fault occurs. However in order to define the parametric faults through the fault signature system it is

first necessary to establish how faults on the plant are represented. Given a parametric fault θ assume that the plant can be defined as an upper LFT as shown in Eq. (13), where G_{zw}, G_{zu}, G_{yw} and G_{yu} are defined using only the fault free plant and the parametric fault θ. θ is given as a diagonal matrix where each diagonal element, denoted θ_i, corresponds with a parametric fault.

$$G(\theta) = \mathcal{F}_u\left(\begin{bmatrix} G_{zw} & G_{zu} \\ G_{yw} & G_{yu} \end{bmatrix}, \theta\right) \tag{13}$$

Instead of expressing the plant G as a function of θ it is advantageous to formulate the fault signature system as a function of the unknown parametric faults θ. Given faults in the form presented in Eq. (13) it was shown in [10] that the fault signature system can be expressed as:

$$S(\theta) = \mathcal{F}_l\left(\begin{bmatrix} 0 & \tilde{M}G_{yw} \\ G_{zu}M & G_{zw} + G_{zu}U\tilde{M}G_{yw} \end{bmatrix}, \theta\right) \tag{14}$$

It is clear from Eq. (14) that the fault signature system $S(\theta)$ is a non-linear function with regards to the parametric faults. The gain and the phase shift of the fault signature system depends on the parametric fault and are therefore of interest for fault diagnosis. With the fault signature system given with respect to the parametric faults, it is useful to state the diagnosis problem solved in this paper.

The main advantage of using the fault signature system as described in Eq. (14) comes from the fact that $S(\theta)$ is zero in the fault free case i.e

$$S(0) = 0 \tag{15}$$

While it is different from zero when a detectable fault occurs, i.e.

$$S(\theta) \neq 0 \qquad \forall \qquad \theta \neq 0 \tag{16}$$

The effect of faults on S is thus similar to the effect of faults on the residual generator used for passive fault detection.

3 Detection Problem Formulation

In section 2 the connection between parametric faults and the fault signature system was established based on the system description given in section 2. In

this section the residual signal used for detection is presented and the assumptions used for detector design in the following sections are presented.

Using Eq. (12) the residual signal is

$$\beta[n] = S(\theta)\alpha[n] + (\tilde{M} + S(\theta)\tilde{V})d[n] \tag{17}$$

The residual in Eq. (17) is influenced by white noise d which goes through a filter. The residual signal β is therefore influenced by coloured noise. In active fault diagnosis the goal of the detector is to detect a known signal with unknown amplitude and phase, corrupted by noise, compactly written

$$\beta[n] = A_{S_\theta}\alpha[n - n_0] + (\tilde{M} + S(\theta)\tilde{U})d[n] \qquad n = 0, 1, ..., N - 1 \tag{18}$$

Here $\alpha[n]$ is the known excitation signal at sample n, A_{S_θ} is the gain through the fault signature system of the known excitation signal $\alpha[n]$, n_0 is the delay of the excitation signal through the fault signature system and $d[n]$ is the noise signal which in this paper is assumed to be white gaussian noise. For the transition from Eq. (17) to Eq. (18), it is assumed that the excitation signal α is having a period sufficiently long compared to the sampling period. Furthermore the period of α is possible to describe as a whole multiple of the sampling period.

For the detection methods presented in this paper the noise is modelled as gaussian. However the noise is not required to be gaussian in order to design a matched filter detector, but this requirement is maintained throughout the paper for simplicity. Whiteness of the noise is on the other hand a strict requirement, to be able to give an upper bound to the number of false alarms in the fault free case. Given the method presented the noise on the residual signal is kept white in the fault free case when the system is only subject to white noise. Furthermore it is mentioned briefly how to keep the whiteness requirement for a system subject to both system and measurement noise.

Design of whitening filter

In the first case for a signal as given in Eq. (18) and letting $\mathcal{H}_0$ be the fault free case, since $S(0)$ is zero, the residual signal β simplifies to

$$\mathcal{H}_0 : \beta[n] = \tilde{M}d[n] \tag{19}$$

Since $\tilde{M}$ is a model dependent known system the residual signal is redefined to

$$\mathcal{H}_0 : r[n] = \tilde{M}^{-1}\beta[n] = d[n] \tag{20}$$

It is clear from Eq. (20) that if the noise d is white gaussian, then the noise imposed on the residual signal in Eq. (20) is white gaussian as well. Furthermore the variance of the noise on the residual signal is equivalent to the variance of the measurement noise. Designing the decorrelation filter $\tilde{M}^{-1}$ is only feasible for open loop stable systems. Given any open loop unstable system $\tilde{M}^{-1}$ will be unstable, and instead a stable filter with the same correlation as $\tilde{M}^{-1}$ is required.

Such a filter can be realised by a spectral factorisation, finding a stable filter with the same pre-whitening effect as the unstable filter $\tilde{M}^{-1}$. In this paper all theory is handled in discrete time however a continuous equivalent is also possible by mirroring the right half plane zeros through zero on the real axis.

For the system $\tilde{M}$ containing zeros outside the stability area it is possible to design a system which has no zeros outside the stable area with the same spectrum denoted W. The method can be found in [22] and a transformation which keeps the same spectrum is shown in eq. (21) while transforming the unstable solution into a stable one.

$$W(\bar{z})W^T(z) = \tilde{M}(\bar{z})\tilde{M}^T(z) \tag{21}$$

The stable filter is thus denoted W^{-1} and the detection signal is given in Eq. (22) with the proposed stable filter that makes the noise white on the detector signal in the fault free case.

$$\mathcal{H}_0 : r[n] = W^{-1}\beta[n] = Hd[n] \tag{22}$$

where $H = W^{-1}\tilde{M}$ is a constant diagonal matrix [22]. Since H contains no dynamics the detector signal is again only subject to white gaussian noise, however the method does alter the variance of the noise as shown by the constant H matrix.

The methods presented above are based on the assumption that all noise can be modelled as white gaussian noise on the output. For the case of a white gaussian process and measurement noise, designing a Kalman filter is proposed instead. A Kalman filter ensures that the noise is white on the innovation signal and thereby on β as shown in [23].

In this paper the detectors are designed based on white gaussian output noise only. Therefore if the system is open loop unstable, the residual is given

by Eq. (23) where the variance of the noise d in the fault free case has been subject to the constant diagonal matrix H.

$$r = W^{-1}\tilde{M}G_{yw}\theta(I - (G_{zw} + G_{zu}U\tilde{M}G_{yw})\theta)^{-1}G_{zu}M\alpha + (H + W^{-1}S(\theta)\tilde{U})d \tag{23}$$

For the case that the plant is open loop stable the residual signal can be simplified. The residual signal of interest to detect in white gaussian noise is then with regards to the parametric uncertainties given as

$$r = G_{yw}\theta(I - (G_{zw} + G_{zu}U\tilde{M}G_{yw})\theta)^{-1}G_{zu}M\alpha + (I + \tilde{M}^{-1}S(\theta)\tilde{U})d \tag{24}$$

4 Fault Diagnosis

In this section the detector design is presented together with calculations of the probability of detection and the threshold. The matched filter detector with a moving window is chosen since it is natural to design based on a wanted false alarm rate. The detector design is based on the residual signal given by Eq. (23) which is the general case. It is assumed that several different faults can occur in the plant however multiple faults can't happen simultaneously. In order to detect the faults a moving window is used. The detector is based on selecting 1 input and 1 ouput of the plant to use for diagnosing the faults. This section is structured such that first detection design is presented without any further assumptions. The ability to isolate faults is then discussed and test statistics for the detector design is given. Finally the detector design is presented for the case of unique phase shifts for each of the faults considered.

Detector Design

Using the framework introduced in [24] to design the detector a $\mathcal{H}_0$ hypothesis is constructed in Eq. (25) for the fault free case, and a $\mathcal{H}_1$ hypothesis is constructed in Eq. (26) representing the case that one of the possible faults has occurred.

$$\mathcal{H}_0 : r[n] = Hd[n], \qquad n = 0, 1, ..., N-1 \tag{25}$$

$$\mathcal{H}_1 : r[n] = A_{S_\theta}\alpha[n - n_0] + (H + W^{-1}S(\theta)\tilde{U})d[n], \qquad n = 0, 1, ..., N-1 \tag{26}$$

Here d is white gaussian noise, A_{S_θ} is the amplification of the detector signal through the system $W^{-1}S(\theta)$, which both depends on which fault is occurring

and the magnitude of the fault. n_0 is the unknown delay due to the fault occurring and the magnitude of this fault. Only faults causing parameter degradation are considered in this paper, which limits the relative faults θ_i to $[-1\ 0[$, where 0 corresponds to no fault and -1 corresponds to a complete failure. There is thus no sign change through the whole possible fault range which makes a Neyman-Pearson detector feasible [12].

The design of the detector is based on the $\mathcal{H}_1$ hypothesis given a predetermined possible fault. A moving window is used for the detector such that it is possible to determine when a change occurs. Since the delay is unknown and depends on the fault occurring, it is required to determine the delay of detector signal, which can be accomplished using

$$\phi = \arg\max_{n_0 \in \tau} \left(\sum_{n=n_0}^{n_0+N-1} r[n]\alpha[n-n_0] \right) \tag{27}$$

Here ϕ is the maximum likelihood estimate of the delay, τ is the set of possible delays given a priori knowledge about the parametric faults and N is the window length. With the delay estimated using Eq. (27) the test statistic can be designed. For the generalised case, the test statistic is

$$T(r) = \sum_{n=\phi}^{\phi+N-1} r[n]A_0\alpha[n-\phi] \tag{28}$$

Here A_0 is a predetermined amplification of the signal excitation α through the fault signature system given the initial guess of the magnitude of one of the faults. It is possible to design other test statistics which might be beneficial in special cases.

An example of such a test statistic is given in subsection 4 which for certain assumptions has attributes which simplify the test statistics.

In fault detector design the probability of a false alarm and probability of detection are usually the two design criteria. For a detector as described in Eq. (28) the probability of false alarm is used to determine the threshold γ as shown in Eq. (29)

$$\gamma = \sqrt{\sigma^2\nu}Q^{-1}(P_{FA}) \tag{29}$$

$$\nu = N\frac{A_0^2}{2} \tag{30}$$

Here σ^2 is the variance of the noise, ν is the energy contained in the signal for one window length given a sinusoidal wave, $Q(\cdot)$ is the complementary cumulative distribution and P_{FA} is the allowed frequency of false alarms. It is worth noticing that the threshold is independent of the different possible faults. The $\mathcal{H}_1$ hypothesis chosen by Eq. (27) is discarded if $T(r)$ is below the threshold γ and found to be true if $T(r)$ is above the threshold γ.

With a threshold design based on the allowed probability of a false alarm, the probability of detection is

$$P_D = Q(Q^{-1}(P_{FA}) - \sqrt{D}) \tag{31}$$

The probability of detection is based on the assumption of the noise to be white which it is not in the case when $\mathcal{H}_1$ is true. The variance of the detector signal will therefore be higher than approximated. The deflection coefficient D is

$$D^2 = \frac{(E(T;\mathcal{H}_1|_{\theta_k}) - \mathcal{X})(E(T;\mathcal{H}_1|_{\theta_{A_0}}) - \mathcal{X})}{var(T;\mathcal{H}_0)} \tag{32}$$

The deflection coefficient depends on the fault detected θ_k and the initial guess of the fault θ_{A_0}. It is therefore necessary to calculate the probability of detection separately for each fault considered. It is worth noticing that Eq. (32) is only true when the test statistic in Eq. (28) is used.

Here $\mathcal{X}$ is defined in Eq. (33) and is the expected value of the test statistic given that the $\mathcal{H}_0$ is true.

$$\mathcal{X} = E(T;\mathcal{H}_0) \tag{33}$$

Using Eq. (31) it it possible to determine the smallest parametric fault with an acceptable probability of detection given the desired probability of the false alarm rate.

Design of the excitation signal

It is of paramount importance to be able to design the excitation signal in accordance with predetermined criteria. In this subsection one such criteria is presented so that it is possible to design the excitation signal. It is for simplicity decided to use only one input for the excitation signal and one output of the fault signature system. The relevant fault signature system thus becomes a SISO

system which makes the analysis simpler. The shape of the excitation signal has in this paper been limited to be a single sinusoidal wave with the single degree of freedom being the frequency. It is the task of the excitation signal to maximise the impact of a fault in the residual signal. Thus it is desired to determine the gain of the transfer function from the excitation signal to the residual given as

$$\xi_r(\omega) = |W^{-1}\tilde{M}G_{yw}\theta(I - (G_{zw} + G_{zu}U\tilde{M}G_{yw})\theta)^{-1}G_{zu}M| \tag{34}$$

If the design criteria is simply to maximise the amplitude of the excitation signal the goal is to maximise Eq. (34). However it is believed that for most systems the design of the excitation signal should be a trade off between maximising the signature of faults while minimising the impact of the excitation signal on the system outputs. The highest gain from the excitation signal to the system outputs can be found using Eq. (12) and is

$$\xi_y(\omega) = \bar{\sigma}(N(\omega)) \tag{35}$$

Here $\bar{\sigma}$ denotes the highest singular value [25] which corresponds to the direction with the highest gain for a MIMO system. It is possible to define a criteria for design of the excitation signal with the gain from the excitation signal to the residual and outputs respectively determined as

$$f_\alpha(\omega) = \frac{\xi_r(\omega)}{\xi_y(\omega)} \tag{36}$$

The frequency of the excitation signal is thus chosen.

$$\omega_\alpha = \underset{\omega_1 \leq \omega \leq \omega_2}{\operatorname{argmax}} f_\alpha(\omega) \tag{37}$$

Here ω_1 defines the lowest considered frequency and ω_2 is the highest frequency considered for the sinusoidal excitation signal. For many systems the range of possible frequencies might be limited due to mechanical limitations or the sample speed which would naturally define the upper and lower limit. So far only a single fault is considered for detection. For several possible faults the frequency should be chosen such that the detectability of the fault most difficult to detect is maximised why Eq. (36) is changed to:

$$f_\alpha(\omega) = \min_{\theta=\Delta} \frac{\xi_r(\theta, \omega)}{\xi_y(\omega)} \tag{38}$$

Here Δ denotes the set of different possible faults considered. With Eq. (36) reformulated as Eq. (38) the optimal excitation frequency can again be found using (37).

Isolation of Faults

In this subsection the ability to isolate faults is discussed. The discussion is based on an excitation signal containing a single sinusoidal wave and estimating the phase shift using Eq. (27). It is in the general case not possible to isolate a fault only based on the phase shift, given that the phase shifts of several faults might be the same. An example is given in Figure 0.7 of how two parametric faults that share the same phase shift.

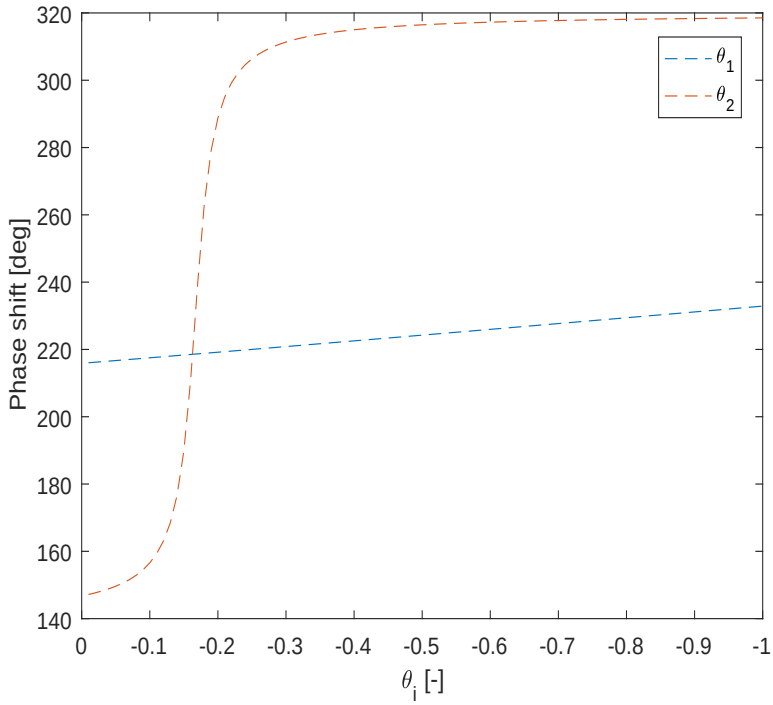

Figure 0.7: Phase shift of a sinusoidal wave for an example system with two possible parametric faults. Here it is seen that all delays that could correspond to parametric fault 1 (θ_1) occurring might as well correspond to parametric fault 2 (θ_2) occurring with a magnitude degradation around 20 %.

It can be seen from Figure 0.7 that the set of possible phase shift for fault 1 is a subset of the set of possible phase shifts for the second parametric fault. It is

therefore not possible to distinguish when fault 1 has occurred from instances of fault 2 occurring solely based on the phase shift. It is thus seen to be convenient to exploit the knowledge about the phase shift and the gain of the fault signature system. Using the test statistic $T(r)$ from Eq. (28) with the moving window N, which are whole periods, the energy of the signal is

$$\kappa = N\frac{A_k A_0}{2} \tag{39}$$

Here A_k is the amplitude of the sinusoidal wave $r[n]$. Using the fact the the noise is Gaussian with a mean of 0, by isolating A_k in Eq. (39) the amplitude of the sinusoidal detector wave can be found as Eq. (40) for an appropriate window length.

$$A_k = \frac{2\kappa}{NA_0} \tag{40}$$

The gain from the excitation signal to the detection signal is thus.

$$A_{S_\theta} = \frac{A_k}{|\alpha|} \tag{41}$$

As with the phase shift, it is also possible to determine how the gain of the excitation signal changes with regard to the magnitude of the fault for a specific frequency of the sinusoidal signal.

The gain of the excitation signal is shown in Figure 0.8 for the same system and same parametric faults as were presented in Figure 0.7. By combining the two it is easy to see that it is possible to isolate which fault has occurred. The fault isolation so far is based on choosing the frequency which makes the job of fault detection easiest. Such a choice does not consider whether the fault characteristics are similar or not and might therefore be a poor choice when it comes to fault isolation. In such a case it can be beneficial to change the frequency of the sinusoidal wave of the excitation signal to maximise the difference between the fault signatures when a fault is detected and isolate the fault through a second test.

Multiple faults without phase shift crossing

The method presented in subsection 4 might for some cases be simplified. Depending on how the phase shift develops if there is a unique mapping between

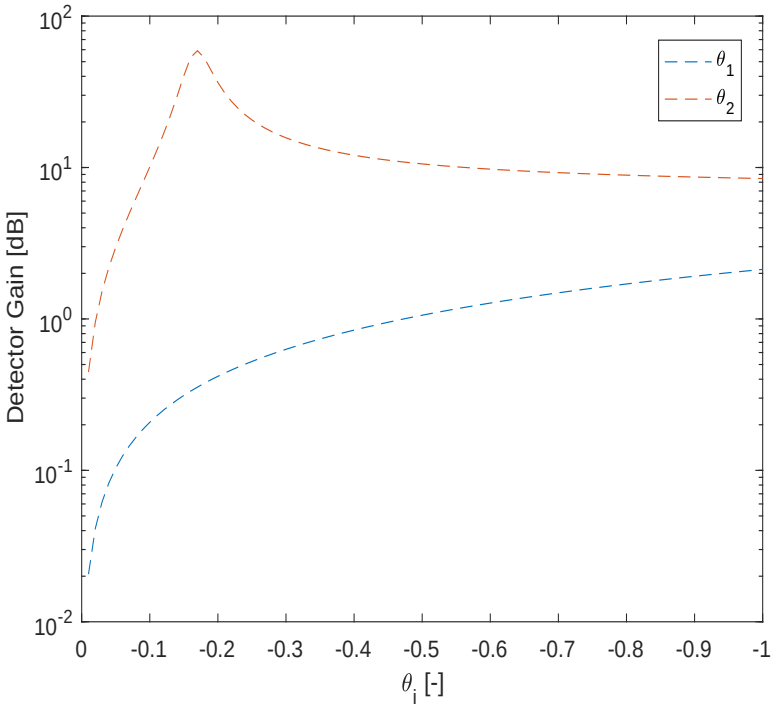

Figure 0.8: Gain of a sinusoidal wave for an example system with two possible parametric faults.

the phase shift and which fault occurs a simplification is possible. This corresponds to the phase shift lines on Figure 0.7 not reaching the same vertical level at any point. If such a mapping is possible the test statistic can be expressed as

$$T(r) = \sum_{n=\phi}^{\phi+N-1} r[n] A_\phi \alpha[n-\phi] \tag{42}$$

Here A_ϕ is the gain from the excitation signal α to the residual signal r based on the fault determined by the delay using Eq. (27). The gain thus changes with regard to the delay identified, which results in a change of the test statistic. Besides changing the test statistic the detector used in Eq. (42) has the advantage of directly identifying which fault is occurring. The threshold is again given as in Eq. (43), but the energy of the signal is now determined by Eq. (44).

$$\gamma = \sqrt{\sigma^2 \nu} Q^{-1}(P_{FA}) \tag{43}$$

$$\nu = N \frac{A_\phi^2}{2} \tag{44}$$

With the threshold determined from Eq. (43) the probability of detection is

$$P_D = Q(Q^{-1}(P_{FA}) - \sqrt{D}) \tag{45}$$

The probability of detection is thus given in the same way for both detectors. The difference is a bit subtle and comes in the change of the definition of the deflection coefficient D. Here D is

$$D^2 = \frac{(E(T; \mathcal{H}_1|_{\theta_k}) - E(T; \mathcal{H}_0))^2}{var(T; \mathcal{H}_0)} \tag{46}$$

The deflection coefficient depends on the fault detected θ_k and must be calculated separately for each fault considered. It is worth noticing that Eq. (46) is only true when the test statistic in Eq. (42) is used, and the deflection coefficient is much more intricate when the assumption of no phase shift crossing cannot be used.

5 Analysis of Model uncertainties

So far a perfect model without any uncertainties has been assumed. It is however important to examine the impact of model uncertainties on the residual signals derived. For this analysis only parametric uncertainties are considered, and the impact of higher order dynamics not contained in the model are disregarded. For parametric uncertainties μ the residual signal is expressed in Eq. (47).

$$r = W^{-1} S(\theta, \mu) \alpha + (H + W^{-1} S(\theta, \mu) \tilde{U}) d \tag{47}$$

The $\mathcal{H}_0$ when no fault occurs is then given in Eq. (48), while the $\mathcal{H}_1$ is given in Eq. (49).

$$\mathcal{H}_0 : r[n] = A_{S_\mu} \alpha[n] + H d[n] \tag{48}$$

$$\mathcal{H}_1 : r[n] = A_{S_{(\theta,\mu)}} \alpha[n - n_0] + (H + W^{-1} S(\theta, \mu) \tilde{U}) d[n] \tag{49}$$

Here A_{S_μ} is the gain through $W^{-1}S(\mu)$ given the frequency of the signal α. μ defines the bound on the uncertainty set, however since the open loop error is non-linear with regards to the parametric uncertainties, the highest amplitude of A_{S_μ} might not be at the boundary. A search in the uncertainty space can thus be conducted in order to find the uncertainty that maximises the gain from the excitation to the residual signal. Such a problem is a N dimensional problem where N is the number of parametric uncertainties. It might therefore be convenient to linearise $W^{-1}S(\mu)$ and determine the gain from the uncertainty bound if the dimension is too large. The threshold is therefore given similarly as the threshold for the case of no uncertainties with the addition of a bias which depends on the uncertainty bound as shown in Eq. (50).

$$\gamma' = \gamma + \nu_\mu = \sqrt{\sigma^2 \nu} Q^{-1}(P_{FA}) + \nu_\mu \tag{50}$$

$$\nu_\mu = N \frac{(A_0 A_{S_\mu})^2}{2} \tag{51}$$

Here A_0 is replaced with A_ϕ if it is possible to use the detector presented in Eq. (42), used for the case when no phase shift crossing is present. Furthermore A_{S_μ} is the maximal amplitude of the signal r due to the uncertainty such that the constant ν_μ is the energy of the detector due to the uncertainty and is an upper bound. The threshold is therefore determined such that the number of false alarms never exceeds the allowed amount. The threshold given in Eq. (50) however is only valid when Eq. (52) is true.

$$\bar{\sigma}(H) \gg \bar{\sigma}(W^{-1}S(\theta, \mu)\tilde{U}) \tag{52}$$

If Eq. (52) is true the noise can be seen as approximately white and gaussian in the fault free case. Such an assumption as given in Eq. (52) is usually valid when proper identification of the system has been conducted beforehand.

Summary of method

The theory has been outlined in the previous sections for how to design a matched filter detector for active FDI. The steps to go through for applying the active FDI method is shown in Figure 0.9. The flow chart is divided into three steps; preliminary experimental work, design phase and implementation.

The method was shown to be based a model of the plant, controller and considered faults. Furthermore knowledge about the PDF and correlation of the noise is required. Based on this initial information is was shown possible to design a detector based on a wanted false alarm rate.

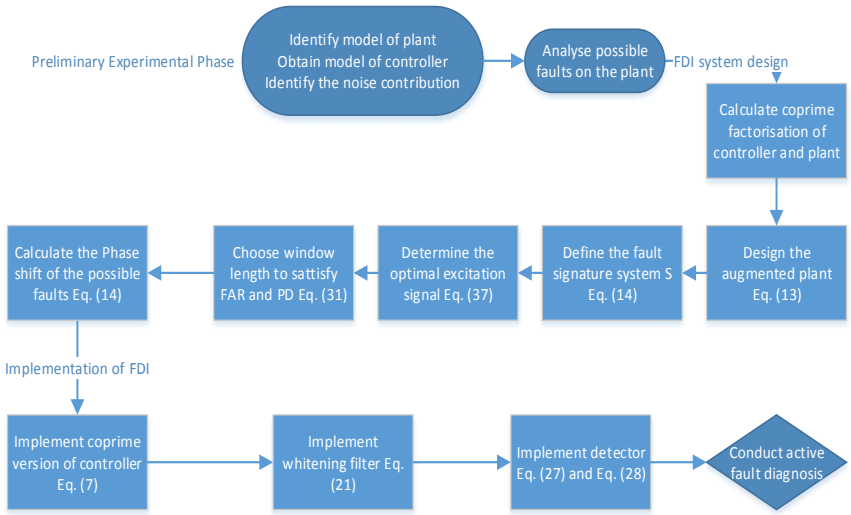

Figure 0.9: Flow chart of the steps involved in using the active FDI method. The round box symbolise information that need to be obtained, the rectangular box symbolise steps derived using already known information and the pointy box symbolise actions.

6 Examples

In this section examples are given to introduce the reader to the method. Simulation examples are given of how to apply the method given in the paper. A discrete second order SISO state space system is used to show how a parametric change can be detected. A MIMO system could as easily be used for the fault detection but is excluded here for simplicity. White gaussian output noise with a variance of 0.11 is applied to the system. The sample time is 1 ms and the 4 matrices of the discrete state space system are given in Eq. (53) to Eq. (56).

$$A = \begin{bmatrix} a_{11} & a_{12} \\ a_{21} & a_{22} \end{bmatrix} = \begin{bmatrix} 1 & -0.3 \\ -0.5 & 0.2 \end{bmatrix} \tag{53}$$

$$B = \begin{bmatrix} b_1 \\ b_2 \end{bmatrix} = \begin{bmatrix} 2 \\ 3 \end{bmatrix} \tag{54}$$

$$C = \begin{bmatrix} c_1 & c_2 \end{bmatrix} = \begin{bmatrix} -1 & 4 \end{bmatrix} \tag{55}$$

$$D = \begin{bmatrix} 0 \end{bmatrix} \tag{56}$$

The state space system used for the example here has a pole outside the unit circle and it is therefore an open loop unstable system. In order to stabilise the

system an observer is designed with a LQR state feedback and observer gain. Furthermore the input gains b_1 and b_2 are prone to multiplicative faults. The input matrix is therefore redefined as in Eq. (57).

$$B = \begin{bmatrix} b_1(1+\theta_1) \\ b_2(1+\theta_2) \end{bmatrix} \tag{57}$$

The augmented system taking the faults into account is given in Eq. (58) using the system description presented in Eq. (13).

$$\begin{bmatrix} z \\ y \end{bmatrix} = \left[\begin{array}{cc|ccc} a_{11} & a_{12} & b_1 & 0 & b_1 \\ a_{21} & a_{22} & 0 & b_2 & b_2 \\ \hline 0 & 0 & 0 & 0 & 1 \\ 0 & 0 & 0 & 0 & 1 \\ c_1 & c_2 & 0 & 0 & 0 \end{array}\right] \begin{bmatrix} w \\ u \end{bmatrix} \tag{58}$$

$$w = \begin{bmatrix} \theta_1 & 0 \\ 0 & \theta_2 \end{bmatrix} z \tag{59}$$

The frequency of the excitation signal was chosen based on the method described in 4. Using Eq. (37) and Eq. (38) the lower bound ω_1 is chosen to be 10 rad/s. The upper bound ω_2 is chosen to be 125 rad/s such that the sampling time is still sufficiently higher.

$$\omega_\alpha = \underset{10 \leq \omega \leq 125}{\operatorname{argmax}} f_\alpha(\omega) = 125 \tag{60}$$

Using Eq. (60) the frequency of the excitation signal is chosen to be 125 rad/s. An illustrative plot of the efficiency for detecting each of the two possible faults using Eq. (36) is shown on Figure 0.10 where θ_1 and θ_2 equal to -0.1 have been considered respectively.

Using Figure 0.10 it is easy to see that the fault which is most difficult to detect is easier to detect as the frequency of the excitation signal is increased. With the augmented system description presented in Eq. (58) and the excitation signal chosen to be a sinusoidal wave of 125 rad/s it is possible to determine the relationship between the phase shift and the magnitude of the fault occurring. Due to the pole location outside the unit circle, the detector signal is given by Eq. (22). The phase shift with regard to the magnitude of the fault is thus as shown on Figure 0.11.

Before designing the detector it is important to verify that the noise is white on the residual signal. It is possible to verify the whiteness of the residual signal by looking at the auto correlation of the signal in the fault free case.

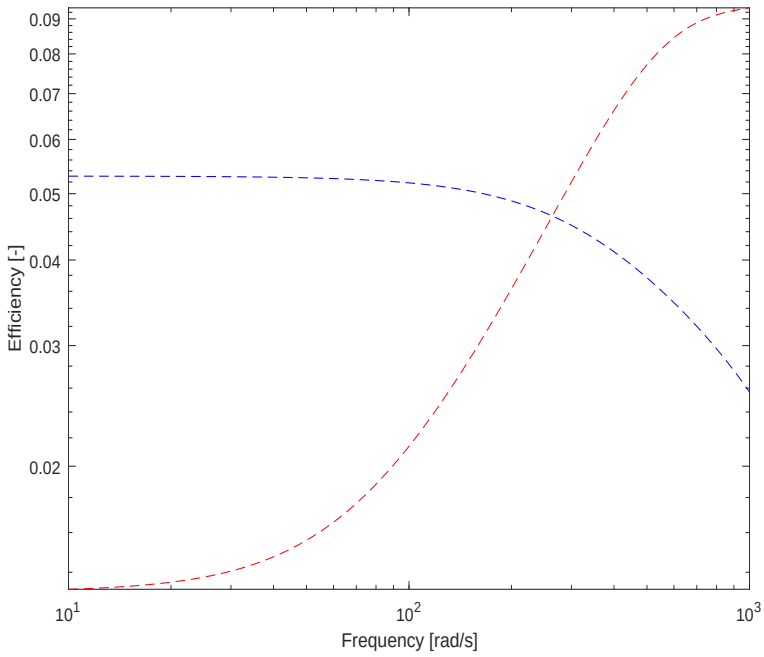

Figure 0.10: Plot of $f_\alpha(\omega)$ for θ_1 of -0.1 (blue) and for θ_2 of -0.1 (red).

The auto correlation of the innovation signal and the innovation signal with the whitening filter W applied is presented on Figure 0.12. The filter W is used since the system itself contains an unstable pole outside the unit circle and $\tilde{M}^{-1}$ is thus not stable. From Figure 0.12 it is seen that the noise is white after applying the whitening filter W and thus a detector can be designed. Furthermore by measuring the residual signal in the fault free case the variance of the noise was found to be 0.14 on the residual signal and A_0 was decided to be a 10% fault on θ_1, which is equal to the fault introduced in the example. Using Eq. (30) the energy in the detector signal can be determined as shown in Eq. (61) where A_0 is found using Eq. (23).

$$\nu = N\frac{A_0^2}{2} = 200\frac{0.29^2}{2} = 8.3 \tag{61}$$

With the energy and the variance of the signal determined the threshold is found using Eq. (29) as

$$\gamma = \sqrt{\sigma^2\nu}Q^{-1}(P_{FA}) = \sqrt{0.14 \cdot 8.3}Q^{-1}(0.0001) = 4 \tag{62}$$

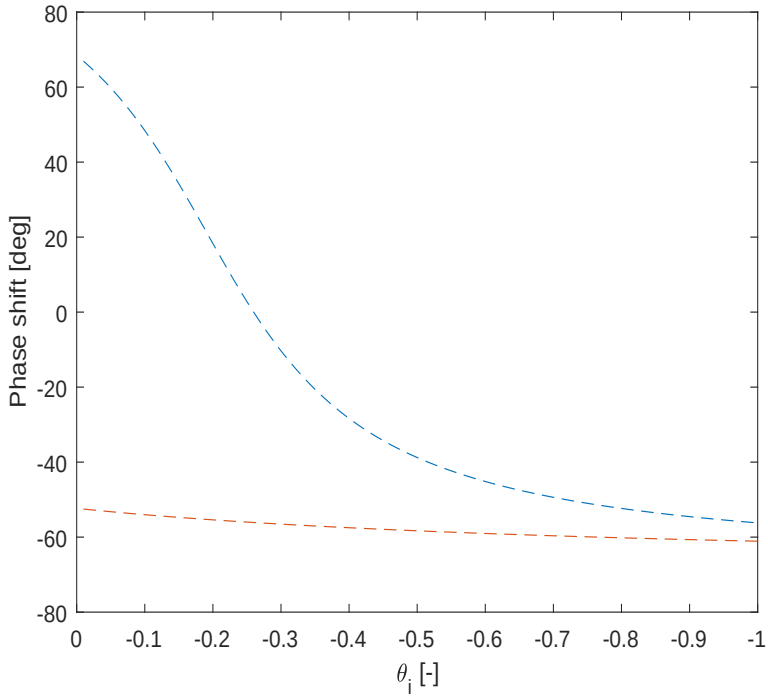

Figure 0.11: Phase shift of a sinusoidal wave of 125 rad/s introduced as the α signal upon the residual signal r. The blue dashed line corresponds to θ_1 and the red dashed line corresponds to θ_2. The phase shift is shown for each fault from the fault free case to the case of a complete failure.

The fault on either parameter 1 or 2 is expected to be a 10% reduction in the gain, which result in a 48.4 degree phase shift of the detector signal if it is fault 1 and a 306 degree phase shift if it is fault 2. The set of possible phase shifts of the detector signal is limited to the set of no fault or a 10% reduction in either of the parameters. The set of possible phase shifts is thus

$$\tau = \{0, 48.4, 306\} \tag{63}$$

This is a very limited set and could easily be expanded. It is however for the sake of clarity chosen to be rather small in this example.

In case the magnitude of the possible fault is unknown the set τ is simply expanded to cover the fault range in an appropriate manner. Given a window length of 200 samples and a sinusoidal excitation signal with an amplitude of 0.1,

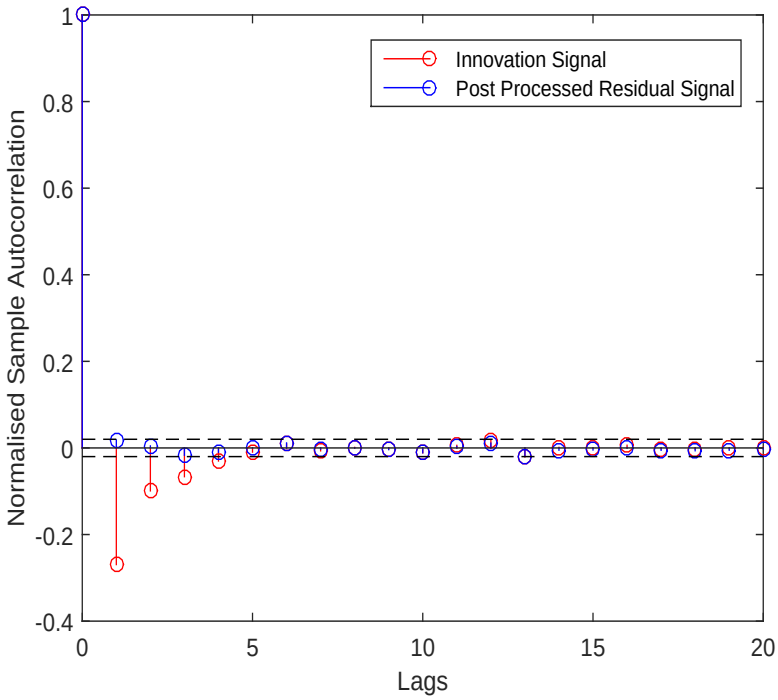

Figure 0.12: Autocorrelation plot of the innovation signal and residual signal respectively. The circles show the normalised autocorrelation for the respective sample delay. The black stippled lines show the 95% confidence bounds.

for a fault θ_1 occurring at 5 seconds, the decision algorithm Eq. (27) produces decisions as shown on Figure 0.13.

With the decision algorithm indicating a fault after 5 seconds the threshold is determined such that one false alarm is on average happening within the simulation period. The threshold is then calculated using Eq. (29) and detection of a fault is shown on Figure 0.14a.

It is possible to increase the probability of detection simply by increasing the window length. However it is important to notice that the window length directly imposes a delay between the occurrence of a fault and the detection of it. The window length should therefore be chosen in accordance with the tolerable delay of detection.

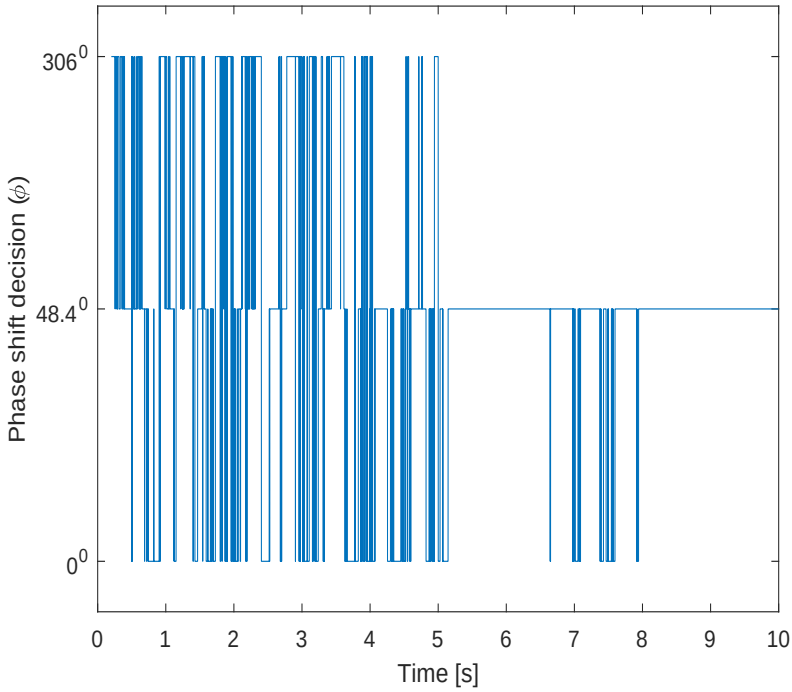

Figure 0.13: Plot of the decision at each time step. The possible phase shifts have been chosen such that a fault of 10% in either θ_1 or θ_2 or no fault at all are searched for. A fault is occurring at 5 seconds on θ_1.

Fault detection with uncertainty

The example system above is now used to show the impact of parametric uncertainties. The system is modified with a parametric uncertainty of the first parameter in the system matrix. The system is thus redefined by the new system matrix

$$A = \begin{bmatrix} a_{11}(1+\mu) & a_{12} \\ a_{21} & a_{22} \end{bmatrix} = \begin{bmatrix} 1+\mu & -0.3 \\ -0.5 & 0.2 \end{bmatrix} \tag{64}$$

This is the same system as used in the first example with the addition of the small parametric uncertainty μ. The bound of the uncertainty is given as $|\mu| = 0.01$. Again parametric faults of the gains from the input to the two states are considered as shown in Eq. (57). The augmented system taking the faults and uncertainty into account is

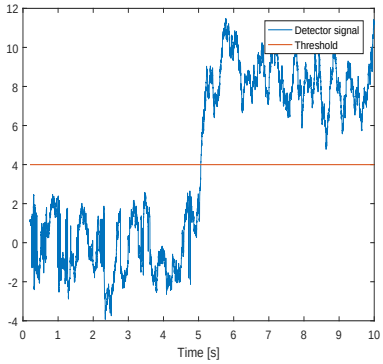

(a) Plot of the test statistic given fault θ_1 occurring after 5 seconds.

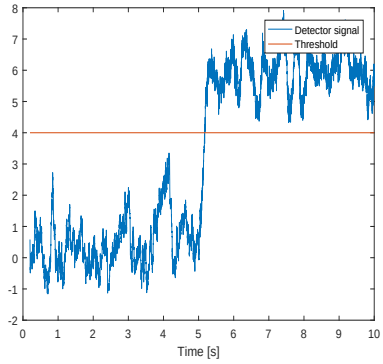

(b) Plot of the test statistic given fault θ_2 occurring after 5 seconds.

Figure 0.14

$$\begin{bmatrix} z \\ \Delta y \\ y \end{bmatrix} = \left[\begin{array}{cc|cccc} a_{11} & a_{12} & b_1 & 0 & b_1 & b_1 \\ a_{21} & a_{22} & 0 & b_2 & 0 & b_2 \\ \hline 0 & 0 & 0 & 0 & 0 & 1 \\ 0 & 0 & 0 & 0 & 0 & 1 \\ 1 & 0 & 0 & 0 & 0 & 0 \\ c_1 & c_2 & 0 & 0 & 0 & 0 \end{array}\right] \begin{bmatrix} w \\ \Delta u \\ u \end{bmatrix} \tag{65}$$

$$\begin{bmatrix} w \\ \Delta u \end{bmatrix} = \begin{bmatrix} \theta_1 & 0 & 0 \\ 0 & \theta_2 & 0 \\ 0 & 0 & \mu \end{bmatrix} \begin{bmatrix} z \\ \Delta y \end{bmatrix} \tag{66}$$

Here Eq. (66) presents the faults and uncertainties as a single complete diagonal system with the vectors z and w having an entry for each of the two faults

considered. This uncertainty introduces an uncertainty region for the phase shift as well as the amplitude of the residual. However for a properly identified system the impact of the uncertainties on the phase shift and amplitude should always be insignificant compared to the impact of the fault in the faulty case. An analysis however is possible to determine the phase shift regions of each fault when taking the bounds of the uncertainties into account. On Figure 0.15 the bounds of the phase shift is shown for fault θ_1 and θ_2.

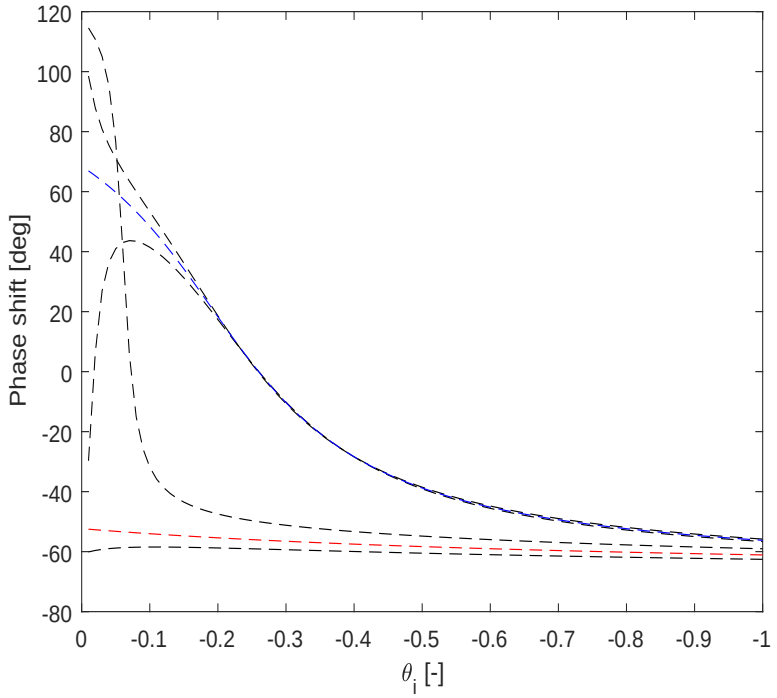

Figure 0.15: Plot of the predicted phase shift of the residual signal r given the fault θ_1 (blue) or the fault θ_2 (red). The black dashed lines represent the bounds on the phase shift given the uncertainty bound, and the red and blue lines are the phase shift introduced by the fault when the uncertainty is not considered.

From Figure 0.15 it is clear that as the magnitude of the fault is increased the impact of the uncertainty on the phase shift decreases as expected. In order to determine the threshold such that the probability of a false alarm does not exceed the predetermined value from the previous example the energy added due to the uncertainty is calculated. The bias added to the threshold due to the uncertainty is found, using Eq. (67), to be 0.1, which guarantees that the number of false alarms does not exceed the previously determined acceptable

limit.

$$\nu_\mu = N\frac{(A_0 A_{S_\mu})^2}{2} = 0.1 \tag{67}$$

$$\gamma' = \gamma + \nu_\mu = 4.1 \tag{68}$$

With the re-evaluated threshold the decision response is shown on Figure 0.16a. Here the set of possible phase shifts has been kept the same as in the previous example since the two possible faults are still clearly separated.

The addition to the threshold using Eq. (67) is based on the assumption that the noise is white for the fault free case, which is not true due to the uncertainty. However the uncertainty in this example has a relatively insignificant impact on the whiteness of the noise and thus the approximation works.

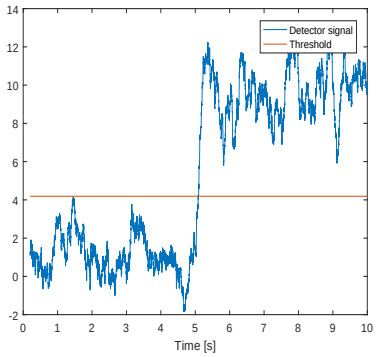

(a) Plot of the test statistic given the uncertainty on the system matrix and the fault θ_1 occurring after 5 seconds.

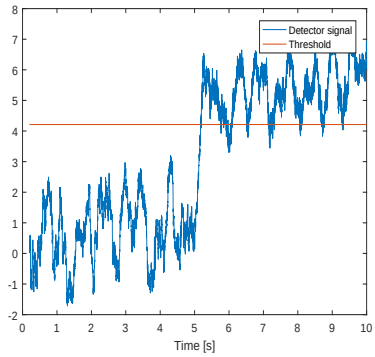

(b) Plot of the test statistic given the uncertainty on the system matrix and the fault θ_2 occurring after 5 seconds.

Figure 0.16

It may be noticed that the threshold is hardly increased due to the uncertainty. This is because the uncertainty introduced in the example has a much larger impact on the phase shift than the magnitude and was thus chosen with a magnitude that provides almost no energy to the detector. It is still possible to distinguish fault from no fault but the variance of the detector signal has increased due to the uncertainty. The example shows that the ability to detect and isolate faults is reduced and a bit more involved when an imperfect model has to be taken into account.

7 Conclusion

A method for design of an optimal detector for active fault detection of a plant in a closed loop system was presented in this paper. It was shown possible to decorrelate the noise for both open loop stable and unstable systems. This made it possible to design optimal detectors based on the Neyman-Pearson detector. Furthermore it was shown how the detector design makes it possible to isolate parametric faults using only a single excitation signal by exploiting knowledge about the phase shift and amplitude of the fault detection signal. A general method was proposed for detector design which could cope with multiple possible parametric faults, and a special case was given which greatly simplified the deflection coefficient. Lastly a simulation example of an open loop unstable system was given. It was shown possible for such a system to generate a residual signal with white noise and design a detector able to both isolate and detect faults of the system for both a system with and without uncertainties.

Bibliography

[1] M. Blanke, M. Kinnaert, J. Lunze, M. Staroswiecki, and J. Schröder, *Diagnosis and fault-tolerant control*. Springer, 2016, vol. 3.

[2] R. Isermann, "Model-based fault-detection and diagnosis–status and applications," *Annual Reviews in control*, vol. 29, no. 1, pp. 71–85, 2005.

[3] P. Frank, S. Ding, and T. Marcu, "Model-based fault diagnosis in technical processes," *Transactions of the Institute of Measurement and Control*, vol. 22, no. 1, pp. 57–101, 2000.

[4] I. Punčochář, J. Širokỳ, and M. Šimandl, "Constrained active fault detection and control," *IEEE Transactions on Automatic Control*, vol. 60, no. 1, pp. 253–258, 2015.

[5] F. Kerestecioğlu* and I. Cetin, "Optimal input design for the detection of changes towards unknown hypotheses," *International Journal of Systems Science*, vol. 35, no. 7, pp. 435–444, 2004.

[6] S. L. Campbell, K. G. Horton, and R. Nikoukhah, "Auxiliary signal design for rapid multi-model identification using optimization," *Automatica*, vol. 38, no. 8, pp. 1313–1325, 2002.

[7] L. H. Chiang, E. L. Russell, and R. D. Braatz, *Fault detection and diagnosis in industrial systems*. Springer Science & Business Media, 2000.

[8] N. Poulsen and H. Niemann, "Active fault diagnosis based on stochastic tests," *International Journal of Applied Mathematics and Computer Science*, vol. 18, no. 4, pp. 487–496, 2008.

[9] H. Niemann* and J. Stoustrup, "An architecture for fault tolerant controllers," *International Journal of Control*, vol. 78, no. 14, pp. 1091–1110, 2005.

[10] H. Niemann and N. K. Poulsen, "Estimation of parametric fault in closed-loop systems," in *2015 American Control Conference (ACC)*. IEEE, 2015, pp. 201–206.

[11] ——, "Active fault detection in MIMO systems," in *2014 American Control Conference*. IEEE, 2014, pp. 1975–1980.

[12] S. M. Kay, "Fundamentals of statistical signal processing: Detection theory, vol. 2," 1998.

[13] N. K. Poulsen and H. H. Niemann, "Active fault isolation and estimation," *Diagnosis of Processes and Systems*, 2009.

[14] A. Sekunda, H. Niemann, N. Kjølstad *et al.*, "Active fault detection based on a statistical test," in *Control and Fault-Tolerant Systems (SysTol), 2016 3rd Conference on*. IEEE, 2016, pp. 511–518.

[15] G. R. Marseglia and D. M. Raimondo, "Active fault diagnosis: A multi-parametric approach," *Automatica*, vol. 79, pp. 223–230, 2017.

[16] M. Vidyasagar, H. Schneider, and B. A. Francis, "Algebraic and topological aspects of feedback stabilization," *IEEE Transactions on Automatic Control*, vol. 27, pp. 880–894, August 1982.

[17] T. T. Tay, I. M. Y. Mareels, and J. B. Moore, Eds., *High Performance Control*. Chicago: Birkhauser, 1998.

[18] B. D. Anderson, "From Youla-Kucera to identification, adaptive and nonlinear control," *Automatica*, vol. 34, pp. 1485–1506, 1998.

[19] A. Sekunda, H. Niemann, N. K. Poulsen, and I. Santos, "Closed loop identification using a modified hansen scheme," *Journal of Physics: Conference Series*, vol. 659, no. 1, p. 012009, 2015. [Online]. Available: http://stacks.iop.org/1742-6596/659/i=1/a=012009

[20] D. Youla, H. Jabr, and J. Bongiorno, "Modern wiener-hopf design of optimal controllers–part ii: The multivariable case," *IEEE Transactions on Automatic Control*, vol. 21, no. 3, pp. 319–338, 1976.

[21] H. Niemann, "Dual youla parameterisation," *IEEE Proc.-Control Theory Appl*, vol. 150, September 2003.

[22] F. Gustafsson and F. Gustafsson, *Adaptive filtering and change detection*. Wiley New York, 2000, vol. 1.

[23] H. Niemann, "A yjbk based architecture for fault diagnosis and fault-tolerant control, linear system theory," 2015.

[24] M. Basseville, I. V. Nikiforov *et al.*, *Detection of abrupt changes: theory and application*. Prentice Hall Englewood Cliffs, 1993, vol. 104.

[25] A. Packard and J. Doyle, "The complex structured singular value," *Automatica*, vol. 29, no. 1, pp. 71–109, 1993.

Publication P5

Parametric Fault Diagnosis of an Active Gas Bearing

Parametric Fault Diagnosis of an Active Gas Bearing

André K. Sekunda[1], H Niemann[1], N Kjølstad Poulsen[2] and Ilmar Santos[3]

[1]) Department of Electrical Engineering, Technical Unversity of Denmark, Kgs. Lyngby, Denmark

[2]) Department of Applied Mathematics and Computer Science, Technical Unversity of Denmark, Kgs. Lyngby, Denmark

[3]) Department of Mechanical Engineering, Technical University of Denmark, Dk-2800 Kgs. Lyngby, Denmark

E-mail: aksek@elektro.dtu.dk, hhn@elektro.dtu.dk, nkpo@dtu.dk, ifs@mek.dtu.dk

Abstract

Recently research into active gas bearings has had an increase in popularity. There are several factors that can make the use of gas bearings favourable. Firstly gas bearings have extremely low friction due to the usage of gas as the lubricant which reduce the needed maintenance. Secondly gas bearings is a clean technology which makes it possible to use for food processing, air condition and so on. Active gas bearings are therefore useful for applications where downtime is expensive and dirty lubricants such as oil are inapplicable. In order to keep as low downtime as possible it is important to be able to determine when a fault occurs. Fault diagnosis of active gas bearings is able to minimize the necessary downtime by making certain the system is only taken off-line when a fault has occurred. It is in this paper shown possible to apply active fault diagnosis to diagnose parametric faults on a controllable gas bearing. The fault diagnosis is based on a statistical detector which is able to quantify the quality of the diagnosis scheme.

Keywords— Active Fault Diagnosis, Active gas bearing, Parametric Faults, Laboratory Experiment, Closed Loop Fault Diagnosis

1 Introduction

Control of active radial gas bearings by means of piezoelectric actuation is an interesting subject that can significantly extend gas bearing technology in the framework of industry 4.0. Until recently all multiphysical mathematical models derived based on the first principles, linking fundamental equations coming from the fields of rotordynamics, fluid dynamics, material science and control techniques, presented considerable deviations from experimental results, as it can be concluded from [1, 2, 3, 4, 5]. Not long ago there wasn't any proper models available for control design of active radial gas bearings via piezoelectric actuation. Pierart and Santos [6, 7, 8, 9] developed accurate mathematical models based on the first principles leading to high order models consisting 144 states. After model reduction, it was shown by the authors to be possible to use them to effectively design model-based controllers. Lately it was shown by [10] that identification of low order models of the position of a shaft held in place by an active gas bearing using a 6th order linear model is possible. With such a model it is possible to design advanced controllers such as done in [10]. The goal of all the controllers applied to the gas bearings has been to reject external disturbances. This is possible as long as the system is not changing. Fault detection is thus relevant to determine when and how the system changes such that appropriate action can be conducted and performance regained. It has previously been shown how to detect and isolate faults for several different mechanical systems such as induction engines [11], gearboxes [12] and bearings [13]. In all these cases the goal of the fault diagnosis was to regain performance or stop the system before it broke down.

Fault diagnosis can be divided into two subcategories, active and passive fault detection. Where passive fault diagnosis makes it possible to diagnose faults by information gained from redundancy, active fault detection introduces an excitation signal in order to gain information usable for diagnosis of faults. The gas bearing system used in this paper has a fixed non-redundant number of sensors which can become problematic for fault diagnosis based on passive fault diagnosis. For such a system, as the active gas bearing, isolation of several faults using passive fault diagnosis can become unrealistic to achieve. Active fault detection add information, through an excitation signal, to the diagnosis scheme and is therefore seen as a more appropriate approach for fault diagnosis of the active gas bearing.

Active fault diagnosis has been studied extensively with the research branching into two directions. One branch treats the fault diagnosis problem as a discrete bank of different possible systems and compares the measured output with that predicted given each of the systems in the bank. One of the systems

represents the healthy system while the others represent the system subject to one of the possible faults. Extensive effort has been put into defining the framework and the optimal input for the diagnosis of such a problem statement [14, 15, 16, 17, 18, 19, 20]. Another approach for defining the effect of the fault has been proposed in [21]. Here a fault signature system is designed and the effect of each of the faults on the fault signature system is instead used for diagnosis [22, 23]. The approach is based on the system being part of a closed loop scheme and automatically decouple the noise from the residual. The active gas bearing should always have an controller active when faults are introduced due to safety where this feature becomes extra convenient.

The main contribution of this paper is to diagnose faults on an active gas bearing. The active gas bearing test rig used is a multiple input multiple output system with two inputs(piezo actuators) and two measured outputs(displacement sensors). It is shown possible to diagnose faults occurring both on the piezo actuators and the displacement sensors. The fault detection is conducted by designing a fault signature system and using a matched filter detector for diagnosis of the faults. The method was proposed in [24] where examples using a simple second order system were given. All faults considered are here modelled as parametric faults. It is here shown possible to successfully diagnose different faults for the gas bearing under non-rotating as well as rotating conditions. Furthermore experiments have been conducted using both a simple proportional controller as well as a linear-quadratic controller. Lastly a whitening filter proposed in [24] was implemented and shown able to whiten the noise on the residual signal. The whitening of the noise makes the residual into a standard form for design of statistical detectors.

This paper is structured as follows: In Section 2 the model of the gas bearing is introduced together with the identification results; In Section 3 the controller design and augmented controller scheme is presented; In Section 4 the parametric faults considered are defined; In Section 5 an analysis of the excitation signal design is conducted; In Section 6 the detector design is presented; In Section 5 an analysis of the excitation signal design is conducted; In Section 7 the experimental results are presented, and finally, in Section 8, a discussion of the results and future possible improvements are given.

2 Model Structure

An active gas bearing is used for the experimental work conducted in this paper. A schematic of the gas bearing considered is shown on Figure 0.1.

The vertical piezo actuators denoted **b** and the horizontal piezo actuators

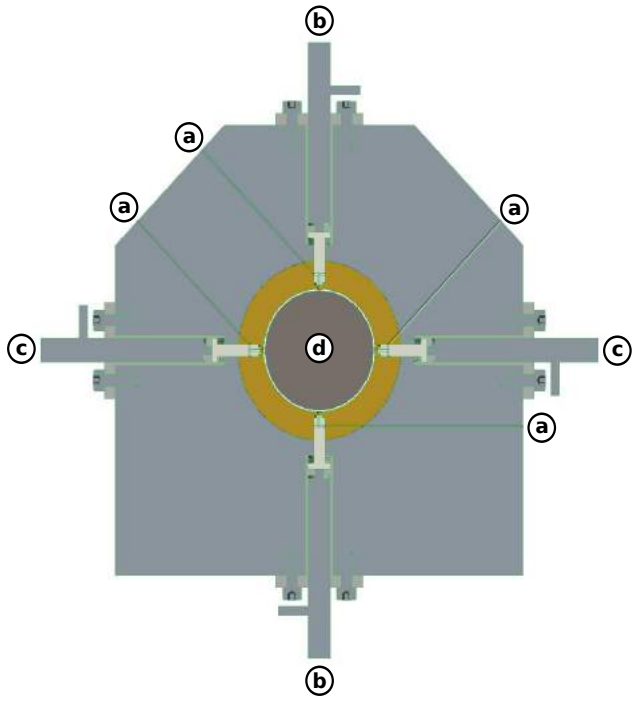

Figure 0.1: A cross section schematic of the active gas bearing. The air is pumped in through the 4 inlets denoted by **a**. The piezo actuators denoted **c** open and close the flow of air from the horizontal direction. Likewise the piezo actuators denoted **c** open and close the flow of air towards the shaft **d** in the vertical direction.

denoted **c** on Figure 0.1 have each respectively been lumped together as a single controllable input. The goal is to keep a rotor in place using only the active gas bearing. This is done by pumping air into the gas bearing through the tubes **a** using the piezo actuators **b** and **c**. The rotor and gas bearing are connected by a flexible shaft. The horizontal and vertical positions of the rotor are measured and used for feedback control. A picture of the experimental test rig is shown on Figure 0.2 where the location of the displacement sensors and actuators can be seen.

A low order physical model structure was identified in [25] which can describe the main dynamics. The model describe the dynamics from the piezo actuators to the position of the disc. It was shown that the model depends on

the rotational speed of the rotor and injection pressure of the lubricant injected into the bearing gap. In this work a constant rotational speed and fixed pressure of the gas in the active gas bearing is chosen for each experiment. The state vector is defined in equation (1).

$$x_{6x1} = \begin{bmatrix} l \\ \dot{l} \\ \mathcal{M} \end{bmatrix} \tag{1}$$

Here l is a column vector denoting the lateral displacement of the rotor in the horizontal and vertical direction respectively. $\mathcal{M}$ is a column vector denoting the state of the actuator dynamics described by the linear position of the piezo electric stacks. Let the system be described by the standard state space description given by equation (2).

$$\begin{aligned} \dot{x} &= Ax + Bu \\ y &= Cx + Du \end{aligned} \tag{2}$$

Where:

$$G = \left[\begin{array}{c|c} A & B \\ \hline C & D \end{array}\right] \tag{3}$$

The model structure is thus given in Eq . (4) - (7) using a standard state space description of the system as given in equation (2).

$$\mathbf{A}_{6x6} = \begin{bmatrix} 0 & \mathbf{I} & 0 \\ \mathcal{K} & \mathcal{D} & \mathcal{B} \\ 0 & 0 & -\mathcal{P} \end{bmatrix} \tag{4}$$

$$\mathbf{B}_{6x2} = \begin{bmatrix} 0 \\ 0 \\ \mathcal{P} \end{bmatrix} \tag{5}$$

$$\mathbf{C}_{2x6} = \begin{bmatrix} \mathbf{I} & 0 & 0 \end{bmatrix} \tag{6}$$

$$\mathbf{D}_{2x2} = \begin{bmatrix} 0 \end{bmatrix} \tag{7}$$

Here $\mathcal{K}$ is the stiffness matrix of the system and is in $[\frac{N}{kg\ \mu m}]$, $\mathcal{D}$ is the damping matrix of the system expressed in $[\frac{Ns}{kg\ \mu m}]$ and $\mathcal{B}$ is the input gain matrix in $[\frac{N}{kg\ V}]$.

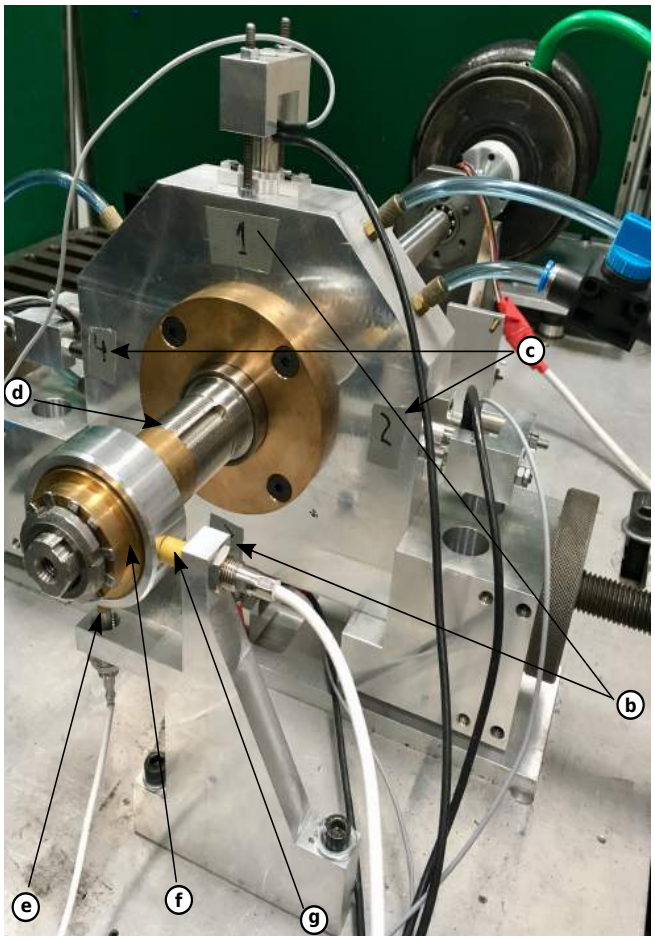

Figure 0.2: Picture of the experimental test rig used for conducting active fault detection. The different parts of the test rig are as follows: **b** are the piezo actuators which pump air into the controllable gas bearing in the vertical direction, **c** are the piezo actuators which pump air into the controllable gas bearing in the horizontal direction, **d** is the flexible shaft, **e** is the sensor measuring the vertical displacement of the disc, **f** is the disc and **g** is the sensor measuring the horizontal displacement of the disc.

The matrix $\mathcal{P}$ is designed as a diagonal matrix with each element p_j defined by equation (8) as a low pass filter describing the actuator dynamics, i.e linear displacement of piezo actuators as a function of the input voltage:

$$h_j(s) = \frac{p_j}{s + p_j} \qquad j \in \{1, 2\} \tag{8}$$

h_j is the first order low pass filter through which the system is actuated.

The model parameters have been identified using a grey box open loop prediction error method. The parameters are given in Table 0.1 for the gas bearing without rotation and in Table 0.2 when the shaft is rotating at 1100 RPM. A rotational speed of 1100 RPM has been chosen as a prove of concept to show that it is possible to diagnose faults during rotation.

$$\mathcal{K} = \begin{bmatrix} -1.79 \cdot 10^6 & 1.726 \cdot 10^4 \\ 1.061 \cdot 10^4 & -1.926 \cdot 10^6 \end{bmatrix}$$

$$\mathcal{D} = \begin{bmatrix} -283.2 & -13.82 \\ -8.152 & -219.7 \end{bmatrix}$$

$$\mathcal{B} = \begin{bmatrix} 4.318 \cdot 10^6 & -2.672 \cdot 10^5 \\ 9.204 \cdot 10^4 & 4.81 \cdot 10^6 \end{bmatrix}$$

$$\mathcal{P} = \begin{bmatrix} 1021 & 0 \\ 0 & 944.5 \end{bmatrix}$$

Table 0.1: Table of the identified parameters for the model of the active gas bearing when the shaft is not rotating.

The identified model is discretised using the zero order hold method for design and implementation of controllers on the active gas bearing. A sampling rate of 5000 Hz (sampling time = 0.0002s) is chosen for the discrete model.

3 Controller Setup

Two different controllers are discussed and implemented to examine the effect of different control architectures in connection with fault diagnosis of the active gas bearings. The first controller implemented is a simple P-controller where the gain is determined by examining its root, while the second controller is an observer based LQR controller.

$$\begin{aligned}
\mathcal{K} &= \begin{bmatrix} -1.79 \cdot 10^6 & 3.43 \cdot 10^4 \\ 3.171 \cdot 10^4 & -1.931 \cdot 10^6 \end{bmatrix} \\
\mathcal{D} &= \begin{bmatrix} -241.6 & 45.97 \\ 7.94 & 212.1 \end{bmatrix} \\
\mathcal{B} &= \begin{bmatrix} -4.446 \cdot 10^6 & 7887 \cdot 10^4 \\ 6085 & 4.853 \cdot 10^6 \end{bmatrix} \\
\mathcal{P} &= \begin{bmatrix} 898.9 & 0 \\ 0 & 955.7 \end{bmatrix}
\end{aligned}$$

Table 0.2: Table of the identified parameters for the model of the active gas bearing when the shaft is rotating with 1100 RPM.

Design of P controller

In order to be able to examine the root of the closed loop system poles the controller is given as in equation (9).

$$K = k \begin{bmatrix} 1 & 0 \\ 0 & 1 \end{bmatrix} \tag{9}$$

Using same control in both directions is found appropriate due to the similar dynamics for the two directions. This description of the controller with k being a scalar makes it possible to follow the loci of the poles where as for a proper MIMO controller, with non-diagonal elements different from zero, the Gershgorin circle theorem would be applicable instead. The root locus plot is shown on Figure 0.3 for the control design given in equation (9).

Using Figure 0.3 the controller gain k was chosen to be -0.2 and the final controller is thus given in equation (10).

$$K = \begin{bmatrix} -0.2 & 0 \\ 0 & -0.2 \end{bmatrix} [V/\mu m] \tag{10}$$

The controller design was chosen to examine the effect of a simple controller without considering any cross coupling.

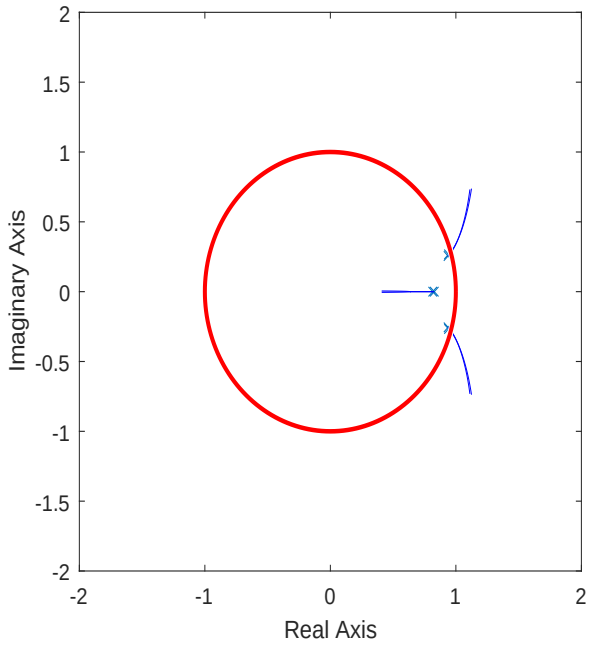

Figure 0.3: Root locus plot of the rotor gas bearing a proportional gain between 0 and -10. The system is found to be stable for a gain from each position error to each input of 0.2 or smaller.

Design of LQR controller

The second controller used for experiments is a LQR controller designed using a full order observer. The observer gain is shown in equation (11) and the state feedback gain is given in equation (12).

$$\mathbf{L} = \begin{bmatrix} -0.17 & 0.00 \\ 0.00 & -0.19 \\ -3.99 & 1.94 \\ 2.62 & -15.77 \\ -0.02 & -0.00 \\ 0.00 & -0.02 \end{bmatrix} \tag{11}$$

$$\mathbf{F} = \begin{bmatrix} -0.08 & 2.36 \\ 2.5 & 0.10 \\ 0.00 & -0.00 \\ -0.00 & -0.00 \\ 0.04 & -5.16 \\ -5.70 & 0.04 \end{bmatrix}^{\mathbf{T}} \tag{12}$$

Controller Implementation

With both a proportional and observer based control design the detectors are implemented using the active fault diagnosis scheme as presented on Figure 0.4.

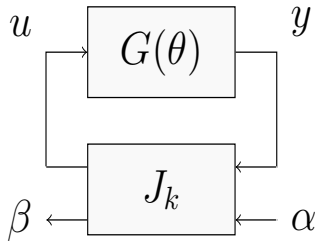

Figure 0.4: Experimental test setup. $G(\theta)$ represents the gas bearing, J_k is the nominal controller augmented with the two signals α which is the excitation signal and β which is the residual signal.

Here J_k is the controller augmented with the vector signals (α,β) and θ denotes the parametric faults in the system. The noise has been omitted from Figure 0.4 and will be considered in section 6. For an observer based controller design the setup in Figure 0.4 is realised by letting the signal β be the innovation signal and by letting α be a control signal of J_k, see Figure 0.4. With the controller architecture from Figure 0.4 the detection signal β is given by equation (13).

$$\beta = \begin{bmatrix} \beta_h \\ \beta_v \end{bmatrix} = S(\theta)\alpha = S(\theta) \begin{bmatrix} \alpha_h \\ \alpha_v \end{bmatrix} \tag{13}$$

Here $S(\theta)$ is the fault signature system. β_h is the residual in the horizontal direction and β_v is the residual in the vertical direction. Equivalently α_h is the excitation signal in the horizontal direction and α_v is the excitation signal in the vertical direction. The fault signature system has the property of being zero in the fault free case and non-zero when a fault has occurred or as written in equation (14).

$$S(\theta) = 0|_{\theta=0} \tag{14}$$

It is always possible to design an augmented controller scheme as in Figure 0.4 by a coprime factorisation of controller and plant. The method is explained in the supplemental material where it is shown how to design J_k and find the Youla-Kucera factorisation given different controller designs.

The ability of the gas bearing to suppress disturbances is shown on Figure 0.5 for both the nominal gas bearing and for each of the two implemented controllers. The plot shows that both controllers give the system increased disturbance rejection compared to the open loop system.

4 Fault Description

In this section the possible faults considered are discussed and the fault signature system is derived based on the faults to be detected. Typically faults on an active gas bearing are due to wear of the actuators and defective sensors. The model structure established in section 2 forms the basis for the fault structure introduced in this section.

In this paper the faults considered are represented as parametric faults. Faults on the actuators are represented as a decrease in the input gain, while a fault on a sensor is modelled as a decrease in the sensor readings. The different possible faults have been summarised in Table 0.3 together with the bounds associated with each of the faults. With the bounds as shown in Table 0.3, the fault free case corresponds to $\theta_i = 0$ where as a complete failure hence a fault of 100% corresponds to θ_i = -1 where i represent the specific fault.

The possible faults are described using a linear fractional transformation as shown in equation (15).

$$G(\theta) = \mathcal{F}_u(G_{aug}, \theta) \tag{15}$$

Further, the connection between z and w is given by equation (16).

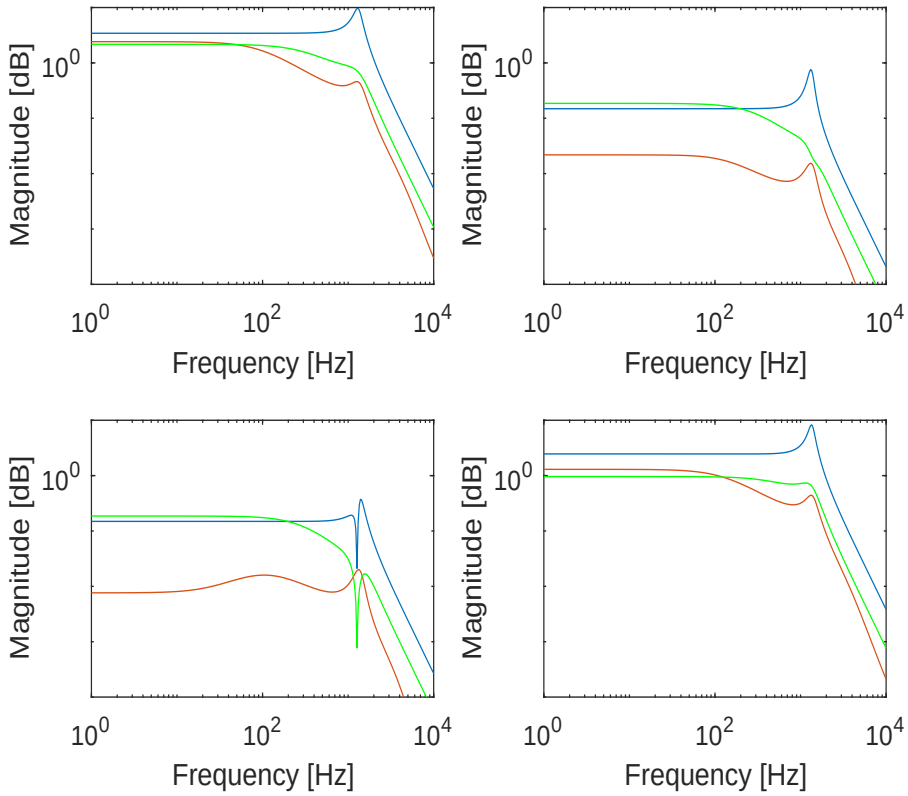

Figure 0.5: Plot of the gain from a displacement disturbance to the displacement of the rotor for when the rotor is not rotating. The left column is for a disturbance in the horizontal direction while the right column is for a disturbance in the vertical direction. Equivalently the top row is for the position of the rotor in the horizontal direction while the bottom row is for the position in the vertical direction. The blue line represent the gas bearing without any control, the red line represent the gas bearing with the LQR controller implemented and the green line represent the gas bearing with the proportional controller implemented.

$$w = \theta z \tag{16}$$

Where θ is a diagonal matrix with the four faults considered, i.e.

Fault description	Notation	Bound	Description
Horizontal actuator	θ_1	[0 -1]	The fault on the opening degree of the horizontal actuator is $100 \cdot (-\theta_1)\%$ is expected to be. This results in a reduction of the horizontal input gain.
Vertical actuator	θ_2	[0 -1]	The fault on the opening degree of the vertical actuator is $100 \cdot (-\theta_2)\%$ is expected to be. This results in a reduction of the vertical input gain.
Horizontal sensor	θ_3	[0 -1]	The fault on the measured distance of the horizontal displacement sensor is $100 \cdot (-\theta_3)\%$. This is equivalent to a reduction in the horizontal output gain and the controller is then demanding wrong actuation.
Vertical sensor	θ_4	[0 -1]	The fault on the measured distance of the vertical displacement sensor is $100 \cdot (-\theta_4)\%$. This is equivalent to a reduction in the vertical output gain and the controller is then demanding wrong actuation.

Table 0.3: Lookup table for the different possible faults

$$\theta = \begin{bmatrix} \theta_1 & 0 & 0 & 0 \\ 0 & \theta_2 & 0 & 0 \\ 0 & 0 & \theta_3 & 0 \\ 0 & 0 & 0 & \theta_4 \end{bmatrix} \tag{17}$$

Where the augmented system is defined as in equation (18).

$$G_{aug} = \begin{bmatrix} G_{zw} & G_{zu} \\ G_{yw} & G_{yu} \end{bmatrix} \tag{18}$$

The augmented plant G_{aug} is shown in equation (19).

$$G_{aug} = \left[\begin{array}{ccc|ccc} 0 & \mathbf{I} & 0 & 0 & 0 & 0 \\ \mathcal{K} & \mathcal{D} & \mathcal{B} & 0 & 0 & 0 \\ 0 & 0 & -\mathcal{P} & \mathcal{P} & 0 & \mathcal{P} \\ \hline \mathbf{I} & 0 & 0 & 0 & 0 & \mathbf{I} \\ 0 & 0 & 0 & \mathbf{I} & 0 & 0 \\ \mathbf{I} & 0 & 0 & 0 & 0 & 0 \end{array}\right] \tag{19}$$

5 Design of the excitation signal

During fault diagnosis, the process is disturbed by the excitation signal. Reducing the disturbance to the production is imperative so that the performance degradation is minimised during fault diagnosis. It is therefore convenient to use an excitation signal that makes it possible to detect the faults while trying not to disturb the process. A method for determining the frequency of the sinusoidal excitation signal was introduced in [24]. The goal of the method is to

maximise the impact of faults on the fault signature system while minimising the impact of the excitation signal on the outputs.

Based on Fig. 0.4 the transfer function from the excitation signal to the residual signal is found. It is thus possible to determine the impact of the faults on the residual signal. It is worth noting that the transfer function from the excitation signal to the residual signal depends on the specific fault occurring and the known nominal model as well as controller parameters. Equivalently the transfer function from the excitation signal to the outputs of the system is required to define an efficiency criteria:

$$f_\alpha = \frac{\xi_r(\omega)}{\xi_y(\omega)} \tag{20}$$

Here $\xi_r(\omega)$ is the frequency dependent gain from the excitation signal α to the output of the fault signature system β. Equally $\xi_y(\omega)$ is the frequency dependent highest singular value for the single input multiple output system from the excitation signal α to the outputs y. With f_α defined in equation (20) the frequency of the excitation signal can be determined as shown in equation (21).

$$\omega_\alpha = \underset{\omega_1 \leq \omega \leq \omega_2}{\operatorname{argmax}} f_\alpha(\omega) \tag{21}$$

Here ω_1 and ω_2 are chosen as the bound for the frequencies considered using for the excitation signal. The active gas bearing has two possible inputs for the excitation signal and two possible residual signals where four different combinations are possible and should be considered. A plot of the efficiency gain of the residual for a fault corresponding to a gain degradation of 50% for each of the four faults, using the proportional controller is shown on Figure 0.6a to Figure 0.6d where the four different possible excitation and residual signal combinations have been tested.

From Figure 0.6a to Figure 0.6d it is seen that f_α increases as the frequency of the excitation signal is increased. The frequency of the excitation signal was found using equation (21) with $\omega_1 = 1 rad/s$ and $\omega_2 = 62 rad/s$. The excitation has been chosen to be 62 rad/s, such that the excitation signal is kept smooth given the sampling rate. With the frequency of the excitation signal selected it is necessary to examine the phase shift of the residual signal given the fault signature system for each of the 4 different parametric faults. It is possible to calculate the phase shift for the interval, fault free to failure, given the chosen

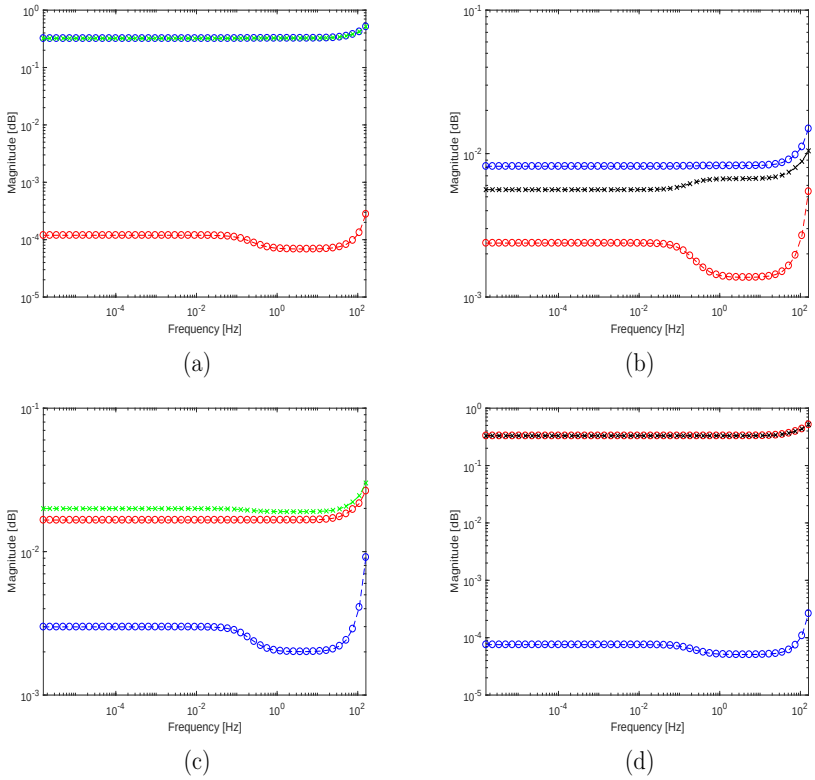

Figure 0.6: Plot of f_α versus the frequency of the excitation signal where α_h and β_h is used in Figure 0.6a, α_h and β_v in Figure 0.6b, α_v and β_h in Figure 0.6c and α_v and β_v in Figure 0.6d. The blue line represent f_α given a fault on the horizontal actuator, the red line is for a fault on the vertical actuator, the green line represent the horizontal sensor and the black line represent the vertical sensor. Faults on the horizontal sensor cannot be detected when using β_v and faults on the vertical sensor cannot be detected when using β_h.

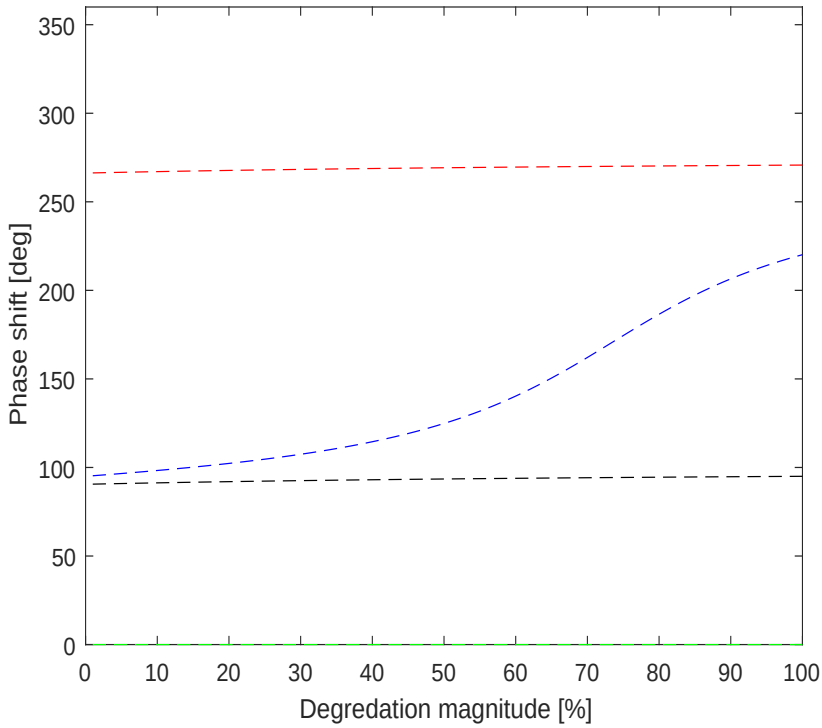

Figure 0.7: Plot of the phase shift versus the magnitude of each of the 4 faults considered using the horizontal α signal and vertical β signal. The blue line represents a fault on the horizontal actuator, the red line is for a fault on the vertical actuator, the green is for a fault on the horizontal sensor and the black represents the vertical sensor.

excitation signal. The phase shift versus the magnitude of the faults is shown on Figure 0.7 using the excitation signal α_h and residual signal β_v.

Based on Figure 0.7 the phase shift given each of the four possible faults is found with an excitation signal frequency of 62 rad/s when using the excitation signal α_h and residual signal β_v. It is possible to make similar plots given the other combinations of excitation and residual signals.

It is not possible to detect faults on the horizontal displacement sensor using the horizontal residual as seen from Figure 0.6b and 0.6d. Equivalently it is found impossible to detect faults on the vertical displacement sensor using the vertical residual signal as seen on Figure 0.6a and 0.6c. It is therefore found necessary to use both the vertical and horizontal residual signals to be able to detect all the predetermined possible faults.

6 Detector Design

A detector design is required in order to detect and isolate faults. It is decided in this paper to use a matched filter detector design. Such a matched filter detector design was introduced in [26] and it was shown in [24] how to apply it to the case of active fault detection based on the fault signature system. Based on Figure 0.8, diagnosis is based on equation (22) where the disturbance is introduced.

$$\beta = S\alpha + d \tag{22}$$

The signal β is as shown in equation (23) used as the residual signal denoted r in keeping with common practice, i.e

$$r = \beta \tag{23}$$

Here the disturbance d is assumed to be white gaussian noise (WGN). Based on the results in [26] it is possible to formulate a $\mathcal{H}_0$ hypothesis as in equation (24) and a $\mathcal{H}_1$ hypothesis as in equation (25).

$$\mathcal{H}_0 : r[n] = d[n] \tag{24}$$
$$\mathcal{H}_1 : r[n] = |S(\theta)|\alpha[n - n_\phi] + d[n] \tag{25}$$

Here $r[n]$ is the fault signature signal as given in equation (23), α is the excitation signal and $|S(\theta)|$ is the gain of the fault signature system given the selected excitation frequency and n_ϕ is the delay of the excitation signal though the fault signature system. The fault free case thus results in simply white noise, while the faulty case results in a known signal with an unknown delay and unknown amplitude. The unknown delay and amplitude both depend on the specific fault occurring and the magnitude of the fault. Identifying the delay and amplitude thus make it possible to isolate the faults. A correlator design as presented in equation (26) is implemented to determine which fault most likely occurred.

$$n_\phi = \arg\max_{n_0 \in \tau}\Big(\sum_{n=n_0}^{n_0+m-1} r[n]\alpha[n - n_0]\Big) \tag{26}$$

Here n_ϕ is the identified delay of the fault signature signal through the fault signature system, m is the length of the matched filter window and τ is the set

of possible delays considered. With the delay identified a test statistic can be generated using equation (27).

$$T[n] = \sum_{n=0}^{m-1} r[n]\alpha[n - n_\phi] \tag{27}$$

A schematic of the detector design explored in this section is shown in Figure 0.8.

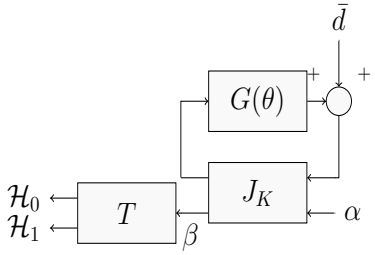

Figure 0.8: Experimental test setup. $G(\theta)$ represents the gas bearing, J_k is the augmented controller, α is the excitation signal, β is the residual signal. The block T is the statistical detector implemented.

Based on this test statistic it is possible to determine the threshold(γ) and probability of detection(P_D). It is in this paper decided to base the threshold on the probability of a false alarm(P_{FA}). Before the threshold can be determined it is furthermore required to quantify the detector signals energy. In equation (28) the energy of the detector is given.

$$\varepsilon = m\frac{A_{|S(\theta)|}}{2} \tag{28}$$

Here $A_{|S(\theta)|}$ is the amplitude of the fault signature signal. Since more than one fault is considered $A_{|S(\theta)|}$ is chosen to be the highest amplitude of the fault signature signal given the faults and fault magnitudes considered possible. With the energy of the signal determine it is possible to decide on a threshold for the test statistic given a probability of false alarm as shown in equation (29).

$$\gamma = \sqrt{\sigma^2\varepsilon}Q^{-1}(P_{FA}) \tag{29}$$

Here σ^2 is the variance of the measurement noise and $Q(*)$ is the complementary cumulative distribution function. With the use of the of the determined

probability of a false alarm the probability of detection can be calculated using equation (30).

$$P_D = Q(Q^{-1}(P_{FA}) - \sqrt{\mathcal{D}}) \tag{30}$$

Here $\mathcal{D}$ is given in equation (31) and is the deflection coefficient which is based on the expected value of the test statistic for the case of a fault and no fault together with the variance of the test statistic in the fault free case.

$$\mathcal{D}^2 = \frac{(E(T; \mathcal{H}_1|_{F_k}) - E(T; \mathcal{H}_0))^2}{var(T; H_0)} \tag{31}$$

F_k is the notation for which of the considered faults that has occurred, thus the deflection coefficient and hence the probability of the detection changes depending on which fault that is considered.

Design and Performance of the Whitening Filter

The residual signal used in [21] and here denoted as β is filtering a systems noise signals through a linear filter. The detector design is based on the noise in equation (24) being white. This will in general not be satisfied when using the β signal as the residual for fault detection on the active gas bearing. A whitening filter is therefore needed.

The main contributor to noise (d) on the active gas bearing is identified to be the displacement sensors and a open loop experiment without any excitation was conducted which showed the noise to be approximately Gaussian and white. Using the signal β as the residual signal results in that the measurement noise is subject to a linear filter. It was proposed in [24] to design a whitening filter for the fault free case. Since the active gas bearing is open loop stable it is possible to find a whitening filter that also keep the variance of the noise the same on the residual signal as on the measurements. The residual signal is therefore reformulated in equation (32) using the known signal β and a linear whitening filter W.

$$r = W\beta \tag{32}$$

The whitening filter W is designed such that the measurement noise on the active gas bearing is white in the fault free case on the residual signal. A throughout description of how to design the whitening filter can be found in [24]. A block diagram where the filter is implemented and the identified source of the noise is shown is shown in Figure 0.9.

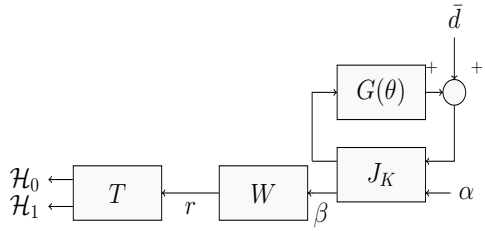

Figure 0.9: Experimental test setup. $G(\theta)$ represents the gas bearing, J_k the augmented controller, α is the excitation signal, β is the residual signal subject to non-white noise, W is the whitening filter and r is the residual signal subject to white noise.

7 Experiments

Based on the possible faults described in section 4, four experiments are conducted in order to show that it is possible to detect and isolate each of the four different faults considered using a one excitation signal and one residual signal. Each of the faults considered are induced as $\theta_i = -0.5$. Even though the faults are quite severe a gain reduction of 50% on the actuators is found to be likely. Such a reduction can be due to pressure loss or something getting stuck in the tube letting air into the active gas bearing. Due to the severity of the faults a linearised version of the fault signature system cannot be considered for the fault diagnosis.

Analysis of the noise on the Gas bearing

Firstly the effect of the whitening filter is examined. In order to examine the effect of the whitening filter W a residual signal has been obtained for the fault free gas bearing without any excitation signal applied. On Figure 0.10 the normalised autocorrelation is shown using the signal β which is the residual signal before any whitening has been conducted.

It is clear from Figure 0.10 that the signal is not white even though the noise the system originally was subject to is. Equivalently the same test can be conducted using equation (32) as the fault signature system. In this case the normalised autocorrelation is shown on Figure 0.11.

From Figure 0.11 it is seen that the residual signal is much closer to being white in the fault free case. For a perfect model this experiment could be conducted with an active excitation signal applied, however even though the model is able to produce a good fit it is not considered perfect and the excitation signal would thus pollute the experiment. This imperfection of the model is

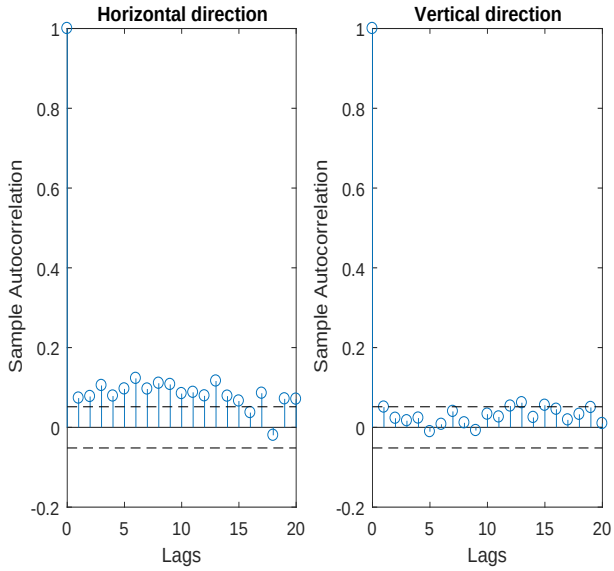

Figure 0.10: Plot of the autocorrelation of β in the fault free case. The stems show the correlation depending on the number of lags, while the black stippled lines are the upper and lower confidence bounds.

also possible to see in that the residual signal, even though it is closer to being white, it is still not within the bounds of the statistical uncertainty for the autocorrelation function.

With the whitening filter verified an analysis of the noise on the residual signal is required. The residual signal has been monitored without any excitation signal applied and a normalised histogram is shown on Figure 0.12 for the horizontal direction and vertical direction.

It is clear from the two histograms that the residual signal is subject to approximately gaussian noise with a mean of zero in both directions. The variance was found in the horizontal direction to be 0.12 and in the vertical direction to be 0.15.

Diagnosing faults using a P-controller

In the first experiment the residual signal from the horizontal direction is used whose variance the threshold is thus based upon. In this experiment the disc is not rotating. Before detection can be conducted it is needed to calculate the energy in the signal depending on the fault occurring and the magnitude of the possible fault. A plot of the gain through the fault signature system is shown

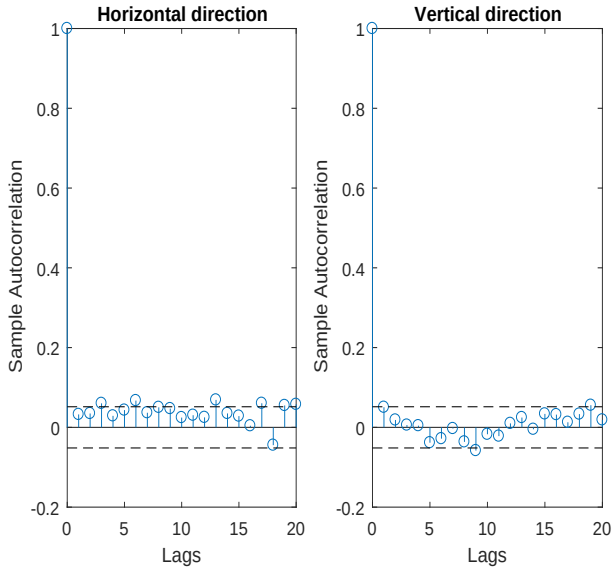

Figure 0.11: Plot of the autocorrelation of r in the fault free case. The stems show the correlation depending on the number of lags, while the black stippled lines are the upper and lower confidence bounds.

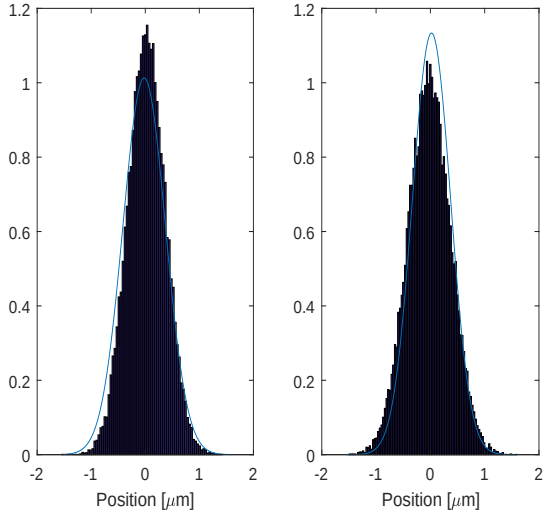

Figure 0.12: Histogram of the signal r in the fault free case with the horizontal direction on the left hand side and the vertical direction on the right hand side.

on Figure 0.13.

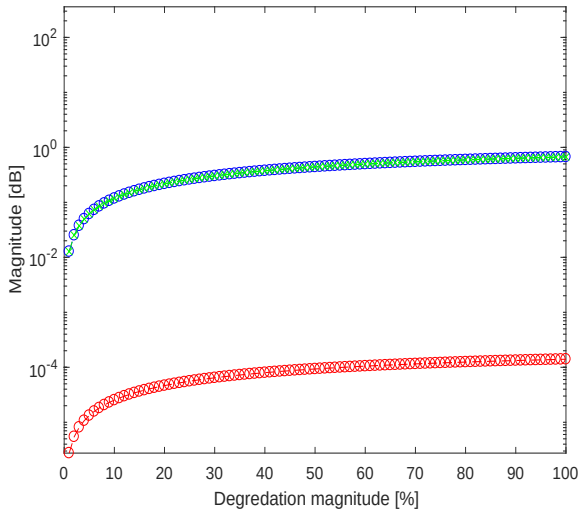

Figure 0.13: Plot of the gain from the horizontal excitation signal α to the horizontal residual signal r given each of the possible faults. The blue line represent a fault on the horizontal actuator, the red line is for a fault on the vertical actuator, the green is for a fault on the horizontal sensor and the black represent the vertical sensor.

From Figure 0.13 the gain through the fault signature system is found to be close to 1 for a fault on the horizontal piezo electric actuator of 50% and around 0.0003 for a fault on the vertical actuator of 50%. A fault of 50% reduction in the opening degree was introduced on the horizontal actuator after 4 seconds. To determine whether it is possible to detect the fault a test statistic as shown in equation (27) is implemented. The threshold is determined using equation (29) as shown in equation (33).

$$\begin{aligned} \gamma &= \sqrt{\sigma^2 \varepsilon} \cdot Q^{-1}(P_{FA}) \\ &= \sqrt{0.42^2 \cdot 31275} \cdot Q^{-1}(2 \cdot 10^{-5}) = 305 \end{aligned} \tag{33}$$

The test statistic is then shown on Figure 0.14 for a fault on the horizontal actuator.

It is clear from Figure 0.14 that it is possible to detect a fault on the horizontal actuator using the horizontal input and horizontal output. In order to determine which fault occur equation (26) is utilised. In order to determine the

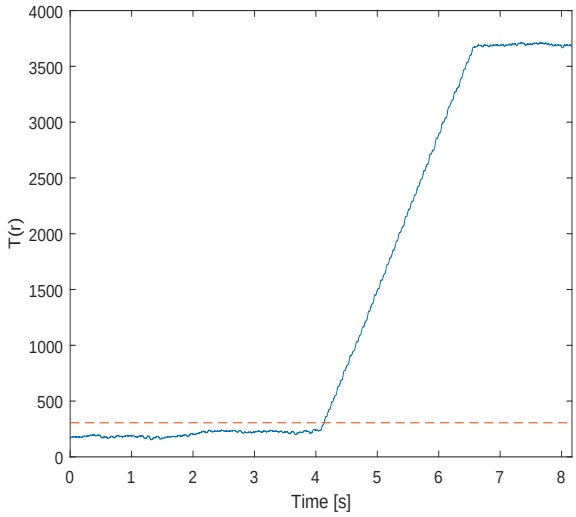

Figure 0.14: Detector signal T where a fault occurs after 4 seconds on the horizontal actuator. A window length of 2.5 seconds is used for the diagnosis.

phase shift of the residual signal 4 different possible phase shifts are considered and are given in equation (34).

$$\tau = [93, 89, 94, 0] \tag{34}$$

The phase shift set corresponds to the phase shift introduced given a 50% degradation ($\theta_i = -0.5$) of each of the possible faults shown in Table 0.3. The phase shift was found as the phase shift of the fault signature system $S(\theta)$ for each of the 4 different possible faults respectively. The result of the decision algorithm is shown on Figure 0.15 using equation (26).

It is clear from Figure 0.15 that the fault is isolated almost 2 seconds after it has actually occurred and is detected. With a window of 2.5 seconds almost the whole window is used.

The decision algorithm determine a horizontal sensor fault to be most likely in the fault free case. There can be several reasons why the decision algorithm does not change between all the possible faults in the fault free case. The most obvious reason is because the model is not a perfect representation of the active gas bearings, thus the fault signature system is not zero in the fault free case. Furthermore the window length is chosen to be 2.5 seconds which makes small model deviations have a relative higher impact on the fault decision compared to the noise. This is clearly seen from Figure 0.16 where the window has been shortened to 0.2 seconds.

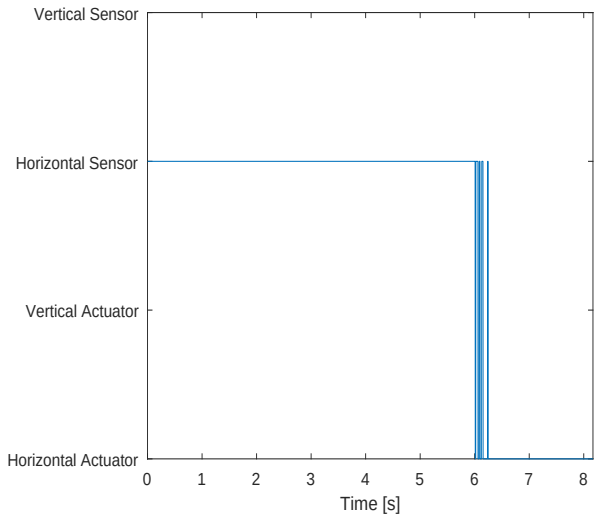

Figure 0.15: Plot of the decision n_ϕ where a fault has been introduced on the horizontal actuator after 4 seconds.

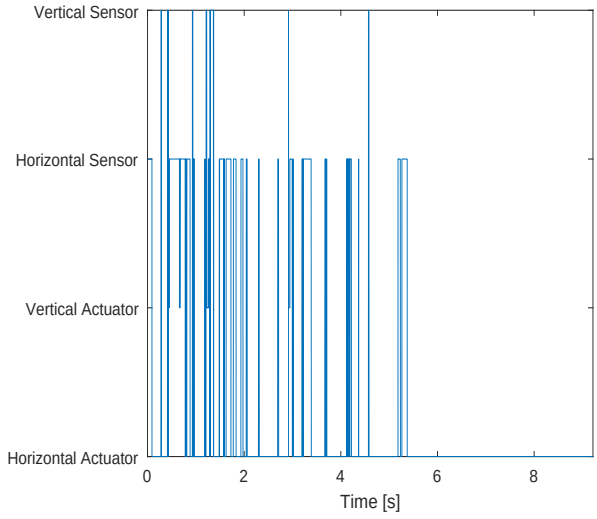

Figure 0.16: Plot of the decision n_ϕ where a fault has been introduced on the horizontal actuator after 2.5 seconds. The window m has here been reduced to 0.2 seconds.

From Figure 0.16 it is seen that the noise is dominant for the fault free case. Again the decision algorithm is able to isolate the correct fault, however in the

fault free case the decision switches between all possible faults instead of being stuck at one as seen on Figure 0.15. The window length of 2.5 seconds was found unnecessary for detecting faults on the horizontal piezo actuator. However in the case of possible faults on the vertical actuator such a window size becomes relevant due to the much lower gain of the fault signature system in case of such a fault occurring. A fault of 50% degradation, is imposed on the vertical piezo actuator after 4 seconds and the detection signal $T(r)$ is shown on Figure 0.17. We recall that such a fault corresponds to the valve opening half the expected amount, hence the input gain of the system has been reduced.

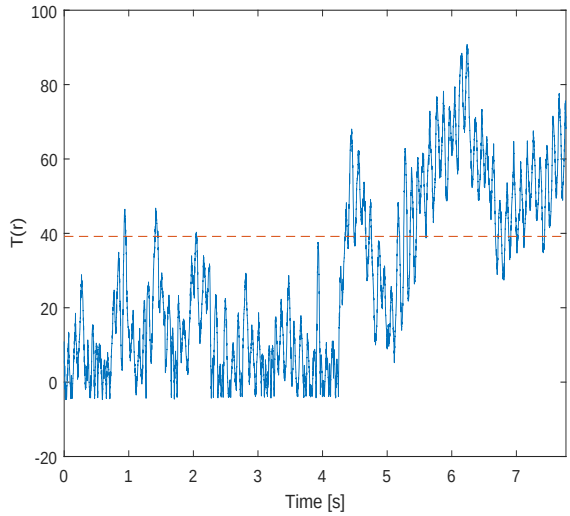

Figure 0.17: Detector signal T where a fault occurs after 4 seconds on the vertical actuator.

Recall that a false alarm occurs every time that the signal $T(r)$ goes above the stippled line before 4 seconds. We notice that we get more false alarms than we expected from the designed threshold. The unexpected amount of false alarms is assumed to be caused by the model uncertainties which has a higher impact on a vertical actuator fault than on the horizontal one in this experiment. This is due to the relative small gain through the fault signature system from the vertical excitation to the horizontal residual signal.

Again using equation (26) a decision on the possible fault occurring at each time step is shown on Figure 0.18.

It is again found possible to isolate the fault which has been introduced to the active gas bearing using equation (26).

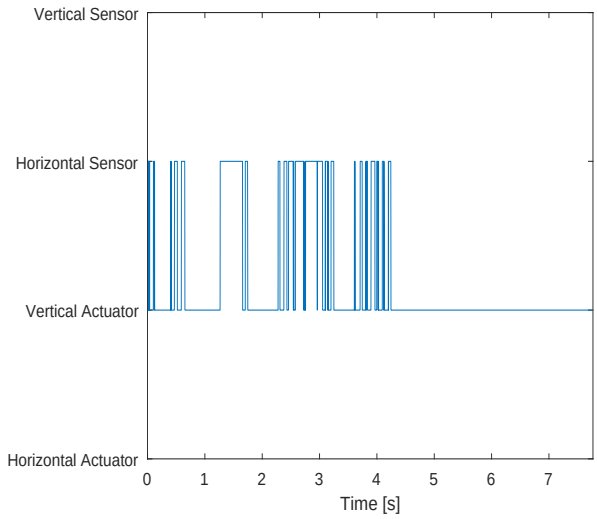

Figure 0.18: Plot of the decision n_ϕ where a fault has been introduced on the vertical actuator after 4 seconds.

Diagnosing faults using cross coupling

It has been shown possible to detect parametric actuator and sensor faults using a horizontal excitation and residual signal. It is in this experiment shown that it is possible to detect faults based on the cross coupling as well. Here it is done using a horizontal excitation signal and the vertical residual signal where again the disc is not rotating. As with the previous example the delay introduced to the residual signal given each of the possible parametric faults is found as shown in equation (35).

$$\tau = [125, 269, 0, 93] \tag{35}$$

Experiments are conducted where each of the 4 possible parametric faults are introduced to the active gas bearing. A detection algorithm as presented in equation (27) is applied and the result for each of the 4 cases is shown in Figure 0.19.

It is seen form Figure 0.19 that by applying an excitation signal in the horizontal direction and using the vertical output of the fault signature system it is possible to detect faults on both the vertical and horizontal actuators. Where as it was expected that a fault on the horizontal actuator would not be detectable a fault on the vertical actuator should be. However the fault on the vertical displacement sensor is not detected due to the low gain from

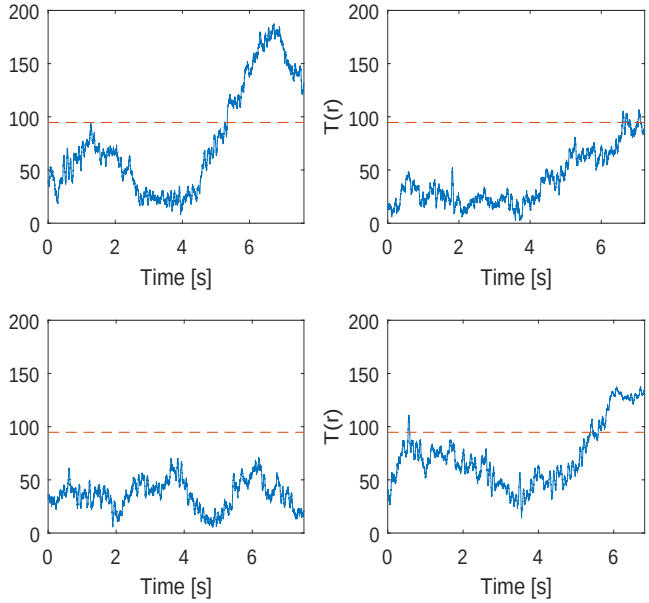

Figure 0.19: Plot of $T[n]$ for the gas bearing when each of the 4 possible parametric faults is introduced respectively. A horizontal excitation signal is applied and the vertical output of the fault signature system is used for detection purposes. The top left plot is for a fault on the horizontal actuator where as the top right is for a fault on the vertical actuator. On the bottom left plot a fault is introduced on the horizontal sensor and on the bottom right a fault has been introduced on the vertical sensor instead.

the excitation signal to the residual given a fault on the vertical displacement sensor.

Detecting faults while the gas bearing is rotating.

An experiment has been conducted where the shaft held in place by the active gas bearing has been set to rotate with a rotational speed of 1100 rounds per minute (RPM). The plant has been identified at a rotational speed of 1100 RPM and the plant has been diagnosed where a parametric fault of 50% has been introduced on the horizontal actuator. A plot of the detector ($T[n]$) is shown on Figure 0.20.

The fault is introduced just after 4 seconds and a window length of 0.2 seconds is used. It is seen on Figure 0.20 that the fault is detected.

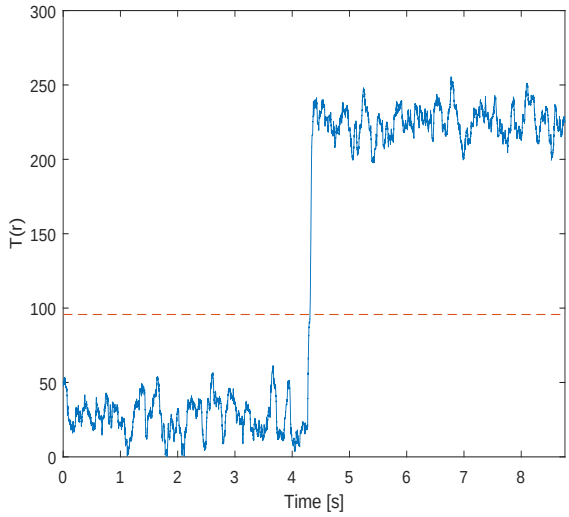

Figure 0.20: Plot of $T[n]$ for the gas bearing when the shaft is rotating with 1100 RPM and a fault is introduced to the horizontal actuator. The excitation signal has been introduced in the horizontal direction and the horizontal output of the fault signature system has been used for the detection

Diagnosing faults using a LQR based controller

For all the previous experiments the same proportional controller is used. An observer based controller is instead investigated here as described in section 3. An excitation signal is used in the vertical direction and each of the 4 faults has been introduced to show the detectors ability to detect faults. The detection signal for each of the 4 faults being introduced is shown in Figure 0.21.

It is seen from Figure 0.21 that it is still possible to detect different faults when the control scheme is changed. The method is thus shown able to apply with whichever linear control design used for the system. The isolation of the fault occurring is shown on Figure 0.22 for the fault on the vertical sensor.

Again it is noted that a delay is present between a fault being detected and the isolation. The fault is proper isolated when the whole window is using data from after the fault has occurred.

8 Conclusion

It has been experimentally shown possible to detect and isolate different parametric faults on an active gas bearing using active fault diagnosis. It was shown

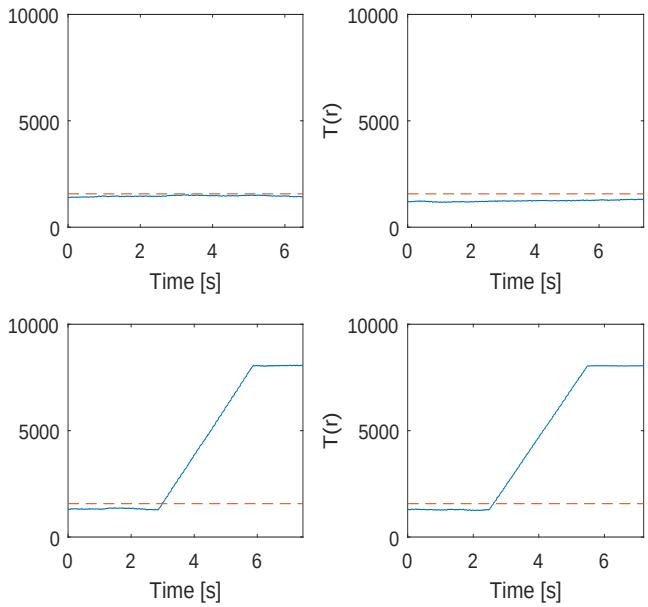

Figure 0.21: Plot of $T[n]$ for the gas bearing when each of the 4 possible parametric fault is introduced respectively. A window length of 2.5 seconds is used. A vertical excitation signal is applied and the vertical output of the fault signature system is used for detection purposes. The top left plot is for a fault on the horizontal actuator where as the top right is for a fault on the vertical actuator. On the bottom left plot a fault is introduced on the horizontal sensor and on the bottom right a fault has been introduced on the vertical sensor instead.

advantageous to apply an active fault diagnosis method to an experimental active gas bearing test rig for diagnosis of parametric faults. The active fault diagnosis was based on the fault signature system. A maximum likelihood estimator was successfully applied to the problem. Two different controller architectures were tested, a proportional and an observer based, to show the methods flexibility. Both faults on the actuators and the sensors could be detected and isolated using the proposed control architectures. The results were achieved by the use of a sinusoidal excitation signal found to minimize the disturbance on the system under the requirement of detectability of the considered faults. The results thus showed consistency with the theory throughout the experiments. Furthermore threshold design with a whitening filter applied was shown to work. The assumptions used for the active fault diagnosis design was therefore found appropriate.

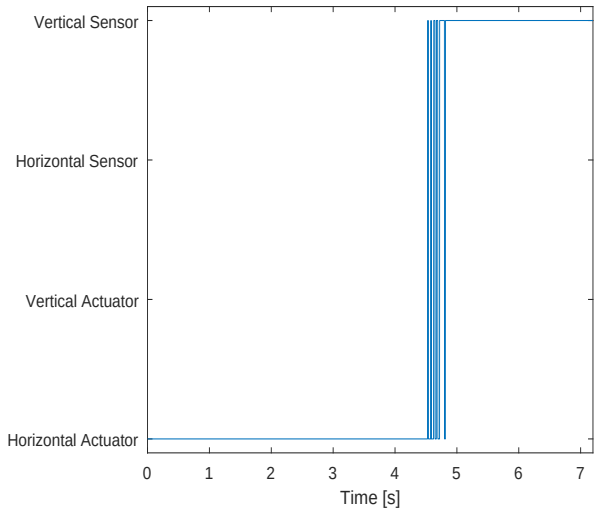

Figure 0.22: Plot of the decision n_ϕ where a fault has been introduced on the vertical sensor after 3 seconds.

Conflict of interest
The authors declare no conflict of interest in preparing this article.

Funding
This research received no specific grant from any funding agency in the public, commercial, or not-for-profit sectors.

Bibliography

[1] I. F. Santos, "On the future of controllable fluid film bearings," *Mechanics & Industry*, vol. 12, no. 4, pp. 275–281, 2011.

[2] B. T. Paulsen, S. Morosi, and I. F. Santos, "Static, dynamic, and thermal properties of compressible fluid film journal bearings," *Tribology Transactions*, vol. 54, no. 2, pp. 282–299, 2011.

[3] S. Morosi and I. F. Santos, "On the modelling of hybrid aerostatic-gas

journal bearings," *Proceedings of the Institution of Mechanical Engineers, Part J: Journal of Engineering Tribology*, vol. 225, no. 7, pp. 641–653, 2011.

[4] ——, "Active lubrication applied to radial gas journal bearings. part 1: Modeling," *Tribology International*, vol. 44, no. 12, pp. 1949–1958, 2011.

[5] ——, "Experimental investigations of active air bearings," in *Proceedings of ASME turbo expo*, vol. 7, 2012, pp. 901–910.

[6] F. G. Pierart and I. F. Santos, "Steady state characteristics of an adjustable hybrid gas bearing–computational fluid dynamics, modified reynolds equation and experimental validation," *Proceedings of the Institution of Mechanical Engineers, Part J: Journal of Engineering Tribology*, vol. 229, no. 7, pp. 807–822, 2015.

[7] ——, "Active lubrication applied to radial gas journal bearings. part 2: Modelling improvement and experimental validation," *Tribology International*, vol. 96, pp. 237–246, 2016.

[8] ——, "Adjustable hybrid gas bearing–influence of piezoelectrically adjusted injection on damping factors and natural frequencies of a flexible rotor operating under critical speeds," *Proceedings of the Institution of Mechanical Engineers, Part J: Journal of Engineering Tribology*, vol. 230, no. 10, pp. 1209–1220, 2016.

[9] ——, "Lateral vibration control of a flexible overcritical rotor via an active gas bearing–theoretical and experimental comparisons," *Journal of Sound and Vibration*, vol. 383, pp. 20–34, 2016.

[10] L. R. Theisen, H. H. Niemann, R. Galeazzi, and I. F. Santos, "Enhancing damping of gas bearings using linear parameter-varying control," *Journal of Sound and Vibration*, vol. 395, pp. 48–64, 2017.

[11] J. P. Amezquita-Sanchez, M. Valtierra-Rodriguez, D. Camarena-Martinez, D. Granados-Lieberman, R. J. Romero-Troncoso, and A. Dominguez-Gonzalez, "Fractal dimension-based approach for detection of multiple combined faults on induction motors," *Journal of Vibration and Control*, vol. 22, no. 17, pp. 3638–3648, 2016.

[12] C. Lin and V. Makis, "Optimal bayesian maintenance policy and early fault detection for a gearbox operating under varying load," *Journal of Vibration and Control*, vol. 22, no. 15, pp. 3312–3325, 2016.

[13] W. Moustafa, O. Cousinard, F. Bolaers, K. Sghir, and J. Dron, "Low speed bearings fault detection and size estimation using instantaneous angular speed," *Journal of Vibration and Control*, vol. 22, no. 15, pp. 3413–3425, 2016.

[14] I. Punčochár and M. Šmandl, "On infinite horizon active fault diagnosis for a class of non-linear non-gaussian systems," *International Journal of Applied Mathematics and Computer Science*, vol. 24, no. 4, pp. 795–807, 2014.

[15] A. E. Ashari, R. Nikoukhah, and S. L. Campbell, "Active robust fault detection in closed-loop systems: Quadratic optimization approach," *IEEE Transactions on Automatic Control*, vol. 57, no. 10, pp. 2532–2544, 2012.

[16] J. K. Scott, R. Findeisen, R. D. Braatz, and D. M. Raimondo, "Input design for guaranteed fault diagnosis using zonotopes," *Automatica*, vol. 50, no. 6, pp. 1580–1589, 2014.

[17] G. R. Marseglia and D. M. Raimondo, "Active fault diagnosis: A multi-parametric approach," *Automatica*, vol. 79, pp. 223–230, 2017.

[18] S. M. Tabatabaeipour, "Active fault detection and isolation of discrete-time linear time-varying systems: a set-membership approach," *International Journal of Systems Science*, vol. 46, no. 11, pp. 1917–1933, 2015.

[19] M. Šimandl and I. Punčochář, "Active fault detection and control: Unified formulation and optimal design," *Automatica*, vol. 45, no. 9, pp. 2052–2059, 2009.

[20] S. L. Campbell and R. Nikoukhah, *Auxiliary signal design for failure detection*. Princeton University Press, 2015.

[21] N. Poulsen and H. Niemann, "Active fault diagnosis based on stochastic tests," *International Journal of Applied Mathematics and Computer Science*, vol. 18, no. 4, pp. 487–496, 2008.

[22] H. Niemann and N. K. Poulsen, "Active fault detection in mimo systems," in *2014 American Control Conference*. IEEE, 2014, pp. 1975–1980.

[23] H. Niemann and N. Poulsen, "Estimation of parametric fault in closed-loop systems," in *2015 American Control Conference (ACC)*. IEEE, 2015, pp. 201–206.

[24] A. Sekunda, H. Niemann, and N. Poulsen, "Detector design for active fault diagnosis in closed loop systems," *Submitted to journal of adaptive control and signal processing for publication*, 2017.

[25] L. R. S. Theisen, "Advanced control of active bearings-modelling, design and experiments," *Technical University of Denmark, Department of Electrical Engineering*, 2016.

[26] S. M. Kay, Ed., *Fundamentals of statistical signal processing, Vol. II: Detection theory.* USA: Prentice Hall, 1998.

[27] H. Niemann, Ed., *A YJBK based Architecture for Fault Diagnosis and Fault-Tolerant Control, Linear System Theory.* Denmark: DTU publications, 2015.

[28] T. T. Tay, I. M. Y. Mareels, and J. B. Moore, Eds., *High Performance Control.* Chicago: Birkhauser, 1998.

Coprime Representation

The work presented in this paper exploits a coprime factorisation of the controller and plant in order to design residual signals for active fault detection. The fault free plant G(0) can be written as a coprime factorisation as shown in equation (36) and the controller K can be represented as a coprime factorisation as shown in equation (37).

$$G(0) = NM^{-1} = \tilde{M}^{-1}\tilde{N}, \qquad N, M, \tilde{M}, \tilde{N} \in \mathcal{RH}_\infty \tag{36}$$

$$K(0) = UV^{-1} = \tilde{V}^{-1}\tilde{U}, \qquad U, V, \tilde{V}, \tilde{U} \in \mathcal{RH}_\infty \tag{37}$$

Here the matrices denoted with a $\tilde{0}$ are known as the left coprime factorisation while those without are the right coprime factorisation. For such a coprime factorisation as shown in equation (36) and equation (37) the bezout identity as shown in equation (38) is satisfied.

$$\begin{aligned} \begin{bmatrix} I & 0 \\ 0 & I \end{bmatrix} &= \begin{bmatrix} M & U \\ N & V \end{bmatrix} \begin{bmatrix} \tilde{V} & -\tilde{U} \\ -\tilde{N} & \tilde{M} \end{bmatrix} \\ &= \begin{bmatrix} \tilde{V} & -\tilde{U} \\ -\tilde{N} & \tilde{M} \end{bmatrix} \begin{bmatrix} M & U \\ N & V \end{bmatrix} \end{aligned} \tag{38}$$

Using the coprime factorisation of the nominal plant $G(0)$ and controller K it is possible to define all controller that stabilise the nominal plant as shown in equation (39).

$$K(Q) = (\tilde{V} + Q\tilde{N})^{-1}(\tilde{U} + Q\tilde{M}), \quad Q \in \mathcal{RH}_\infty \tag{39}$$

It is possible to define an equivalent representation of all controller stabilising the nominal plant using the right factorisation as well. Such a controller can be implemented as shown on Figure .23.

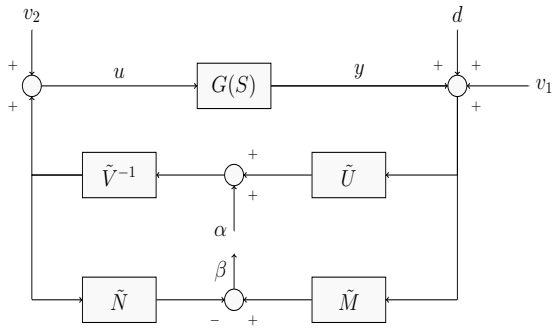

Figure .23: Experimental test setup. $G(S)$ represents the gas bearing, α is the excitation signal and G is the nominal model of the gas bearing.

Here S describe the system dynamics diverging from the nominal model, which in this paper is known as the system faults. How the system S influence the plant is shown in equation (40) using the right coprime factorisation and in equation (41) using the left coprime factorisation.

$$G(S) = (N + VS)(M + US)^{-1}, \quad S \in \mathcal{RH}_\infty \tag{40}$$

$$G(S) = (\tilde{N} + S\tilde{V})^{-1}(\tilde{M} + S\tilde{U}), \quad S \in \mathcal{RH}_\infty \tag{41}$$

Furthermore the two signals α and β has been introduced on Figure .23 which are used for injecting the excitation signal used for active fault detection and design of the residual generator. It was shown in [24] that for a system as shown in Figure .23 the transfer functions from the inputs to outputs are given as shown in equation (42).

$$\begin{bmatrix} y \\ u \\ \beta \end{bmatrix} = T_{cl}(S) \begin{bmatrix} d \\ v_1 \\ v_2 \\ \alpha \end{bmatrix} \tag{42}$$

Where T_{cl} is

$$\begin{bmatrix} (N+VS)\tilde{U} & (N+VS)\tilde{U} & (N+VS)\tilde{V} & N+VS \\ (M+US)\tilde{U} & (M+US)\tilde{U} & (M+US)\tilde{V} & M+US \\ \tilde{M}+S\tilde{V} & \tilde{M}+S\tilde{V} & \tilde{N}+S\tilde{U} & S \end{bmatrix}$$

With the controller designed it is possible to calculate the Youla-Kucera factorisation. One such factorisation for a P-controller can be found in [27] and is given in equation (43) for the right coprime factorisation and in equation (44) for the left coprime factorisation.

$$\begin{bmatrix} M & U \\ N & V \end{bmatrix} = \left(\begin{array}{c|cc} A+BF & B & 0 \\ \hline F & I & K \\ C & 0 & I \end{array} \right) \tag{43}$$

$$\begin{bmatrix} \tilde{V} & -\tilde{U} \\ -\tilde{N} & -\tilde{M} \end{bmatrix} = \left(\begin{array}{c|cc} A+BPC & -B & BK \\ \hline F-PC & I & -K \\ C & 0 & I \end{array} \right) \tag{44}$$

Here F is a fictitious gain that satisfy all eigenvalues of $A+BF$ are in the stable left half plane. Equivalently it is possible to calculate the Youla-Kucera factorisation for the observer based controller. For such a controller the right factorisation is shown in equation (45) and the left factorisation is shown in equation (46).

$$\begin{bmatrix} M & U \\ N & V \end{bmatrix} = \left(\begin{array}{c|cc} A+BF & B & -L \\ \hline F & I & 0 \\ C & 0 & I \end{array} \right) \tag{45}$$

$$\begin{bmatrix} \tilde{V} & -\tilde{U} \\ -\tilde{N} & -\tilde{M} \end{bmatrix} = \left(\begin{array}{c|cc} A+LC & -B & L \\ \hline F & I & 0 \\ C & 0 & I \end{array} \right) \tag{46}$$

Here F is the state feedback matrix and L is the observer gain matrix. Using the coprime factorisation of controller and plant the augmented controller can be expressed as in equation (47).

$$J_k = \begin{bmatrix} UV^{-1} & \tilde{V}^{-1} \\ V^{-1} & -V^{-1}N \end{bmatrix} \tag{47}$$

For an augmented controller as presented in equation (47) it might seem that the order is higher than for the nominal controller. The order of the two controllers has been shown to be the same in [28]. In the case of the observer based control design the controller J_k can be written in state space form as in equation (47).

$$J_k = \left[\begin{array}{c|cc} A+BF+LC+LDF & -L & B+LD \\ \hline F & 0 & I \\ -(C+DF) & I & -D \end{array}\right] \tag{48}$$

Since a full order observer has been implemented the order of the nominal controller is the same as for the plant. From equation (48) it is easy to see that the augmented controller has the same order as well why the computational effort is the same with the nominal controller and the augmented.

Publication P6

Closed Loop Identification of a Piezo Electrically-Controlled Radial Gas Bearing - Theory & Experiment

Closed Loop Identification of a Piezo Electrically-Controlled Radial Gas Bearing - Theory & Experiment

André K. Sekunda[1], H Niemann[1], N Kjølstad Poulsen[2] and Ilmar Santos[3]

[1]) Department of Electrical Engineering, Technical Unversity of Denmark, Kgs. Lyngby, Denmark

[2]) Department of Applied Mathematics and Computer Science, Technical Unversity of Denmark, Kgs. Lyngby, Denmark

[3]) Department of Mechanical Engineering, Technical University of Denmark, Dk-2800 Kgs. Lyngby, Denmark

E-mail: aksek@elektro.dtu.dk, hhn@elektro.dtu.dk, nkpo@dtu.dk, ifs@mek.dtu.dk

Abstract

Gas bearing systems have extremely small damping properties. Feedback control is thus employed to increase the damping of gas bearings. Such a feedback loop correlates the input with the measurement noise which in turn makes the assumptions for direct identification invalid. The originality of this paper lies in the investigation of the impact of using different identification methods to identify a rotor-bearing systems dynamic model when a feedback loop is active. Two different identification methods are employed. The first method is open loop Prediction Error Method (PEM) while the other method is the modified Hansen scheme. Identification based on the modified Hansen scheme is conducted by identifying the Youla deviation system using subspace identification. Identification of the Youla deviation system is based on the Youla-Jabr-Bongiorno-Kucera (YJBK) parametrisation of plant and controller. By using the modified Hansen scheme, identification based on standard subspace identification methods can be used to identify the Youla deviation system of the gas bearing. This procedure ensures the input to the Youla deviation system and the noise are uncorrelated even though the system is subject to feedback control. The effect of identifying the Youla deviation system compared to direct subspace identification of the gas bearing is further investigated through a simulation example. Experiments are conducted on the piezoelectrically-controlled radial gas bearing. A dynamic model

is identified using the modified Hansen scheme as well as using PEM identification. The resulting models are compared for different imperfect nominal models, to examine under which conditions each method should be used.

Keywords— Experiment, Gas Bearing, Closed-loop Identification, Coprime Factorisation, Subspace Identification

1 Introduction

Active gas bearings are an interesting alternative to more commonly used bearings such as ball and magnetic bearings. Compared to ball bearings, active gas bearings have extremely low friction. At the same time active gas bearings are open loop stable for appropriately low rotational speeds, unlike magnetic bearings, which are always open loop unstable. The active gas film itself delivers low damping. Because of the low damping the rotor system may become unstable due to self-excited rotor whirling. Control is therefore still required although it is less limited than for unstable systems. Designing models of gas bearings has however been shown to be less straightforward, compared to the frictionless alternative of magnetic bearings. A successful mathematchical model for active gas bearings was first introduced in [1] with extensions to the model presented in [2, 3, 4]. Recently a low order model able to describe the dynamics of the active gas bearing was presented in [5]. Such low order models greatly simplify the control design phase.

Identification of gas bearings have been a subject of some interest recently [6, 7]. It has been shown possible to identify appropriately low order models that mimic the behaviour of the gas bearing in a satisfying manner when no feedback loop is active. Usually the gas bearing will operate under conditions at which the damping is so small that feedback control is needed for safe operation. It is therefore of extreme relevance to be able to identify an appropriate model for the gas bearing under conditions where it is only possible to obtain identification data while the gas bearing is part of a closed loop system.

There are plenty of different methods for identifying closed loop systems. One of such methods transforms the closed loop identification problem of the plant into an open loop identification problem by using the Youla parameterization. Well known subspace identification methods are in this paper used for identifying the Youla deviation system. It has become increasingly popular to use subspace identification methods due to their natural connection to multiple-input and multiple-output state space models [8]. Some of the most well known subspace identification methods are the Numerical algorithm for Subspace IDentification (N4SID) proposed in [9] and the Multivariable Output-

Error State-sPace (MOESP) proposed in [10]. Both methods, as with most subspace identification methods, assume the noise and input to be uncorrelated, hence the methods are based on assumptions that are only valid for open loop identification. Some work has been done on extending the subspace identification methods to identification of closed loop systems. Several different methods for coping with feedback connection have been proposed[8]. However, often such methods show the same weakness of depending on being able to identify the noise signal imposed on the system.

One possible indirect identification method is subspace identification of the Youla deviation system. The Youla deviation system is used to reformulate the identification problem from a closed loop to an open loop identification problem using a coprime factorisation of the nominal plant model and the controller. This identification procedure is known as the Hansen scheme and was first introduced in [11]. The original version of the Hansen scheme used external excitation signals to indirectly excite the Youla deviation system. A modified version of the Hansen scheme, first introduced in [12], is used instead in this paper which makes it possible to directly impose an excitation signal onto the Youla deviation system. A gas bearing easily becomes an unstable system when the rotational speed is increased. However the Youla deviation system identified by the modified Hansen scheme will always be stable. The open loop identification technique is thus applicable where direct open loop identification of the gas bearing is not. The modified Hansen scheme however, has the drawback of loss of physical understanding of the system.

The key contribution of this paper is to offer insight into when it can be advantageous to identify an active gas bearing using the modified Hansen scheme instead of the more traditional Prediction Error Method (PEM) identification. This paper thus focuses on comparing known identification techniques for identification of a gas bearing when being part of a closed loop system. The results are gathered by a combination of simulations and experiments conducted on a laboratory installation.

The paper is structured as follows: In the following section the model of the gas bearing is introduced; In the third section some preliminary theory is introduced in order to let the paper stand alone; In the fourth section the three methods used for identification of the gas bearing are discussed; In the fifth section the identification procedure is given and the quality of the nominal model is discussed; In sixth section the experimental methods are presented and the resulting model identified using each of the 3 different identification methods are shown. Finally, in the last section, a discussion of the results and future possible improvements are given.

2 Gas Bearing System

The gas bearing test rig used in this paper has already been subject to different identification methods, with the focus on its physical behavior in [13, 2, 14] and on the system dynamics in [6, 7, 15]. These methods however, have all been both conducted and verified under open loop conditions. All identification in this paper are based on the gas bearing being subject to feedback control. The nominal model is based on the model structure introduced in [15] which showed it possible to model the vertical and horizontal position of a disc attached to a flexible shaft. The shaft is held in position by the gas bearing, using gas injected into the bearing in both the horizontal and vertical directions using a 6'th order model. A picture of the test rig is presented on Fig. 0.1a.

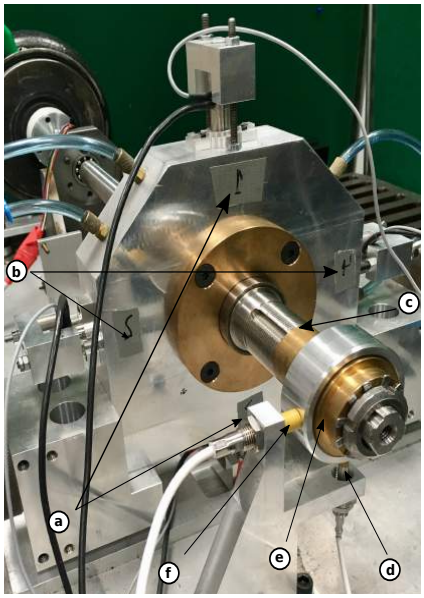

(a) Picture of the experimental test rig used for conducting active fault detection. The different parts of the test rig is as follows: **a**; vertical piezo actuator, **b**; horizontal piezo actuators, **c**; flexible shaft, **d**; vertical displacement sensor, **e**; disc and **f** horizontal displacement sensor.

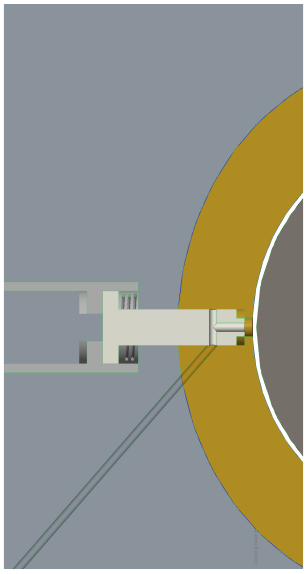

(b) Cross section illustration of the actuator. The further out the pin is moved the more air is able to flow in which increase the pressure. The position of the shaft is thus controlled by changing the flow of air through the inlet valve.

Figure 0.1

A illustration of the gas bearing actuators is shown on Figure 0.1b. The air is going into the bearing through the small pipe, a piezo electric actuator is attached which controls how much air is able to get into the bearing and thus

controls the preasure inside the bearing.

The model of the gas bearing is based on the mass-springer-damper-model in Eq. (1) for the non rotating case.

$$\ddot{\mathbf{l}} - \mathbf{D}\dot{\mathbf{l}} - \mathbf{K}\mathbf{l} = \mathbf{B}\mathbf{m} \tag{1}$$

Here $\mathbf{l}$ is a vector with the position in the horizontal and vertical direction and $\mathbf{m}$ is the state of the actuator dynamics. $\mathbf{K}$ is the specific stiffness matrix given in $[\frac{N}{kg\ \mu m}]$, $\mathbf{D}$ is the specific damping matrix in $[\frac{Ns}{kg\ \mu m}]$, and $\mathbf{B}$ is the actuator gain matrix in $[\frac{N}{kg\ V}]$. Using Eq. (1) the state vector is defined in Eq. (2).

$$\mathbf{x} = \begin{bmatrix} \mathbf{l} \\ \dot{\mathbf{l}} \\ \mathbf{m} \end{bmatrix} \tag{2}$$

The structure of the state space model is given in Eq. (3) to Eq. (6) where each element is a 2x2 matrix

$$\mathbf{A} = \begin{bmatrix} 0 & \mathbf{I} & 0 \\ \mathbf{K} & \mathbf{D} & \mathbf{B} \\ 0 & 0 & -\mathbf{P} \end{bmatrix} \tag{3}$$

$$\mathbf{B} = \begin{bmatrix} 0 \\ 0 \\ \mathbf{P} \end{bmatrix} \tag{4}$$

$$\mathbf{C} = \begin{bmatrix} \mathbf{I} & 0 & 0 \end{bmatrix} \tag{5}$$

$$\mathbf{D} = \begin{bmatrix} 0 \end{bmatrix} \tag{6}$$

The matrix $\mathbf{P}$ is a diagonal matrix with each element p_j defined by Eq. (7).

$$h_j(s) = \frac{p_j}{s + p_j} \qquad j \in \{1, 2\} \tag{7}$$

h_j is the first order low pass filter through which the system is actuated. The state space model is thus given in Eq. (8).

$$G := \begin{Bmatrix} \dot{x} & = \mathbf{A}x + \mathbf{B}u \\ y & = \mathbf{C}x + \mathbf{D}u \end{Bmatrix} \tag{8}$$

In order to conduct closed loop identification of the system, the parameters of the model have been identified with the disc not rotating as part of an open loop scheme. The identified matrices are given in Eq. (9) to Eq. (12)

$$D = \begin{bmatrix} -224.9 & 3.97 \\ 9.12 & -267.7 \end{bmatrix} \tag{9}$$

$$K = \begin{bmatrix} -1.869 \cdot 10^6 & -8577 \\ -9510 & -1.737 \cdot 10^6 \end{bmatrix} \tag{10}$$

$$B = \begin{bmatrix} -6.126 \cdot 10^6 & 3.154 \cdot 10^5 \\ -1.571 \cdot 10^5 & -4.516 \cdot 10^6 \end{bmatrix} \tag{11}$$

$$P = \begin{bmatrix} 989 & 0 \\ 0 & 942.5 \end{bmatrix} \tag{12}$$

3 Theory

The first part of this section is dedicated to presenting some definitions to the reader in order to make the rest of the paper stand alone. A nominal plant is given by $G(0)$ and a stabilizing controller is given by K. The coprime factorization of $G(0)$ and K are given by:

$$G(0) = NM^{-1} = \tilde{M}^{-1}\tilde{N}, \quad N, M, \tilde{N}, \tilde{M} \in RH_\infty \tag{13}$$

$$K = UV^{-1} = \tilde{V}^{-1}\tilde{U}, \quad U, V, \tilde{U}, \tilde{V} \in RH_\infty \tag{14}$$

Here N and M denote the right coprime factorisation of the nominal plant and $\tilde{N}$ and $\tilde{M}$ denote the left coprime factorisation of the nominal plant. Equivalently the right coprime factorisation of the controller is given by V and U, and the left coprime factorisation is given by $\tilde{V}$ and $\tilde{U}$ such that the Bezout identity given in Eq. (15) is satisfied.

$$\begin{bmatrix} I & 0 \\ 0 & I \end{bmatrix} = \begin{bmatrix} M & U \\ N & V \end{bmatrix} \begin{bmatrix} \tilde{V} & -\tilde{U} \\ -\tilde{N} & \tilde{M} \end{bmatrix} = \begin{bmatrix} \tilde{V} & -\tilde{U} \\ -\tilde{N} & \tilde{M} \end{bmatrix} \begin{bmatrix} M & U \\ N & V \end{bmatrix} \tag{15}$$

It will be assumed in this paper that K is a stabilizing controller for both the nominal plant as well as for the real plant $G(S)$. This is the case if Eq. (15) is true. Here S is the Youla deviation system describing the divergence between the nominal model and the real plant. With the controller and plant

model factorisations defined in Eq. (13) and (14) the real plant is given by Eq. (16) using the right coprime factorisation and Eq. (17) using the left corpime factorisation.

$$G(S) = (N + VS)(M + US)^{-1},\ S \in \mathcal{RH}_\infty \tag{16}$$

$$G(S) = (\tilde{M} + S\tilde{U})^{-1}(\tilde{N} + S\tilde{V}),\ S \in \mathcal{RH}_\infty \tag{17}$$

With a formulation of the true plant as in Eq. (17) only the Youla deviation system(S) is unknown and needs to be identified. G(S) from Eq. (16) can be formulated using a linear fractional transformation (LFT) given by:

$$G(S) = \mathcal{F}_u(J_G, S) \tag{18}$$

where:

$$J_G = \begin{bmatrix} -M^{-1}U & M^{-1} \\ \tilde{M}^{-1} & G(0) \end{bmatrix}$$

Here the input and output signals of J_G is presented in Eq. (19).

$$\begin{bmatrix} \eta \\ y \end{bmatrix} = J_G \begin{bmatrix} \epsilon \\ u \end{bmatrix} \tag{19}$$

The closed-loop system using the system description in Eq. (18) is shown in Fig. 0.2, where v_1 and v_2 are two possible excitation signals and n is the noise.

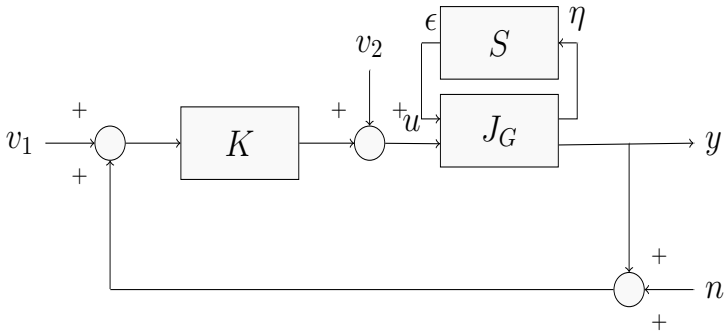

Figure 0.2: Closed loop system with the plant represented as a nominal part(J_G) and the unknown Youla deviation system S.

Using Eq. (18) and the setup in Fig. 0.2, the vector introduced, ϵ, is given in Eq. (20).

$$\epsilon = S\eta \tag{20}$$

Eq. (20) shows that the identification of S is straightforward using the signals η and ϵ. The two signals ϵ and η in Eq. (20) are not directly accessible. However, it is shown that using the available signal vectors v_1, v_2, y and u it is possible to generate ϵ and η. It is therefore not possible to inject η directly for the open loop identification of S [11]. Instead, including the Youla parametrization of all controllers in the closed-loop, it will be possible to have a direct access to ϵ and η as shown further on. Let the Youla parametrization of all stabilizing controllers for the nominal system $G(0)$ be given by the following LFT description:

$$K(Q) = \mathcal{F}_l(J_K, Q) \tag{21}$$

where:

$$J_K = \begin{bmatrix} K & \tilde{V}^{-1} \\ V^{-1} & -V^{-1}N \end{bmatrix}$$

The input and output signals of J_K are in Eq. (22).

$$\begin{bmatrix} u \\ \beta \end{bmatrix} = J_K \begin{bmatrix} y \\ \alpha \end{bmatrix} \tag{22}$$

Again it is possible to introduce two new signals in order to determine Q.

$$\alpha = Q\beta \tag{23}$$

The two new signals β and α are part of the controller and can thus be directly measured and inserted. The relationship between the signals in the plant and controller can therefore give a significant advantage for direct identification of S.

The relationship between the signals η, ϵ, β and α can be calculated as a Redheffer star product as defined in [16]. The resulting relationship is shown in Eq. (24).

$$\begin{bmatrix} \alpha \\ \beta \end{bmatrix} = J_G \star J_K = \begin{bmatrix} 1 & 0 \\ 0 & 1 \end{bmatrix} \begin{bmatrix} \eta \\ \epsilon \end{bmatrix} \tag{24}$$

Here $\star$ denotes the redheffer star product. The Youla deviation system is therefore possible to identify using the signals found in the controller, which is used for the closed loop identification. Based on the system description given on Figure 0.2 the Youla deviation system can thus be identified using Eq. (25).

$$\beta = S\alpha + (\tilde{M} + S\tilde{U})n \tag{25}$$

This ability to directly impose the excitation signal on the Youla deviation system S is the advantage of the modified Hansen scheme compared to the original version. The modification is believed to make the identification more intuitive and was first introduced in [12].

4 Identification methods

In all tests conducted the plant is subject to a feedback loop with an a priori designed controller. In order to conduct a proper comparison between the methods, all methods use data from the same experiment. Furthermore the noise (n) has been found to be approximately white gaussian from an open loop dataset without any excitation.

Identification using the modified Hansen Scheme

It was argued in [12] that the signals should be obtained directly from the controller by modifying it to the form shown in Fig. 0.3

Using the signals α and β it is possible to cast an identification problem as given in Eq. (25) by taking advantage of the relationship found in Eq. (24). Since α does not depend on the noise n as shown in [17] it is clear from Eq. (25) that the noise and excitation signal are not correlated. The system S is identified using the subspace method N4SID for identification. The choice of using a subspace method for identification is two-fold. One of the great advantages of using subspace identification is the direct identification of MIMO state space models. The other important advantages of choosing a subspace identification method is that the methods are based on zero a priori knowledge. Unlike the true system $G(S)$ it is rather difficult to determine a proper initial structure of the Youla deviation system S. This comes from the fact that the nominal system is believed to be the best initial guess possible. All prior knowledge therefore points towards the Youla devitation system being 0.

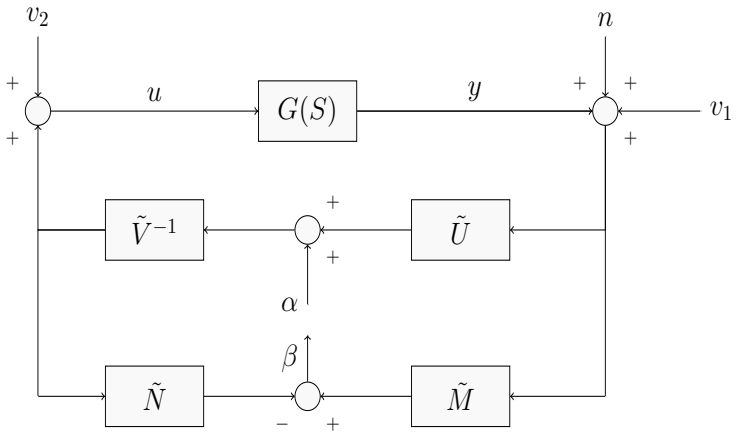

Figure 0.3: Representation of a YJKB parametrised controller for generation of signals for identification.

Direct Grey Box Identification

This identification method, as the name suggests, does not use any information regarding the feedback loop and the controller to determine the model. The method was presented in [18] and is based on obtaining input and output data of the plant and determining the model. In this paper it is implemented as a PEM. The method uses the input-output data together with a nominal model as the information for parameter identification.

5 Preliminary open loop identification

Identification is conducted in two separate steps. First, a nominal model is generated to use as a basis for identification of the plant when part of a closed loop scheme. Such a model is obtained using data acquired from an open loop experiment conducted when the active gas bearing is not rotating. The identification results for the nominal model are based on the method described in [7].

The identified nominal model is able to predict the displacement to an acceptable degree. The parameters identified through the experiment were presented in section 2. In order to give a quantitative measure of the quality of the different identification procedures used during the experiments, a goodness fit is calculated using Eq. (26) which is the normalised root mean square error.

$$R^2 = 1 - \frac{||y - \hat{y}||}{||y - \bar{y}||} \tag{26}$$

Here y is the measured output, $\bar{y}$ is the mean of the measured output and $\hat{y}$ is the estimated output using the model. Based on the nominal model, a controller is designed and a coprime factorisation is conducted. In the experiment only the left factorised form is used. In order to show the effect of the closed loop identification, the nominal model has been degraded in several different ways to examine the ability of the different identification procedures when the plant is part of a closed loop scheme. Lastly, a controller is been designed using the LQR function in MATLAB and implemented using the controller design presented in Fig. 0.3.

6 Simulation Results

It is in this section investigated which benefits there are from identifying the Youla deviation system. Identifying the Youla deviation system is compared to other more well known methods. It is decided to compare the method with grey box PEM identification and subspace identification. Normal subspace identification is independent of the nominal model. Grey box PEM identification on the other hand uses information from the nominal model.

Inferior a priori knowledge of the system dynamics

A definition of the inferior model from which the system has to be identified is needed to compare the identification methods. For the first test inferior knowledge about the system dynamics has been investigated. The system matrix of the initial model is defined in Eq. (27) where A_{model} has inferior knowledge relative to the real system matrix A.

$$A_{model} = (1 - \theta) \cdot A \tag{27}$$

Here A is the system matrix of the system to be identified, A_{model} is the system matrix of the nominal model and θ is a uniformly distributed random variable in the interval 0 to 1. The nominal model thus contains a system matrix where all elements are smaller than for the real plant. A simulation has been conducted where 500 different initial models were constructed using Eq. (27). For each model a controller was designed that would stabilise the

initial model and the real plant. Noise has been added as output noise and the system has been excited using a series of square waves. For each initial model an input-output set has been gathered and an identification has been conducted. In each case a second verification data set has been obtained where noise was omitted from the system. The identification results are shown on Fig. 0.4 for identification using PEM and subspace identification of the Youla deviation system.

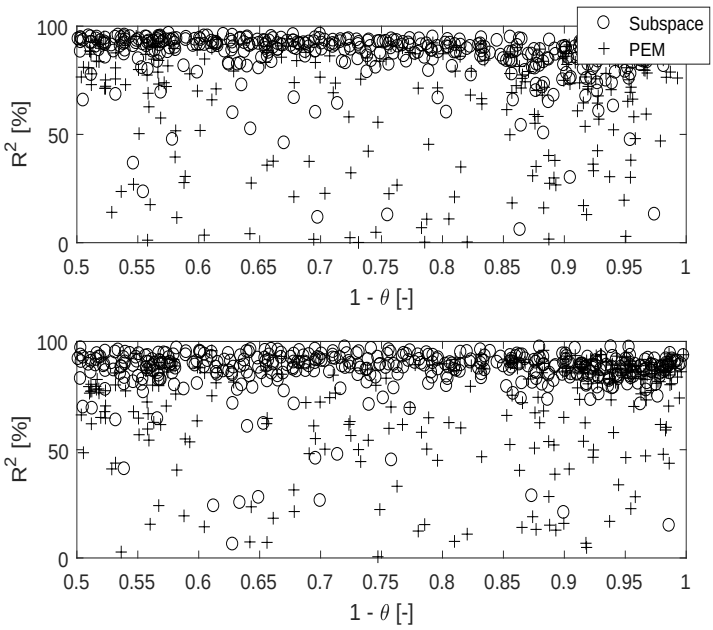

Figure 0.4: Plot of the R^2 fit in the horizontal direction (Top plot) and vertical direction (bottom plot) using the PEM for identification and subspace identification of the Youla system.

It can be seen from Fig. 0.4 that for small deviations between the real system and the initial model both methods produce similar results. However as θ is increased the PEM identification starts to produce a lower R^2 fit.

With the methods compared it is concluded that identification of the Youla deviation system using subspace identification is resulting in higher R^2 fit when sufficient a priori knowledge of the system dynamics is lacking. Identifying the Youla deviation system instead of the plant directly, increases the complexity. The effect has therefore been examined when compared to direct subspace identification of the plant. Again 500 initial models were constructed using Eq. (27). Identification was conducted using subspace identification to identify the plant

directly and to identify the Youla deviation system. A box plot of the resulting fit of the identified models is shown in Fig. 0.5.

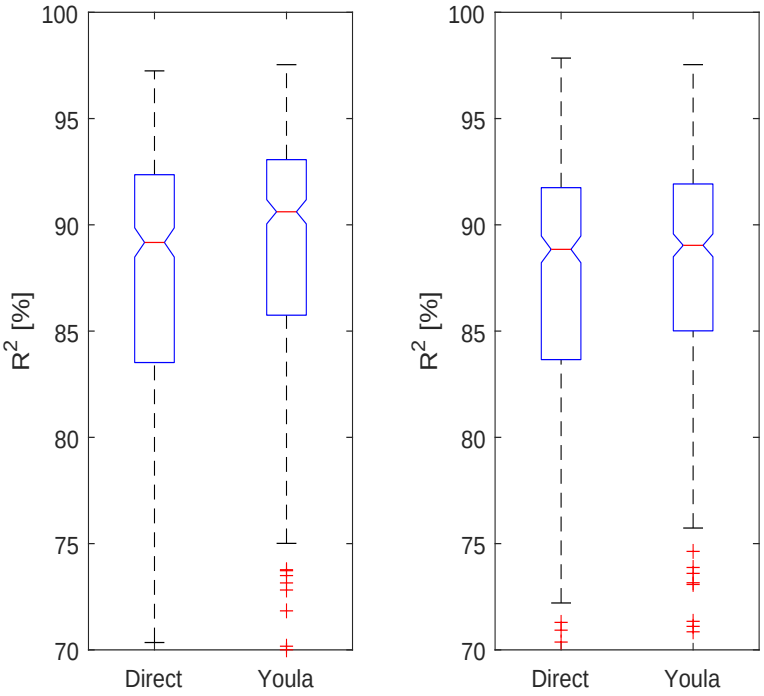

Figure 0.5: Boxplot of the R^2 fit given direct identification of the plant and identification of the Youla deviation system. The left plot is for the horizontal direction where as the right plot is for the vertical direction.

It is seen from Fig. 0.5 that when the plant is directly identified, using a subspace identification method, the variance of the R^2 fit increases. Furthermore the mean of the R^2 fit is higher when identifying the Youla deviation system. Identifying the plant indirectly by identification of the Youla deviation system thus produces better results. Since both methods suffer from the loss of physical understanding of the models produced it is decided not to look further into direct subspace identification.

7 Experiments & Results

With the controller designed and nominal model identified using the method described in [15], experiments have been conducted under 3 different conditions.

The results have been summarised in Table 0.1 for all 3 experiments. In all experiments the same 2 identification methods have been applied; PEM using a fixed a priori model structure and identification of the Youla deviation system. The identification signals are found as Eq. (28) for direct identification of S. The system has been excited using the input signal denoted α on Fig. 0.3.

$$\beta = \tilde{M}y - \tilde{N}u \tag{28}$$

The Youla devitation system is the identified based on Eq. (25). The first experiment is conducted where the disc is non-rotating, and the nominal model has been degraded so that it is not able to mimic the plant dynamic in a satisfying manner. The degradation of the nominal model was achieved by multiplying all elements of the system matrix with 0.5. The result of the identification is shown in Fig. 0.6 where the nominal model and the 2 identified models have been compared with a verification dataset.

It is shown in Fig. 0.6 that with a poor nominal model, identification of the Youla deviation system is able to recover the system dynamics. It is also noticed that the PEM is unable to identify a model of the same quality and obtains a lower R^2 fit when the nominal model is of such low quality. The same trend was observed in section 6 when θ is equal to 0.5. The result is summarised as column 2 in Table 0.1.

To further examine the effect of the identification methods for low quality nominal models, an experiment is conducted where the disc is rotating with 2500 revolutions per minute. Here it has instead been chosen to multiply all elements of the input matrix with 0.7 so that the input gain is higher than expected. The verification data together with the predicted output for each of the models are shown in Fig. 0.7.

The nominal model is better than in the previous example at predicting the position of the disc, however the nominal model is still having a fit lower than what is expected possible to obtain. This is seen from the relatively large increase in the fit for each of the identification methods. The result is summarised as column 1 in Table 0.1. Lastly an experiment is conducted to examine the identification methods ability to recover small deviations. Again the nominal model has been tampered with to degrade its performance. The elements of the system matrix have been multiplied by 0.97 so that the dynamics of the real plant is slightly faster than for the nominal model. Identification of the Youla deviation system using Eq. (28) has thus been conducted, and a plot of the signal β measured and predicted using the identified system are shown in Fig. 0.8.

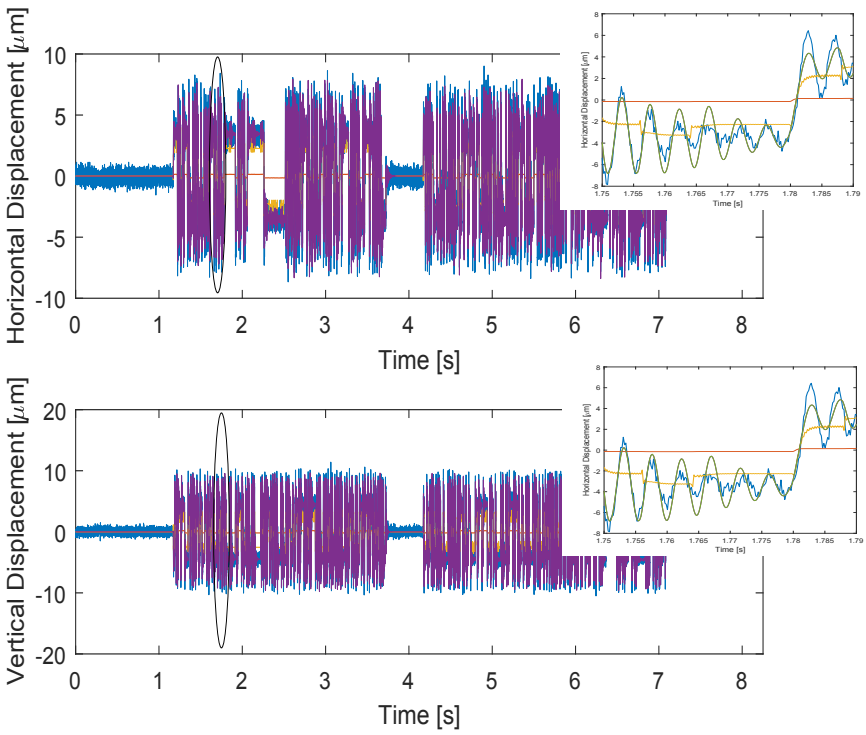

Figure 0.6: Comparison of a verification signal (blue) with the predicted output given the nominal model (red) and each of the 3 identified models. The nominal model G was found to have a fit of 3.188% in the horizontal direction and 2.999% in the vertical direction. The PEM (yellow) was found to have a fit of 48.91% in the horizontal direction and of 39.47 in the vertical direction. Identification of the Youla deviation system (purple) gave a fit of 76.76% in the horizontal direction and of 83.58% in the vertical direction.

The nominal model and plant are fairly similar why noise is expected to dominated the β signal. This is seen on Fig. 0.8 where the measured signal β is presented. It is clear that the signal contain a dominant noise part in the horizontal direction. It is clear from Fig. 0.8 that the identification should improve the model in the vertical direction mainly. Again the identified model has been compared with a verification signal which is shown in Fig. 0.9.

It can be seen from Fig. 0.9 that the nominal model does indeed produce a better fit. Still, both methods are able to improve the model. As clearly seen from Fig. 0.8 the improvement of the identified model was mostly in the vertical direction. A zoom on the verification experiment is shown in Fig. 0.10.

It is clear from Fig. 0.10 that the identified models have improved the predic-

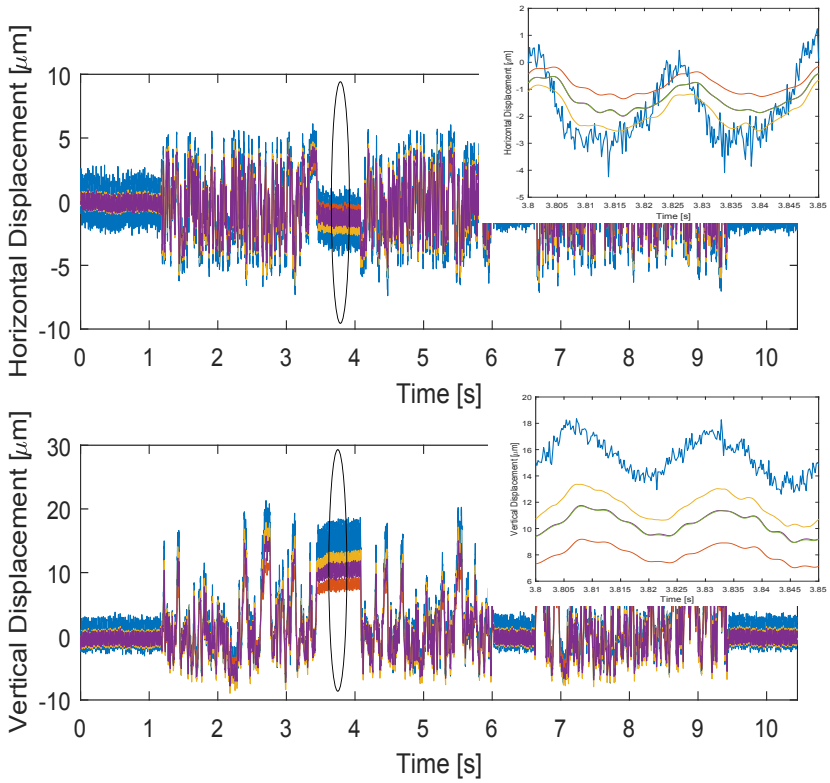

Figure 0.7: Comparison of a verification signal (blue) with the predicted output given the nominal model (red) and each of the 3 identified models. The nominal model G was found to have a fit of 51.36% in the horizontal direction and 54.13% in the vertical direction. The PEM (yellow) was found to have a fit of 62.87% in the horizontal direction and of 75.78 in the vertical direction. Identification of the Youla deviation system (purple) gave a fit of 61.04% in the horizontal direction and of 69.19% in the vertical direction.

tion accuracy in the vertical direction. Both models show a clear improvement compared to the nominal case as shown in the 3'rd column of Table 0.1. The result of the 3 experiments for each of the identification methods using Eq. (26) to determine the quality of the identified model are shown in Table 0.1 together with the fit of the nominal model.

As seen in Table 0.1, using PEM or subspace identification of the Youla deviation system based on the modified Hansen scheme ($G(S)$) gives similar results for small deviations. However in the case where the nominal model lack significant insight to the plant(low fit for nominal model) the PEM results in a

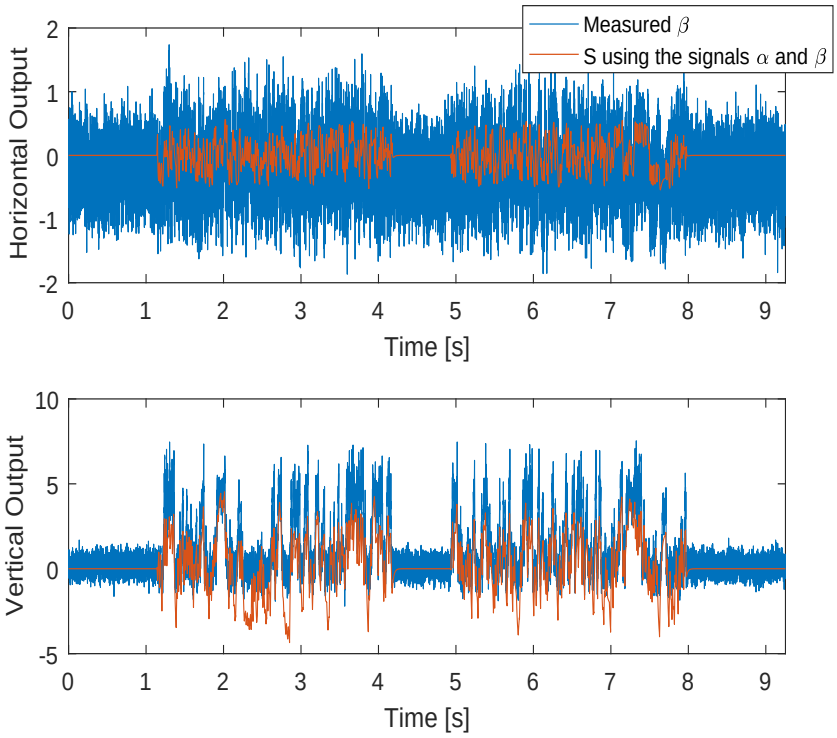

Figure 0.8: Comparison of the measured β signal with the predicted β signal, using the two identified models of the Youla deviation system. The blue line represents the measured signals, the red line is the predicted signals given an Youla deviation system identified using the modified Hansen Scheme.

	2500 RPM		high deviation 0 RPM		small deviation 0 RPM	
	Horizontal	Vertical	Horizontal	Vertical	Horizontal	Vertical
Nominal model	51.36%	54.13%	3.19%	3%	83.21%	76.12%
Open loop PEM model	62.87%	75.78%	48.91%	39.47%	83.9%	84.63%
Modified Hansen scheme $G(S)$	61.94%	69.19%	76.76%	83.58%	83.53%	81.18%
Modified Hansen scheme $G_{red}(S)$	60.71%	69.33%	76.73%	83.53%	83.07%	79.59%

Table 0.1: Model fit using each of the two identification methods. The fit is R^2 fit shown in Eq. (26)

lower fit.

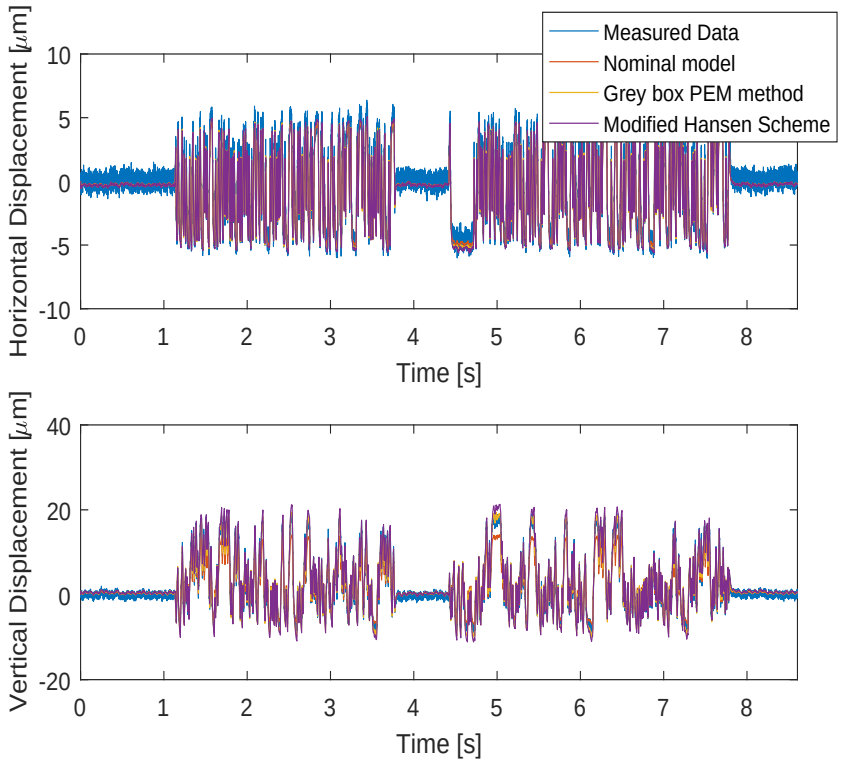

Figure 0.9: Comparison of a verification signal (blue) with the predicted output given the nominal model (red) and each of the 3 identified models. The nominal model G was found to have a fit of 81.93% in the horizontal direction and 76.12% in the vertical direction. The PEM (yellow) was found to have a fit of 83.9% in the horizontal direction and of 84.63 in the vertical direction. Identification of the Youla deviation system (purple) gave a fit of 83.53% in the horizontal direction and of 81.18% in the vertical direction.

Model reduction of the identified models

The models identified using the modified Hansen scheme are all of a inconveniently high order. This is a well known result of the identification method and it is therefore found useful to investigate the impact on the quality of the identification when model reduction is conducted. Model reduction has in this paper been conducted by requiring all models to be of the same order as the nominal model (6′th order). The same systems as identified previously have been compared in Table 0.1 where those systems identified using the Hansen scheme have been reduced to be of 6′th order. The identified plant after model reduction is

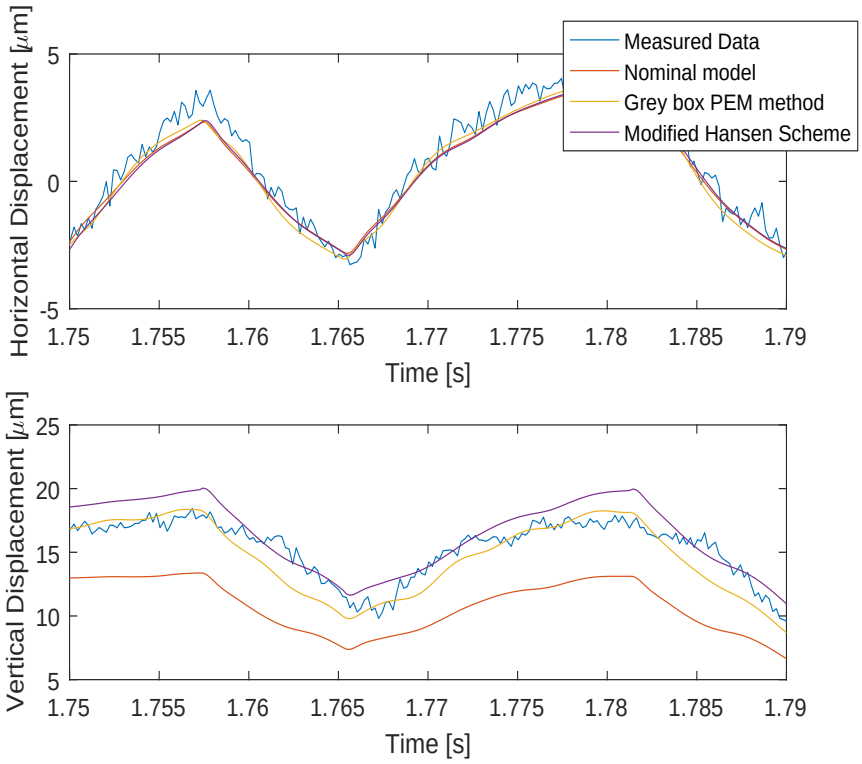

Figure 0.10: Zoom in on the comparison of a verification signal(blue) with the predicted output given the nominal model (red) and each of the 2 identified models, PEM (yellow) and Youla deviation system (purple)

given in Eq. (29).

$$G_{red}(S) = modred(G(S)) \tag{29}$$

Here $modered()$ denotes the model reduction function used and $G(S)$ is the originally identifed plant using the modified Hansen scheme. The results of the models for which model reduction has been conducted are shown in Table 0.1. The model reduction technique used is described in [19] and the resulting $6'$th order approximations shows to have a similar fit to the full order identified systems as shown in Tab. 0.1. It is worth noting that the initially identified models had as much as 40 states, which makes control design problematic.

8 Conclusion

Identification of a gas bearing as part of a closed loop system has been conducted. It was shown possible to identify the gas bearing, as part of a closed loop system, by reformulating the problem into identification of the Youla deviation system which is a standard open loop identification problem. Furthermore, using an open loop PEM method for identification gives similar results when the nominal model predicts the system dynamics with high accuracy. A simulation example was given which pointed towards the identification of the youla deviation system to produce better results on average for poor knowledge of the plant dynamics. Experiments showed that for a poor nominal model the modified Hansen scheme method did indeed produce better results, with a fit 28% in the horizontal direction and 44% higher in the vertical direction for poor a priori knowledge of the plant dynamics. The PEM method furthermore used considerably longer time to identify a model than the subspace identification method used to determine the Youla deviation system. This result might be due to how the PEM method is restricted to the model structure determined while the modified Hansen scheme is not. The identified systems using the Youla deviation system however also has some disadvantages. Any physical understanding related to model parameters of the gas bearing is lost when using the modified Hansen scheme. Furthermore the methods produced models of higher order than the nominal model and the plant identified using the PEM for identification. This tendency of order increase comes naturally from the construction of the plant when the Youla deviation system has been identified. Unnecessary high order model solutions is thus a well known consequence when using the modified Hansen scheme. Model reduction has therefore been conducted which was able to produce acceptable results. It have thus been shown that the method has its clear advantage over PEM identification when model expert knowledge is lacking.

Conflict of interest
The authors declare no conflict of interest in preparing this article.

Funding
This research received no specific grant from any funding agency in the public, commercial, or not-for-profit sectors.

Bibliography

[1] F. G. Pierart and I. F. Santos, "Steady state characteristics of an adjustable hybrid gas bearing–computational fluid dynamics, modified reynolds equation and experimental validation," *Proceedings of the Institution of Mechanical Engineers, Part J: Journal of Engineering Tribology*, vol. 229, no. 7, pp. 807–822, 2015.

[2] ——, "Active lubrication applied to radial gas journal bearings. part 2: Modelling improvement and experimental validation," *Tribology International*, vol. 96, pp. 237–246, 2016.

[3] ——, "Adjustable hybrid gas bearing–influence of piezoelectrically adjusted injection on damping factors and natural frequencies of a flexible rotor operating under critical speeds," *Proceedings of the Institution of Mechanical Engineers, Part J: Journal of Engineering Tribology*, vol. 230, no. 10, pp. 1209–1220, 2016.

[4] ——, "Lateral vibration control of a flexible overcritical rotor via an active gas bearing–theoretical and experimental comparisons," *Journal of Sound and Vibration*, vol. 383, pp. 20–34, 2016.

[5] L. R. Theisen, H. H. Niemann, R. Galeazzi, and I. F. Santos, "Enhancing damping of gas bearings using linear parameter-varying control," *Journal of Sound and Vibration*, vol. 395, pp. 48–64, 2017.

[6] L. R. S. Theisen and H. Niemann, "Modelling of rotor-gas bearings for feedback controller design," in *Journal of Physics: Conference Series*, vol. 570. IOP Publishing, 2014, p. 052005.

[7] L. R. S. Theisen, F. G. Pierart, H. Niemann, I. F. Santos, and M. Blanke, "Experimental grey box model identification and control of an active gas bearing," in *Vibration Engineering and Technology of Machinery*. Springer, 2015, pp. 963–976.

[8] S. J. Qin, "An overview of subspace identification," *Computers & chemical engineering*, vol. 30, no. 10, pp. 1502–1513, 2006.

[9] P. Van Overschee and B. De Moor, "N4SID: Subspace algorithms for the identification of combined deterministic-stochastic systems," *Automatica*, vol. 30, no. 1, pp. 75–93, 1994.

[10] M. Verhaegen and P. Dewilde, "Subspace model identification part 1. the output-error state-space model identification class of algorithms," *International journal of control*, vol. 56, no. 5, pp. 1187–1210, 1992.

[11] F. Hansen, G. Franklin, and R. Kosut, "Closed-loop identification via the fractional representation: Experiment design," in *1989 American Control Conference*, 1989, pp. 1422–1427.

[12] A. Sekunda, H. Niemann, N. K. Poulsen, and I. Santos, "Closed loop identification using a modified hansen scheme," *Journal of Physics: Conference Series*, vol. 659, no. 1, p. 012009, 2015. [Online]. Available: http://stacks.iop.org/1742-6596/659/i=1/a=012009

[13] S. Morosi and I. F. Santos, "Active lubrication applied to radial gas journal bearings. part 1: Modeling," *Tribology International*, vol. 44, no. 12, pp. 1949–1958, 2011.

[14] F. G. P. Vásquez, "Model-based control design for flexible rotors supported by active gas bearings-theory & experiment," *Technical University of Denmark*, 2016.

[15] L. R. Theisen, H. H. Niemann, R. Galeazzi, and I. F. Santos, "Enhancing damping of gas bearings using linear parameter-varying control," *Journal of Sound and Vibration*, 2017.

[16] K. Zhou and J. C. Doyle, *Essentials of robust control*. Prentice hall Upper Saddle River, NJ, 1998, vol. 104.

[17] B. D. Anderson, "From Youla-Kucera to identification, adaptive and nonlinear control," *Automatica*, vol. 34, pp. 1485–1506, 1998.

[18] L. Ljung, "System identification," in *Signal Analysis and Prediction*. Springer, 1998, pp. 163–173.

[19] A. Varga, "Balancing free square-root algorithm for computing singular perturbation approximations," in *Decision and Control, 1991., Proceedings of the 30th IEEE Conference on*. IEEE, 1991, pp. 1062–1065.

Technical University of Denmark
Department of Electro Engineering
Section of Automation and Control
Elektro vej, Building 326
DK-2800 Kgs. Lyngby
Denmark
Phone: (+45) 45 25 34 76
Email: info@elektro.dtu.dk
www.elektro.dtu.dk